universität wien

DISSERTATION | DOCTORAL THESIS

Titel | Title

Variational modeling of molecular geometries

verfasst von | submitted by

Manuel Seitz BSc MSc

angestrebter akademischer Grad | in partial fulfilment of the requirements for the degree of

Doktor der Naturwissenschaften (Dr.rer.nat.)

Wien | Vienna, 2024

Studienkennzahl lt. Studienblatt | Degree programme code as it appears on the student record sheet:	UA 796 605 405
Dissertationsgebiet lt. Studienblatt | Field of study as it appears on the student record sheet:	Mathematik
Betreut von | Supervisor:	Univ.-Prof. Ulisse Stefanelli PhD

Abstract

Deriving macroscopic properties from atomistic systems is a challenging yet rewarding task. In this thesis, we are concerned with three instances in this direction. First, we characterize three-dimensional ground states of a two dimensional mass-spring model featuring a three body potential preferring angles of π. The competition between closest nearest-neighbor interaction and the three-body potential causes flat squares to become kinked into the third dimension. This gives rise to the question of characterizing tilings with nonflat squares. We show that such arrangements admit ripples, bending and even roll-up, but essentially only in one dimension.

It has been shown that mass-spring models converge to classical linear elasticity in the simultaneous atomistic-to-continuum and linearization limit. In the second contribution, we extend this result to the dynamic setting. More precisely, we prove that solutions to the atomistic equation of motion featuring also viscosity effects converge to the momentum equation for the linear elastic energy.

Whereas in classical continuum mechanics stresses are described solely via contact forces, the atomistic approach has the advantage of featuring also long-range interactions. These two paradigms have been combined into a nonlocal continuum model, called *Peridynamics*. In some cases, it is possible to recover classical continuum-mechanics formulations in the nonlocal-to-local limit, i.e., when the horizon of the nonlocal interactions tends to 0. We present a dynamic nonlocal-to-local convergence result, considering the quasi static evolution of a viscoelastic peridynamic model with nonlocal viscosity potential. This can be interpreted as a nonlocal version of a Kelvin-Voigt rheological model. We prove that solutions of the nonlocal model converge to the solution of the local equation in the nonlocal-to-local convergence.

Acknowledgments

First and foremost, I would like to express my deepest gratitude to my supervisor Ulisse Stefanelli. He guided me through the first steps into the wonderful world of Mathematics. And although I may not continue this path, I do not want to miss any of these steps along the journey.

I also want to thank Manuel Friedrich, who involuntarily become a second supervisor by all accounts. It was a pleasure!

Through all these years at the University of Vienna, I met so many great people – professors, fellow students, administration personnel, the SSC, etc. There were too many to name them all and I am very grateful to have met each and everyone of them. Still, I specifically want to thank Bettina Hiebl and Matteo Tommasini and their other-worldly organizational skills.

Naturalmente, also a big thank you to all the guys and gals from the 4th floor! I very much enjoyed all the lunch and coffee breaks with you, filled with chats about the world, math and music. May the force beer with you!

I would also like to thank my family and friends for their efforts of keeping me sane.

And of course Steffi, who had to put up with me when sanity was nowhere to be found. I couldn't have done this without you.

Contents

1 Introduction

The ability to describe and predict a material's mechanical response to forces and stresses is crucial for applications in engineering, geology, physics, chemistry, but also in biology and medicine. Not only effective mathematical models and numerical simulations are needed, but also their rigorous justification is required. Classically, materials are considered as a continuum and stresses are described via internal contact forces transmitted from point to point in the continuum. The classical theory of continuum mechanics is already well-developed [83, 87], although essential questions still ask for consideration [12, 13].

In this thesis, however, we take on a different viewpoint, namely, we consider materials as a collection of mutually interacting atoms [6, 92]. To put it crudely, we think of real world objects as an assemblage of tiny spheres, connected via (elastic) springs corresponding to the interatomic bonds. Those so-called *atomistic models* allow for long-range interactions and are well-suited for a wide range of applications, ranging from modeling material failure [40], to understanding crystallization [89], to essential tasks in material science [90] and chemistry [41].

An important question is the compatibility between discrete (atomistic) and continuum models [15, 23]. In particular, one hopes to obtain macroscopic properties of a specimen from microscopic models when letting the number of atoms tend to infinity (or equivalently, letting the interatomic distance tend to 0).

In order to give a mathematical description of the structure of a crystal, one needs to keep track of the positions of the individual atoms. An elegant way to do so, is to consider maps capturing the deformation of a chosen reference lattice $\mathcal{L} \subset \mathbb{R}^d$ due to the atomic interactions, body forces, and contact forces at the boundary. Naturally, such maps $y : \mathcal{L} \to \mathbb{R}^d$ are called *deformations* and $y(\mathcal{L})$ corresponds to the positions of the atoms of the *deformed configuration*. To capture the effects of the interatomic forces, we associate to each deformation a *configurational energy* depending on the positions of the atoms in the deformed configuration. For example, we could sum up the potential energy of the stretched or compressed springs that make up the atomic bonds. We expect those configurations that (locally or globally) minimize the configurational energy to model actual, observable deformations. Apart from modeling aspects, this approach leads to many questions. Do minimizers of the energy actually exist? Are they unique? Can we characterize the minimizers and if so, what are their properties? Are the atomistic and the continuum approach compatible, i.e., can we recover classical continuum models from the atomistic description?

In this thesis, we address some of those questions. In fact, we

(i) characterize minimizers of an energy (featuring two- and three-body potentials)

of three-dimensional deformations of the square lattice (thus providing a simple model for Tellurene or Selenene, already capturing some of their essential traits) (Chapter 2),

(ii) investigate the convergence of a specific elastic atomistic model to a linearized continuum one, aiming at recovering the classical equations of linear elastodynamics (Chapter 3), and

(iii) study the convergence of a nonlocal *Peridynamic* continuum model, where the governing energy comes from atomistic-inspired point interactions, when the interaction radius tends to 0 (Chapter 4).

The Chapters 2, 3, 4 are based on the papers [73], [71], and [72], respectively.

We give a summary of the main results of the thesis in Section 1.1 and collect some preliminaries in Section 1.2.

1.1 Outline and main results

Let us now describe the organization of the thesis and give an overview of the results. We defer the reader to the corresponding introductory sections of each chapter for all the necessary detail and a discussion of the relevant literature.

In Chapter 2, we characterize arrangements of identical nonflat squares in 3D. The nonflatness of the tiles gives rise to nontrivial geometries with configurations bending, wrinkling, or even rolling up in one direction. We prove that the fine geometry of such arrangements is completely characterized in terms of patterns of mutual orientations of the squares and that these patterns are periodic and one-dimensional. This chapter is based on the paper [73] in collaboration with Manuel Friedrich and Ulisse Stefanelli.

Chapter 3 is devoted to an atomistic-to-continuum linearization result in atomistic dynamics. Moving within the framework of [123], we prove that solutions of the equation of motion driven by atomistic deformation energies converge to the solutions of the momentum equation for the corresponding continuum energy of linearized elasticity. By recasting the evolution problems in their equivalent energy-dissipation-inertia-principle form, we directly argue at the variational level of evolutionary Γ-convergence [110, 119]. This chapter is based on the paper [71] in collaboration with Manuel Friedrich and Ulisse Stefanelli.

In the final Chapter 4, we study the quasistatic evolution of a linear peridynamic Kelvin-Voigt viscoelastic material. More specifically, we consider the gradient flow of a nonlocal elastic energy with respect to a nonlocal viscous dissipation. Following an evolutionary Γ-convergence approach, we prove that the solutions of the nonlocal problem converge to the solution of the local problem when the peridynamic horizon tends to 0, that is, in the nonlocal-to-local limit. This chapter is based on the paper [72] in collaboration with Manuel Friedrich and Ulisse Stefanelli.

In the remainder of this section, we summarize the main results and the proof ideas, referring to the individual chapters for the details.

1.1.1 Chapter 2 – Tilings with nonflat squares

In [73], we characterize all minimizers of a configurational energy featuring nearest and closest next-to-nearest neighbor interactions and three-body potentials preferring specific the bond angles.

The model and the main result. Let $y : \mathbb{Z}^2 \to \mathbb{R}^3$ be a three-dimensional deformation of the reference lattice $\mathbb{Z}^2$. The configurational energy under investigation is given by (a suitably normalized variant of)

$$E(y) := \frac{1}{2} \sum_{(x,x')\in N_1} v_2\big(|y(x) - y(x')|\big) + \frac{1}{2} \sum_{(x,x')\in N_2} v_2\big(|y(x) - y(x')|\big) + \frac{1}{2} \sum_{(x,x',x'')\in T} v_3\big(\measuredangle y(x)\, y(x')\, y(x'')\big), \tag{1.1}$$

where N_1 is the set of *nearest-neighbors*, N_2 the set of *closest next-to-nearest-neighbors*, and T the set of *triplets*, i.e., triples (x, x', x'') with $(x, x'), (x', x'') \in N_1$. Here, v_2 is a Lennard-Jones-type two-body potential and v_3 a smooth and strictly convex three-body potential with minimum $v_3(\pi) = 0$. Note that each bond gets counted twice, calling for the normalization factor of $1/2$.

Minimizers of the energy can be shown to have equal bond length. i.e., $|y(x)-y(x')| = \ell$ for all $(x, x') \in N_1$ for some $\ell > 0$, and map orthogonal bonds to bonds with optimal angle $\theta^* < \pi/2$. The latter is essentially due to the competition between closest next-to-nearest-neighbor interaction and the three-body-potential. The angle deficiency causes flat squares in $\mathbb{Z}^2$ to get mapped to *regular nonflat squares*. From this perspective, ground states can be interpreted as *tilings* with nonflat tiles. Additionally, bonds forming a straight line in the reference lattice, i.e., $x' - x = x'' - x' = \pm e_i$ with $i = 1, 2$ (e_i denoting unit vectors in $\mathbb{Z}^2$) are getting mapped to form a specific optimal angle $\delta^* = \measuredangle y(x)y(x')y(x'') < \pi$. In particular, these three optimality conditions imply that the four neighbors of each atom are coplanar in a ground state.

The main result is the characterization of all admissible tilings of identical regular nonflat squares in 3D under the condition that the four neighbors of each atom are coplanar. We show that they can bend, wrinkle, and roll in one direction and that such flexural behavior is completely characterized by specifying a suitably defined section of the configuration in the bending direction.

Proof idea. The core idea of the proof is to consider collections of four nonflat squares sharing one common atom, so-called *4-tiles*, and their categorization into six *classes*. The *boundary* of such a 4-tile consists of two bonds joining in a specific angle, which constitutes the *boundary type* of the 4-tile. This observation paves the way to applying combinatorial arguments, as only 4-tiles with the same boundary type can be attached.

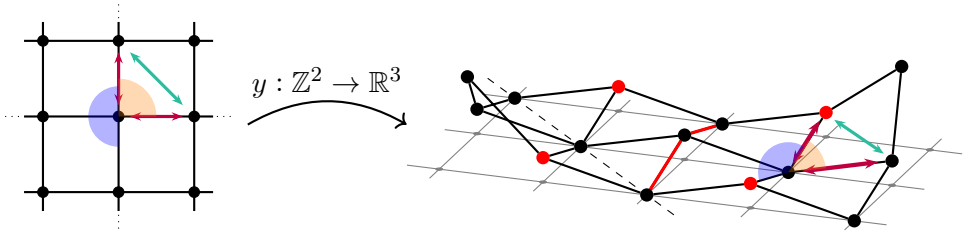

Figure 1.1: The deformation energy (1.1) encompasses nearest neighbor interaction (purple), the closest next-to-nearest neighbor interaction (green), and a three-body potential depending on the indicated angles (orange and blue). On the right, two attached 4-tiles are depicted. Their mutual boundary (red) is the "backbone" of the 4-tile with red corners. The structure is periodic along the dashed line and therefore roll-up occurs only orthogonal to the dashed diagonal.

Since the mutual boundary, at which two 4-tiles are attached, is again the "backbone" of another 4-tile (by simply shifting the reference lattice by either $(1,0)$ or $(0,1)$), it has to be of the optimal angle δ^* as well, as otherwise the deformation under consideration cannot be a ground state, see Figure 1.1. Carrying out this argument carefully, one proves that only three of the six classes are admissible, giving rise to essentially one-dimensional configurations, that can only roll-up/roll-down along either diagonal $(1,1)$ or $(-1,1)$.

1.1.2 Chapter 3 – Atomistic-to-continuum linearization in atomistic dynamics

In the paper [71], we show that solutions of the equation of motion driven by atomistic deformation energies converge to the solution of the momentum equation for the corresponding continuum energy of linearized elasticity.

The model and the main result. In [35, 123], the authors recovered linear elasticity models as Γ-limits of atomistic energies in the simultaneous atomistic-to-continuum and linearization limit. We indicate by $\Omega \subset \mathbb{R}^d$ the macroscopic reference configuration of the specimen and consider all points of the scaled d-dimensional Bravais lattice $\varepsilon\mathcal{L} := \varepsilon A \cdot \mathbb{Z}^d$ in Ω. Here, $\varepsilon > 0$ models the interatomic distance and $A \in \mathbb{R}^{d\times d}$ is an invertible matrix. In the small-deformation setting of linear elasticity, the parameter $\delta > 0$ is involved, quantifying the distance of deformations $y : \varepsilon\mathcal{L} \cap \Omega \to \mathbb{R}^d$ from the identity. For a scaled lattice displacement $u = (y - \mathrm{id})/\delta : \varepsilon\mathcal{L} \cap \Omega \to \mathbb{R}^d$, the atomistic energy in the small-strain regime is then given by

$$I_{\varepsilon\delta}(u) = \frac{\varepsilon^d \det A}{\delta^2} \sum_{\text{cells}} W(Z + \delta\bar{\nabla}u) + \text{surface terms},$$

where $\bar{\nabla}y$ is the *discrete deformation gradient*, describing the relative displacement of the atoms of a single cell. The scaling $\varepsilon^d \det A$ corresponds to the volume of a single cell,

whereas the factor δ^{-2} is instrumental for obtaining the correct limit in the small-strain regime [48]. The function W models the elastic cell energy and is assumed to be suitably smooth. In particular, it can be chosen to correspond to mass-spring models.

The main result of [123] is the Γ-convergence of $I_{\varepsilon\delta}$ as $\varepsilon, \delta \to 0$ to the classical linear elastic energy

$$I(w) = \frac{1}{2}\int_\Omega \nabla^s w : \mathbb{C} : \nabla^s w \,\mathrm{d}x,$$

where $w\colon \Omega \to \mathbb{R}^d$ is now the *macroscopic displacement* of the body, $\nabla^s w := (\nabla w + \nabla w^\top)/2$ is its symmetrized gradient, and $\mathbb{C}$ the fourth-order *elasticity tensor*, which can be directly computed from the Hessian of the cell energy.

In [71], we extend this theory to the dynamic setting by including inertial and viscous effects. Given initial a scaled lattice displacement u_ε^0 and a velocity u_ε^1, we consider the *atomistic equation of motion* given by

$$\begin{cases} \rho\ddot{u}_{\varepsilon\delta}(t) + \nu\dot{u}_{\varepsilon\delta}(t) + \partial I_{\varepsilon\delta}(u_{\varepsilon\delta}(t)) = 0 \quad \forall t \in (0,T), & \text{(1.2a)} \\ u_{\varepsilon\delta}(0) = u_\varepsilon^0, & \text{(1.2b)} \\ \dot{u}_{\varepsilon\delta}(0) = u_\varepsilon^1. & \text{(1.2c)} \end{cases}$$

The gradient $\partial I_{\varepsilon,\delta} u_{\varepsilon,\delta}$ is computed with respect to an atomistic L^2-like topology. We show that (specific interpolations of) solutions to the atomistic equation of motion above converge strongly in L^2 to the solution to the *momentum equation for the limiting linear elastic energy* in the simultaneous limit $\varepsilon, \delta \to 0$, which is given by

$$\begin{cases} \rho\partial_{tt} w + \nu\partial_t w - \operatorname{div}(\mathbb{C} : \nabla^s w) = 0 & \text{in } (0,T)\times\Omega, & \text{(1.3a)} \\ w = 0 & \text{on } (0,T)\times\partial\Omega, & \text{(1.3b)} \\ w(0,\cdot) = w^0 & \text{in } \Omega, & \text{(1.3c)} \\ \partial_t w(0,\cdot) = w^1 & \text{in } \Omega. & \text{(1.3d)} \end{cases}$$

Here w^0 and w^1 are suitable limits of u_ε^0 and u_ε^1, respectively.

Proof sketch. We prove convergence of solutions to the atomistic equation by directly passing to the limit in equation (1.2a). To this end, we reformulate (1.2a) as *energy-dissipation-inertia equality*, which reads as

$$\begin{aligned} &\frac{\rho}{2}\|\dot{u}_{\varepsilon\delta}(t)\|_\varepsilon^2 + I_{\varepsilon\delta}(u_{\varepsilon\delta}(t)) + \frac{1}{2\nu}\int_0^t \|\rho\ddot{u}_{\varepsilon\delta} + \partial I_{\varepsilon\delta}(u_{\varepsilon\delta})\|_\varepsilon^2 \,\mathrm{d}s + \frac{\nu}{2}\int_0^t \|\dot{u}_{\varepsilon\delta}\|_\varepsilon^2 \,\mathrm{d}s \\ &= \frac{\rho}{2}\|\dot{u}_{\varepsilon\delta}(0)\|_\varepsilon^2 + I_{\varepsilon\delta}(u_{\varepsilon\delta}(0)) \qquad \forall t \in [0,T]. \end{aligned} \tag{1.4}$$

This allows for establishing a priori estimates and hence also compactness by identifying the atomistic deformations with specific interpolations (based on the idea of Schmidt [123]). Identifying the weak limits eventually proves that solutions to (1.2) converge to solutions to (1.3). This approach however only entails weak convergence of gradients. Therefore, we improve this result in a second step, by showing energy convergence along

the sequence of solutions. This allows us to obtain the strong convergence of the gradients which prevents oscillations in the sequence of atomistic solutions and can therefore be interpreted a justification of the classical Cauchy-Born hypothesis [45, 78].

To this end, we follow an *evolutionary* Γ*-convergence* result [110, 119], based on passing to the liminf in (1.4) by means of a suite of liminf inequalities.

Note that arguing directly by employing the evolutionary Γ-convergence approach is not possible, as for reformulating the continuum equation of motion (1.3a) as energy-dissipation-inertia inequality, the chain rule is needed.

1.1.3 Chapter 4 – Nonlocal-to-local limit in linearized viscoelasticity

In [72], we are interested in the quasistatic evolution of linear peridynamic Kelvin–Voigt viscoelastic materials.

The model and the main result. Let $\Omega \subset \mathbb{R}^d$ ($d \geq 2$) be a bounded reference domain and indicate by $u\colon [0,T] \times \Omega \to \mathbb{R}^d$ the *time dependent displacement*. Following [101] and moving within the framework of (state-based) peridynamics, we define the *nonlocal elastic energy* of a homogeneous, isotropic material as

$$\begin{aligned} E_\rho(u) =& \frac{\beta}{2} \int_\Omega (\mathfrak{D}_\rho(u)(x))^2 \,\mathrm{d}x \\ &+ \frac{\alpha}{2} \int_\Omega \int_\Omega \rho(x'-x) \left(\mathscr{D}(u)(x',x) - \frac{1}{d}\,\mathfrak{D}_\rho(u)(x) \right)^2 \mathrm{d}x' \,\mathrm{d}x. \end{aligned} \tag{1.5}$$

Here, $\rho : \mathbb{R}^d \to [0,\infty)$ is a radially symmetric kernel, weighting the strength of nonlocal interactions. We assume that $\rho(\xi) = 0$ for $|\xi| > h$, where h is the so-called *peridynamic horizon*. We denote by

$$\mathscr{D}(u)(x',x) := \frac{(u(x') - u(x)) \cdot (x'-x)}{|x'-x|^2}$$

the *nonlocal strain* in the direction $(x'-x)/|x'-x|$. The weighted nonlocal strain, given by

$$\mathfrak{D}_\rho(u)(x) = \text{pv-}\int_\Omega \rho(x'-x)\mathscr{D}(u)(x',x)\,\mathrm{d}x',$$

is called *nonlocal divergence*. Here 'pv' indicates the Cauchy principle value. The constants $\alpha, \beta > 0$ are material parameters related to the shear and bulk modulus, respectively.

Mengesha and Du [101] showed that E_ρ admits a unique minimizer and proved that E_ρ Γ-converges with respect to the strong L^2-topology to the *local elastic energy*

$$E(u) = \frac{\lambda}{2} \int_\Omega \operatorname{div} u(x)^2 \,\mathrm{d}x + \frac{\mu}{2} \int_\Omega |\nabla^s u(x)|^2 \,\mathrm{d}x$$

when passing from the nonlocal to the local problem, that is, when $\rho \to \delta_0$ suitably. Here, $\nabla^s u = (\nabla u + (\nabla u)^\top)/2$ denotes the symmetric gradient of u.

We extend this result to the dynamic setting. To capture viscous effects, we introduce the *nonlocal potential of viscous forces* as

$$D_\rho(\dot{u}) = \frac{1}{2}\int_\Omega \int_\Omega \rho(x'-x)|\mathscr{D}(\dot{u})(x',x)|^2 \,\mathrm{d}x'\,\mathrm{d}x,$$

where $\dot{u}$ denotes the time-derivative of u.

Let us denote by $\mathcal{S}_\rho(\Omega;\mathbb{R}^d)$ the Hilbert space of L^2-deformations of finite nonlocal energy.

Given some *initial displacement* $u_{\rho,0} \in \mathcal{S}_\rho(\Omega;\mathbb{R}^d)$, we look for a solution $u_\rho \in H^1(0,T;\mathcal{S}_\rho(\Omega;\mathbb{R}^d))$ to the *nonlocal viscoelastic problem* given by

$$\begin{cases} \mathrm{d}_\rho D_\rho(\dot{u}_\rho) + \mathrm{d}_\rho E_\rho(u_\rho) = 0 & \text{in } \mathcal{S}_\rho(\Omega;\mathbb{R}^d)^* \text{ for } t\in[0,T], \quad (1.6a)\\ u_\rho(0,\cdot) = u_{\rho,0} & \text{in } \Omega, \quad (1.6b)\\ u(t,\cdot) = 0 & \text{in } \mathbb{R}^d\setminus\Omega. \quad (1.6c) \end{cases}$$

Here, $\mathrm{d}_\rho D_\rho$, $\mathrm{d}_\rho E_\rho\colon \mathcal{S}_\rho(\Omega;\mathbb{R}^d) \to \mathcal{S}_\rho(\Omega;\mathbb{R}^d)^*$ (dual space) are the Fréchet differentials of the quadratic functionals D_ρ and E_ρ. A specific integration by parts argument requires us to prescribe homogeneous Dirichlet boundary conditions, see Remark 4.5.7.

We show that the solutions to the nonlocal viscoelastic problems converge to a solution to the *local viscoelastic problem* in the nonlocal-to-local limit, that is, when the kernel ρ converge to δ_0 in a suitable sense. The *local viscoelastic problem* is that of finding a weak solution $u \in H^1(0,T;H^1_0(\Omega;\mathbb{R}^d))$ of

$$\begin{cases} -\nabla\cdot(\mathbb{D}\nabla^s\dot{u} + \mathbb{C}\nabla^s u) = 0 & \text{in } (0,T)\times\Omega, \quad (1.7a)\\ u(0,\cdot) = u_0 & \text{in } \Omega, \quad (1.7b) \end{cases}$$

where $u_0 \in H^1_0(\Omega;\mathbb{R}^d)$ is a suitable nonlocal-to-local limit of $u_{\rho,0}$.

Proof sketch. Existence and uniqueness of the nonlocal problem follows by the classical Picard Theorem in Banach spaces. In order to prove convergence of solutions, we again adopt the evolutionary Γ-convergence approach [110, 119]. To this end, we reformulate (1.6a) as *energy dissipation equality* and then pass to the limit by means of three liminf-inequalities. As the Γ-liminf inequality has already been established in [101], the key ingredients are the two liminf inequalities

$$\liminf_{\rho\to\delta_0}\int_0^t D_\rho(\dot{u}_\rho(s))\,\mathrm{d}s \geq \int_0^t D(\dot{u}(s))\,\mathrm{d}s, \quad (1.8)$$

$$\liminf_{\rho\to\delta_0}\int_0^t D_\rho^*\big(-\mathrm{d}_\rho E_\rho(u_\rho(s))\big)\,\mathrm{d}s \geq \int_0^t D^*\big(-\mathrm{d}E(u(s))\big)\,\mathrm{d}s. \quad (1.9)$$

Showing (1.8) and (1.9) relies on checking the convergence of $\mathrm{d}_\rho E_\rho(u_\rho)$ and $\mathrm{d}_\rho D_\rho(u_\rho)$, for which one is required to study the convergence of

$$\int_\Omega\int_\Omega \rho(x'-x)\mathscr{D}(u_\rho)(x',x)\mathscr{D}(v)(x',x)\,\mathrm{d}x'\,\mathrm{d}x,$$

along solutions to the nonlocal problem. Here, $v \in C^\infty(\Omega;\mathbb{R}^d)$ is a smooth test function. The problem in our setting, as compared to many nonlocal-to-local convergence results from the literature, is that u_ρ also depends on the kernel ρ. Indeed, as only L^2-compactness is available, one relies on an integration by parts formula to obtain

$$\int_\Omega \int_\Omega \rho(x'-x)\mathscr{D}(u_\rho)(x',x)\mathscr{D}(v)(x',x)\,\mathrm{d}x'\,\mathrm{d}x = \int_\Omega u_\rho(x)\mathscr{D}_\rho^*(\mathscr{D}(v))(x)\,\mathrm{d}x$$

and is thus left with proving a uniform bound on $\mathscr{D}_\rho^*(\mathscr{D}(v))$.

1.2 Preliminaries

Let us now collect some preliminaries.

1.2.1 Molecular Mechanics

In this section, we comment on why the picture of mass-spring-models is a useful approximation and briefly discuss some of the problems, that occur when dealing with atomistic-to-continuum convergence. In particular, we want to answer the following questions in an overview fashion. Why it is actually a good idea to minimize a configurational energy to describe the behavior of atomistic structures? Or in other words, why is thinking of atoms as spheres connected via springs a good approximation of real world molecules? Indeed, to fully characterize molecules and therefore derive micro- and macroscopic properties from first principles, one would actually have to start from the Schrödinger equation see, e.g., [91, 92, 129, 142]. As this is unfeasible, even for most simple molecules, we introduce the *Born-Oppenheimer approximation* and then discuss further coarse-graining methods.

For illustration purposes, let us assume the nuclei and electrons are point masses and neglect spin and relativistic interactions. Let $(X_1,\dots,X_M) \in \mathbb{R}^{3M}$ be the nuclear positions with atomic numbers Z_i and mass m_i for $i = 1,\dots,M$ and $(x_1,\dots,x_N) \in \mathbb{R}^{3N}$ be the electronic positions with mass m_e and electric charge e. Then the *wave function* is given by $\Psi : \mathbb{R} \times \mathbb{R}^{3M} \times \mathbb{R}^{3N} \to \mathbb{C}$, satisfying specific symmetry, regularity and normalization properties, see, e.g., [91, 92].

If we assume that the external potential is time-independent, a separation-of-variables approach $\Psi(t,x) = f(t)\psi(x)$ allows to split the Schrödinger equation into two differential equations [91]. As the time ODE can be readily solved, we are only concerned with time-independent case, that is the *time-independent Schrödinger equation* given by the following eigenvalue problem

$$\hat{H}\psi = E\psi.$$

Here, $\hat{H}$ is the *molecular Hamiltonian* consisting of

$$\hat{H} = -T_n - T_e + V_{nn} + V_{ne} + V_{ee}, \tag{1.10}$$

where

$$T_n = \frac{\hbar^2}{2}\sum_{i=1}^{M}\frac{1}{m_i}\nabla_{X_i}^2 \qquad \text{is the kinetic energy of nuclei,}$$

$$T_e = \frac{\hbar^2}{2m_e}\sum_{i}\nabla_{x_i}^2 \qquad \text{is the kinetic energy of electrons,}$$

$$V_{nn} = \sum_{i=1}^{M}\sum_{j>i}\frac{Z_i Z_j e^2}{|X_i - X_j|} \qquad \text{is the pot. energy of repulsions between nuclei,}$$

$$V_{ne} = \sum_{i=1}^{M}\sum_{j=1}^{N}\frac{Z_i e^2}{|X_i - x_j|} \qquad \text{is the pot. energy of attraction of electrons and nuclei,}$$

$$V_{ee} = \sum_{i=1}^{N}\sum_{j>i}\frac{e^2}{|x_i - x_j|} \qquad \text{is the pot. energy of repulsion of electrons.}$$

The Born-Oppenheimer approximation rests on the observation that the nuclei of atoms are much heavier compared to the electrons and thus the position of the nuclei changes substantially more slowly. This motivates a multiplicative splitting of the wave function into an electronic and a nuclear part, $\psi = \psi_e \phi_n$. Moreover, one can neglect the kinetic energy of the nuclei and the position of the atomic nuclei now enter as parameter. More precisely, we are now considering the *electronic Schrödinger equation* given by

$$(\hat{H}_e + V_{nn})\psi_e = U_e \psi_e, \tag{1.11}$$

where the *electronic Hamiltonian* $\hat{H}_e$ is given by

$$\hat{H}_e = -\frac{\hbar^2}{2m_e}\sum_{i=1}^{N}\nabla_{x_i}^2 + \sum_{i=1}^{M}\sum_{j=1}^{N}\frac{Z_i e^2}{|X_i - x_j|} + \sum_{i=1}^{N}\sum_{j>i}\frac{e^2}{|x_i - x_j|}, \text{ and}$$

$$V_{nn} = \sum_{i=1}^{M}\sum_{j>i}\frac{Z_i Z_j e^2}{|X_i - X_j|}.$$

The eigenvalue $U_e(X_1, \ldots, X_M)$ of (1.11) is the energy of the system depending on the position of the nuclei and is called *potential energy surface (PES)*. Since we are interested in the *ground state* of the system, that is, the stationary state of lowest energy, we can find the so-called *Born-Oppenheimer potential energy surface* via

$$E_{BO}(X) = \min_{\psi_e \in \mathcal{A}} U_e(X, \psi_e),$$

where

$$U_e(X, \psi_e) = \int_{\mathbb{R}^{3N}} \psi_e^* \hat{H}_e \psi_e$$

and $\mathcal{A}$ is the set of admissible electronic wave functions encoding the physical symmetry and normalization assumptions [77].

The so derived PES is now a function depending on $3M$ variables and assigning to a possible configuration of the molecule its configurational energy. This approximation is called *Born-Oppenheimer approximation*, originally introduced by Born and Oppenheimer in 1927 [20]. Note however that numerically computing the PES is highly nontrivial, even for small systems, and becomes unfeasible for larger systems.

Therefore, several *coarse-graining* methods were developed to reduce the number of degrees of freedom. Some examples include the Hartree-Fock method, the Cauchy-Born rule, and density-functional-theory methods. Another common approach, which we also adopt in this thesis, is to resort to so-called *classical potentials*, in which the energy of the atomic arrangement is given explicitly depending on the position of the nuclei. Such explicit formulas are obtained either by experimental data and/or quantum mechanical simulations. For example, one can set

$$E_{\text{classical}}(X) = \sum_{1\leq i<j\leq M} v_2(|X_i - X_j|),$$

where v_2 is a *two-body potential* only depending on the distance between the nuclei. A typical example chosen for v_2 is the *(6,12)-Lennard-Jones potential*, introduced by Lennard-Jones in a series of articles in the 1920s and '30s [66] and given by

$$v_{LJ}(r) = ar^{-12} - br^{-6},$$

where $a, b > 0$ are empirical parameters. It consists of the long-range attraction r^{-6} due to the London dispersion force and the short-range repulsion r^{-12} corresponding to the Pauli exclusion principle. Additionally, also three body-potentials or even higher interactions can be included, such that the energy now reads as

$$E_{\text{classical}}(X) = \sum_{1\leq i<j\leq M} v_2(|X_i - X_j|) + \sum_{1\leq i<j<k\leq M} v_3(X_i, X_j, X_k) + \dots.$$

Common examples for three-body potentials are the Tersoff [132], the Brenner [38] (both developed for carbon bonds) and the Stillinger-Weber [131] (introduced to model silicon) potential.

This approach is based on the classical Newtonian mechanics and is therefore also termed *Molecular Mechanics* or *forcefield methods*, see, e.g., [92, Chapter 3], [6]. Predicting the three-dimensional arrangement of the molecule via minimizing the energy is called *geometry optimization* [77]. This paves the way for applying techniques from *Calculus of Variations* [81, 117]. In particular, the *Direct Method of the Calculus of Variations* [46] gives a criterion for existence of minimizers.

However, providing an explicit characterization is in general a very difficult task, which very often can only be achieved under strong assumptions on the energy. In particular, the numerically observed fact that optimizers of classical energies arrange themselves into periodic configuration, that is, a crystal, still lacks a full rigorous mathematical justification and can only be checked for simplified models [17, 57, 84, 133].

In the second chapter of this thesis, we tackle such a characterization problem. In fact, we prove a characterization result for an energy depending on deformations of the square lattice, penalizing the distance of neighbors and next-neighbors and angles between bonds. The competition between the energy contribution of minimizing the distance of next-neighbors and the angles causes the flat squares to be bent into the third dimension. This phenomenon of two dimensional (multi-)lattices wrinkling up and appearing as three-dimensional structures can indeed be observed in nature, for example in graphene [96, 109] or selenene. It is conjectured that this contributes to its energetic stability, as the existence of two dimensional periodic structures are prevented from the so called Mermin-Wagner Theorem [106, 107].

To close this section, we mention another commonly used way to obtain a PES, the *Cauchy-Born rule (CB-rule)*. It asserts that the microscopic deformation follows the macroscopic one. More precisely, let $y : \Omega \cap \mathcal{L} \to \mathbb{R}^d$ be a deformation of a bounded portion of a d-dimensional Bravais lattice $\mathcal{L}$ and consider an elastic energy $E_\Omega(y)$. We say that the Cauchy-Born rule holds for a matrix F, if the minimizer of $E_\Omega(y)$ subject to the affine boundary condition $y(x) = Fx$ for $x \in \partial\Omega$ is exactly given by the affine deformation $y(x) = Fx$ for $x \in \Omega \cap \mathcal{L}$. In this case, the elastic energy can be easily calculated by

$$E_{\mathrm{CB}} = \lim_{r\to\infty} \frac{E_{r\Omega}(Fx)}{|r\Omega|}.$$

However, the validity of the CR-rule cannot be guaranteed in every setting. In fact, in the seminal paper [78], Friesecke and Theil proved the validity of the CR-Rule for a specific two-dimensional mass spring model, but also gave explicit examples for its failure. We do not present all details, but refer to [26, 45, 58, 59, 63] and the references therein. Instead we comment on the Cauchy-Born rule as it naturally appears in the setting of Chapter 3, that we sketched in Section 1.1.2 above. There, energy convergence implies strong convergence of the atomistic gradients, i.e., the atomistic deformation gradient follows the macroscopic (continuum) deformation gradient. Moreover, the strong convergence prevents the presence of oscillations in the sequence of atomistic solutions, and hence the emergence of microstructures. This can be interpreted as evidence for the validity of the classical Cauchy-Born hypothesis.

1.2.2 Bridging the scales – Γ-convergence

In Chapter 3, we are concerned with the question whether we are able to recover equations from classical continuum mechanics, when starting out from an atomistic model and letting the interatomic distance tend to 0.

As a first step towards this goal, one requires minimizers of the atomistic model to converge to minimizers of the continuum model in the atomistic-to-continuum limit. This calls for a notion of convergence of functionals respecting the variational nature of the problem, that is, we wish for convergence of minimizers and minima, when the functionals converge. Often the considered energy is depending on an additional parameter, e.g., in problems of homogenization, phase-transition, dimension-reduction, etc. One then is

asked to find an effective energy, that governs the behavior in the limiting case, e.g., when the given parameter tends to zero. De Giorgi's Γ-convergence is exactly the right tool, as, assuming equicoercivity, it guarantees the convergence of minima and minimizers. For the sake of completeness, we will recall Γ-convergence also here, but we refer to the by now standard monographs [22, 24, 47].

Definition 1.2.1. Let $F_n, F : X \to \mathbb{R} \cup \{+\infty\}$ be functionals defined on a separable metric space X. We say that F_n Γ-*converges* to F, written as $F_n \xrightarrow{\Gamma} F$, if for all $x \in X$, we have

(i) a liminf inequality: for every sequence $x_n \to x$ we have $F(x) \leq \liminf_{n\to\infty} F_n(x_n)$, and

(ii) a recovery sequence: $\forall x \in X$ there exists a sequence $x_n \to x$, such that $F(x) = \lim_{n\to\infty} F_n(x_n)$.

Condition (ii) can be replaced by the following limsup-inequality: For every x there is a sequence $x_n \to x$ such that $F(x) \geq \limsup_{n\to\infty} F_n(x_n)$.

As already mentioned, Γ-convergence respects convergence of minimizers and minimal values, provided F_n satisfies some mild uniform compactness property.

Theorem 1.2.1 (Fundamental Theorem of Γ-convergence, [24, Theorem 2.1])**.** *Let X be a metric space and $F_n, F : X \to \mathbb{R} \cup \{\pm\infty\}$ be such that $F_n \xrightarrow{\Gamma} F$. If F_n additionally satisfies that*

$$\exists K \subset X \text{ compact for which } \inf_X F_n = \inf_K F_n \text{ for all } n \in \mathbb{N}, \tag{1.12}$$

we have

(i) *Convergence of minimal values:* $\inf_X F = \min_X F = \lim_{n\to\infty}(\inf_X F_n)$, *and*

(ii) *Convergence of minimizers: If x_{n_k} is a minimizing sequence for some subsequence (F_{n_k}), i.e., $F_{n_k}(x_{n_k}) = \inf_X F_n + o(1)$, which converges to some $\bar{x}$, then its limit is a minimizer of F.*

Condition (1.12) in the above theorem is sometimes called *equi-mildly coercivity* of F_n. Note that Theorem 1.2.1 does not imply that all minimizers of F can be approximated by minimizers of F_n. From this perspective, Γ-convergence acts as selection criterion, a viewpoint that has been adapted by Ortner in [115] to the gradient flow setting of atomistic-to-continuum convergence.

Besides implying convergence of minima and minimizers, Γ-convergence enjoys another very useful property: It is stable under continuous perturbations. Let $G : X \to \mathbb{R}\cup\{+\infty\}$ be continuous with respect to the metric on X. Then, from $F_n \xrightarrow{\Gamma} F$, one automatically obtains $F_n + G \xrightarrow{\Gamma} F + G$. This follows readily from the definition, as for any x and x_n with $x_n \to x$, we have

$$F(x) + G(x) \leq \liminf_{n\to\infty} F_n(x_n) + \lim_{n\to\infty} G(x_n) \leq \liminf_{n\to\infty}(F_n(x_n) + G(x_n)).$$

Furthermore, for a recovery sequence $x_n \to x$ of F, it holds that

$$F(x) + G(x) = \lim_{n\to\infty} F_n(x_n) + \lim_{n\to\infty} G(x_n) = \lim_{n\to\infty} (F_n(x_n) + G(x_n)).$$

This feature is remarkable, as Γ-convergence is not linear. Consider for example $X = \mathbb{R}$ and $F_n := \sin(nx)$ and $G_n(x) := -\sin(nx)$. Then, F_n and G_n both Γ-converge to -1 (the liminf inequality is clear, for a recovery sequence for F_n take $x_n = \frac{3\pi\lfloor nx \rfloor}{2n}$). However, $F_n + G_n = 0$ for all $n \in \mathbb{N}$.

This stability under continuous perturbations is particularly useful, because it allows us to directly add body forces, such as gravity, to our model. For example the model of Chapter 4, outlined in Section 1.1.3 above, could be augmented to feature loading terms of the form

$$L(u) = \int_\Omega l(x) \cdot u(x) \, \mathrm{d}x,$$

for a $l \in L^2(\Omega; \mathbb{R}^d)$. Then, by the arguments above the nonlocal energy (1.5) satisfies $E_\rho + L \xrightarrow{\Gamma} E + L$.

1.2.3 Evolutionary Γ-convergence

From Definition 1.2.1, we see that Γ-convergence is a purely static notion. In Chapters 3–4, we are however considering dynamic problems in the structure of the *parameter-dependent gradient flow*, as

$$\begin{cases} \dot{x}_n = -\nabla F_n(x_n), & \text{(1.13a)} \\ x_n(0) = x_n^0. & \text{(1.13b)} \end{cases}$$

For illustrational purpose, we consider here a family of maps $F_n : X \to \mathbb{R} \cup \{+\infty\}$ on a Hilbert space X and a map $x : [0, T] \times X \to X$.

To extend the variational convergence to the dynamic setting, there are two related ways. The approach in [24] essentially adapts the minimizing movement scheme [7] to also allow for parametrized energies. As taking limits of the time scale parameter of the minimizing movement scheme $\tau \to 0$ and the Γ-limit may not commute [24, Chapter 8], one has to couple τ and n in a specific way, giving rise to the notion of a *minimizing movement along a sequence of functionals at the scale* τ. This calls for criteria, when the limit of minimizing movements along a sequence is a minimizing movement for the limit [24, 27].

One criterion guaranteeing that solutions of (1.13) converge to a solution of the corresponding limiting gradient flow problem is the by now well-established *evolutionary* Γ*-convergence approach*, inspired by Sandier and Serfaty [119], see also [110]. Here, one reformulates the evolution equation in terms of an energy dissipation inequality, see, e.g., [120], and then passes to the limit by means of specific liminf-inequalities. In addition, the limit must fulfill a chain rule to ensure equivalence of the energy dissipation inequality in the limit and the corresponding gradient flow problem.

Although this is a standard method by now, let us sketch the idea for the simple case of a gradient flow in $\mathbb{R}^d$ driven by the potential $F : \mathbb{R}^d \to \mathbb{R}$

$$\begin{cases} \dot{x} = -\nabla F(x) & \text{(1.14a)} \\ x(0) = x_0. & \text{(1.14b)} \end{cases}$$

Here, $\dot{x}$ denotes the time derivative of $x : [0,T] \times \mathbb{R}^d \to \mathbb{R}^d$ and $x_0 \in \mathbb{R}^d$ is some initial condition. We then assume that F_n from (1.13) Γ-converges to F and ask ourselves the question, when solutions x_n to (1.13) converge to solutions to (1.14).

We first sketch how to obtain the aforementioned energy-dissipation-inequality for (1.14), although it works analogously for (1.13). For the sake of simplicity, let us assume smoothness. Testing (1.14a) against $\dot{x}$, integrating in time, and using the chain rule, we arrive at

$$F(x(0)) - F(x(T)) = \int_0^T |\dot{x}(t)|^2 \, \mathrm{d}t. \tag{1.15}$$

Relation (1.15) entails $|\dot{x}|^2 = -\nabla F(x) \cdot \dot{x}$, but not that x is a solution to (1.14a). To resolve this issue, we invoke the Cauchy-Schwarz and the Young Inequality, giving us

$$|\dot{x}|^2 = -\nabla F(x) \cdot \dot{x} \leq |\nabla F(x)| \, |\dot{x}| \leq \frac{|\dot{u}|^2}{2} + \frac{|\nabla F(x)|^2}{2}. \tag{1.16}$$

Equality in (1.16) holds if and only if we have equality for the Cauchy-Schwarz and Young's Inequality, which again occurs if and only if $\dot{x} = -\nabla F(x)$, that is, if x solves (1.14a). Putting this together, we get that x solves (1.14a) if and only if x fulfills

$$F(x(0)) - F(x(T)) \geq \frac{1}{2} \int_0^T |\dot{x}(t)|^2 \, \mathrm{d}t + \frac{1}{2} \int_0^T |\nabla F(x(t))|^2 \, \mathrm{d}t. \tag{1.17}$$

Inequality (1.17) is called *Energy Dissipation Inequality*. This reformulation allows to generalize gradient flows to the setting of metric spaces, such as the space of probability measures. In particular, this formulation allows us to extend the notion of Γ-convergence to the dynamical setting. To this end, assume that we can find a solution x_n to the parameter-dependent gradient flow (1.13) and that $F_n \xrightarrow{\Gamma} F$. Additionally, we suppose that the initial conditions are *well-prepared*, that is, $x_n^0 \to x^0$ and $F_n(x_n^0) \to F(x^0)$. Then, we get from the well-preparedness, the Γ-convergence and the Energy Dissipation Inequality for x_n that

$$\begin{aligned} F(x(0)) - F(x(T)) &\geq \liminf_{n\to\infty} (F_n(x_n(0)) - F_n(x_n(T)) \\ &\geq \liminf_{n\to\infty} \frac{1}{2} \int_0^T |\dot{x}_n(t)|^2 \, \mathrm{d}t + \liminf_{n\to\infty} \frac{1}{2} \int_0^T |\nabla F_n(x_n(t))|^2 \, \mathrm{d}t. \end{aligned} \tag{1.18}$$

If we now assume that the following liminf-inequalities hold

$$\liminf_{n\to\infty} \int_0^T |\dot{x}_n(t)|^2 \, \mathrm{d}t \geq \int_0^T |\dot{x}(t)|^2 \, \mathrm{d}t \tag{1.19}$$

$$\liminf_{n\to\infty} \int_0^T |\nabla F_n(x_n(t))|^2 \, \mathrm{d}t \geq \int_0^T |\nabla F(x(t))|^2 \, \mathrm{d}t, \tag{1.20}$$

we can pass to the limit in (1.18) and eventually get that

$$F(x(0)) - F(x(T)) \geq \frac{1}{2}\int_0^T |\dot{x}(t)|^2 \,\mathrm{d}t + \frac{1}{2}\int_0^T |\nabla F(x(t))|^2 \,\mathrm{d}t.$$

Thus, we have shown that x is actually a solution to the limiting gradient flow, as it satisfies (1.17). This method has been coined *Evolutionary* Γ*-convergence* [110].

Summarizing this section, we see that it is therefore instrumental to show compactness, Γ-convergence and the liminf-inequalities (1.19)–(1.20) to prove the convergence of solutions to the parameterized gradient flow. This sets up the roadmap for the results in Chapter 3 and 4.

1.2.4 Peridynamics

One drawback of the continuum setting, compared to the atomistic one is, that it is poorly suited to model discontinuities, such as cracks, dislocations, etc. This is the reason, why Silling introduced a nonlocal continuum model in [127], called *Peridynamics*. Here, one considers the reference domain as continuum, but still models the governing potential energy as it would come from interaction between atoms. This way, discontinuities, e.g., cracks, can be described easily. We model the *force density due to interaction with other particles* by

$$L_\rho(x) = \int_\Omega \rho(x' - x) f(y(x') - y(x), x' - x) \,\mathrm{d}x', \tag{1.21}$$

where f is the *pairwise force function*, i.e., force that x' exerts on x weighted by the kernel ρ, which is assumed to satisfy $\rho(x' - x) = 0$ if $|x' - x| \geq \delta$. The parameter δ is called *(peridynamic) horizon*. Introducing this additional length scale in the form of the horizon paves the way to multiscale models, see, e.g., [9, 18]. Moreover, by choosing the kernel ρ suitably, one can model anisotropies, voids, or different material phases. In this thesis, we assume that ρ is radially symmetric, corresponding to an isotropic material, and normalized such that $\|\rho\|_{L^1(\Omega)} = d$.

This approach gives rise to a nonlocal model. The natural question is, can we also recover the classical continuum equations, when we let the range of interactions vanish, that is, let the horizon tend to 0? In the static setting, this question had been answered affirmatively by Mengesha and Du in [101] for a model in linear elasticity. The dynamic case has also attracted some attention, however, only inertia effects have been studied, see, e.g., [60, 61] and the references therein. Rigorous results concerning viscous effects are still lacking, although viscous peridynamic rheological models are commonly used by the engineering community, see the discussion in Section 4.1.

Already in [127], it has been noticed that the so-called *bond-based* model outlined above only applies to isotropic materials with Poisson ratio 1/4. Consequently, the more elaborate *state-based* peridynamic model has been introduced in 2007 [128] to resolve this problem. There, the interaction between atoms is governed by a so called *force state* that is similar to the classical stress tensor. In fact, this allows for describing the

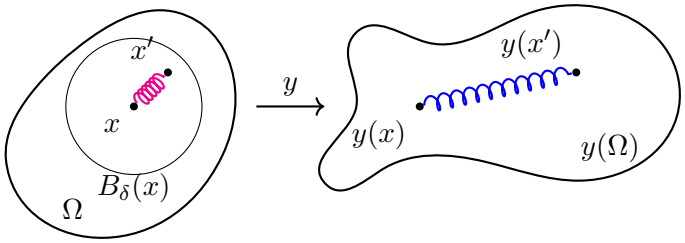

Figure 1.2: Idea of (bond-based) Peridynamics. The total force an atom at $y(x)$ is exerted to is the contribution of all the forces of the elastic springs, which get stretched or compressed due to the deformation.

collective response of all bonds in a neighborhood, whereas for the bond-based model each bonds' response is independent of all other bonds.

Let us now sketch the derivation of the energy (1.5). As starting from state-based peridynamics would require the more technical notion of a *state*, we resort to the simpler setting of bond-based peridynamics [127] instead. The derivation of the energy from state-based constitutive modeling runs along the same lines.

Following [127], a bond-based peridynamic material is called *microelastic*, if the pairwise force function f from (1.21) is *conservative*, that is, if there is a *pairwise potential function* w such that,

$$f(\eta, \xi) = \frac{\partial w(\eta, \xi)}{\partial \eta}. \tag{1.22}$$

Here, we abbreviated the bond in the reference configuration by $\xi = x' - x$ and the deformed bond by $\eta = y(x') - y(x)$. Definition (1.22) resembles the classical notion of hyperelasticity, where the Cauchy-stress is determined as the derivative of a stored energy function depending on the deformation gradient, see, e.g., [87, Chapter 2.3]. This allows us to define the *macroelastic energy density* W_y as

$$W_y(x) = \frac{1}{2} \int_\Omega w(y(x') - y(x), x' - x) \, \mathrm{d}x'$$

and consequently the *total macroelastic energy* or *total strain energy* E as

$$E(y) = \int_\Omega W_y(x) \, \mathrm{d}x.$$

Note that in stated-based peridynamics, the macroelastic energy density is a function of vector states. Its (suitably defined) derivative would then correspond to generalized force due to atomic interaction.

The aim is to derive the nonlocal strain energy corresponding to an isotropic elastic material. We therefore start from the classical decomposition of strains in a *spherical*

(also called hydrostatic) and *deviatoric* (also called shear) part, that is, for $A \in \mathbb{R}^{d\times d}$, we set $A = \operatorname{sph} A + \operatorname{dev} A$ with

$$\operatorname{sph} A := \frac{\operatorname{tr} A}{d}\mathbb{I}, \qquad \operatorname{dev} A := A - \operatorname{sph} A = A - \frac{\operatorname{tr} A}{d}\mathbb{I}.$$

Here, $\mathbb{I} \in \mathbb{R}^{d\times d}$ denotes the unit matrix. Then, a Lamé material with coefficients λ and μ at small strains has the quadratic stored energy

$$W(\nabla^s u) = \frac{1}{2}\lambda(\operatorname{tr}\nabla^s u)^2 + \mu|\nabla^s u|^2 = \frac{d}{2}k|\operatorname{sph}\nabla^s u|^2 + \mu|\operatorname{dev}\nabla^s u|^2, \tag{1.23}$$

where k is the *bulk modulus* and μ the second Lamé coefficient also corresponding to the *shear modulus*. For the derivation, see [87, Formula (6.7.9)]. Recall that $\nabla^s u = (\nabla u + \nabla u^\top)/2$ denotes the symmetric gradient.

Following [128] and drawing inspiration from classical materials, we aim at rewriting the energy of an elastic material in the small strain regime as

$$E(u) = \int_\Omega W_u(x)\,\mathrm{d}x = \int_\Omega W_{\mathrm{dil}}(x)\,\mathrm{d}x + \int_\Omega W_{\mathrm{dev}}(x)\,\mathrm{d}x.$$

Here, $W_{\mathrm{dil}}(x)$ is the strain energy density associated with dilations and $W_{\mathrm{dev}}(x)$ denotes the strain energy density associated with deviatoric portion of deformation. Moreover, analogously to (1.23), we write

$$W_{\mathrm{dil}} = \frac{d}{2}k(s_{\mathrm{dil}}, s_{\mathrm{dil}})_\rho, \qquad W_{\mathrm{dev}} = \mu(s_{\mathrm{dev}}, s_{\mathrm{dev}})_\rho,$$

where s_{dil} is the dilatational nonlocal strain, s_{dev} is the deviatoric nonlocal strain and $(\,\cdot\,,\,\cdot\,)_\rho$ is the weighted L^2-inner product.

In order to transfer this idea to the nonlocal case, we investigate how a bond $x' - x$ with $x', x \in \Omega \cap B_\delta(x)$, gets stretched or compressed due to the deformation. Thus, we define *(bond) elongation* e and the *nonlocal strain* s as

$$e(x', x) = |y(x') - y(x)| - |x' - x|, \qquad s(x', x) = e(x', x)/|x' - x|.$$

In the classical setting, the dilatational part of the strain would be given by $\operatorname{sph}\nabla y = 1/d\sum_{i=1}^d \partial_i y_i$, i.e., as the sum over all normal strains in direction e_i, $i = 1, \dots, d$. Following this idea, and additionally including the weight ρ, we define the *nonlocal dilatation*, that is, the surrogate of $\operatorname{tr}\nabla^s u$, as

$$\theta(x) = \int_\Omega \rho(x' - x)s(x', x)\,\mathrm{d}x'. \tag{1.24}$$

This corresponds to the trace of the strain tensor for small homogeneous deformations. Indeed, let us consider a deformation $y(x) = (1 + \varepsilon)x$. The deformation gradient is then

$\nabla y = (1+\varepsilon)\mathbb{I}$ and hence $\operatorname{sph}\nabla y = \frac{d(1+\varepsilon)}{d}\mathbb{I} = (1+\varepsilon)\mathbb{I}$. Considering the trace of the linearized strain given by $\nabla^s u = (\nabla u^\top + \nabla u)/2$ and $y = u + \mathrm{id}$, we get

$$\operatorname{tr}\nabla^s u = \sum_{i=1}^{d} \partial_i u_i = \sum_{i=1}^{d} \partial_i y_i - d = d + \varepsilon d - d = d\varepsilon.$$

Next, we consider the nonlocal case. We have $e(x', x) = \varepsilon|x' - x|$ and thus, $s(x', x) = \varepsilon$. This gives $\theta = \int_\Omega \rho(x' - x)s(x', x)\,\mathrm{d}x' = \varepsilon\int_\Omega \rho(x' - x)\,\mathrm{d}x' = \varepsilon d$, which is also in correspondence to $\operatorname{sph}\nabla^s u = \varepsilon = \frac{\theta}{d}$.

This motivates the definitions

$$s_{\mathrm{dil}} = \frac{\theta}{d}, \qquad s_{\mathrm{dev}}(x', x) = s(x', x) - s_{\mathrm{dil}} = s(x', x) - \frac{1}{d}\theta.$$

In the current linearized elasticity setting, we consider (uniformly) small displacements, i.e., $\sup_{|x'-x|<\delta} |u(x') - u(x)| \ll 1$ and assume for the moment that y is smooth. Then, a Taylor-expansion yields

$$\begin{aligned} e(x', x) =& |y(x') - y(x)| - |x' - x| \\ =& |x' - x + u(x') - u(x)| - |x' - x| \\ =& (u(x') - u(x))^\top \frac{x' - x}{|x' - x|} + O(|u(x') - u(x)|). \end{aligned}$$

So we can set

$$\begin{aligned} e(x', x) &\approx (u(x') - u(x))^\top \frac{x' - x}{|x' - x|} =: \mathscr{D}(u)(x', x)|x' - x|, \\ \tilde{s}(x', x) &= \mathscr{D}(u)(x', x). \end{aligned}$$

Substituting these into (1.24), the linearized version of nonlocal dilation θ reads as

$$\tilde{\theta}(x) = \int_\Omega \rho(x' - x)\mathscr{D}(u)(x', x)\,\mathrm{d}x' = \mathfrak{D}_\rho(u)(x)$$

and therefore the linearized dilatational strain is given by

$$\tilde{s}_{\mathrm{dil}} = \frac{\tilde{\theta}}{d}.$$

Note that the above linearization procedure is only formal. However, rigorous mathematical justification as in the classical setting [48] are available for the bond-based peridynamic material [103]. A linearized model for state-based peridynamics has been introduced in [126], again derived as a first order approximation.

Analogously to (1.23), the strain energy density associated with the dilatational part in the small strain regime is given by

$$\begin{aligned} W_{\mathrm{dil}}(x) &= d\frac{k}{2}(\tilde{s}_{\mathrm{dil}}, \tilde{s}_{\mathrm{dil}})_\rho = d\frac{k}{2}\int_\Omega \rho(x' - x)(\tilde{s}_{\mathrm{dil}})^2\,\mathrm{d}x' \\ &= d\frac{k}{2}\frac{\tilde{\theta}^2}{d^2}\int_\Omega \rho(x' - x)\,\mathrm{d}x' = \frac{k}{2}(\mathfrak{D}_\rho(u)(x))^2. \end{aligned}$$

where we used the normalization of ρ, namely, $\|\rho\|_{L^1(\Omega)} = d$.

The deviatoric part of the nonlocal strain $s(x', x)$ is then given by $s(x', x) - \frac{1}{d}\theta(x)$. Therefore, we obtain for the energy density corresponding of the linearized deviatoric nonlocal strain

$$W_{\mathrm{dev}}(x) = \frac{\alpha}{2}(\tilde{s}_{\mathrm{dev}}, \tilde{s}_{\mathrm{dev}})_\rho = \frac{\alpha}{2}\int_\Omega \rho(x' - x)\left(s(x', x) - \frac{1}{d}\theta(x)\right)^2 \mathrm{d}x',$$

where α is scalar proportional to shear modulus.

Collecting the linearized strain energies, we arrive at the potential energy of the linear problem (1.5) that was given by

$$\begin{aligned} E_\rho(u) =& \int_\Omega W_{\mathrm{dil}}(x) + W_{\mathrm{dev}}(x)\,\mathrm{d}x \\ =& \frac{k}{2}\int_\Omega (\mathfrak{D}_\rho(u)(x))^2\,\mathrm{d}x + \frac{\alpha}{2}\int_\Omega\int_\Omega \rho_n(x' - x)\left(\mathscr{D}(u)(x', x) - \frac{1}{d}\mathfrak{D}_\rho(u)(x)\right)^2 \mathrm{d}x'\,\mathrm{d}x. \end{aligned}$$

Isotropy of the material is simply modeled by assuming that the kernel ρ is radially symmetric. We thus have derived the potential energy for a linear isotropic homogeneous elastic material. This corresponds to a nonlocal version of the classical Navier-Lamé potential energy, which can be recovered in the nonlocal-to-local limit, see [101].

2 Tilings with nonflat squares: a characterization

This chapter consists of the paper [73] in collaboration with Manuel Friedrich and Ulisse Stefanelli.

Abstract

Inspired by the modelization of 2D materials systems, we characterize arrangements of identical nonflat squares in 3D. We prove that the fine geometry of such arrangements is completely characterized in terms of patterns of mutual orientations of the squares and that these patterns are periodic and one-dimensional. In contrast to the flat case, the nonflatness of the tiles gives rise to nontrivial geometries, with configurations bending, wrinkling, or even rolling up in one direction.

2.1 Introduction

The serendipitous isolation of graphene in 2004 [113] attracted enormous interest on the physics of 2D materials systems. Driven by their fascinating electronic and mechanical properties [144], research on 2D systems is currently witnessing an exponential growth. Beyond graphene [5, 80], 2D material systems are continuously syntetized and investigated [42, 49, 94, 145] and findings are emerging at an always increasing pace, ranging from fundamental understanding to applications [2].

Free standing 2D material samples are often not flat, but rather present rippling patterns at specific length scales [93]. The origin of such nonflatness is currently debated, one possible explanation being the instability of perfectly flat arrangements at finite temperatures, as predicted by the classical Mermin-Wagner theory [106, 107]. In the case of graphene, ripples have been experimentally observed [96, 109], computationally investigated [65], and analytically assessed [74, 75]. The phenomenon is however not restricted to graphene, and surface rippling has been detected in other 2D systems as well [21, 136]. Understanding the global geometry of 2D materials is of the greatest importance, as flatness is known to influence crucially the electronic, thermal, and mechanical behavior of these systems [43, 52, 139, 143].

In this chapter, we tackle the question of flatness of 2D systems with square symmetry. Our interest is theoretical and our arguments are not tailored to a specific material system. Still, we remark that square-like 2D crystals have been predicted in selenene and tellurene [138]. We formulate the problem in the setting of molecular mechanics [6, 92, 116] by associating to each point configuration a scalar *configurational energy* and

focusing on its ground states in the quest for optimal geometries [17, 77]. In the square-symmetric case, each atom has four first neighbors and the topology of the configuration is that of the square lattice $\mathbb{Z}^2$ [98]. The configurational energy is assumed to feature both two- and three-body effects [38, 131, 132], depending on bond lengths (distances between atoms) and angles between bonds, respectively. We present conditions ensuring that global minimizers of the configurational energy have all bonds of equal length, all angles formed by bonds to first neighbors of equal amplitude θ^*, and the four first neighbors of each atom are coplanar. As a result, minimal cycles of four atoms form *regular* squares featuring equal sides and equal angles θ^*, see Figure 2.1. Such identical squares arrange then in an infinite 3D configuration, which under the above provisions we call *admissible* and which we interpret as the actual geometry of the crystal.

The goal of this chapter is to classify all admissible configurations, namely all possible 3D arrangements of identical regular squares. In case the squares are flat, namely if $\theta^* = \pi/2$, the result is straightforward: the only configuration of flat squares where all first neighbors of each atom are coplanar is the plane. In order to tackle genuinely 3D geometries, we hence need to focus on the case $\theta^* < \pi/2$ instead, which induces nonflatness, as per Figure 2.1.

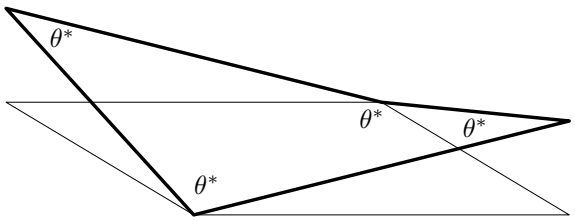

Figure 2.1: The regular nonflat square

Our main result is a complete characterization of admissible arrangements of identical regular nonflat squares in 3D, see Theorem 2.2.8. We prove in particular that admissible configurations can bend, wrinkle, and roll in one direction and that such flexural behavior is completely characterized by specifying a suitably defined section of the configuration in the bending direction, see Figure 2.4 below. More precisely, one classifies patches of four squares sharing an atom (*4-tiles*) in six different *classes*, in terms of their mutual orientation, see Figure 2.6. We prove that just *three* of these classes actually give rise to admissible configurations, that the whole geometry is specified by knowing the pattern of such classes, and that such pattern is periodic.

One can visualize the square in Figure 2.1 as (the boundary of) a nonflat tile. Our result can hence be interpreted as a classification of all possible *tilings* with such nonflat tiles under the condition that the four neighbors of each atom are coplanar. The relevance of this coplanarity condition is revealed by considering the limiting flat case. In case tiles are flat and the four neighbors of each atom are coplanar, the only possible tiling is the plane. By dropping the coplanarity requirement, we however allow for tilings ensuing from foldings of the reference square lattice $\mathbb{Z}^2$ along a set of parallel coordinate directions. Thus, the coplanarity requirement serves the purpose of excluding the effect

of the symmetry of the reference lattice on the onset of nontrivial geometries.

In the case of hexagonal symmetry, the characterization of global arrangements of regular nonflat hexagons has been obtained in [74, 75]. To some extent, the results in this chapter for squares are akin to the hexagonal case, for in both cases the arrangement shows some distinguished one-dimensional patterning. Compared with the hexagonal setting, the present square-symmetric case is however much more involved. This is an effect of the different symmetry of the underlying reference lattices. In the square case, arguments require to consider the detailed geometry of patches of up to sixteen neighboring squares, which makes the combinatorial picture much richer.

The chapter is organized as follows. Section 2.2 is devoted to the statement of our main results. The molecular-mechanical model is discussed first and the detailed geometry of ground states is assessed. A first description of admissible configurations is presented in Theorem 2.2.2. We then introduce the concept of 4-*tile* and of its *type*, collect all possible types and classes, and discuss the possibility of attaching two 4-tiles by analyzing the corresponding boundary, see Lemma 2.2.6. This eventually paves the way to the statement of our main result, namely the characterization of Theorem 2.2.8. Section 2.3 is entirely devoted to the proof of the main result, hinging both on combinatorial and geometrical arguments. Some proofs are postponed to Section 2.4 in order to enhance the readability of the arguments.

2.2 The setting and main results

2.2.1 Ground states of configurational energies

We focus on three-dimensional deformations $y\colon \mathbb{Z}^2 \to \mathbb{R}^3$, defined on the two-dimensional *reference lattice* $\mathbb{Z}^2$. For any open subset $\Omega \subset \mathbb{R}^2$ we define the *configurational energy* of a deformation on Ω by

$$\begin{aligned} E(y,\Omega) := \frac{1}{2} \sum_{(x,x')\in N_1(\Omega)} v_2\big(|y(x)-y(x')|\big) + \frac{1}{2} \sum_{(x,x')\in N_2(\Omega)} v_2\big(|y(x)-y(x')|\big) \\ + \frac{1}{2} \sum_{(x,x',x'')\in T(\Omega)} v_3\big(\measuredangle y(x)\, y(x')\, y(x'')\big), \end{aligned} \tag{2.1}$$

where

$$N_1(\Omega) := \big\{(x,x')\colon x,x' \in \mathbb{Z}^2,\, x\in\Omega,\, x'\in\overline{\Omega},\, |x-x'|=1\big\} \tag{2.2}$$

denotes the set of *nearest-neighbors* and

$$\begin{aligned} N_2(\Omega) := \{(x,x')\colon x,x'\in\mathbb{Z}^2\cap\overline{\Omega},\, |x-x'|=\sqrt{2}; \\ (x-x')\cdot e_1 > 0 \text{ if } x\in\partial\Omega \text{ or } x'\in\partial\Omega\} \end{aligned} \tag{2.3}$$

is the set of *closest next-to-nearest-neighbors*. Moreover, by $\measuredangle y(x)\, y(x')\, y(x'')$ we denote the *bond angle* in $[0,\pi]$ at $y(x')$ formed by the the vectors $y(x)-y(x')$ and $y(x'')-y(x')$, where the set of *triplets* $T(\Omega)$ is defined by

$$T(\Omega) := \{(x,x',x'')\colon (x',x)\in N_1(\Omega), (x',x'')\in N_1(\Omega), x\neq x''\}. \tag{2.4}$$

The factor $1/2$ reflects the fact that *bonds* $\{y(x), y(x')\}$, $(x, x') \in N_1(\Omega) \cup N_2(\Omega)$, and bond angles $\measuredangle y(x)\, y(x')\, y(x'')$ appear twice in the corresponding sums. Let us point out that in order to take surface effects at $\partial\Omega$ properly into account, bonds $\{y(x), y(x')\}$ are only counted once if $\{x, x'\} \in N_1(\Omega)$ and either $x \in \partial\Omega$ or $x' \in \partial\Omega$, or if $\{x, x'\} \in N_2(\Omega)$ and $x \in \partial\Omega$ or $x' \in \partial\Omega$. Bonds where $\{x, x'\} \in N_1(\Omega)$ with $x \in \partial\Omega$ and $x' \in \partial\Omega$ are not counted at all. This asymmetry of counting bonds is motivated by the specific choice of the cell energy, see Section 2.4.5.

We assume the *two-body* interaction potential $v_2 \colon \mathbb{R}^+ \to [-1, \infty)$ to be of short-range repulsive and long-range attractive type. In particular, we assume that v_2 is continuous and attains its minimum value only at 1 with $v_2(1) = -1$. Moreover, we suppose that v_2 is decreasing on $(0, 1)$, increasing on $[1, \infty)$, and that v_2 is continuously differentiable on $(1, 2]$ with $v_2' > 0$ on $(1, 2]$. The *three-body* interaction density $v_3 \colon [0, \pi] \to [0, \infty)$ is assumed to be strictly convex and smooth, with $v_3(\pi) = 0$.

In the following, we will be interested in minimizing the energy of a configuration on the *whole* reference lattice. To this end, we define the *normalized energy* of $y \colon \mathbb{Z}^2 \to \mathbb{R}^3$ by

$$E(y) = \sup_{m \in \mathbb{N}} \frac{1}{(2m-1)^2} E(y, Q_m), \tag{2.5}$$

where $Q_m \subset \mathbb{R}^2$ is the open square centered at 0 with sidelength $2m$. A deformation is called a *ground state* if it minimizes the energy E.

For a fine characterization of the minimizers, some additional qualification on v_2 and v_3 will be needed. More precisely, we suppose that there exist small parameters $\eta, \varepsilon > 0$ such that

$$v_2(1-\eta) > 3 + 4v_2(\sqrt{2}) + 8v_3(\pi/2), \tag{2.6}$$

$$v_2(1+\eta) > -1 + 4v_2(\sqrt{2}) - 4v_2(\sqrt{2}(1-\eta)^2) + 8v_3(\pi/2), \tag{2.7}$$

$$v_3(\theta) > 2 + 2v_2(\sqrt{2}) + 4v_3(\pi/2) \text{ if } \theta \le \pi/2 - \eta, \tag{2.8}$$

$$\begin{aligned} &(\ell_1, \ell_2, \theta) \mapsto \frac{1}{4} v_2(\ell_1) + \frac{1}{4} v_2(\ell_2) + v_2\left(\left(\ell_1^2 + \ell_2^2 - 2\ell_1\ell_2\cos\theta\right)^{1/2}\right) + v_3(\theta) \\ &\qquad \text{strictly convex on } [1-\eta, 1+\eta]^2 \times [\pi/2 - \eta, \pi] \text{ and} \\ &\qquad \text{strongly convex for } \theta \in [\pi/2 - \eta, \pi/2 + 3\eta], \end{aligned} \tag{2.9}$$

$$|v_3|, |v_3'| \le \varepsilon \text{ in a neighborhood of } \pi, \tag{2.10}$$

$$\begin{aligned} &0 < -2\sqrt{2}\sqrt{1-\cos\theta}\, v_3'(\theta) < \ell \sin\theta\, v_2'\big(\sqrt{2}\ell\sqrt{1-\cos\theta}\big) \\ &\qquad \text{for } \ell \in [1-\eta, 1] \text{ and } \theta \in [\pi/2 - \eta, \pi]. \end{aligned} \tag{2.11}$$

Properties (2.6)–(2.7) entail that first-neighbor bond lengths range between $1-\eta$ and $1+\eta$, whereas (2.8) ensures that bond angles are not significantly smaller than $\pi/2$. Eventually, assumptions (2.9)–(2.11) yield that the contributions of first and second neighbors are strong enough to induce local geometric symmetry of ground states, i.e., bonds and bond angles will be constant, see (2.12)–(2.14) below.

Note that the assumptions (2.6)–(2.11) are compatible with a choice of a density v_2 growing sufficiently fast out of its minimum. In particular, the quantitative Lennard-Jones-like case of Theil [133] (see also [57, 64]) can be reconciled with assumptions (2.6)–(2.7), upon suitably choosing densities and parameters. Let us however remark that the specific form of (2.6)–(2.11) is here chosen for the sake of definiteness and simplicity. Indeed, these assumptions could be weakened, at the expense of additional notational intricacies. Under the above assumptions we have the following result, where we set $N_1 := N_1(\mathbb{R}^2)$, $N_2 := N_2(\mathbb{R}^2)$, and $T := T(\mathbb{R}^2)$ (see (2.2)–(2.4)).

Proposition 2.2.1 (Ground states)**.** *Let v_2 and v_3 be the above-introduced two- and three-body-potentials satisfying assumptions (2.6)–(2.11). For η small enough and $\varepsilon = \varepsilon(\eta)$ small enough there exist $\ell \leq 1$, $\theta < \pi/2$, and $\delta_\theta < \pi$ only depending on v_2 and v_3 such that a deformation $y\colon \mathbb{Z}^2 \to \mathbb{R}^3$ is a ground state of the energy E if and only if y satisfies*

$$|y(x) - y(x')| = \ell \text{ for all } (x, x') \in N_1, \tag{2.12}$$

and

$$\measuredangle y(x)\, y(x')\, y(x'') = \theta \text{ for all } (x, x', x'') \in T \text{ with } (x, x'') \in N_2, \tag{2.13}$$

as well as

$$\measuredangle y(x)\, y(x')\, y(x'') = \delta_\theta \text{ for all } (x, x', x'') \in T \text{ with } (x, x'') \notin N_2. \tag{2.14}$$

Here, the conditions $(x, x'') \in N_2$ and $(x, x'') \notin N_2$ correspond to the case that the vectors $x - x'$ and $x'' - x'$ form an angle $\pi/2$ or π, respectively, in the reference lattice. We will see later that δ_θ is uniquely determined by θ due to a geometric compatibility condition, see Lemma 2.2.4 below.

The proof of Proposition 2.2.1 is similar to the one in [74, Proposition 3.1] and is postponed to Section 2.4.5. At this stage, let us just comment on the effect of condition $v_2' > 0$ in a neighborhood of $\sqrt{2}$, see (2.11), which guarantees that θ is strictly smaller than $\pi/2$. Indeed if $v_2' = 0$ in a neighborhood of $\sqrt{2}$, we would obtain $\ell = 1$ and $\theta = \pi/2$, i.e., $y(\mathbb{Z}^2)$ would coincide with $\mathbb{Z}^2$ up to isometries. For $\theta < \pi/2$ instead, ground states exhibit interesting nontrivial geometries. The aim of this chapter is precisely that of characterizing these nontrivial geometries.

2.2.2 Necessary conditions for admissibility

Deformations $y\colon \mathbb{Z}^2 \to \mathbb{R}^3$ satisfying the conditions (2.12)–(2.14) are called *admissible*. Without restriction, we suppose for notational convenience that $\ell = 1$. Indeed, this can be achieved by replacing y by $\frac{1}{\ell} y$ without effecting the geometry of admissible configurations.

Obviously, conditions (2.12)–(2.13) constrain the local geometry of configurations: let $\{x_1, x_2, x_3, x_4\}$ be a simple cycle in $\mathbb{Z}^2$, called a *reference cell*, where here and in the following the labeling is counterclockwise and counted modulo 4. The image via y is the

simple cycle $\{y_1, y_2, y_3, y_4\}$, where $y_i = y(x_i)$, called an *optimal cell*. Since $\theta < \pi/2$ from (2.13), optimal cells are not flat. Indeed, the sum of interior angles is strictly less then 2π, i.e., $\sum_{i=1}^{4} \measuredangle y_{i-1}\, y_i\, y_{i+1} = 4\theta < 2\pi$, see also Figure 2.2.

The kink of an optimal cell can equivalently be visualized as occurring along the diagonal $x_3 - x_1$ or along the diagonal $x_4 - x_2$ of the corresponding reference cell. We set $m_1 := (y_1 + y_3)/2$ and $m_2 := (y_2 + y_4)/2$ and define $p := m_1 - m_2$. Let n be the normal vector of the triangle formed by y_1, y_2, and y_4, in direction $(y_2 - y_1) \times (y_4 - y_2)$. Then, we say that the optimal cell is of *form* $\diagdown$ if $p \cdot n > 0$ and of *form* $\diagup$ if $p \cdot n < 0$, see Figure 2.2. An optimal cell of any form can be transformed into a cell of the other form simply via a rotation by $\pi/2$ along the vector p or via a reflection with respect to the plane with normal p.

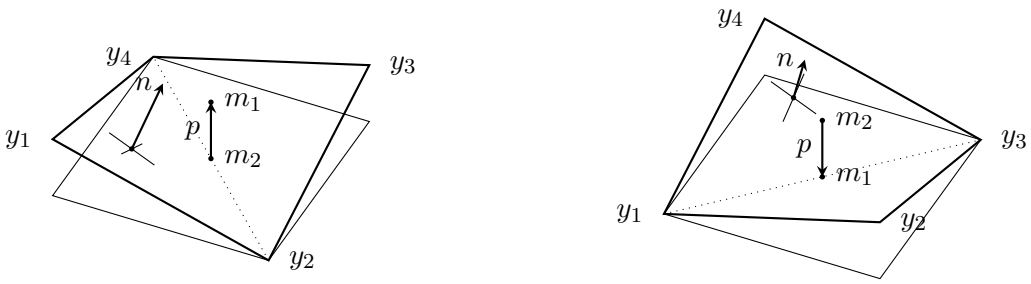

(A) Optimal cell of form $\diagdown$

(B) Optimal cell of form $\diagup$

Figure 2.2: The two optimal cells, defined via the vector p and the normal vector of one face. For the sake of illustration, they are positioned in such a way that p is parallel to e_3, which is why here $y_1 \cdot e_3 = y_3 \cdot e_3$ and $y_2 \cdot e_3 = y_4 \cdot e_3$. In symbols, we indicate optimal cells with $\diagup$ or $\diagdown$, according to the direction of the lower diagonal.

Our goal is to provide a complete characterization of admissible configurations. In a first step, we will present necessary conditions for admissibility in terms of *optimal cells*. To obtain a complete characterization, we will subsequently present a refined formulation in terms of so-called 4-*tiles*, namely, 2×2 groups of optimal cells, see Subsection 2.2.5. To state our first main result, we need to introduce some further notation.

Form function. Given a reference cell $\{x_1, x_2, x_3, x_4\}$ labeled in such a way that for the lower-left corner x_1 we have $x_1 = (s, t)$, we define the *barycenter* z of the reference cell via $z(s, t) := (1/2 + s, 1/2 + t)$. Thus, $z(\mathbb{Z}^2) = \mathbb{Z}^{2^*}$, where $\mathbb{Z}^{2^*}$ denotes the dual lattice of $\mathbb{Z}^2$. For an admissible configuration y, we define the *form function* on the dual lattice $\tau_y \colon \mathbb{Z}^{2^*} \to \{\diagdown, \diagup\}$ as the map assigning to each reference cell the form of the optimal cell in the deformed configuration. In other words, the deformation y maps a reference cell with barycenter $z(s, t)$ to an optimal cell of form $\tau_y(z(s, t))$. In the sequel, we simply write τ for notational convenience.

Incidence angles. We define the diagonals $d_1 = (1, 1)$ and $d_2 = (-1, 1)$. For $i = 1, 2$, we indicate *signed incidence angles along the diagonal* d_i for each bond of the configuration via the mappings $\gamma_i \colon ((\mathbb{Z} + 1/2) \times \mathbb{Z}) \cup (\mathbb{Z} \times (\mathbb{Z} + 1/2)) \to [-\pi, \pi]$ defined as follows:

first, for $s,t \in \mathbb{Z}$, $(s+1/2,t)$ parametrizes the horizontal bond in the reference lattice connecting (s,t) and $(s+1,t)$, and $(s,t+1/2)$ parametrizes the vertical bond in the reference lattice connecting (s,t) and $(s,t+1)$, see Figure 2.3 A. In the following, we explicitly give the definition of the incidence angle $\gamma_i(s+1/2,t)$, $i=1,2$, for horizontal bonds. The definition associated to vertical bonds follows analogously, up to a rotation of the reference lattice by $\pi/2$.

Consider a horizontal bond parametrized by $(s+1/2,t)$, which is shared by the two cells with barycenters $z(s,t-1)=(s+1/2,t-1/2)$ and $z(s,t)=(s+1/2,t+1/2)$. By n^i_{top} we denote the unit normal vector to the plane spanned by the points $y(s,t)$, $y(s+1,t)$, and $y^i_{\mathrm{top}} := y((s,t)+v_i)$, with direction $(y(s+1,t)-y(s,t))\times(y^i_{\mathrm{top}}-y(s,t))$, where for convenience we set $v_1 := d_1 = (1,1)$ and $v_2 := (0,1)$. Analogously, we let n^i_{bot} be the unit normal vector to the plane spanned by $y(s,t)$, $y(s+1,t)$, and $y^i_{\mathrm{bot}} := y((s+1,t)-v_i)$ with direction $(y(s,t)-y(s+1,t))\times(y^i_{\mathrm{bot}}-y(s+1,t))$, see Figure 2.3 B.

Then, for all $s,t\in\mathbb{Z}$, the *signed incidence angles along the diagonal* d_i of horizontal bonds are given by

$$\gamma_i(s+1/2,t) = \begin{cases} \arccos(n^i_{\mathrm{top}}\cdot n^i_{\mathrm{bot}}) & \text{if } (y^i_{\mathrm{top}}-y^i_{\mathrm{bot}})\cdot(n^i_{\mathrm{top}}-n^i_{\mathrm{bot}})\geq 0 \\ -\arccos(n^i_{\mathrm{top}}\cdot n^i_{\mathrm{bot}}) & \text{if } (y^i_{\mathrm{top}}-y^i_{\mathrm{bot}})\cdot(n^i_{\mathrm{top}}-n^i_{\mathrm{bot}})<0. \end{cases} \tag{2.15}$$

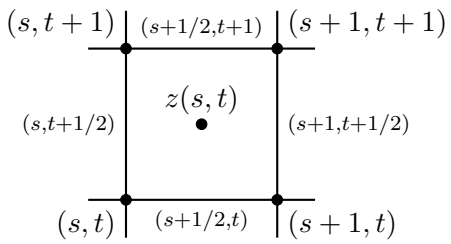

(A) Parametrization in the reference lattice.

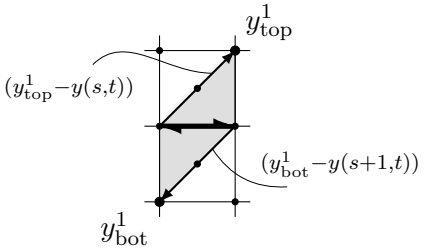

(B) Definition of the incidence angle along d_1 for a horizontal bond. The shaded areas correspond to the bond planes.

Figure 2.3: Notions for Theorem 2.2.2.

Making use of the introduced notation, we are now in the position of formulating our first result. This is a simplified version of the later Theorem 2.2.8 and provides *necessary* conditions on the existence of admissible configurations.

Theorem 2.2.2 (Basic structure of admissible configurations)**.** *There exists $\gamma^*\in(0,\pi)$, depending only on θ, such that for every admissible configuration $y\colon\mathbb{Z}^2\to\mathbb{R}^3$, possibly up to reorientation of the reference lattice, the following holds true:*

- *(Constant form function along d_1) We have $\tau(s,t)=\tau(s+1,t+1)$ for all $s,t\in\mathbb{Z}$.*
- *(Vanishing incidence angle along d_1) We have $\gamma_1(s+1/2,t)=0=\gamma_1(s,t+1/2)$ for all $s,t\in\mathbb{Z}$.*

- *(Incidence angle along d_2) It holds that* $\gamma_2(s,t) = \gamma_2(s+1/2, t+1/2) \in \{\pm\gamma^*, 0\}$ *for all* $s,t \in \frac{1}{2}\mathbb{Z}$ *with* $s+t \in \mathbb{Z}+1/2$.

This theorem implies that ground states are essentially one-dimensional, in the sense that they can be characterized as two-dimensional deformations of one-dimensional chains, see Figure 2.4. Indeed, due to τ being constant along d_1, any cross section along d_2 contains the same information. In particular, admissible configurations can be any combination of flat, rolled-up/down areas in relation to the fact that the incidence angle along d_2 can be 0 (flat areas), $-\gamma^*$ (rolled-up areas) or $+\gamma^*$ (rolled-down areas).

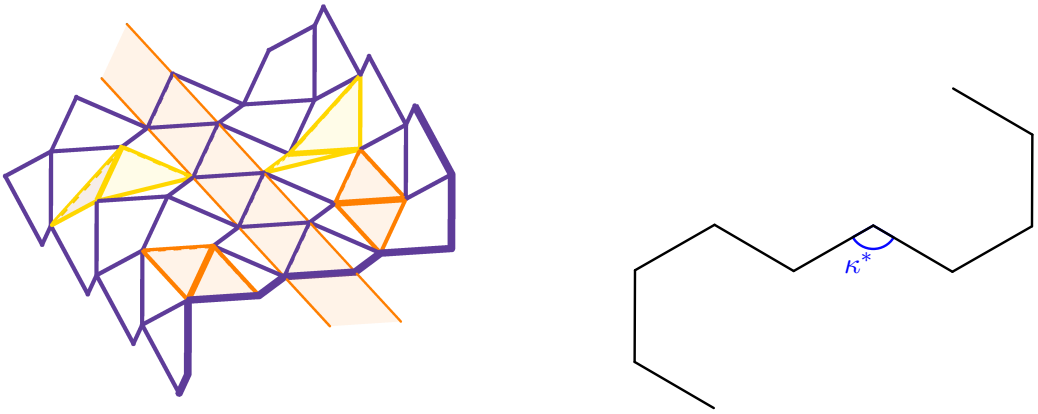

Figure 2.4: An admissible configuration (left). Since the form function is constant along the diagonal d_1, as indicated by the orange area, the same pattern repeats periodically and all necessary information is contained in one cross section as shown on the right. The angle κ^* is defined in (2.17). The defining bond planes for vertical (on the right) and horizontal (on the left) bonds of the incidence angles γ_1 (orange) and γ_2 (yellow) are marked, indicating that $\gamma_1 = 0 \neq \gamma_2$.

In the next subsections, we will present a refined version of Theorem 2.2.2, namely Theorem 2.2.8. We will show that Theorem 2.2.8 below implies Theorem 2.2.2. In Section 2.3 we then prove Theorem 2.2.8, which then also implies Theorem 2.2.2.

2.2.3 Geometry of optimal cells and construction of 4-tiles

We aim at obtaining a complete characterization of admissible configurations, by resorting to so-called 4-*tiles*. To introduce this concept, we first need to investigate the geometry of optimal cells in more detail. First, we consider an admissible deformation y and an optimal cell of the configuration, consisting of the points $y_1, \dots, y_4$ and the corresponding midpoints $m_1 = (y_1+y_3)/2$ and $m_2 = (y_2+y_4)/2$, as indicated in Figure 2.2. We denote the length of the diagonal by $2v := |y_1 - y_3| = |y_2 - y_4|$. By the cosine rule we have

$$v = \sqrt{(1-\cos\theta)/2}. \tag{2.16}$$

Setting $d := |y_1 - m_2| = |y_3 - m_2| = |y_2 - m_1| = |y_4 - m_1|$, we obtain by Pythagoras' theorem $d = \sqrt{1 - v^2} = \sqrt{(1 + \cos\theta)/2}$. This allows us to calculate the *kink angle* κ^* of an optimal cell by

$$\kappa^* = \pi - 2\kappa, \qquad \text{where } \kappa := \arccos(v/d) = \arctan(h/v), \tag{2.17}$$

with $h = \sqrt{1 - 2v^2}$, see also Lemma 2.2.5. We refer to Figure 2.5 with the optimal cell formed by $\{C, M_2, E_2, M_3\}$ for an illustration. For $\theta = \pi/2$ we have $v/d = 1$, and thus $\kappa^* = \pi$. In this case, as expected, optimal cells are flat. Let us firstly observe that an optimal cell is uniquely determined by the coordinates of three points and the choice of the cell form.

Lemma 2.2.3 (Optimal cell)**.** *Given any three points $y_1, y_2, y_4 \in \mathbb{R}^3$ of an optimal cell, i.e., points satisfying $|y_1 - y_4| = |y_1 - y_2| = 1$ and $\measuredangle y_4 y_1 y_2 = \theta$, there exists a unique fourth point $y_3^{\diagdown}$ and $y_3^{\diagup}$, respectively, such that $\{y_1, y_2, y_3^{\diagdown}, y_4\}$ is optimal of form $\diagdown$ and $\{y_1, y_2, y_3^{\diagup}, y_4\}$ is optimal of form $\diagup$.*

For the proof, we refer to Subsection 2.4.1. A priori, by prescribing only the common angle θ, many configurations are conceivable as each optimal cell can be of form $\diagdown$ or form $\diagup$, and neighboring cells can in principle be attached to each other with an arbitrary incidence angle. Condition (2.14) is therefore essential to reduce the number of admissible deformations. To take (2.14) into account, we now consider sub-configurations consisting of four optimal cells which are arranged in a square sharing one common point. Such structures are called 4-*tiles*, and we refer to Figure 2.5 for an illustration.

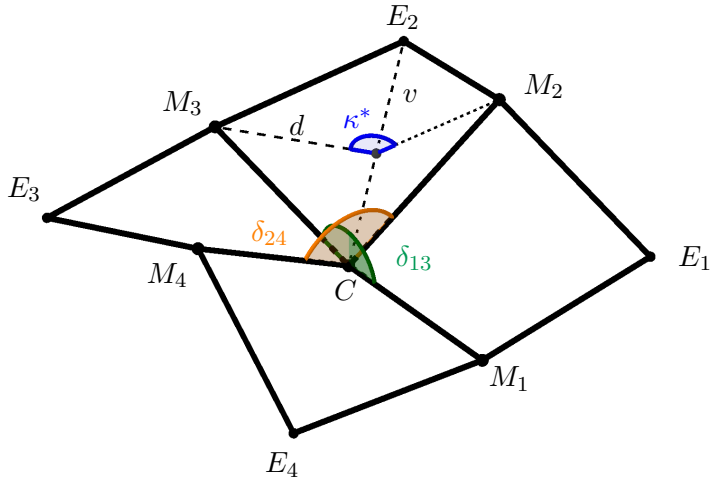

Figure 2.5: Example of a 4-tile with center C, middle points $M_1, \dots, M_4$ and corner points $E_1, \dots, E_4$. We have also indicated v, d, and κ^* of the optimal cell $\{C, M_2, E_2, M_3\}$.

The point shared by all four optimal cells is called *center* and is denoted by C. The additional four points shared by two optimal cells are called *middle points* (as they are

in the middle of the boundary of the 4-tile), are denoted by M_i for $i = 1, \dots, 4$, and are labeled counter-clockwise such that

$$y^{-1}(M_1) - y^{-1}(M_3) = 2e_1 \qquad \text{and} \qquad y^{-1}(M_2) - y^{-1}(M_4) = 2e_2.$$

By construction, we have $\measuredangle M_i\, C\, M_{i+1} = \theta < \pi/2$ which implies that the five points C and $(M_i)_{i=1}^4$ cannot be coplanar. We introduce the *nonplanarity angles* δ_{13} and δ_{24} by

$$\delta_{13} := \measuredangle M_1\, C\, M_3 \quad \text{and} \quad \delta_{24} := \measuredangle M_2\, C\, M_4. \tag{2.18}$$

Note that $|\delta_{13} - \pi|$ and $|\delta_{24} - \pi|$ indicate how far the five points C and $(M_i)_{i=1}^4$ are from being coplanar, and again refer to Figure 2.5 for an illustration. The nonplanarity angles δ_{13} and δ_{24} are related by the following lemma.

Lemma 2.2.4 (Nonplanarity angles)**.** *The nonplanarity angles δ_{13} and δ_{24} satisfy*

$$\cos\left(\delta_{13}/2\right) \cos\left(\delta_{24}/2\right) = \cos\theta. \tag{2.19}$$

In particular, δ_{13} and δ_{24} coincide if and only if

$$\delta_{13} = \delta_{24} = \delta_\theta = 2\arccos(\sqrt{\cos\theta}).$$

Indeed, by (2.14) we always have $\delta_{13} = \delta_{24}$ for every 4-tile of an admissible configurations since M_1, C, M_3 and M_2, C, M_4 fulfill the condition in (2.14). This yields that $\delta_\theta = 2\arccos(\sqrt{\cos\theta})$ is solely determined by θ. The proof relies on the geometry of optimal cells, i.e., on assumptions (2.12) and (2.13), and will be given in Subsection 2.4.1.

We denote the four corner points of the 4-tile by E_i, $i = 1, \dots, 4$, as indicated in Figure 2.5. For the classification of all different 4-tiles, it is convenient to frame 4-tiles in a *reference position*, as given in the following proposition.

Lemma 2.2.5 (Reference position)**.** (i) *By applying a suitable isometry, every 4-tile can be positioned in such a way that the center C coincides with the origin, and we have*

$$M_1 = (s, 0, \varsigma h), \quad M_2 = (0, s, \varsigma h), \quad M_3 = (-s, 0, \varsigma h), \quad M_4 = (0, -s, \varsigma h),$$

where $s = \sqrt{2}v$ (see (2.16)), $h = \sqrt{1 - 2v^2}$, and $\varsigma \in \{-1, 1\}$.
(ii) *Fixing $\varsigma \in \{-1, 1\}$, and the form of each of the four optimal cells, the positions of $(M_i)_{i=1}^4$ and $(E_i)_{i=1}^4$ are uniquely determined, up to isometry.*

For the proof, we again refer to Subsection 2.4.1. Lemma 2.2.5 entails that the middle points $(M_i)_{i=1}^4$ are coplanar. For this reason, we call 4-tiles *coplanar* in the following. By (2.14) coplanarity is a necessary condition for the admissibility of 4-tiles.

In view of Lemma 2.2.5(ii), there are 32 different *types* of 4-tiles. Indeed, there are $2^4 = 16$ possibilities to distribute either a form $\diagdown$ or a form $\diagup$ optimal cell to the four positions of a 4-tile. Additionally, one can do this construction for $\varsigma = 1$ or $\varsigma = -1$. As we show next, the different types can be classified into six *classes* which are invariant under rotation by $\pi/2$ and reflection along the e_1-e_2-plane, see Table 2.1. A representative of

each class is shown in Figure 2.6. The names of the classes are inspired by their geometry: the I-tile is intermediate between the zigzag-shaped Z-tile and the diagonally rolled-up D-tile (cf. the example in (2.22)). Similarly, the J-tile joins the arrowhead-shaped A-tile with the E-tile, whose periodic pattern resembles to egg cartons.

To denote a 4-tile we use a matrix-like notation, where the form of the optimal cell in the square is represented by $\diagdown$ or $\diagup$ in the respective position in the matrix. The case of $\varsigma = -1$ is indicated with a $+$-symbol in the center of the matrix, and $\varsigma = 1$ is denoted with a $-$-symbol. We use this notation since, given a 4-tile in reference position, we have that for $i = 1, \dots, 4$ the center satisfies $(C - M_i) \cdot e_3 > 0$ if $\varsigma = -1$ (e.g. in Figure 2.6 D) and $(C - M_i) \cdot e_3 < 0$ if $\varsigma = 1$ (e.g. in Figure 2.5), see Lemma 2.2.5(i).

Reflection of a 4-tile in reference position with respect to the e_1-e_2-plane interchanges the index $+$ with $-$. Moreover, $\diagup$ and $\diagdown$ are exchanged, as observed in Subsection 2.2.2. Also a rotation by $\pi/2$ interchanges the forms of the optimal cells, i.e., swaps $\diagdown$ and $\diagup$, see again Subsection 2.2.2. In addition, note that, by applying a $\pi/2$ rotation, one needs to permute the entries of the matrix accordingly, e.g.,

$$A \mapsto A^T \begin{pmatrix} 0 & 1 \\ 1 & 0 \end{pmatrix}$$

for a clockwise rotation of the entries.

A-tile	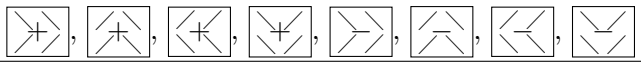	Figure 2.6 A
I-tile	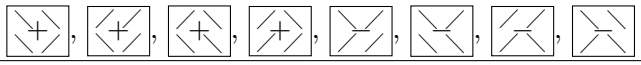	Figure 2.6 B
J-tile	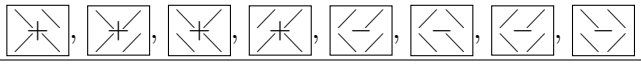	Figure 2.6 C
Z-tile	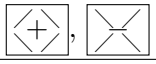	Figure 2.6 D
E-tile	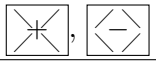	Figure 2.6 E
D-tile	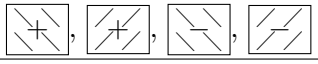	Figure 2.6 F

Table 2.1: Full classification of all possible 4-tiles.

As an example, rotation leaves the 4-tile invariant, as interchanging $\diagup$ and $\diagdown$ yields  and the rotation of the entries then leads to  . However, rotating 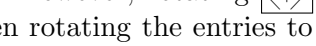 clockwise, i.e., first swapping $\diagdown$ and $\diagup$ to obtain  and then rotating the entries to , yields an 4-tile of the same class, but with different type, see Table 2.1.

2.2.4 Boundary orientation and boundary angles

In this subsection, we further refine the characterization of 4-tiles by introducing a notion of boundary orientation. To this end, consider a 4-tile with notation as indicated

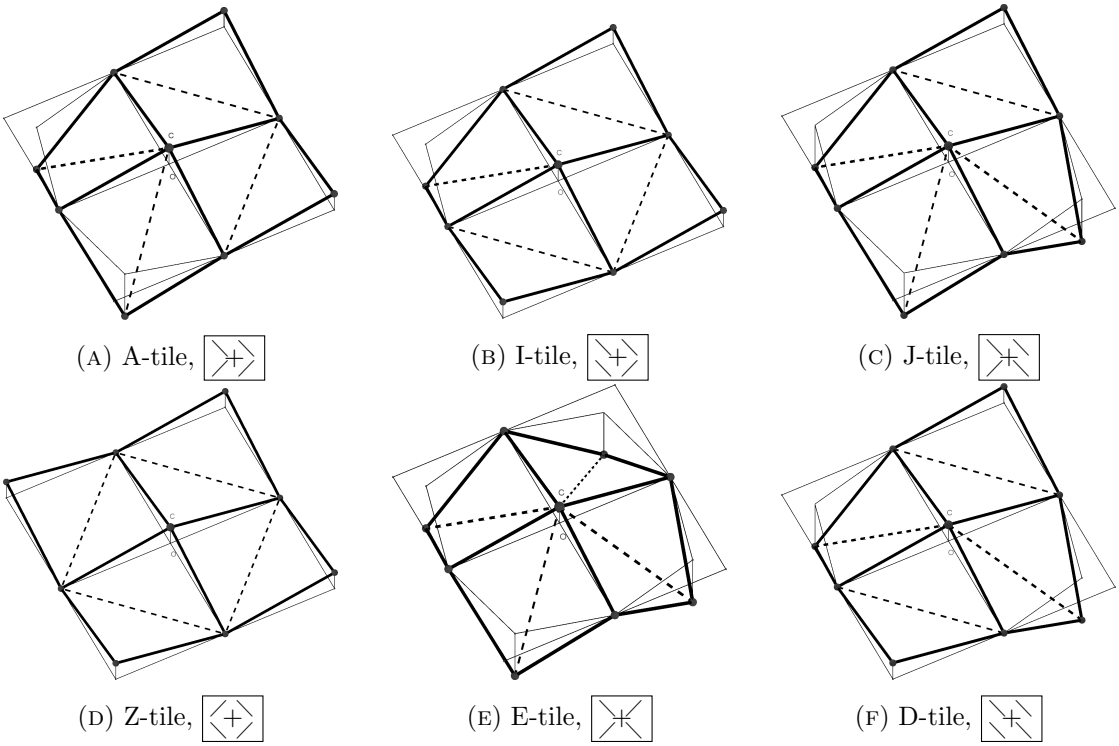

(A) A-tile, (B) I-tile, (C) J-tile,

(D) Z-tile, (E) E-tile, (F) D-tile,

Figure 2.6: Representative 4-tiles of each class.

in Figure 2.5, placed in reference position. We call three points E_{i-1}, M_i, and E_i, and the two bonds in between a *boundary* of the 4-tile, where the indices have again to be understood modulo 4. We define the *boundary orientation* of $E_{i-1}\, M_i\, E_i$ by

$$\mathcal{O}(E_{i-1}\, M_i\, E_i) := \begin{cases} \wedge & \text{if} \quad (E_i + E_{i-1}) \cdot e_3/2 < M_i \cdot e_3, \\ \vee & \text{if} \quad (E_i + E_{i-1}) \cdot e_3/2 > M_i \cdot e_3, \end{cases} \tag{2.20}$$

and the corresponding *boundary angle* by

$$\measuredangle E_i\, M_i\, E_{i-1}. \tag{2.21}$$

Intuitively, the orientation describes the fact that the boundary points upwards (orientation $\wedge$) or downwards (orientation $\vee$), see Figure 2.6 for an illustration. Boundary orientation and boundary angle are crucial for classifying admissible configurations as they provide compatibility conditions for neighboring 4-tiles. To formalize this, we now introduce the notion of *attached 4-tiles*.

Given two 4-tiles T and $\tilde{T}$ with centers C and $\tilde{C}$, we say that the 4-tiles are *attached to each other* if $y^{-1}(C) - y^{-1}(\tilde{C}) \in \{2e_1, -2e_1, 2e_2, -2e_2\}$. Note that T and $\tilde{T}$ share exactly one of the middle points $(M_i)_{i=1}^4$ and $(\tilde{M}_i)_{i=1}^4$ (and the adjacent two corner points). This shared middle point is the center of the so-called *middle 4-tile* which is formed by two optimal cells of T and two optimal cells of $\tilde{T}$.

The following result will be a key tool for the classification of admissible configurations.

Lemma 2.2.6 (Attachment of two 4-tiles)**.** *If two 4-tiles are attached to each other, the boundary angles and the boundary orientation at the shared boundary coincide. If the boundary orientation is* $\wedge$*, the corresponding middle 4-tile satisfies* $\varsigma = -1$ *(see Lemma 2.2.5(i)), otherwise we have* $\varsigma = 1$*.*

Lemma 2.2.6 will be proved in Subsection 2.4.2. The statement delivers necessary conditions for attaching two 4-tiles. In fact, a crucial idea for proving the main theorem, Theorem 2.2.8, is excluding many situations by checking that boundary angles or boundary orientations do not match. In particular, this reasoning will allow us to prove that admissible configurations *exclusively* contain Z-, D-, and I-tiles. To ease the readability, from now on we include the boundary orientation in the notation, at least for the relevant tiles, i.e., the Z-, D-, and I-tiles. This allows for an easy check whether the boundary orientations match or not.

On lateral boundaries, we denote boundaries with orientation $\wedge$ by $<$. Likewise, lateral boundaries with boundary orientation $\vee$ are indicated by $>$. Table 2.2 gives an overview of admissible 4-tiles with the new notation.

Z-tile	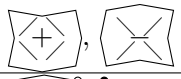
D-tile	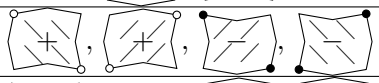
I-tile	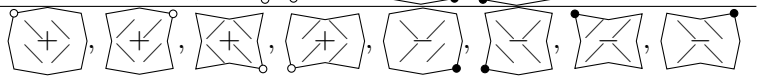

Table 2.2: A table of all admissible Z-, D-, and I-tiles with corresponding boundary orientations.

In the notation, we also denote corner points pointing downwards with $\circ$ and corner points pointing upwards with $\bullet$ (of course, always assuming that the 4-tile is in reference position). As an example, we refer to (B) and (F) in Figure 2.6 for  and  , respectively. Note that this notation is not part of the characterization of types, but is included only to visualize the directions along which the boundary rolls up or down, respectively. (In fact, a $+$ in the center along with $\diagup$ pointing towards $+$ yields $\circ$ in the corresponding corner. In a similar fashion, a $-$ in the center along with $\diagup$ *not* pointing towards $-$ yields $\bullet$.) This notation facilitates to determine the class of the 4-tile as Z-tiles have no $\bullet/\circ$, D-tiles have two, and I-tiles have exactly one.

Lemma 2.2.7 (Boundary orientations)**.** *The boundary orientations of the different boundaries of the Z-, D-, and I-tiles are given as indicated in Table 2.2.*

Lemma 2.2.7 will be proved in Subsection 2.4.2. We close this subsection with an example illustrating Lemma 2.2.6. Let us attach the Z-tile  and the D-tile  . From the notation we can directly see that by attaching via

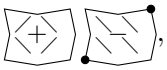 (2.22)

the boundary orientation match at the shared boundary, i.e., the 4-tiles can be attached to each other provided that also the boundary angles coincide. (This indeed holds true, as we will see later in Lemma 2.3.1.) The type of the middle 4-tile can be determined directly by considering the forms of the four optimal cells in the middle, i.e.,  . As the shared boundary has orientation $>$, which corresponds to $\vee$, Lemma 2.2.6 implies that the middle 4-tile satisfies $\varsigma = 1$. The latter implies a $-$-symbol in the middle of the matrix, see the discussion below Lemma 2.2.5. Therefore, the middle 4-tile is the I-tile  . Clearly, the procedure applies to all combinations of 4-tiles.

2.2.5 Main result: Characterization in terms of 4-tiles

After having introduced the necessary notation and concepts in the previous subsections, we are ready to formulate our main result on the characterization of admissible configurations in terms of 4-tiles. To this end, we need a variant of the form function, the so-called *type functions*: consider an admissible deformation y and let $S_1 = 0$, $S_2 = (1,0)$, $S_3 = (0,1)$, and $S_4 = (1,1)$. For $i = 1,\dots,4$, we let σ_i be the function defined on $2\mathbb{Z}^2$ such that $\sigma_i(k,l)$ for $(k,l) \in 2\mathbb{Z}^2$ indicates the type of the 4-cell with center $y(S_i + (k,l))$. The four different functions account for the fact that a translation of $\mathbb{Z}^2$ by $(0,0)$, $(1,0)$, $(0,1)$, or $(1,1)$ leaves the deformed configuration invariant, but groups together different optimal cells to form 4-tiles. With this definition at hand, we now state the main result of this chapter.

Theorem 2.2.8 (Characterization of all admissible configurations)**.** *A deformation y is admissible if and only if, possibly up to rotation of the lattice $\mathbb{Z}^2$ by $\pi/2$, the following holds true:*

Only particular types of Z-, D-, and I-tiles are admissible, namely, for $i = 1,\dots,4$ we have

$$\sigma_i \colon 2\mathbb{Z}^2 \to \left\{ \text{ 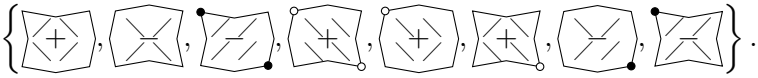 } \right\}. \tag{2.23}$$

Moreover, the type function is constant along d_1, i.e., $\sigma_i(s,t) = \sigma_i(s+2,t+2)$ for all $s,t \in 2\mathbb{Z}$ and the following matching conditions are satisfied:

(M1) *for all $s,t \in 2\mathbb{Z}$ we have*

$$\sigma_i(s,t) \in \left\{ \text{ 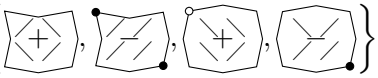 } \right\} \quad \Longleftrightarrow$$
$$\sigma_i(s,t-2) \in \left\{ \text{ 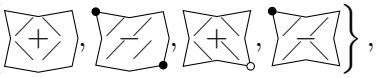 } \right\},$$

(M2) *for all $s,t \in 2\mathbb{Z}$ we have*

$$\sigma_i(s,t) \in \left\{ \text{ 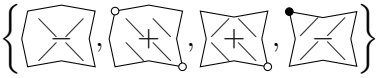 } \right\} \quad \Longleftrightarrow$$
$$\sigma_i(s,t-2) \in \left\{ \text{ 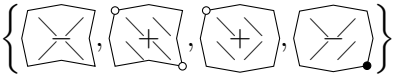 } \right\}.$$

The theorem gives a *complete characterization* of all admissible configurations. First, it shows that only Z-, D-, and I-tiles are admissible. More precisely, we see that only such D-, and I-tiles from Table 2.2 are admissible, which roll-up/down along the same diagonal, and that the type function is constant along the other diagonal. In particular, no change between the direction of rolling-up/down is admissible. This observation allows for a clear geometric interpretation: Z-tiles correspond to flat areas and D-tiles induce rolled-up/down areas. In order to match such 4-tiles, the I-tile arises naturally as a combination of the Z-tile and D-tile. (See, e.g., Figure 2.6 B, which is a D-tile left and a Z-tile right. See also the example in (2.22).) Clearly, rolling-up/down exclusively along the other diagonal is admissible as well, corresponding exactly to the other collection of D-, and I-tiles from Table 2.2. However, after a rotation of the lattice $\mathbb{Z}^2$ by $\pi/2$, one can always reduce to (2.23). Eventually, the matching conditions (M1) and (M2) further restrict the admissible combination of 4-tiles, and account for the fact that the boundary orientations at shared boundaries of two attached 4-tiles need to match, see Lemma 2.2.6. We close this discussion by noting that the characterization cannot be simplified further, i.e., there are indeed admissible configurations y which contain all eight types given in (2.23).

Let us now stress that Theorem 2.2.8 implies Theorem 2.2.2. To see this, we observe that the type functions σ_i, $i = 1, \dots, 4$, are constant along the diagonal d_1. This along with the fact that all types in (2.23) have the same form of optimal cell ($\diagdown$ or $\diagup$) along the diagonal d_1 (i.e., in the lower left and upper right entry) shows that the form function τ introduced in Subsection 2.2.2 satisfies $\tau(s,t) = \tau(s+1,t+1)$ for all $s,t \in \mathbb{Z}$.

The fact that all incidence angles along d_1 vanish and that all incidence angles along d_2 lie in $\{0, \gamma^*, -\gamma^*\}$ (with the property that the value is constant along d_1) follows by an elementary computation. We defer the exact calculation to Section 2.4.4. At this stage, we only mention that inside Z-tiles, all incidence angles along both diagonals are equal to zero. On the other hand, for the D-tile  the incidence angle along d_2 is γ^* and for  it is $-\gamma^*$. I-tiles have incidence angles 0 and $\pm\gamma^*$, where the sign depends on $\bullet$ or $\circ$ in the notation.

2.3 The proof of the main theorem

This section is devoted to the proof of Theorem 2.2.8. This hinges on two facts, namely, that (1) attaching two 4-tiles is only possible if the boundary orientation at shared boundaries match and (2) that such attachment needs to lead to an admissible, i.e., coplanar middle 4-tile. Firstly, we use these ideas to show that actually only Z-, D-, and I-tiles are admissible, see Proposition 2.3.2. In a second step, we further restrict the set of admissible types by showing that D- and I-tiles necessarily need to roll-up/down along the same diagonal, see Proposition 2.3.3. This is achieved by considering four 4-tiles arranged in a square and exploiting the aforementioned compatibility conditions. With similar techniques, we subsequently show that along one diagonal the type has to be constant, see Proposition 2.3.4. Eventually, we provide another auxiliary result

(Proposition 2.3.5) stating that four 4-tiles arranged in a square can be indeed realized by an admissible configuration y if all compatibility conditions, including the matching conditions stated in Theorem 2.2.8, are satisfied. With these results at hand, we are then able to prove Theorem 2.2.8.

2.3.1 Admissible classes of 4-tiles

In this subsection, we show that admissible configurations contain only Z-, D-, and I-tiles and that pairs of such tiles can be attached. This is achieved in two steps. We start by calculating the different boundary angles introduced in (2.21). Then, by discussing the possibility of attaching two 4-tiles along a boundary with the same boundary angle and the same boundary orientation, see (2.20), we are able to show that Z-, D-, and I-tiles are admissible, while E-, A-, and J-tiles are not.

We start by observing that there are exactly three different boundary types. In view of Lemma 2.2.5, we see that the three points forming a boundary (e.g., E_{i-1}, M_i, and E_i, see Figure 2.5) are completely characterized by $\varsigma \in \{-1, 1\}$ and the form, i.e., form $\diagdown$ or form $\diagup$, of the two optimal cells adjacent to the boundary. (Strictly speaking, in Lemma 2.2.5(ii), this was only shown once the forms of all four optimal cells are fixed, but the argument clearly localizes at each boundary.)

This leads to at most $2^3 = 8$ different boundary types, as indicated in Table 2.3. Given a 4-tile in reference position, the boundary type remains invariant under reflection of the 4-tile along the e_1-e_2-plane and the e_2-e_3-plane. This shows that the number of different boundary types reduces to three. We indicate the corresponding boundaries as *Z-, D-, and E-boundaries*, respectively, as the corresponding 4-tiles have exclusively such boundaries, compare also Table 2.3 with Table 2.1. We also mention that I-tiles have both Z- and D-boundaries, but no E-boundaries, and that J- and A-tiles contain E-boundaries.

Z-boundary	D-boundary	E-boundary
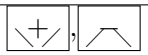	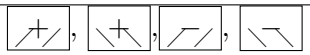	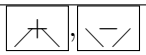

Table 2.3: Classification of the three types of boundaries.

Lemma 2.3.1 (Boundary angles)**.** *The Z-boundary angle and D-boundary angle of coplanar 4-tiles are given by* $\delta_\theta = 2\arccos\left(\sqrt{\cos\theta}\right)$*. The E-boundary angle of coplanar 4-tiles is strictly smaller than* δ_θ*.*

Proof. We start by considering the Z-boundary angle. Without restriction we consider a Z-tile in reference position with notation as indicated in Figure 2.5, satisfying $M_2 = (0, s, h)$ for $s, h > 0$, where s and h are given in Lemma 2.2.5. We observe that the isometry $x = (x_1, x_2, x_3) \mapsto (x_1, x_2, -x_3) + (0, s, h)$ maps M_1 to E_1, C to M_2, and M_3 to E_2. This yields that the Z-boundary angle coincides with δ_θ, see (2.14) and (2.18). The fact that the D-boundary angle coincides with the Z-boundary angle is postponed

to Corollary 2.4.3, and relies on the fact that two 4-tiles with the respective boundaries can be attached to each other, cf. Lemma 2.4.2.

Eventually, we show that the E-boundary angle is strictly smaller. To this end, we let $E_1 = (s, s, 0)$, $M_2 = (0, s, h)$, $E_2 = (-s, s, 0)$ be again the points of the Z-tile considered above. The corresponding points of an E-tile in reference position are denoted by $\tilde{E}_1$, $\tilde{M}_2$, and $\tilde{E}_2$. (They are obtained by changing the form of the optimal cells containing E_1 and E_2, respectively.) By simple geometric considerations we find

$$\tilde{E}_1 = E_1 + (-p, -p, q), \qquad \tilde{M}_2 = M_2, \qquad \tilde{E}_2 = E_2 + (p, -p, q) \tag{2.24}$$

for some $p, q > 0$. One can check that $q = \tilde{E}_1 \cdot e_3 = \tilde{E}_2 \cdot e_3 > 2h$, see Lemma 2.4.1(iv) below. Given that $|\tilde{E}_1 - \tilde{M}_2| = |\tilde{E}_2 - \tilde{M}_2| = 1$, the E-boundary angle is calculated by $\arccos((\tilde{E}_1 - \tilde{M}_2) \cdot (\tilde{E}_2 - \tilde{M}_2))$. We now compute by using (2.24) and $q > 2h$ that

$$\begin{aligned}(\tilde{E}_1 - \tilde{M}_2) \cdot (\tilde{E}_2 - \tilde{M}_2) &= (E_1 - M_2) \cdot (E_2 - M_2) + \begin{pmatrix} -p \\ -p \\ q \end{pmatrix} \cdot \begin{pmatrix} -s \\ 0 \\ -h \end{pmatrix} \\ &\quad + \begin{pmatrix} p \\ -p \\ q \end{pmatrix} \cdot \begin{pmatrix} s \\ 0 \\ -h \end{pmatrix} + \begin{pmatrix} -p \\ -p \\ q \end{pmatrix} \cdot \begin{pmatrix} p \\ -p \\ q \end{pmatrix} \\ &= (E_1 - M_2) \cdot (E_2 - M_2) + 2ps - 2qh + q^2 \\ &> (E_1 - M_2) \cdot (E_2 - M_2).\end{aligned}$$

As $\delta_\theta = \arccos((E_1 - M_2) \cdot (E_2 - M_2))$ and arccos is strictly decreasing on $[-1, 1]$ we find that the E-boundary angle is smaller than δ_θ. This concludes the proof. □

Proposition 2.3.2 (Nonadmissible classes of 4-tiles)**.** *An admissible configuration does not contain E-, A-, and J-tiles.*

Proof. Suppose by contradiction that the configuration contains a 4-tile of class E, A, or J. As each E-, A-, or J-tile contains at least one E-boundary, see Table 2.3 and Table 2.1, by Lemma 2.2.6 and Lemma 2.3.1 we deduce that the configuration contains at least two adjacent 4-tiles in these three classes such that the shared boundary has an E-boundary angle. For the corresponding middle 4-tile between the two 4-tiles we thus get that the corresponding δ_{13} or δ_{24} as defined in (2.18) coincides with the E-boundary angle which is strictly smaller than δ_θ by Lemma 2.3.1. On the other hand, by (2.14) we have $\delta_{13} = \delta_{24} = \delta_\theta$ for the nonplanarity angles of the middle tile, a contradiction. □

2.3.2 Proof of the main result

In this subsection we give the proof of Theorem 2.2.8. The argument rests upon two propositions, showing that only certain arrangements of Z-, D-, and I-tiles are admissible. A third auxiliary result verifies that such arrangements are indeed admissible. We start by stating these results, whose proofs are postponed to the next subsections. Recall the notation of the 4-tiles in Table 2.2.

Proposition 2.3.3 (Roll-up/down along one diagonal)**.** *Consider any four adjacent* 4*-tiles of class Z, D, or I of an admissible configuration arranged in a square. Then all D- and I-tiles locally roll-up/down along the same diagonal, i.e., the type of the four* 4*-tiles is either exclusively contained in* $\mathcal{A}$ *or exclusively contained in* $\mathcal{B}$*, where*

$\mathcal{A} :=$ 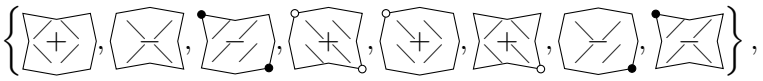 , (2.25)

and

$\mathcal{B} :=$ 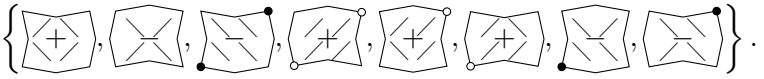 . (2.26)

Note that $\mathcal{B}$ can be obtained from $\mathcal{A}$ through a rotation of the reference lattice by $\pi/2$, and vice versa. The proposition shows that locally only 4-tiles which roll along the same diagonal can be attached to each other. The following result states that locally admissible configurations have the same type along one of the diagonals.

Proposition 2.3.4 (Arrangements along diagonals)**.** *Consider four adjacent* 4*-tiles of an admissible configuration with types either in* $\mathcal{A}$ *or in* $\mathcal{B}$*, see* (2.25)–(2.26)*, arranged in a square and denoted by*

$$\boxed{\mathfrak{A}}\,\boxed{\mathfrak{D}}$$
$$\boxed{\mathfrak{B}}\,\boxed{\mathfrak{C}}.$$

If the types are in $\mathcal{A}$*, we have* $\mathfrak{B} = \mathfrak{D}$*, and if the types are in* $\mathcal{B}$*, we have* $\mathfrak{A} = \mathfrak{C}$*.*

The previous two results yield restrictions for the arrangement of 4-tiles in admissible configurations. The next result shows that such arrangements are indeed admissible.

Proposition 2.3.5 (Admissible arrangements of 4-tiles)**.** (i) *If two coplanar* 4*-tiles in* $\mathcal{A}$ *are attached along a boundary with matching boundary orientation, the resulting middle* 4*-tile is a coplanar* 4*-tile in* $\mathcal{A}$*.*
(ii) *If four adjacent coplanar* 4*-tiles with types in* $\mathcal{A}$ *are arranged as*

$$\boxed{\mathfrak{A}}\,\boxed{\mathfrak{D}}$$
$$\boxed{\mathfrak{B}}\,\boxed{\mathfrak{C}} \tag{2.27}$$

such that $\mathfrak{B} = \mathfrak{D}$ *and such that the four* 4*-tiles satisfy the matching conditions* (M1)–(M2) *stated in Theorem 2.2.8, there exists an admissible deformation* $y\colon \{0,1,2,3,4\}^2 \to \mathbb{R}^3$ *such that the* 4*-tiles of* $y(\{0,1,2,3,4\}^2)$ *have the types indicated in* (2.27)*.*

A similar statement holds for 4-tiles with types in $\mathcal{B}$ by rotation of the reference lattice by $\pi/2$. We are now in a position to prove our main result.

Proof of Theorem 2.2.8. Step 1: $\Rightarrow$. We recall the definition of σ_i, $i = 1,\dots,4$, before the statement of Theorem 2.2.8. Without restriction we only consider σ_1 in the following

proof. By Proposition 2.3.2 we have that the configuration only contains Z-, D-, and I-tiles.

We next show that all types are either in $\mathcal{A}$ or in $\mathcal{B}$, see (2.25)–(2.26), i.e., rolling up/down occurs at most along one diagonal. Assume by contradiction that there were two 4-tiles rolling along different diagonals, i.e., $T_1 \in \mathcal{A} \setminus \mathcal{B}$ and $T_2 \in \mathcal{B} \setminus \mathcal{A}$. Choose $s_i, t_i \in 2\mathbb{Z}$, $i = 1, 2$, such that $\sigma_1(s_1, t_1) = T_1$ and $\sigma_1(s_2, t_2) = T_2$. By Proposition 2.3.3 we can apply Proposition 2.3.4 and thus find $\sigma_1(s_1+r, t_1+r) = T_1$ and $\sigma_1(s_2+r', t_2-r') = T_2$ for all $r, r' \in 2\mathbb{Z}$. For a particular choice of r and r' this entails $T_1 = T_2$ or that T_1 is adjacent to T_2. In both cases, we obtain a contradiction to Proposition 2.3.3.

This shows that all types of 4-tiles are either in $\mathcal{A}$ or $\mathcal{B}$. Up to a rotation of the reference lattice by $\pi/2$, we may suppose that all types of 4-tiles lie in $\mathcal{A}$, which corresponds to the notation of Theorem 2.2.8. By Proposition 2.3.4 we get that the type function is constant along d_1, i.e., $\sigma_i(s, t) = \sigma_i(s + 2, t + 2)$ for all $s, t \in 2\mathbb{Z}$ and all $i = 1, \dots, 4$.

It remains to show that the *matching conditions* (M1) and (M2) hold true as indicated in the statement. These properties rely on the fact that the boundary orientations of each two attaching 4-tiles need to match, cf. Lemma 2.2.6.

We only prove matching condition (M1) as the proof for (M2) follows along similar lines. Since the type function is constant along d_1, i.e., $\sigma_1(s, t) = \sigma_1(s + 2, t + 2)$ $(s, t \in 2\mathbb{Z})$, for any $s, t \in 2\mathbb{Z}$ such that $\sigma_1(s, t) \in$  , we have one of the two possibilities

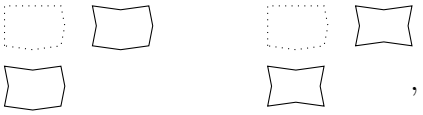

where the boundaries of the 4-tiles with type $\sigma_1(s, t) = \sigma_1(s + 2, t + 2)$ are depicted with solid lines. The given boundary orientations and Lemma 2.2.6 imply that only a 4-tile from (compare Table 2.2)  can be attached in the blank position top left indicated by the dotted 4-tile (where its straight boundaries represent arbitrary boundary orientations). Within the class of admissible 4-tiles $\mathcal{A}$ in (2.25), exactly the four choices  match this boundary orientation. Conversely, for $s, t \in 2\mathbb{Z}$ such that $\sigma_1(s, t) \in$ 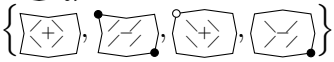 an arrangement as above yields one of the two possibilities

However, due to the given boundary orientations, the 4-tiles in 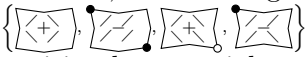 are the only 4-tiles from $\mathcal{A}$ which can be attached in the blank position bottom-right, again indicated with the dotted 4-tile. This concludes the check of the matching conditions (M1).

Step 2: $\Leftarrow$. The existence of an admissible configuration $y\colon \mathbb{Z}^2 \to \mathbb{R}^3$ follows directly from Proposition 2.3.5 (ii) and an induction argument. Indeed, (2.12) and (2.13) are

satisfied since each cell is optimal. To see (2.14), it suffices to check that all 4-tiles are coplanar. In fact, then (2.14) follows from Lemma 2.2.4. First, by construction in Proposition 2.3.5(ii) we get that all 4-tiles related to the type function σ_1 are coplanar. By using Proposition 2.3.5(i) we find that also the 4-tiles related to the other type functions σ_i, $i = 2, 3, 4$, are in $\mathcal{A}$ and are coplanar. This shows that all 4-tiles are coplanar, as desired. □

2.3.3 Rolling along one diagonal

This subsection is devoted to the proof of Proposition 2.3.3. The proof fundamentally relies on Lemma 2.2.6, i.e., the fact that the boundary orientations of attached 4-tiles match. To this end, we will make extensive use of the matrix diagrams introduced in Table 2.2 in order to exclude certain arrangements of 4-tiles. Unfortunately, not all nonadmissible cases can be ruled out by such compatibility analysis and we also need to consider some more refined tools, based on the real three-dimensional geometry of the 4-tiles. For this reason, we will use the following lemma concerning the attachment of four coplanar 4-tiles. Recall the types of 4-tiles $\mathcal{A}$ and $\mathcal{B}$ introduced in (2.25)–(2.26), as well as the different types of boundaries in Table 2.3.

Lemma 2.3.6 (Arrangements of four 4-tiles)**.** *Consider four adjacent 4-tiles of an admissible configuration with types either in $\mathcal{A}$ or in $\mathcal{B}$, see (2.25)–(2.26), arranged in a square and denoted by*

$$\begin{array}{|c|c|}\hline \mathfrak{A} & \mathfrak{D} \\ \hline \mathfrak{B} & \mathfrak{C} \\ \hline \end{array}\,. \tag{2.28}$$

Then: (i) *If three tiles are Z-tiles and one tile is an D-tile, then the D-tile is in $\{\mathfrak{A}, \mathfrak{C}\}$ (case $\mathcal{A}$) or in $\{\mathfrak{B}, \mathfrak{D}\}$ (case $\mathcal{B}$).*
(ii) *If two tiles are Z-tiles and two tiles are D-tiles, then the Z-tiles are arranged along one diagonal and the D-tiles along the other diagonal.*
(iii) *If three tiles are D-tiles and one tile is a Z-tile, then the Z-tile is in $\{\mathfrak{A}, \mathfrak{C}\}$ (case $\mathcal{A}$) or in $\{\mathfrak{B}, \mathfrak{D}\}$ (case $\mathcal{B}$).*
(iv) *The arrangement*

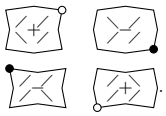

(2.29)

is not admissible.

We postpone the proof of this lemma to Section 2.4.3 and proceed with the proof of Proposition 2.3.3.

Proof of Proposition 2.3.3. We proceed in two steps: in Step 1 we show that two attached 4-tiles cannot roll-up/down along different diagonals. In Step 2 we show that in four adjacent 4-tiles arranged in a square, the two pairs of diagonal 4-tiles cannot roll-up/down along different diagonals. These two steps imply the statement.

Step 1: Attached 4-tiles. Up to interchanging the roles of • and ∘, and up to reflection along the e_1- or the e_2-axis, there are six different cases to address:

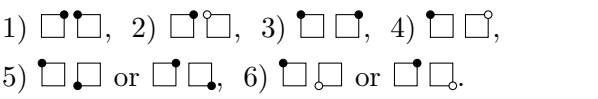

Here, the symbol is a placeholder both for the corresponding I-tile  and the D-tile  . The meaning of the other symbols is analogous. For the proof, we refer the reader to Table 2.2 which collects all possible 4-tiles.

Case 1: . This case leads to a contradiction to Proposition 2.3.2 as necessarily the middle 4-tile is the A-tile . As an example, among the four possibilities, we consider the case where both 4-tiles are I-tiles. In this case, we have  .

Case 2: . This case ensues if two 4-tiles with different boundary orientations are attached, which contradicts Lemma 2.2.6. As an example, among the four possibilities, we consider the case where both 4-tiles are D-tiles. In this case, we have 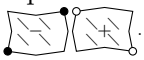 .

Case 3: . First, if both 4-tiles are D-tiles, then up to a reflection along the e_2-axis, we are in Case 1 and obtain a contradiction as explained before. In the case that one is a D-tile and the other is an I-tile, we obtain a contradiction to Lemma 2.2.6 as then the boundary orientations do not match. In fact, these two last cases are 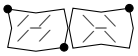 and 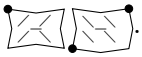 .

We can therefore assume that both 4-tiles are I-tiles, i.e., take the form 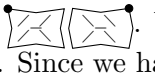 . We will now consider which 4-tiles are admissible on top of the given 4-tiles. Since we have already ruled out Case 1 and the boundary orientations need to match by Lemma 2.2.6, we see that on top of the left I-tile we can only have  , and on top of the right I-tile we can only have 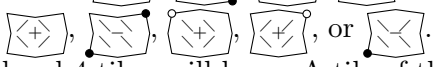 . In any case, the 4-tile in the middle of the four considered 4-tiles, will be an A-tile of the form 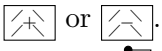 or . This contradicts Proposition 2.3.2 and concludes the proof of Case 3.

Case 4: . If both 4-tiles are D-tiles, then up to a reflection along the e_2-axis, we are in Case 2 and obtain a contradiction as explained before. If both 4-tiles are I-tiles, we have 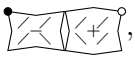 , i.e., the boundary orientations are different and we obtain a contradiction to Lemma 2.2.6. The two remaining possibilities are 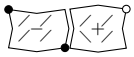 and 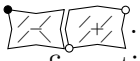 . We prove the contradiction only for the first configuration as the second configuration can be treated along similar lines. In order to do so, we proceed as in Case 3 and attach 4-tiles at the top, yielding

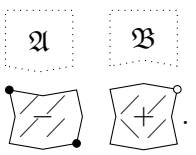

(2.30)

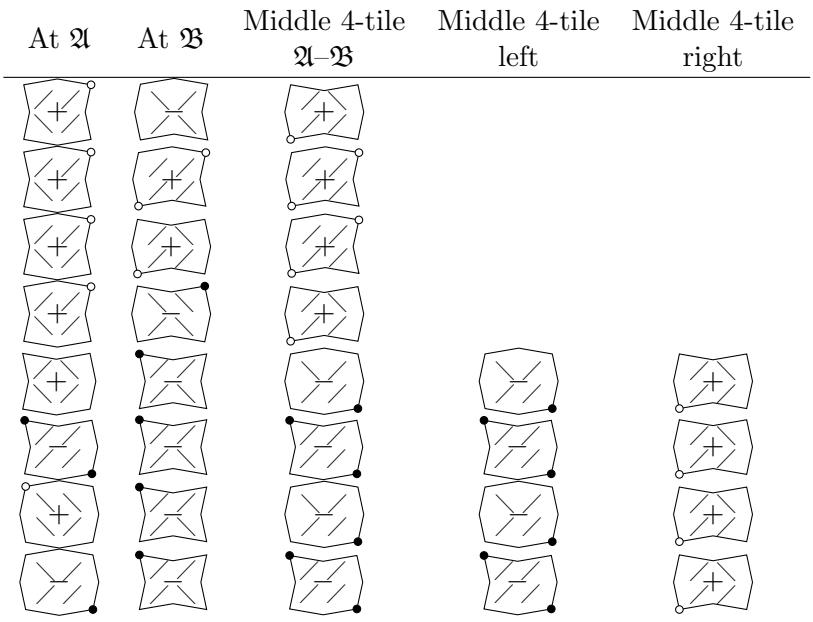

Table 2.4: The eight different cases considered in Case 4.

In (2.30), the straight dotted lines encompass all possible boundary orientations. We start by noting that the I-tile in the middle of 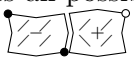 is of the form  .

Since we have already ruled out Case 1 and the boundary orientations need to match by Lemma 2.2.6, only the 4-tiles 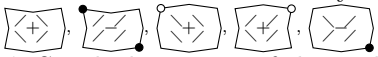 can be attached on top of the D-tile (left), i.e., at position 𝔄. Similarly, on top of the I-tile (right) at position 𝔅 we can only attach the 4-tiles  , see Table 2.2. As the boundary orientations between 𝔄 and 𝔅 have to match as well, there are only eight possibilities of the upper two 4-tiles which are indicated in the first two columns of Table 2.4. The two upper 4-tiles 𝔄 and 𝔅 form middle 4-tiles which are indicated in the third column of Table 2.4. Note that the 4-tile attached on the bottom of this 4-tile is exactly the middle 4-tile between the original two 4-tiles, i.e.,  . Therefore, in the first four cases we obtain a contradiction to Lemma 2.2.6 since the boundary orientations of the shared boundary of the two middle 4-tiles do not match.

For the second four cases we need a different argument instead. To this end, we consider also the middle 4-tile between the D-tile and 𝔄 (left middle 4-tile) and the middle 4-tile between the I-tile and 𝔅 (right middle 4-tile), see the last two columns in Table 2.4. We observe that in none of the cases the boundary orientations of the shared boundary of the left and right middle 4-tiles match. This is again a contradiction to Lemma 2.2.6, concluding the check of Case 4.

Case 5:  or : Without restriction we address only the first case as the second can be treated analogously (and, in fact, obtained by a rotation). We have to distinguish two cases. Firstly, the 4-tile on the left is a D-tile, i.e.,  . Then up to a reflection

along the e_2-axis, we are in Case 1 and obtain a contradiction as explained before. Secondly, if the left 4-tile is not a D-tile, it has to be an I-tile. We obtain the two possible configurations 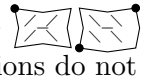 and 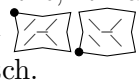 which both contradict Lemma 2.2.6 as the boundary orientations do not match.

Case 6:  or  . Without restriction we address only the first case as the second can be treated analogously. If the 4-tile on the left is a D-tile, then we have the two possibilities 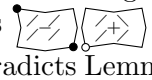 and 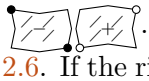 . Thus, the boundary orientations do not match which contradicts Lemma 2.2.6. If the right 4-tile is a D-tile, we are in Case 4 and obtain a contradiction as explained before.

Therefore, both 4-tiles have to be I-tiles, i.e., we have

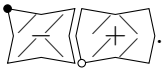 (2.31)

As in Case 4, we consider two 4-tiles attached on the top. By using arguments similar to the ones above, we will show that the only possible choice how to assemble the four 4-tiles would be given by

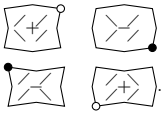 (2.32)

This, however, is excluded by Lemma 2.3.6(iv). To see (2.32), in view of the fact that we have already ruled out Cases 1–5 and the boundary orientations need to match by Lemma 2.2.6, only the 4-tiles

 (2.33)

can be attached on top of the left I-tile in (2.31). Analogously, on top of the right I-tile in (2.31) we can only attach the 4-tiles

 (2.34)

see Table 2.2. As in Case 4 we consider the middle 4-tile between the left I-tile in (2.31) and the 4-tile on top of it (left middle 4-tile) and the middle 4-tile between the right I-tile in (2.31) and the 4-tile on top of it (right middle 4-tile). In view of (2.33)–(2.34), there are only the cases indicated in Table 2.5. From Table 2.5 we see that the boundary orientations of the shared boundary of the two middle 4-tiles can only match if the right middle 4-tile is of type  . By (2.34) this shows that only  can be attached on top of the right I-tile  . Then, in view of (2.33), only  can be attached on top of the left I-tile  as the other four 4-tiles in (2.33) do not math the boundary orientation of  . This shows that (2.32) holds, and concludes the proof of Case 6.

Step 2: 4-tiles on the diagonal. We now show that in four adjacent 4-tiles arranged in a square, the two pairs of diagonal 4-tiles cannot roll-up/down along different diagonals.

Middle 4-tile left	Middle 4-tile right
	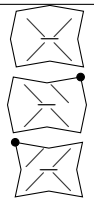

Table 2.5: The different possible middle 4-tiles in Case 6.

Up to interchanging the roles of $\bullet$ and $\circ$, and up to reflection along the e_1- or the e_2-axis, there are two cases to consider, where Case 1 represents one of the eight situations

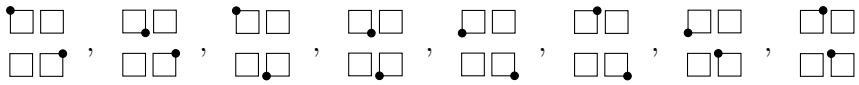

and Case 2 represents one of the eight situations

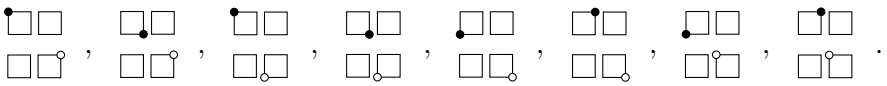

Here, as in Step 1, the symbols $\bullet$ and $\circ$ indicate both the corresponding I-tile and D-tile. Without restriction we address only the first configuration in both cases as all other situations can be treated along similar lines.

Case 1. We start by introducing the labeling

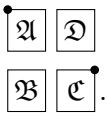

We preliminarily note that, in view of Step 1, for $\mathfrak{B}$ and $\mathfrak{D}$ only 4-tiles in $\mathcal{A} \cap \mathcal{B}$ are admissible, see (2.25)–(2.26), i.e., the two Z-tiles  and  . We distinguish three different subcases:

Case 1.1. If $\mathfrak{A}$ is the unique I-tile, then Lemma 2.2.6 for the boundary between $\mathfrak{A}$ and $\mathfrak{D}$ as well as the boundary between $\mathfrak{D}$ and $\mathfrak{C}$ implies that the 4-tile $\mathfrak{D}$ cannot be a Z-tile. In fact, the boundary orientation of $\mathfrak{A}$ on the right is $\wedge$ (indicated by $<$ in the notation) and the boundary orientation of $\mathfrak{C}$ on top is $\vee$.

Case 1.2. By a similar reasoning, if $\mathfrak{A}$ is the unique D-tile and $\mathfrak{C}$ is the unique I-tile, Lemma 2.2.6 implies that the 4-tile $\mathfrak{B}$ cannot be a Z-tile.

Case 1.3. If both $\mathfrak{A}$ and $\mathfrak{C}$ are D-tiles, we again use Lemma 2.2.6 and see that the 4-tiles $\mathfrak{B}$ and $\mathfrak{D}$ can only be of type  . Therefore, we need to consider the configuration

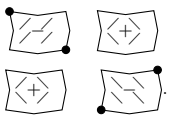

The middle 4-tile between $\mathfrak{A}$ and $\mathfrak{B}$ is given by  and the middle 4-tile between $\mathfrak{C}$ and $\mathfrak{D}$ is given by  . Their shared boundary have mismatching boundary orientations, contradicting Lemma 2.2.6.

Case 2. We start by introducing the labeling

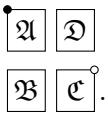

As in Case 1, due to Step 1, for $\mathfrak{B}$ and $\mathfrak{D}$ only the two Z-tiles  and  are admissible. We distinguish four different subcases:

Case 2.1. If both $\mathfrak{A}$ and $\mathfrak{C}$ are I-tiles, Lemma 2.2.6 implies that the 4-tile $\mathfrak{B}$ cannot be a Z-tile.

Case 2.2. If both $\mathfrak{A}$ and $\mathfrak{C}$ are D-tiles, then Lemma 2.2.6 implies that the 4-tile $\mathfrak{B}$ cannot be a Z-tile.

Case 2.3. If $\mathfrak{A}$ is the unique D-tile and $\mathfrak{C}$ is the unique I-tile, then Lemma 2.2.6 implies that the 4-tile $\mathfrak{D}$ cannot be a Z-tile.

Case 2.4. Now suppose that $\mathfrak{A}$ is the unique I-tile and $\mathfrak{C}$ is the unique D-tile. Then $\mathfrak{B}$ and $\mathfrak{D}$ need to be of type  . Therefore, we need to consider the configuration

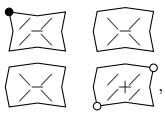 (2.35)

and show that it is also not admissible. The I-tile rolls up in direction top left, which has no influence in this (sub-)configuration. In other words, by replacing in (2.35) the tile $\mathfrak{A}$ with the Z-tile  and showing that this modified configuration is not admissible, we also find that (2.35) is not admissible. In fact, in view of Lemma 2.3.6(i) and the fact that the D-tile  lies in $\mathcal{B}$ (see (2.26)), we see that the modified version of (2.35) is not admissible. This concludes this step of the proof. □

2.3.4 Constant type along the diagonal

This subsection is devoted to the proof of Proposition 2.3.4.

Proof of Proposition 2.3.4. We assume without restriction that all four 4-tiles lie in $\mathcal{A}$, see (2.25), as the other case is completely analogous. We consider

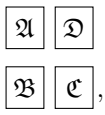

and note that we need to show that $\mathfrak{B}$ and $\mathfrak{D}$ are of the same type. We proceed in two steps: first, we show that $\mathfrak{B}$ and $\mathfrak{D}$ are of the same *class,* i.e., both have to be either Z-, I-, or D-tiles. In the second step, we then conclude that they even have to be of

the same *type*. In the proof, we will use the following observation which directly follows from the definition of $\mathcal{A}$:

- Z- and D-tiles: All four boundary orientations are identical,
- I-tiles: Left and upper boundary orientations are identical, right and lower boundary orientations are identical. (2.36)

Step 1. In this step, we show that $\mathfrak{B}$ and $\mathfrak{D}$ are necessarily of the same class.
Case 1.1. If exactly one of the two tiles $\mathfrak{B}$ and $\mathfrak{D}$ is an I-tile, in view of (2.36), we obtain a contradiction to Lemma 2.2.6 as not all boundary orientations of the four shared boundaries can match.

Thus, we can now assume that none of the tiles $\mathfrak{B}, \mathfrak{D}$ is an I-tile. Actually, it is also not restrictive to assume that the tiles $\mathfrak{A}$ and $\mathfrak{C}$ are not of class I. Indeed, the upper left optimal cell of $\mathfrak{A}$ and the lower right optimal $\mathfrak{C}$ have no influence on the subsequent arguments in Cases 1.2–1.4 and can readily be replaced by the other type. This allows to replace tiles of class I by types of class Z or D in $\mathcal{A}$, without affecting the following arguments. Summarizing, it suffices to consider the case that all four 4-tiles are Z- or D-tiles.
Case 1.2. If three 4-tiles are D-tiles and one tile is a Z-tile, we only have that $\mathfrak{B}$ and $\mathfrak{D}$ are not of the same class if the Z-tile lies in $\{\mathfrak{B}, \mathfrak{D}\}$. This contradicts Lemma 2.3.6(iii).
Case 1.3. If three 4-tiles are Z-tiles and one tile is a D-tile, we only have that $\mathfrak{B}$ and $\mathfrak{D}$ are not of the same class if the D-tile lies in $\{\mathfrak{B}, \mathfrak{D}\}$. This contradicts Lemma 2.3.6(i).
Case 1.4. If two 4-tiles are of class Z and two of class D, the claim follows directly from Lemma 2.3.6(ii).
Step 2. In this second step we show that not only the class but also the type has to be constant along the diagonal. First, if we had different Z-tiles or D-tiles along the diagonal, in view of (2.25), these two 4-tiles would have different boundary orientations. Again by using (2.36), we obtain a contradiction to Lemma 2.2.6 as not all boundary orientations of the four shared boundaries can match.

We now address the case that $\mathfrak{B}$ and $\mathfrak{D}$ are I-tiles. Again in view of (2.36) and the definition of $\mathcal{A}$, we find

either a) $\mathfrak{B}, \mathfrak{D} \in$  or b) $\mathfrak{B}, \mathfrak{D} \in$ 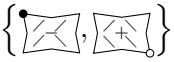

since otherwise the boundary orientations do not match, contradicting Lemma 2.2.6. Whenever the type is not constant along the diagonal, the 4-tile in the middle of the four 4-tiles is an A-tile which contradicts Proposition 2.3.2. For simplicity, we show this only in case a) as case b) follows along similar lines. In fact, by Lemma 2.2.6 we find that $\mathfrak{A}$ can only be of type  ,  ,  , or  , and $\mathfrak{C}$ can only be of type  ,  ,  , or  . Consequently, if $\mathfrak{B}$ is of type  , in the middle we find the A-tile  or  , and if $\mathfrak{B}$ is of type  , we find the A-tile  or  , see Table 2.1. □

2.3.5 Admissible arrangement of 4-tiles

This subsection is devoted to the proof of Proposition 2.3.5.

Proof of Proposition 2.3.5. Without restriction we perform the proof only for the types $\mathcal{A}$ defined in (2.25).
(i) We start by observing that each pair of 4-tiles in $\mathcal{A}$ with matching boundary orientations can be attached since all boundary angles are either Z- or D-boundary angles, see Table 2.3 and Table 2.1, and both angles coincide with δ_θ, see Lemma 2.3.1. We first show that the 4-tile in the middle is again in $\mathcal{A}$. In a second step, we check that the middle 4-tile is also coplanar.

We recall that the type of the middle 4-tile can by determined by considering the matrix notation, as exemplified in (2.22). In view of (2.25), we obtain the following six cases:
Case 1. Attaching two Z-tiles, we find that the two tiles are of same type and the middle tile is the Z-tile of the other type.
Case 2. Attaching two D-tiles, we find that the two tiles are of same type and the middle tile is again of this type.
Case 3. Attaching two I-tiles, we can obtain all possible 4-tiles in $\mathcal{A}$.
Case 4. Attaching a Z- and a D-tile, we obtain an I-tile in $\mathcal{A}$.
Case 5. Attaching a Z- and an I-tile, we obtain any Z- and I-tile in $\mathcal{A}$.
Case 6. Attaching a D- and an I-tile, we obtain any D- and I-tile in $\mathcal{A}$.

Note that in all cases above exactly 4-tiles from $\mathcal{A}$ can occur, and no more than those.

It remains to show that the resulting middle 4-tile is also coplanar. As attaching two 4-tiles does not change the optimal angle θ, also the middle 4-tile consists of four optimal cells with angle θ. Therefore, relation (2.19) holds for the middle 4-tile as well. To conclude the proof, it suffices to show that one of the nonplanarity angles δ_{13} and δ_{24} of the middle 4-tile is equal to δ_θ. To this end, note that one of these angles coincides with the boundary angle of the shared boundary of the two 4-tiles. By Lemma 2.3.1 this angle is equal to δ_θ.
(ii) We proceed constructively to show that every configuration consisting of four 4-tiles from $\mathcal{A}$ arranged in a square satisfying the matching conditions (M1)–(M2) is admissible, i.e., can be realized by an admissible deformation y. By assumption, $\mathfrak{B}$ and $\mathfrak{D}$ are of the same type. Then, one can check that, for any choice of $\mathfrak{A}, \mathfrak{C} \in \mathcal{A}$ satisfying the matching conditions (M1)–(M2), the boundary orientations of $\mathfrak{A}, \mathfrak{C}$ match with those of $\mathfrak{B}$ and $\mathfrak{D}$. In view of Lemma 2.4.1(i), fixing $\mathfrak{B}$ in reference configuration and translating $\mathfrak{D}$ from its reference position by the vector $(2s, 2s, 0)$, we see that these two 4-tiles share exactly one corner point, and we have $|P - \tilde{P}| = |Q - \tilde{Q}| = \sqrt{(2s)^2 + (2s)^2} = 4v$, where $P, Q \in \mathfrak{B}$ and $\tilde{P}, \tilde{Q} \in \mathfrak{D}$ are the corner vertices indicated in Figure 2.7. By Lemma 2.4.1(i) the opposite corner points along the diagonal d_1 have distance $4v$, i.e., $|E_1^{\mathfrak{A}} - E_3^{\mathfrak{A}}| = |E_1^{\mathfrak{C}} - E_3^{\mathfrak{C}}| = 4v$. Therefore, we can translate $\mathfrak{A}$ and $\mathfrak{C}$ from their reference positions such that their opposite corner points coincide with P and $\tilde{P}$ and Q and $\tilde{Q}$, respectively. Since, for every 4-tile the distance between its center and a corner point equals $\sqrt{s^2 + s^2} = 2v$, see (2.16) and Lemma 2.2.5(i), after rotating $\mathfrak{A}$ and $\mathfrak{C}$ about

$(0, 2s, 0) + \mathbb{R}(1, 1, 0)$ and $(2s, 0, 0) + \mathbb{R}(1, 1, 0)$, respectively, as indicated in Figure 2.7, the corner points of $\mathfrak{A}$, $\mathfrak{B}$, $\mathfrak{C}$, and $\mathfrak{D}$ in the interior of the configuration coincide. As the boundary orientations match by (M1)–(M2) and the boundary angles coincide by Lemma 2.3.1, also the respective middle points coincide after rotation of $\mathfrak{A}$ and $\mathfrak{C}$. This along with part (i) of the statement shows that the configuration is indeed realizable by an admissible configuration $y\colon \{0,1,2,3,4\}^2 \to \mathbb{R}^3$. This concludes the proof. □

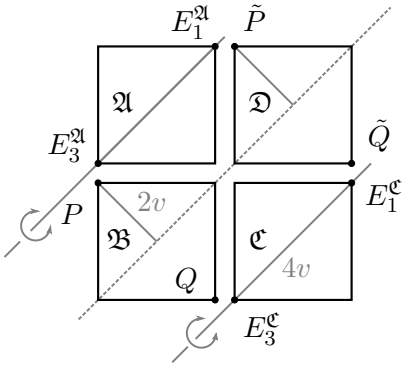

Figure 2.7: The points and rotations indicated in the proof of Proposition 2.3.5.

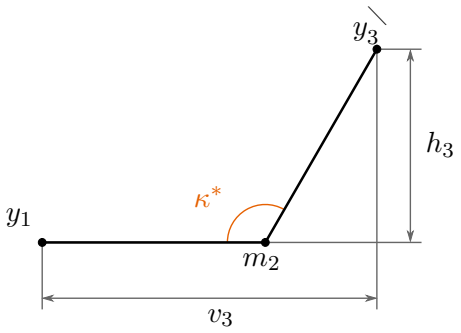

Figure 2.8: Cross section along the plane spanned by a and n, as defined in the proof of Lemma 2.2.3. From this perspective the points y_2, m_2, and y_4 coincide.

2.4 Remaining proofs

2.4.1 Geometry of optimal cells and 4-tiles

This subsection is devoted to the proofs of the lemmas stated in Subsection 2.2.3.

Proof of Lemma 2.2.3. Recall that $m_2 := (y_2 + y_4)/2$ is the middle point between y_2 and y_4, cf. Figure 2.2. We define $a = m_2 - y_1$, with $|a| = d$. Let n be a normal vector to the plane spanned by y_1, y_2, and y_4, in direction $(y_2 - y_1) \times (y_4 - y_1)$.

Observe that by assumption the fourth point y_3 has to satisfy $|y_2 - y_3| = |y_4 - y_3| = 1$ and thus has to lie on the plane spanned by a and n. Therefore, we can make the ansatz

$$y_3 = y_1 + v_3\, a \pm h_3\, n,$$

where v_3 and h_3 are to be determined, see Figure 2.8. Note that in $\pm$ we choose $+$ for form $\diagdown$ and $-$ for form $\diagup$. To conclude, we are left to prove that v_3 and h_3 can be determined uniquely. Since the cell is optimal, we have $\measuredangle y_3\, m_2\, y_1 = \kappa^*$ (see (2.17)) as well as $|a| = |m_2 - y_1| = |m_2 - y_3| = d$. Consequently, the triangle with vertices y_1, m_2, and y_3 and thus also the values of v_3 and h_3 are uniquely determined. □

For convenience, we proceed with the proof of Lemma 2.2.5 and show Lemma 2.2.4 afterwards.

Proof of Lemma 2.2.5. In the proof, we again use the notation indicated in Figure 2.5. We recall the definition in (2.18) and drop for the moment the condition $\delta_{13} = \delta_{24}$ induced by (2.14). To verify that every 4-tile can be placed in reference position, we first rotate and translate the 4-tile such that $C = 0$ and $M_1 = (s_1, 0, h_1)$, and $M_3 = (-s_1, 0, h_1)$, where a simple trigonometric relation yields

$$s_1 = \cos\left(\frac{\pi - \delta_{13}}{2}\right) = \sin(\delta_{13}/2), \quad h_1 = \sin\left(\frac{\pi - \delta_{13}}{2}\right) = \cos(\delta_{13}/2). \tag{2.37}$$

Here, we note that $s_1 > 0$, while h_1 is negative whenever $\delta_{13} > \pi$. We now show that the coordinates of M_2 and M_4 are given by

$$M_2 = (0, s_2, h_2), \qquad M_4 = (0, -s_2, h_2), \tag{2.38}$$

where $s_2 = \sin(\delta_{24}/2)$ and $h_2 = \cos(\delta_{24}/2)$. We focus on M_2 since the argument for M_4 is analogous. For convenience, we write $M_2 = (p_1, p_2, p_3)$ and use the definition of optimal cells, i.e., $\measuredangle M_1\, C\, M_2 = \theta = \measuredangle M_2\, C\, M_3$ and $|M_1| = |M_2| = |M_3| = 1$, to find

$$\cos\theta = M_1 \cdot M_2 = p_1 s_1 + p_3 h_1, \qquad \cos\theta = M_3 \cdot M_2 = -p_1 s_1 + p_3 h_1.$$

By combining the two equalities we get $p_1 = 0$. In view of (2.37), p_3 is then given by

$$p_3 = \frac{\cos\theta}{h_1} = \frac{\cos\theta}{\cos(\delta_{13}/2)}, \tag{2.39}$$

and, since $|M_2| = 1$, we find $p_2 = \sqrt{1 - p_3^2}$. Thus, we have $M_2 = (0, p_2, p_3)$. By a similar argument we find $M_4 = (0, -p_2, p_3)$. To conclude for (2.38), we need to find the relation between p_2 and p_3. To this end, we use the fact that $\measuredangle M_2\, C\, M_4 = \delta_{24}$ to calculate $\cos(\delta_{24}) = M_2 \cdot M_4 = p_3^2 - p_2^2$. This, together with $p_2^2 + p_3^2 = 1$, verifies that $p_3 = \sqrt{(1 + \cos(\delta_{24}))/2} = \cos(\delta_{24}/2)$ by using the double-angle formula. Correspondingly, we find $p_2 = \sin(\delta_{24}/2)$. This proves (2.38). Let us remark for later purposes that (2.39) implies

$$\cos(\delta_{13}/2)\cos(\delta_{24}/2) = \cos\theta. \tag{2.40}$$

From the condition $\delta_{13} = \delta_{24}$ we get that $s = s_1 = s_2$ and $h = |h_1| = |h_2| = \sqrt{1 - s^2}$. We also let $\varsigma = \operatorname{sgn}(h_1) = \operatorname{sgn}(h_2)$. To conclude the proof of (i), it remains to check that $s = \sqrt{2}v$, where v is defined in (2.16), i.e., is chosen in such a way that $2v$ indicates the length of a diagonal in an optimal cell. This length can indeed be expressed as $|M_i - M_{i+1}| = \sqrt{2}s$ for $i = 1, \dots, 4$, which yields the desired relation.

We proceed with the proof of (ii). By fixing θ, the angle δ_θ is also determined and, by (i), also fixing $\operatorname{sgn}(h_1)$ determines completely the positions of the points $(M_i)_{i=1}^4$. In view of Lemma 2.2.3, the positions of $(E_i)_{i=1}^4$ are determined as well, as soon as the forms of the four optimal cells are given. □

Proof of Lemma 2.2.4. In the proof of Lemma 2.2.5 we have already verified (2.19), see (2.40). Consider $f_\theta\colon [0,\pi] \to \mathbb{R}$ defined by

$$f_\theta(\delta) = 2\arccos(\cos\theta/\cos(\delta/2)).$$

As $\cos\theta > 0$, f_θ is decreasing and thus has at most one fixed point. Hence, f_θ has exactly one fixed point given by $\delta_\theta = 2\arccos(\sqrt{\cos\theta})$. This eventually shows that δ_{13} and δ_{24} coincide if and only if $\delta_{13} = \delta_{24} = \delta_\theta$. □

We close this subsection with an elementary observation. We again refer to the notation in Figure 2.5.

Lemma 2.4.1. (i) *For any coplanar 4-tile in $\mathcal{A}$ (cf. (2.25)) in reference position, see Lemma 2.2.5* (i)*, we have $E_1 = (s,s,0)$ and $E_3 = (-s,-s,0)$.*
(ii) *For any Z-tile in $\mathcal{A}$ in reference position, we have $E_2 = (-s,s,0)$ and $E_4 = (s,-s,0)$.*
(iii) *For any D-tile in $\mathcal{A}$ in reference position, we have $|E_2 - E_4| < 4v$, where v is given in (2.16).*
(iv) *Assume that an optimal cell $\{y_1,\dots,y_4\}$ is positioned in such a way that $e_3\cdot y_1 = 0$ and $e_3\cdot y_2 = e_3\cdot y_4 = h$. Then, depending on its form, we have $e_3\cdot y_3 = 0$ or $e_3\cdot y_3 > 2h$.*

Similar statements as (ii)–(iv) hold for $\mathcal{B}$ in place of $\mathcal{A}$ by changing the roles of the diagonals.

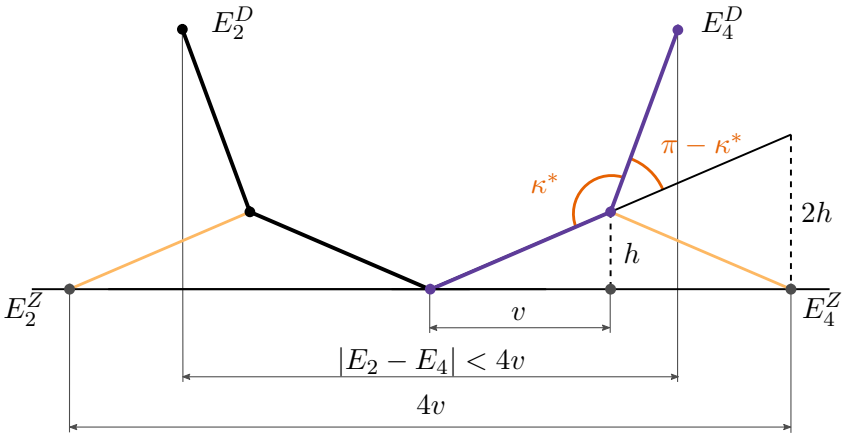

Figure 2.9: Cross section of a D-tile (bold, black and purple) and of a Z-tile (thin lines in light orange), positioned as in Lemma 2.4.1. The distance between the diagonals is $4v$ for the Z-tile and smaller for the D-tile.

Proof. Without restriction, we consider a 4-tile in $\mathcal{A}$ in reference position such that $\varsigma = 1$, cf. Lemma 2.2.5, as the other case only amounts to reflection along the e_1-e_2-plane. By Lemma 2.2.5(i) we have that $M_1 = (s,0,h)$, $M_2 = (0,s,h)$, $M_3 = (-s,0,h)$, and $M_4 = (0,-s,h)$. The optimal cells $\{C,M_1,E_1,M_2\}$ and $\{C,M_3,E_3,M_4\}$ are of

form $\diagup$, see Figure 2.2 and (2.25). Thus, by Lemma 2.2.3 we get $E_1 = (s, s, 0)$ and $E_3 = (-s, -s, 0)$. This shows (i). We now suppose that the 4-tile is either of class Z or of class D, i.e., is of type  or  . Therefore, the two optimal cells $\{C, M_2, E_2, M_3\}$ and $\{C, M_4, E_4, M_1\}$ are of form $\diagup$ (D-tile) and of form $\diagdown$ (Z-tile), which yields to a cross section along the direction $(-1, 1)$ as indicated in Figure 2.9. We now obtain

$$\begin{aligned} E_2^D \cdot e_3 = E_4^D \cdot e_3 > 2h \qquad & \text{for the D-tile and} \\ E_2^Z \cdot e_3 = E_4^Z \cdot e_3 = 0 \qquad & \text{for the Z-tile.} \end{aligned} \tag{2.41}$$

Indeed, for the Z-tile this follows from Lemma 2.2.3. For the D-tile we use Thales' intercept theorem instead, with reference to Figure 2.9. In particular, this implies (ii). Then, as in the Z-cell the distance of the diagonals is $4v = 2\sqrt{2}s$, (2.41) and Figure 2.9 show that in the D-cell we have $|E_2^D - E_4^D| < 4v$. This implies (iii). Eventually, property (iv) follows from (2.41). □

2.4.2 Boundary orientations and attachment of two 4-tiles

This subsection is devoted to the proofs of Lemma 2.2.6 and Lemma 2.2.7.

Proof of Lemma 2.2.6. The statement for the boundary orientation and the boundary angle, defined in (2.20)–(2.21), respectively, follows from the fact that the notions are determined uniquely by the three points which are shared by the two 4-tiles. More precisely, given any 4-tile in reference position, by applying a rotation about the e_3 axis composed with a further small rotation (depending on θ), and a translation one can ensure that a boundary of the 4-tile is contained in the e_2-e_3-plane and is symmetric with respect to the e_1-e_3-plane. Provided that θ is small, one can check that this transformation does not change the inequality in (2.20). Clearly, each two 4-tiles with the same boundary angles can be transformed in this fashion in order to be matched along the shared boundary.

Consider now two attached 4-tiles positioned such that the middle 4-tile is in reference position, in particular, the shared middle point of the boundary is the origin. If the boundary orientation of the shared boundary is $\wedge$, then both shared corner vertices satisfy $E_{i-1} \cdot e_3$, $E_i \cdot e_3 < 0$, see (2.20), and thus for the middle 4-tile we have $\varsigma = -1$. An analogous argument applies if the boundary is $\vee$. □

Proof of Lemma 2.2.7. First, we note that, for any 4-tile in reference position, reflection about the e_1-e_2-plane interchanges all boundary orientations since the reflection changes the sign of any e_3-component. Moreover, rotation around e_3 by $\pi/2$ leaves the boundary orientation invariant. A rotation in the matrix notation therefore simply rotates the corresponding sides and interchanges $\vee$ with $>$ and $\wedge$ with $<$. For example, rotating  by $\pi/2$ counterclockwise, yields  . This entails that it is enough to check the boundary orientations for one representative of any class in Table 2.2.

First, by Lemma 2.2.5 and Lemma 2.4.1 we get that the orientation of all boundaries of the coplanar D-tile  is $\vee$. Indeed, assume that the 4-tile is in reference position

and use the notation of Figure 2.5. Then the corner vertices $E_1 \cdot e_3 = E_3 \cdot e_3 = 0$ and $M_i \cdot e_3 = h$ for $i = 1, \dots, 4$. Moreover, the optimal cells $\{C, M_2, E_2, M_3\}$ and $\{C, M_4, E_4, M_1\}$ are positioned as in Lemma 2.4.1(iv). Thus, we can conclude that the corner vertices E_2 and E_4 have e_3-coordinate strictly larger than $2h$ and hence, in view of (2.20), we find that the boundary orientation is $\vee$.

Consider the Z-tile  in reference position. In this case, the middle points satisfy $M_i \cdot e_3 = h$, $i = 1, \dots, 4$ and, in view of the forms of the four optimal cells, the corner points satisfy $E_i \cdot e_3 = 0$, $i = 1, \dots, 4$. Thus, all four boundaries have orientation $\wedge$.

We observe that the above arguments actually only take into account the relative position of the two optimal cells adjacent to a boundary. Thus, one can repeat the arguments above for the I-tiles. For instance,  has two $\vee$ boundaries top and left, i.e., adjacent to $\bullet$ as in a D-tile, and two $\wedge$ boundaries right and bottom, as in a Z-tile. □

2.4.3 Arrangements of four 4-tiles

In this subsection we prove Lemma 2.3.6. We start by a result about the mutual position of two attached 4-tiles. To this end, recall the types of 4-tiles $\mathcal{A}$ and $\mathcal{B}$ introduced in (2.25)–(2.26), as well as the definition of s and h in Lemma 2.2.5(i).

Lemma 2.4.2. *Let T and $\tilde{T}$ be two attached Z-, I-, or D-tiles of an admissible configuration. Without restriction, up to applying an isometry, suppose that T is in reference position, and that the shared boundary consists of the three points E_1, M_1, E_4 and $\tilde{E}_2$, $\tilde{M}_2$, $\tilde{E}_3$, respectively, referring to the notation in Figure 2.5. We denote the reference position corresponding to $\tilde{T}$ by $\tilde{T}'$. We denote by $R^{\mathcal{A}}_{\alpha}$ the counterclockwise rotation around the axis $(1,1,0)$ by the angle α, and $R^{\mathcal{B}}_{\alpha}$ denotes the counterclockwise rotation around the axis $(-1,1,0)$ by the angle α.*
(1) *If the shared boundary is a Z-boundary of T, and a Z-boundary of $\tilde{T}$, then we have $\tilde{T} = (2s, 0, 0) + \tilde{T}'$.*
(2) *If the shared boundary is a D-boundary of T and a Z-boundary of $\tilde{T}$, we have*

$$\tilde{T} = \begin{cases} R^{\mathcal{A}}_{2\varsigma_T \kappa}((2s,0,0) + \tilde{T}') & \text{if } T \in \mathcal{A}, \\ R^{\mathcal{B}}_{2\varsigma_T \kappa}((2s,0,0) + \tilde{T}') & \text{if } T \in \mathcal{B}, \end{cases}$$

where κ is defined in (2.17), and ς_T corresponding to T is given in Lemma 2.2.5.
(3) *If the shared boundary is a Z-boundary of T and a D-boundary of $\tilde{T}$, we have*

$$\tilde{T} = \begin{cases} (2s,0,0) + R^{\mathcal{A}}_{2\varsigma_{\tilde{T}'} \kappa} \tilde{T}' & \text{if } \tilde{T} \in \mathcal{A}, \\ (2s,0,0) + R^{\mathcal{B}}_{2\varsigma_{\tilde{T}'} \kappa} \tilde{T}' & \text{if } \tilde{T} \in \mathcal{B}, \end{cases}$$

where $\varsigma_{\tilde{T}'}$ corresponds to $\tilde{T}'$.

The case of two shared D-boundaries is not addressed here as we will not need it in the sequel. We warn the reader that, in the applications below without further mentioning, we will apply isometries to the tiles in order to reduce the positions to the ones indicated in the lemma. We postpone the proof of Lemma 2.4.2 to the end of this subsection, and proceed with the proof of Lemma 2.3.6.

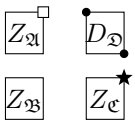

(A) Case (i): Three Z- and one D-tile.

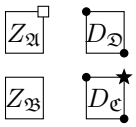

(B) Case (ii): Two Z- and two D-tiles.

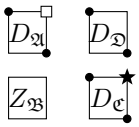

(C) Case (iii): Three D- and one Z-tile.

Figure 2.10: Different cases in the proof of Lemma 2.3.6.

Proof of Lemma 2.3.6. (i) Without restriction we suppose that the tiles lie in $\mathcal{A}$ and we suppose by contradiction that the D-tile is given by $\mathfrak{D}$. We assume that $\mathfrak{B}$ is given in reference position. Then, by Lemma 2.4.2(1) we see that $\mathfrak{C}$ is in reference position shifted by $(2s, 0, 0)$, and $\mathfrak{A}$ is in reference position shifted by $(0, 2s, 0)$. By Lemma 2.2.5 this implies that the coordinates of the points Q and P, indicated with $\square$ and respectively $\star$ in Figure 2.10 A, are given by $Q = (s, 3s, 0)$ and $P = (3s, s, 0)$, respectively. In particular, we have that $|P - Q| = 2\sqrt{2}s = 4v$, cf. (2.16) and Lemma 2.2.5(i), which corresponds to the length of the diagonal in $\mathfrak{D}$. For the D-tile $\mathfrak{D}$ in $\mathcal{A}$, however, having the rolling direction as given in Figure 2.10 A, cf. (2.25), the corresponding diagonal has length smaller than $4v$ by Lemma 2.4.1(iii), a contradiction.

(ii) Without restriction we suppose that the tiles belong to $\mathcal{A}$ and we suppose by contradiction that the Z-tiles are in $\mathfrak{A}$, $\mathfrak{B}$, and that the D-tiles are in $\mathfrak{C}$, $\mathfrak{D}$, as in Figure 2.10 B. We also assume that $\mathfrak{B}$ is given in reference position. By Lemma 2.4.2(1) we see that $\mathfrak{A}$ is in reference position shifted by $(0, 2s, 0)$, and thus the point Q, indicated by $\square$, has coordinates $Q = (s, 3s, 0)$. By Lemma 2.4.2(3) the position of the tile $\mathfrak{C}$ is obtained by taking the tile in reference configuration, rotating around the axis $(1, 1, 0)$ by the angle $\pm 2\kappa$, and then by a shifting by $(2s, 0, 0)$. As the corners where no roll-up occurs are left invariant under the rotation, we find by Lemma 2.4.1(i) that the point P, denoted by a $\star$ in Figure 2.10 B, has coordinates $(3s, s, 0)$. This implies $|P - Q| = 2\sqrt{2}s = 4v$. As in (i), this contradicts Lemma 2.4.1(iii) since the length of the diagonal in the D-tile $\mathfrak{D}$ where the tile rolls-up is less than $4v$.

(iii) Again without restriction we assume that the tiles belong to $\mathcal{A}$ and we suppose by contradiction that the Z-tile is in $\mathfrak{B}$, as in Figure 2.10 C. We assume that $\mathfrak{B}$ is given in reference position. By Lemma 2.4.2(3) the position of $\mathfrak{C}$ is obtained by taking the tile in reference configuration, rotation around the axis $(1, 1, 0)$ by the angle $\pm 2\kappa$, and then by a shifting by $(2s, 0, 0)$ (exactly in this order). As the corners where no roll-up occurs are left invariant under the rotation, we find by Lemma 2.4.1(i) that the point P, marked with $\star$ in Figure 2.10 C, has coordinates $P = (3s, s, 0)$. In a similar fashion, the position of $\mathfrak{A}$ is obtained by taking the tile in reference configuration, rotating around the axis $(1, 1, 0)$ by the angle $\pm 2\kappa$, and then by a shifting by $(0, 2s, 0)$. Lemma 2.4.1(i) yields that the point Q, indicated with $\square$ in Figure 2.10 C, has coordinates $Q = (s, 3s, 0)$. This implies $|P - Q| = 2\sqrt{2}s = 4v$, which as in (i) and (ii) contradicts Lemma 2.4.1(iii) since the length of the diagonal in the D-tile $\mathfrak{D}$ where the tile roll-up is less than $4v$.

(iv) We finally show that (2.29) is not admissible. As before, we denote the 4-tiles by $\mathfrak{A}, \dots, \mathfrak{D}$, as indicated in (2.28). Our strategy hinges on (i)–(iii): we denote by $\tilde{Q}$ the right middle point of $\mathfrak{A}$ and by $\tilde{P}$ the upper middle point of $\mathfrak{C}$. In view of Lemma 2.2.5 (i) applied on $\mathfrak{D}$, their distance necessarily needs to be $\sqrt{2}s = 2v$. We will show, however, that this is impossible.

We first assume that $\mathfrak{B}$ is in reference position. In view of Lemma 2.4.2 (3), the position of the tile $\mathfrak{C}$ is obtained by taking the tile in reference configuration, rotating it around the axis $(-1,1,0)$ by the angle -2κ, and then by a shifting by $(2s,0,0)$ (exactly in this order). In a similar fashion, by Lemma 2.4.2 (2) the position of the tile $\mathfrak{A}$ is obtained by taking the tile in reference configuration, followed by a translation by $(0,2s,0)$, and then by rotation around the axis $(1,1,0)$ by the angle -2κ (exactly in this order).

We will now change the coordinate system to simplify the notational realization of the procedure: we suppose that the common vertex of all three 4-tiles lies in the origin and we reorient the coordinate system such that the rotation axis $(1,1,0)$ coincides with e_1 and the rotation axis $(-1,1,0)$ with e_2, see Figure 2.11. Then, the points $\tilde{Q}$ and $\tilde{P}$ are given by $\tilde{Q} = \mathcal{R}_{2\kappa}^{e_1} Q$ and $\tilde{P} = \mathcal{R}_{2\kappa}^{-e_2} P = \mathcal{R}_{-2\kappa}^{e_2} P$, where $Q = (v,v,-h)$ and $P = (v,-v,-h)$ are calculated by using Lemma 2.2.5, and the rotations are given by

$$\mathcal{R}_{2\kappa}^{e_1} = \begin{pmatrix} 1 & 0 & 0 \\ 0 & \cos(2\kappa) & -\sin(2\kappa) \\ 0 & \sin(2\kappa) & \cos(2\kappa) \end{pmatrix}, \quad \mathcal{R}_{-2\kappa}^{e_2} = \begin{pmatrix} \cos(2\kappa) & 0 & \sin(2\kappa) \\ 0 & 1 & 0 \\ -\sin(2\kappa) & 0 & \cos(2\kappa) \end{pmatrix}.$$

An elementary calculation yields

$$\tilde{Q} = \begin{pmatrix} v \\ v \\ h \end{pmatrix}, \quad \tilde{P} = \begin{pmatrix} 0 \\ -v \\ 0 \end{pmatrix} + \mathcal{R}_{-2\kappa}^{e_2} \begin{pmatrix} v \\ 0 \\ -h \end{pmatrix} = \begin{pmatrix} 0 \\ -v \\ 0 \end{pmatrix} + \mathcal{R}_{-4\kappa}^{e_2} \begin{pmatrix} v \\ 0 \\ h \end{pmatrix},$$

where we used the definition of $\kappa = \arctan(h/v)$, see (2.17), and the trigonometric identities $\cos(2\arctan(x)) = (1-x^2)/(1+x^2)$ and $\sin(2\arctan(x)) = 2x/(1+x^2)$, as well as $(v,0,-h) = \mathcal{R}_{-2\kappa}^{e_2}(v,0,h)$. Consequently, we obtain

$$|\tilde{Q} - \tilde{P}|^2 = (2v)^2 + \left|\left(\mathcal{R}_0^{e_2} - \mathcal{R}_{-4\kappa}^{e_2}\right)(v,0,h)\right|^2$$

which is strictly larger than $(2v)^2$ since $\kappa \in (0,\pi/2)$, see (2.17). This establishes a contradiction since, as stated above, the distance should be $2v$. □

Proof of Lemma 2.4.2. (1) Since the shared boundary is a Z-boundary of T and a Z-boundary of $\tilde{T}$, and the boundary orientations of T and $\tilde{T}$ match at the shared boundary (see Lemma 2.2.6), Table 2.2 and Table 2.3 show that $\varsigma_T = \varsigma_{\tilde{T}}$ and that the middle 4-tile between T and $\tilde{T}$, denoted by T_*, is a Z-tile. By Lemma 2.2.6 we also find $\varsigma_{T_*} = -\varsigma_T$. Then by Lemma 2.4.1(ii) it is elementary to check that $C_{\tilde{T}} - C_T = (2s,0,0)$, where $C_{\tilde{T}}$ and C_T denote the centers of the 4-tiles, respectively.

(2) We prove the result only for the particular case of the two 4-tiles  and  , as depicted in Figure 2.12. In fact, the general case can be reduced to this situation by

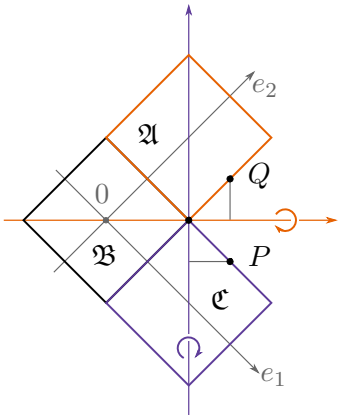

Figure 2.11: The points P and Q are rotated by 2κ around the axis in the respective directions. Note that P rotates clockwise.

(a) replacing the optimal cells which are not adjacent to the shared boundary, as they do not affect the argument; and by (b) applying a suitable rotation or reflection.

Suppose that T is in reference position and denote the reference position of $\tilde{T}$ by $\tilde{T}'$. We define $\tilde{T}'' := \tilde{T}' + (2s, 0, 0)$. In view of Lemma 2.4.1(i),(ii), we see that T and $\tilde{T}''$ share exactly one corner point $E_* = (s, s, 0)$ as depicted in Figure 2.12. Clearly, the rotation around the axis $(1, 1, 0)$ by 2κ leaves E_* invariant. We need to show that under this rotation the points P_i, $i = 1, 2$, are mapped to $\tilde{P}_i$, as depicted in Figure 2.12. We denote by C_i, $i = 1, 2$, the two points on $(1, 1, 0)$ which intersect the plane with normal vector $(1, 1, 0)$ containing P_i and $\tilde{P}_i$. By Lemma 2.2.5 we find that $C_1 = (s/2, s/2, 0)$ and $C_2 = 0$. We need to check that

$$|C_i - P_i| = |C_i - \tilde{P}_i| \quad \text{and} \quad \measuredangle P_i\, C_i\, \tilde{P}_i = 2\kappa \quad \text{for } i = 1, 2. \tag{2.42}$$

We first address $i = 1$. By Lemma 2.2.5, we have $P_1 = (s, 0, -h)$ and $\tilde{P}_1 = (s, 0, h)$. We also note that $s = \sqrt{2}v$. This along with $C_1 = (s/2, s/2, 0)$, $\kappa = \arctan(h/v)$ (see (2.17)), and the trigonometric identity $\cos(2\arctan(x)) = (1 - x^2)/(1 + x^2)$ yields (2.42) by an elementary computation.

We now address $i = 2$. As C_2 and $\tilde{P}_2$ form a diagonal of an optimal cell, see Figure 2.12, by the definition before (2.16) we get $|C_2 - \tilde{P}_2| = 2v = \sqrt{2}s$. On the other hand, by Lemma 2.2.5, we find $P_2 = (s, -s, 0)$ and therefore $|P_2 - C_2| = \sqrt{2}s$. This shows the first part of (2.42). To calculate the angle, we refer to the cross section in Figure 2.13. Since this cross section is the one of an optimal cell in a rotated position, we can calculate the angle $\measuredangle P_2\, C_2\, \tilde{P}_2$ using the definition of κ^* in (2.17) and thus derive that $\gamma = \kappa + (\pi - \kappa^*)/2 = \kappa + \pi/2 - (\pi - 2\kappa)/2 = 2\kappa$. This concludes the proof.

The proof of (3) is similar to (2) by interchanging the roles of the 4-tiles. We omit the details. □

We proceed with a simple consequence for boundary angles defined in (2.21).

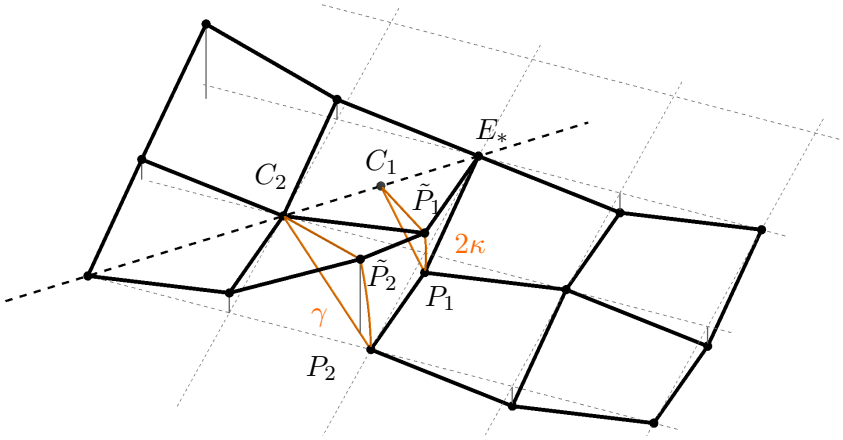

Figure 2.12: Rotation of a Z-tile around the diagonal of a D-tile in order to match the boundaries.

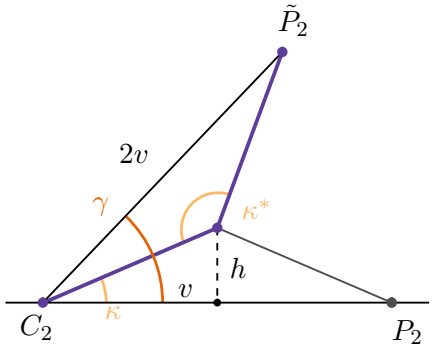

Figure 2.13: Cross section along the plane with normal $(1, 1, 0)$.

Corollary 2.4.3. *The boundary angle of a D-boundary coincides the the boundary angle of a Z-boundary.*

This immediately follows from Lemma 2.4.2(ii). Indeed, if the statement was not true, one could not attach the two 4-tiles, as described in the previous proof.

2.4.4 Incidence angles in coplanar 4-tiles: Theorem 2.2.8 implies Theorem 2.2.2

In this short subsection, we explain that Theorem 2.2.8 implies Theorem 2.2.2. In Subsection 2.2.5, we already addressed the type function. Therefore, it remains to consider the last two items in Theorem 2.2.2, i.e., the incidence angles defined in (2.15) between optimal cells.

Z-tiles. We start by showing that the incidence angles between optimal cells in a Z-tile along both diagonals are given by zero. Observe that reflection about the e_1-e_2-plane only interchanges the sign of the incidence angle. Thus, we assume without restriction that

$\varsigma = 1$ (cf. Lemma 2.2.5). Due to symmetry, it suffices to consider one of the four bonds contained in the 4-tile, e.g., the bond connecting C and M_1, referring to the notation in Figure 2.5. Without restriction we only calculate the incidence angle along d_1 as the other one can be calculated in a similar fashion, again exploiting symmetry. If the 4-tile is in reference position, Lemma 2.2.5(i) implies that $y^1_{\mathrm{top}} = E_1 = (s, s, 0)$, $y^1_{\mathrm{bot}} = M_4 = (0, -s, h)$, $C = 0$, and $M_1 = (s, 0, h)$. Therefore, since n^1_{top} is in direction $M_1 \times E_1$ and n^1_{bot} is in direction $-M_1 \times (M_4 - M_1)$, we find $n^1_{\mathrm{top}} = n^1_{\mathrm{bot}} = \frac{1}{\sqrt{s^2+2h^2}}(-h, h, s)$. Thus, in view of (2.15), we get that the incidence angle is $\arccos(1) = 0$.

D-tiles. We now address a D-tile in (2.23), given in reference configuration. Due to symmetry, it is again not restrictive to consider only the bond connecting C and M_1 and to suppose that $\varsigma = 1$. Note that, due to Lemma 2.2.5 and Lemma 2.4.1(i), we have $E_1 = (s, s, 0)$ and E_4 satisfies $E_4 \cdot e_3 = q$ and $0 < E_4 \cdot e_1 = -E_4 \cdot e_2 = p := \sqrt{s^2 - q^2/2} < s$ for some $q > 0$. Since E_1, M_1, and M_4 have the same position as in a Z-tile, repeating the above calculation we find that the incidence angle along d_1 is zero. We now consider the angle along d_2. To this end, we first find that $y^2_{\mathrm{top}} = M_2 = (0, s, h)$ and $y^2_{\mathrm{bot}} = E_4 = (p, -p, q)$, see Lemma 2.2.5. Therefore, since n^2_{top} is in direction $M_1 \times M_2$ and n^2_{bot} is in direction $-M_1 \times (E_4 - M_1)$, we get $n^2_{\mathrm{top}} = \frac{1}{\sqrt{s^2+2h^2}}(-h, -h, s)$, and an elementary computation yields $n^2_{\mathrm{bot}} = v/|v|$ for $v = (-h, -h, s) + (0, qs/p, 0)$. This implies n^2_{top} and n^2_{bot} are not parallel and therefore by (2.15) the incidence angle, denoted by γ^*, is not zero.

To determine the sign of the non-zero incidence angle, we need to determine the sign of $(y^2_{\mathrm{top}} - y^2_{\mathrm{bot}}) \cdot (n^2_{\mathrm{top}} - n^2_{\mathrm{bot}}) = (y^2_{\mathrm{top}} - y^2_{\mathrm{bot}}) \cdot n^2_{\mathrm{top}} - (y^2_{\mathrm{top}} - y^2_{\mathrm{bot}}) \cdot n^2_{\mathrm{bot}}$. First note that $(y^2_{\mathrm{top}} - y^2_{\mathrm{bot}}) = M_2 - E_4 = (-p, s + p, h - q)$ which yields $(y^2_{\mathrm{top}} - y^2_{\mathrm{bot}}) \cdot n^2_{\mathrm{top}} = -\lambda qs$, with $\lambda = 1/\sqrt{s^2 + 2h^2}$ and $(y^2_{\mathrm{top}} - y^2_{\mathrm{bot}}) \cdot n^2_{\mathrm{bot}} = \mu qs^2/p$, with $\mu = 1/|v|$. Therefore, we obtain $(y^2_{\mathrm{top}} - y^2_{\mathrm{bot}}) \cdot (n^2_{\mathrm{top}} - n^2_{\mathrm{bot}}) = -\lambda qs - \mu qs^2/p < 0$. Hence, the incidence angle has a negative sign, see (2.15). Summarizing, we have shown that in D-tiles the angles are also zero along d_1 and lie in $\{-\gamma^*, \gamma^*\}$ along d_2.

I-tiles. It is obvious that for I-tiles, being combinations of Z- and D-tiles, we find that the incidence angles along d_1 are also 0 and along d_2 they lie in $\{-\gamma^*, 0, \gamma^*\}$.

We close the proof by the observation that, due to the symmetries in Z-, D-, and I-tiles contained in $\mathcal{A}$, see (2.25), it is indeed elementary to check that $\gamma_2(s, t) = \gamma_2(s + 1/2, t + 1/2)$ for all $s, t \in \frac{1}{2}\mathbb{Z}$ with $s + t \in \mathbb{Z} + 1/2$.

2.4.5 Admissible configurations and ground states of the energy

This subsection is devoted to the proof of Proposition 2.2.1.

Proof. Step 1. We start by introducing a specific *unit cell*: fix $x_0 \in \mathbb{Z}^2$ and denote the four neighbors of x_0 by $x_1 = x_0 + e_1$, $x_2 = x_0 + e_2$, $x_3 = x_0 - e_1$, and $x_4 = x_0 - e_2$. Given a deformation $y\colon \{x_0, \dots, x_4\} \to \mathbb{R}^3$, we define $y_i = y(x_i)$ for $i = 0, \dots, 4$, and we

let $y_5 = y_1$. We introduce the *cell energy* by

$$E_{\mathrm{cell}}(y) = \frac{1}{2}\sum_{i=1}^{4} v_2(|y_i - y_0|) + \frac{1}{2}\sum_{i=1}^{4} v_2(|y_i - y_{i+1}|) + \sum_{i=1}^{4} v_3(\theta_i) + v_3(\delta_{13}) + v_3(\delta_{24}), \tag{2.43}$$

where $\theta_i = \measuredangle y_i\, y_0\, y_{i+1}$ for $i = 1, \dots, 4$, as well as $\delta_{13} = \measuredangle y_1\, y_0\, y_3$ and $\delta_{24} = \measuredangle y_2\, y_0\, y_4$. The cell $(y_i)_{i=0}^4$ is called *optimal* if it minimizes (2.43).

Let us start by relating the cell energy to the configurational energy in (2.1). To this end, let $y\colon \mathbb{Z}^2 \to \mathbb{R}^3$ be a deformation, and for $m \in \mathbb{N}$ let Q_m be the open square centered at 0 with sidelength $2m$. For $j \in \mathbb{Z}^2 \cap Q_m$ we denote by $y^j = \{y_0^j, \dots, y_4^j\}$ the cell considered above for $x_0 = j$. Then, in view of (2.1), owing to the fact that bonds related to nearest-neighbors and next-to-nearest-neighbors are contained in two cells (apart from bonds intersecting ∂Q_m), whereas each bond angle is contained in exactly one cell, we find for every $m \in \mathbb{N}$ that

$$E(y, Q_m) = \sum_{j \in \mathbb{Z}^2 \cap Q_m} E_{\mathrm{cell}}(y^j) = (2m-1)^2 \frac{1}{\#(\mathbb{Z}^2 \cap Q_m)} \sum_{j \in \mathbb{Z}^2 \cap Q_m} E_{\mathrm{cell}}(y^j).$$

Then, recalling the definition in (2.5) and by arguing as in [74, Proposition 2.1] we have that $y\colon \mathbb{Z}^2 \to \mathbb{R}^3$ is a ground state if and only if for each $x_0 \in \mathbb{Z}^2$ the corresponding cell $\{y_0, \dots, y_4\}$ is optimal. Note that there exist admissible configurations consisting of optimal cells by Theorem 2.2.8, e.g., a tiling with only Z-tiles. Therefore, in the following it suffices to minimize the cell energy and to show that the unique minimizer is identified by having specific bond lengths and bond angles.

Step 2. Let $\{y_0, y_1, y_2, y_3, y_4\}$ be an optimal cell. We show that $|y_j - y_0| \in (1-\eta, 1+\eta)$ as well as $\theta_j > \pi/2 - \eta$ for $j = 1, \dots, 4$. Assume first by contradiction that $|y_j - y_0| \le 1 - \eta$ for some $j = 1, \dots, 4$. Then by using $v_2 \ge -1$, $v_3 \ge 0$, the fact that v_2 is decreasing on $(0, 1)$, and (2.6) we get

$$\begin{aligned} E_{\mathrm{cell}}(y) &\ge \frac{1}{2}\sum_{i=1}^{4} v_2\left(|y_i - y_0|\right) + \frac{1}{2}\sum_{i=1}^{4} v_2\left(|y_{i+1} - y_i|\right) \\ &\ge \frac{1}{2} v_2(1-\eta) + \frac{1}{2}\sum_{i \neq j} v_2\left(|y_i - y_0|\right) + \frac{1}{2}\sum_{i=1}^{4} v_2\left(|y_{i+1} - y_i|\right) \\ &\ge \frac{1}{2} v_2(1-\eta) - \frac{3}{2} - 2 = \frac{1}{2} v_2(1-\eta) - \frac{7}{2} \\ &\overset{(2.6)}{>} -2 + 2v_2(\sqrt{2}) + 4v_3(\pi/2) = E_{\mathrm{cell}}(x_0, x_1, x_2, x_3, x_4). \end{aligned}$$

In the last equation, we have also used that $v_2(1) = -1$ and $v_3(\pi) = 0$. This estimate contradicts the optimality of the cell.

In a similar fashion, we assume by contradiction that there exists some bond angle θ_j, $j = 1, \dots, 4$, such that $\theta_j \leq \pi/2 - \eta$. Then, by $v_2 \geq -1$, $v_3 \geq 0$, and (2.8) we have

$$\begin{aligned} E_{\text{cell}}(y) &= \frac{1}{2}\sum_{i=1}^{4} v_2\left(|y_i - y_0|\right) + \frac{1}{2}\sum_{i=1}^{4} v_2\left(|y_i - y_{i+1}|\right) \\ &\quad + \sum_{i=1}^{4} v_3(\theta_i) + v_3(\delta_{13}) + v_3(\delta_{24}) \\ &\geq -4 + v_3(\theta_j) \overset{(2.8)}{>} -2 + 2v_2(\sqrt{2}) + 4v_3(\pi/2) \\ &= E_{\text{cell}}(x_0, x_1, x_2, x_3, x_4), \end{aligned}$$

which is again in contradiction with the optimality of y.

We eventually show that for an optimal cell the bond lengths have to be less then $1 + \eta$. Basic trigonometry together with the least size of the bond lengths and bond angles ensures that second-neighbor bonds have at least length

$$\begin{aligned} 2(1-\eta)\sin(\pi/4 - \eta/2) &= 2(1-\eta)\frac{\sqrt{2}}{2}\left(\cos(\eta/2) - \frac{1}{2}\sin(\eta/2)\right) \\ &> \sqrt{2}(1-\eta)^2 > 1, \end{aligned} \tag{2.44}$$

where the last two inequalities hold for η sufficiently small. Assume now that $|y_j - y_0| \geq 1 + \eta$ for some $j = 1, \dots, 4$. Then, we get by $v_2 \geq -1$, $v_3 \geq 0$, the fact that v_2 increasing on $[1, \infty)$, and (2.7) that

$$\begin{aligned} E_{\text{cell}}(y) &= \frac{1}{2}\sum_{i=1}^{4} v_2\left(|y_i - y_0|\right) + \frac{1}{2}\sum_{i=1}^{4} v_2\left(|y_i - y_{i+1}|\right) \\ &\quad + \sum_{i=1}^{4} v_3(\theta_i) + v_3(\delta_{13}) + v_3(\delta_{24}) \\ &\geq -\frac{3}{2} + \frac{1}{2}v_2(1+\eta) + 2v_2(\sqrt{2}(1-\eta)^2) \\ &\overset{(2.7)}{>} -2 + 2v_2(\sqrt{2}) + 4v_3(\pi/2) = E_{\text{cell}}(x_0, x_1, x_2, x_3, x_4). \end{aligned}$$

The latter inequality once again contradicts optimality and we conclude that all first-neighbor bond lengths are at most $1 + \eta$.

Step 3. To simplify notation, we denote the collection of angles by $\boldsymbol{\theta} := (\theta_i)_{i=1}^4 = (\theta_1, \dots, \theta_4)$. We observe that δ_{24} can be written as a function of $\boldsymbol{\theta}$ and δ_{13}, i.e., $\delta_{24} = f(\boldsymbol{\theta}, \delta_{13})$, where the function f is explicitly given in Step 8, see (2.57). We will not need the exact form of this function, but only use that it is smooth for θ_i in a left neighborhood of $\pi/2$ and δ_{13} in a small interval left of π, see Step 8 below. Using Lemma 2.2.4 we find that in a cell with $\theta_1 = \cdots = \theta_4 = \theta$ it holds that $\delta_{24} = f(\theta, \dots, \theta, \delta_{13}) = f_\theta(\delta_{13})$,

where $f_\theta(\delta) := 2\arccos\left(\cos\theta/\cos(\delta/2)\right)$. Note that f_θ has a unique fixed point $\delta_\theta := 2\arccos(\sqrt{\cos\theta})$. We decompose the cell energy E_{cell} defined in (2.43) as

$$E_{\mathrm{cell}}(y) = \sum_{i=1}^{4} F(\ell_i, \ell_{i+1}, \theta_i) + v_3(\delta_{13}) + v_3(f(\boldsymbol{\theta}, \delta_{13})), \tag{2.45}$$

where $\ell_i := |y_i - y_0|$ for $i = 1, \dots, 4$ and

$$\begin{aligned} F(\ell_i, \ell_{i+1}, \theta_i) :=& \frac{1}{4} v_2(\ell_i) + \frac{1}{4} v_2(\ell_{i+1}) \\ &+ \frac{1}{2} v_2\big((\ell_i^2 + \ell_{i+1}^2 - 2\ell_i\ell_{i+1}\cos\theta_i)^{1/2}\big) + v_3(\theta_i). \end{aligned}$$

We have proved that, if $\{y_0, \dots, y_4\}$ is optimal, first-neighbor bond lengths ℓ_i lie in $(1-\eta, 1+\eta)$ and bond angles θ_i lie in $(\pi/2 - \eta, \pi]$. Therefore, by using the convexity assumption (2.9) on F we find

$$\sum_{i=1}^{4} F(\ell_i, \ell_{i+1}, \theta_i) \geq 4F(\bar{\ell}, \bar{\ell}, \bar{\theta}), \tag{2.46}$$

where

$$\bar{\ell} = \frac{1}{4}(\ell_1 + \cdots + \ell_4), \quad \bar{\theta} = \frac{1}{4}(\theta_1 + \cdots + \theta_4). \tag{2.47}$$

Note that the inequality in (2.46) is strict whenever $\ell_i \neq \bar{\ell}$ or $\theta_i \neq \bar{\theta}$ for some $i = 1, \dots, 4$.

Step 4. We check that the map $(\ell, \theta) \mapsto F(\ell, \ell, \theta)$ is minimized on $(1-\eta, 1+\eta) \times (\pi/2 - \eta, \pi]$ at some $\ell^* \leq 1$ and $\theta^* < \pi/2$. If we had $\ell^* > 1$, one could reduce F by reducing ℓ, noting that v_2 is increasing in $(1, \infty)$ and recalling (2.44). This, however, would contradict optimality. We now exclude $\theta^* \geq \pi/2$. Indeed, in this case we could decrease θ^* by $0 < \tilde{\theta} \ll 1$ and by a Taylor expansion we would get that F changes to first order by

$$-v_3'(\theta^*)\tilde{\theta} - v_2'\big(\sqrt{2}\ell\sqrt{1-\cos\theta^*}\big)\frac{\ell}{2\sqrt{2}}\frac{\sin\theta^*\,\tilde{\theta}}{\sqrt{1-\cos\theta^*}}.$$

By $\ell \in (1-\eta, 1]$ and (2.11) we get that the above term is negative, which contradicts minimality.

Step 5. Next, we show that for $\bar{\theta}$ defined in (2.47) it holds that $\bar{\theta} \leq \pi/4 + \theta^*/2$. We also establish a bound from below on δ_{13} and δ_{24}. The argument is based on the observation that by (2.45), (2.46), and the definition of δ_θ we find that $4F(\ell, \ell, \theta) + 2v_3(\delta_\theta)$ is an upper bound for the minimal cell energy for $(\ell, \theta) \in (1-\eta, 1+\eta) \times (\pi/2 - \eta, \pi]$. By definition we have $\delta_\theta \to \pi$ as $\theta \to \pi/2$. Thus, in view of (2.10), the monotonicity of v_3, and $\theta^* \geq \pi/2 - \eta$, we can choose η sufficiently small depending on v_3 and find $\lambda > 0$ small such that $|v_3| \leq \varepsilon$ on $[\pi - \lambda, \pi]$, $|v_3'| \leq \varepsilon$ on $[\pi - 2\lambda, \pi]$, and

$$v_3(\delta) > 2\varepsilon > 2v_3(\delta_{\theta^*}) \quad \text{for } \delta \leq \pi - \lambda. \tag{2.48}$$

We also suppose that ε is chosen small enough depending on v_2, v_3, and θ^* such that

$$F(\ell,\ell,\theta) > F(\ell^*,\ell^*,\theta^*) + 2\varepsilon \quad \text{for } \theta > \frac{\pi}{4} + \frac{\theta^*}{2} \text{ and } \ell \in (1-\eta, 1+\eta). \tag{2.49}$$

Now, we can suppose $\delta_{13}, \delta_{24} \geq \pi - \lambda$ (recall that $\delta_{24} = f(\boldsymbol{\theta}, \delta_{13})$) since otherwise we get

$$E_{\text{cell}}(y) > 4F(\bar{\ell},\bar{\ell},\bar{\theta}) + 2v_3(\delta_{\theta^*}) \geq 4F(\ell^*,\ell^*,\theta^*) + 2v_3(\delta_{\theta^*})$$

by using (2.45), (2.46), and (2.48), which contradicts minimality. In a similar fashion, we can suppose that $\bar{\theta}$ in (2.47) satisfies $\bar{\theta} \leq \frac{\pi}{4} + \frac{\theta^*}{2}$ as otherwise $E_{\text{cell}}(y) > 4F(\ell^*,\ell^*,\theta^*) + 2v_3(\delta_{\theta^*})$ follows using (2.45), (2.46), (2.48), and (2.49).

Step 6. We are left with the case $\delta_{13} \geq \pi - \lambda$ and $\theta_1 + \ldots + \theta_4 = 4\bar{\theta} \leq \pi + 2\theta^* < 2\pi$. In this step, we show that

$$E_{\text{cell}}(y) \geq 4F(\bar{\ell},\bar{\ell},\bar{\theta}) + v_3(\delta_{13}) + v_3(f_{\bar{\theta}}(\delta_{13})) \tag{2.50}$$

with equality only if $\ell_i = \bar{\ell}$ and $\theta_i = \bar{\theta}$ for $i = 1, \ldots, 4$.

We start by noticing that $\theta_1 + \ldots + \theta_4 < 2\pi$ and $\theta_i > \pi/2 - \eta$ for $i = 1, \ldots, 4$ imply $\theta_i < \pi/2 + 3\eta$ for $i = 1, \ldots, 4$. Therefore, the convexity estimate in (2.46) can be improved by using the strong convexity assumption (2.9) on F, and we find

$$\sum_{i=1}^{4} F(\ell_i, \ell_{i+1}, \theta_i) \geq 4F(\bar{\ell},\bar{\ell},\bar{\theta}) + \alpha \sum_{i=1}^{4} |\theta_i - \bar{\theta}|^2 \tag{2.51}$$

for some $\alpha > 0$. Moreover, a simple geometric argument shows that $\delta_{13} = \pi$ implies $\theta_1 + \ldots + \theta_4 = 2\pi$, see Figure 2.14. Therefore, by a continuity argument and $\theta_1 + \ldots + \theta_4 \leq \pi + 2\theta^*$ we get that $\delta_{13} \leq \delta^*$ for some $\delta^* < \pi$ only depending on θ^*. Consequently, we need to consider the case that $\delta_{13} \in [\pi - \lambda, \delta^*]$ and $\theta_i \in (\frac{\pi}{2} - \eta, \frac{\pi}{2} + 3\eta)$.

If $\alpha \sum_{i=1}^{4} |\theta_i - \bar{\theta}|^2 \geq 2\varepsilon$, by (2.45), (2.48), and (2.51) we obtain a contradiction to minimality as $v_3(\delta_{13}) + v_3(f(\boldsymbol{\theta}, \delta_{13})) + \alpha \sum_{i=1}^{4} |\theta_i - \bar{\theta}|^2 \geq 2\varepsilon > 2v_3(\delta_{\theta^*})$.

If $\alpha \sum_{i=1}^{4} |\theta_i - \bar{\theta}|^2 < 2\varepsilon$, we now show that $f_{\bar{\theta}}(\delta_{13})$ cannot be too far away from $f(\boldsymbol{\theta}, \delta_{13})$. Eventually, this will allow us to deduce (2.50). By choosing ε small enough and recalling that $\bar{\theta} < \pi/2$, we get that $\theta_i \leq \pi/2$ for $i = 1, \ldots, 4$. By Taylor's Theorem there exists $\boldsymbol{z} \in \{t\boldsymbol{\theta} + (1-t)\bar{\boldsymbol{\theta}} \,:\, t \in [0,1]\}$, where $\bar{\boldsymbol{\theta}} = (\bar{\theta}, \ldots, \bar{\theta})$, such that

$$\begin{aligned} f(\boldsymbol{\theta}, \delta_{13}) - f_{\bar{\theta}}(\delta_{13}) &= f(\boldsymbol{\theta}, \delta_{13}) - f(\bar{\boldsymbol{\theta}}, \delta_{13}) \\ &= \nabla_{\boldsymbol{\theta}} f(\bar{\boldsymbol{\theta}}, \delta_{13})(\boldsymbol{\theta} - \bar{\boldsymbol{\theta}}) + \frac{1}{2}(\boldsymbol{\theta} - \bar{\boldsymbol{\theta}}) \nabla^2_{\boldsymbol{\theta}} f(\boldsymbol{z}, \delta_{13})(\boldsymbol{\theta} - \bar{\boldsymbol{\theta}}) \\ &= \frac{1}{2}(\boldsymbol{\theta} - \bar{\boldsymbol{\theta}}) \nabla^2_{\boldsymbol{\theta}} f(\boldsymbol{z}, \delta_{13})(\boldsymbol{\theta} - \bar{\boldsymbol{\theta}}) \leq \frac{\lambda_{\max}}{2} |\boldsymbol{\theta} - \bar{\boldsymbol{\theta}}|^2 \\ &= \frac{\lambda_{\max}}{2} \sum_{i=1}^{4} |\theta_i - \bar{\theta}|^2, \end{aligned} \tag{2.52}$$

where we used that $\frac{\partial}{\partial\theta_i} f(\bar{\boldsymbol{\theta}}, \delta_{13}) = \frac{\partial}{\partial\theta_j} f(\bar{\boldsymbol{\theta}}, \delta_{13})$ and thus

$$\nabla_{\boldsymbol{\theta}} f(\bar{\boldsymbol{\theta}}, \delta_{13}) \cdot (\boldsymbol{\theta} - \bar{\boldsymbol{\theta}}) = \tfrac{\partial}{\partial\theta_1} f(\bar{\boldsymbol{\theta}}, \delta_{13}) \left(\sum_i \theta_i - \sum_i \bar{\theta} \right) = 0.$$

In (2.52) we denoted the largest eigenvalue of the Hessian $\nabla^2_{\boldsymbol{\theta}} f(\boldsymbol{z}, \delta_{13})$ with $\lambda_{\max}$. Using the Gershgorin circle theorem, we find $|\lambda_{\max}| \leq 4c_f$ where we use that f is smooth for $\theta_i \in I := [\frac{\pi}{2} - \eta, \frac{\pi}{2}]$ and $\delta_{13} \in [\pi - \lambda, \delta^*]$, and define

$$c_f := \max_{i,j=1,\dots,4} \sup_{\theta_i \in I} \sup_{\delta_{13} \in [\pi-\lambda, \delta^*]} \left| \frac{\partial^2}{\partial\theta_i \partial\theta_j} f(\boldsymbol{\theta}, \delta_{13}) \right| < \infty.$$

The proof of the smoothness of f is deferred to the end of the proof in Step 8. Therefore, we obtained

$$|f(\boldsymbol{\theta}, \delta_{13}) - f_{\bar{\theta}}(\delta_{13})| \leq 2c_f \sum_{i=1}^4 |\theta_i - \bar{\theta}|^2. \tag{2.53}$$

For ε small enough such that $4c_f\varepsilon \leq \alpha\lambda$, due to $\alpha \sum_{i=1}^4 |\theta_i - \bar{\theta}|^2 < 2\varepsilon$, we have

$$|f(\boldsymbol{\theta}, \delta_{13}) - f_{\bar{\theta}}(\delta_{13})| \leq 2c_f \sum_{i=1}^4 |\theta_i - \bar{\theta}|^2 \leq \frac{\alpha\lambda}{2\varepsilon} \sum_{i=1}^4 |\theta_i - \bar{\theta}|^2 \leq \lambda.$$

Hence $f_{\bar{\theta}}(\delta_{13}) \geq \pi - 2\lambda$ as $f(\boldsymbol{\theta}, \delta_{13}) \geq \pi - \lambda$ by Step 5. Therefore, as $|v_3'| \leq \varepsilon$ on $[\pi - 2\lambda, \pi]$ and $\lambda > 0$ small, we obtain by (2.53)

$$\begin{aligned} |v_3(f(\boldsymbol{\theta}, \delta_{13})) - v_3(f_{\bar{\theta}}(\delta_{13}))| &\leq |f(\boldsymbol{\theta}, \delta_{13}) - f_{\bar{\theta}}(\delta_{13})| \sup_{[\pi-2\lambda,\pi]} |v_3'| \\ &\leq 2c_f\varepsilon \sum_{i=1}^4 |\theta_i - \bar{\theta}|^2 \leq \frac{\alpha}{2} \sum_{i=1}^4 |\theta_i - \bar{\theta}|^2. \end{aligned} \tag{2.54}$$

Consequently, (2.50) holds by applying (2.51) and (2.54) to (2.45).

Step 7. We now conclude the proof by showing

$$E_{\mathrm{cell}}(y) \geq 4 \left(\frac{1}{2} v_2(\bar{\ell}) + \frac{1}{2} v_2(\sqrt{2}\bar{\ell}(1 - \cos\bar{\theta})^{1/2}) + v_3(\bar{\theta}) \right) + 2v_3(\delta_{\bar{\theta}}), \tag{2.55}$$

where $\delta_{\bar{\theta}} = 2\arccos(\sqrt{\cos\bar{\theta}})$, and that equality holds only if $\ell_i = \bar{\ell}$ and $\theta_i = \bar{\theta}$ for $i = 1, \dots, 4$. To this end, we further estimate (2.50) by claiming

$$g(\delta_{13}) := v_3(\delta_{13}) + v_3(f_{\bar{\theta}}(\delta_{13})) \geq 2v_3(\delta_{\bar{\theta}}), \tag{2.56}$$

with equality if and only if $\delta_{13} = f_{\bar{\theta}}(\delta_{13})$. Computing $g'(\delta) = v_3'(\delta) + v_3'(f_{\bar{\theta}}(\delta))\, f_{\bar{\theta}}'(\delta)$ shows that $g'(\delta_{\bar{\theta}}) = 0$, because $f_{\bar{\theta}}'(\delta_{\bar{\theta}}) = -1$ and $\delta_{\bar{\theta}} = f_{\bar{\theta}}(\delta_{\bar{\theta}})$. Moreover, we calculate $g''(\delta) = v_3''(\delta) + v_3''(f_{\bar{\theta}}(\delta))\,(f_{\bar{\theta}}'(\delta))^2 + v_3'(f_{\bar{\theta}}(\delta))\, f_{\bar{\theta}}''(\delta) > 0$, where we used the monotonicity

and strict convexity of v_3 and the concavity of $f_{\bar\theta}$, which follows from an elementary computation. This indeed implies (2.56).

This, along with (2.50), implies that (2.55) holds, with equality only if all bonds of an optimal cell have length $\bar\ell$, all angles have amplitude $\bar\theta$, and $\delta_{13} = \delta_{24} = \delta_{\bar\theta}$. Clearly, for an optimal cell, $\bar\ell$ and $\bar\theta$ are given uniquely. We finally observe that $\bar\ell \leq 1$ and $\bar\theta < \pi/2$. For $\bar\ell$, this follows from the fact that $\ell^* \leq 1$, as shown in Step 4, and $\bar\theta < \pi/2$ has been checked in Step 5.

Step 8. Let us conclude by collecting some remarks on the function $f(\boldsymbol{\theta}, \delta_{13})$ used throughout the proof. If $\delta_{13} = \pi$, we have that $\theta_1 + \theta_2 = \theta_3 + \theta_4 = \delta_{13} = \pi$. Therefore, δ_{24} can be chosen arbitrarily in $[0, \pi]$, see Figure 2.14, and $f(\cdot, \pi)$ is hence not defined. For $\delta_{13} < \pi$, the definition is given by

$$f(\boldsymbol{\theta}, \delta_{13}) = \arccos\Big\{ \cos\theta_1 \, \cos\theta_4 + \frac{(\cos\theta_2 - \cos\delta_{13}\cos\theta_1)(\cos\theta_3 - \cos\delta_{13}\cos\theta_4)}{\sin^2\delta_{13}} \\ - \sqrt{1 - \cos^2\theta_1 - \frac{(\cos\theta_2 - \cos\delta_{13}\cos\theta_1)^2}{\sin^2\delta_{13}}} \sqrt{1 - \cos^2\theta_4 - \frac{(\cos\theta_3 - \cos\delta_{13}\cos\theta_4)^2}{\sin^2\delta_{13}}} \Big\}, \tag{2.57}$$

which can be derived by elementary, yet tedious, trigonometry. Let us now check that f is smooth for all $\delta_{13} \in [\pi - \lambda, \delta^*]$ and $\boldsymbol{\theta} \in [\pi/2 - \eta, \pi]^4$ such that $f(\boldsymbol{\theta}, \delta_{13}) = \delta_{24} \in [\pi - \lambda, \delta^*]$ which we need in Step 6 of the proof. First, since $\delta_{24} \in [\pi - \lambda, \delta^*]$ the expression inside of arccos is bounded away from -1 and 1. As $\delta_{13} \in [\pi - \lambda, \delta^*]$, $\sin\delta_{13}$ is bounded away from 0. Thus, it suffices to check that the expressions inside the square roots are bounded away from 0. Indeed, $\boldsymbol{\theta} \in [\pi/2 - \eta, \pi]^4$ implies $\cos\theta_1 \, \cos\theta_4 \to 0$ as $\eta \to 0$ and $(\cos\theta_2 - \cos\delta_{13}\cos\theta_1)(\cos\theta_3 - \cos\delta_{13}\cos\theta_4)/\sin^2\delta_{13} \geq 0$. As $\cos(f(\boldsymbol{\theta}, \delta_{13}))$ lies in a neighborhood of -1, this is indeed only possible if the value of each of the square roots is close to 1. □

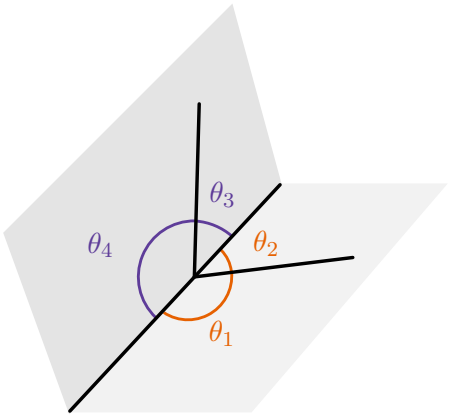

Figure 2.14: If $\delta_{13} = \pi$, then $\theta_1 + \theta_2 = \theta_3 + \theta_4 = \delta_{13} = \pi$ and thus $\theta_1 + \cdots + \theta_4 = 2\pi$. Furthermore, the angle δ_{24} can be chosen arbitrarily.

Acknowledgements

This work is partially supported by the FWF-DFG grant 10.55776/I4354, the FWF grants 10.55776/F65, 10.55776/W1245, 10.55776/I5149, and 10.55776/P32788, and the OeAD-WTZ project CZ 01/2021. This work was supported by the Deutsche Forschungsgemeinschaft (DFG, German Research Foundation) under Germany's Excellence Strategy EXC 2044 -390685587, Mathematics Münster: Dynamics–Geometry–Structure.

3 Discrete-to-continuum linearization in atomistic dynamics

This chapter consists of the paper [71] in collaboration with Manuel Friedrich and Ulisse Stefanelli.

Abstract

In the stationary case, atomistic interaction energies can be proved to Γ-converge to classical elasticity models in the simultaneous atomistic-to-continuum and linearization limit [35, 123]. The aim of this note is that of extending the convergence analysis to the dynamic setting. Moving within the framework of [123], we prove that solutions of the equation of motion driven by atomistic deformation energies converge to the solutions of the momentum equation for the corresponding continuum energy of linearized elasticity. By recasting the evolution problems in their equivalent energy-dissipation-inertia-principle form, we directly argue at the variational level of evolutionary Γ-convergence [110, 119]. This in particular ensures the pointwise in time convergence of the energies.

3.1 Introduction

In recent years, the passage from atomistic models to continuum theories has attracted remarkable attention, originating a variety of different results, see [15, 23] for an overview. The interest in atomistic-to-continuum limits is grounded on the possibility of describing macroscopic behaviors starting from microscopic modeling. The latter relies in specifying interactions between displaced points, resulting from a deformation of a given reference lattice. The atomistic-to-continuum limit then ensues by letting the reference lattice spacing go to 0.

The elective tool to tackle these limits is Γ-convergence [22, 47], see for instance [3, 32]. Alternatively, more pointwise perspectives can be followed [16], which again may contribute to compute Γ-limits in specific cases. These tools were successfully applied to different situations, ranging from the modeling of lower-dimensional structures [28, 122, 124], to analyzing fracture and softening effects in one dimension [29, 31, 33, 121], to deriving cleavage laws in higher dimensions [68–70], to investigating systems of charged particles [108] and multi-body systems [10, 37]. Moreover, surface effects [33, 34, 50, 134], as well as random point clouds and stochastic lattices [4, 25, 118] were also studied using these techniques.

The main reference for our work is the stationary analysis by Braides, Solci, & Vitali [35] and Schmidt [123] who recover elasticity models as Γ-limits of atomistic energies. In both papers, the atomistic-to-continuum limit is combined with a small-deformation

limit, effectively resulting in a linear elastic limiting model. We refer to this combined limiting procedure as *atomistic-to-continuum linearization limit* in the sequel.

Following the general setting of [123], the focus of this note is to extend the atomistic-to-continuum linearization limit procedure to the evolutionary case. We first show that solutions to the equation of motion driven by the gradient of the atomistic deformation energy converge to the solution to the momentum equation for the limiting linear elastic energy by passing to the limit in the equations. By resorting to an equivalent variational formulation of the evolutionary problems in terms of the Energy-Dissipation-Inertia Principle, we present an evolutionary Γ-convergence analysis [24, 110, 119], as well. This entails in particular the pointwise in time convergence of the energies and the strong convergence of the gradients.

Let us mention that atomistic-to-continuum linearization in the evolutionary setting has already attracted some attention. The one-dimensional case is studied by Ortner [115] who proves that the limits of H^1-gradient flows of the Lennard-Jones potential give rise to H^1-gradient flows of an elastic energy.

The one-dimensional model is also considered by Braides, Defranceschi, & Vitali [30], who check that L^2-gradient flows of the Lennard-Jones potential under a different scaling give rise to gradient flows of the Mumford-Shah (or Griffith fracture) functional. Their analysis is based on an analogous limiting procedure at the level of time-discrete minimizing-movements approximations. Compared with these contributions, the novelties here are that the multidimensional case is tackled and inertial effects are taken into account.

Some instances of discrete-to-continuum limits in dynamics have already been considered. E & Ming [58] obtain a dynamic atomistic-to-continuum convergence result, in which they show that, as long as the deformation gradient stays inside a stability region, solutions to the discrete dynamical problem obtained by molecular mechanics are close to the nonlinear continuum problem obtained by the Cauchy-Born rule. A related result has been achieved by Ortner & Theil [114], who prove existence of solutions to the discrete and the nonlinear continuum problem for more general interaction energies and unbounded domains, and likewise quantify the difference in terms of the lattice spacing. Due to the nonlinear nature of the limiting problems and the absence of viscous regularization, in [58] and [114] existence of solutions can be guaranteed for short times only. Existence of global solutions in the bounded-domain case, as well as their asymptotic behavior, has been investigated by Braun [36]. In all mentioned results [36, 58, 114], regularity or smallness assumptions have to be imposed on data. On the contrary, our approach is nonperturbative, thus requiring less restrictions on the data.

Let us now describe our result more closely, postponing however most details to Section 3.2. We indicate by $\Omega \subset \mathbb{R}^d$ the macroscopic reference configuration of the specimen. At the atomistic level, the system consists of all points in Ω of the scaled d-dimensional Bravais lattice $\varepsilon\mathcal{L} := \varepsilon A \cdot \mathbb{Z}^d$, where $\varepsilon > 0$ models the interatomic distance and $A \in \mathbb{R}^{d\times d}$ is an invertible matrix. The atomistic energy $I_\varepsilon(y)$ of a *lattice deformation* $y : \Omega \cap \varepsilon\mathcal{L} \to$

$\mathbb{R}^d$ is modeled by

$$I_\varepsilon(y) = \varepsilon^d \det A \sum_{\text{cells}} W(\bar{\nabla} y) + \text{surface terms}.$$

The latter features the *discrete deformation gradient* $\bar{\nabla} y$, describing the relative displacement of the atoms of a single cell, see (3.5) below. The sum ranges over all scaled cells of the lattice portion $\Omega \cap \varepsilon\mathcal{L}$. The scaling $\varepsilon^d \det A$ corresponds to the volume of a single cell and the function W models the *elastic cell energy*, assumed to be suitably smooth. The treatment of surface energy terms is in general a delicate matter, see [123], and, for the sake of conciseness, will be simplified in this chapter by choosing homogeneous Dirichlet boundary conditions.

In the small-deformation setting, a second small parameter $\delta > 0$ is involved, quantifying the distance of deformations from the identity. More precisely, the atomistic model is rephrased in terms of the *scaled lattice displacement* $u := \delta^{-1}(y - \mathrm{id}) : \Omega \cap \varepsilon\mathcal{L} \to \mathbb{R}^d$ [48] and the energy is suitably rescaled as

$$I_{\varepsilon\delta}(u) = \frac{\varepsilon^d \det A}{\delta^2} \sum_{\text{cells}} W(Z + \delta \bar{\nabla} u) + \text{surface terms},$$

where Z denotes the discrete deformation gradient of id. The main result in [123] is the Γ-convergence of $I_{\varepsilon\delta}$ as $\varepsilon, \delta \to 0$ to the classical linear elastic energy

$$I(w) = \frac{1}{2} \int_\Omega \nabla^s w : \mathbb{C} : \nabla^s w \, \mathrm{d}x,$$

where $w \colon \Omega \to \mathbb{R}^d$ is now the *macroscopic displacement* of the body, $\nabla^s w := (\nabla w + \nabla w^\top)/2$ is its symmetrized gradient, and $\mathbb{C}$ the fourth-order *elasticity tensor*, which can be directly computed from W, see (3.11) below.

Our main result concerns the limiting behavior as $\varepsilon, \delta \to 0$ of the solutions to the atomistic equation of motion

$$\begin{cases} \rho \ddot{u}_{\varepsilon\delta}(t) + \nu \dot{u}_{\varepsilon\delta}(t) + \partial I_{\varepsilon\delta}(u_{\varepsilon\delta}(t)) = 0 \quad \forall t \in (0, T), & \text{(3.1a)} \\ u_{\varepsilon\delta}(0) = u^0_\varepsilon, & \text{(3.1b)} \\ \dot{u}_{\varepsilon\delta}(0) = u^1_\varepsilon, & \text{(3.1c)} \end{cases}$$

for some given initial scaled lattice displacement u^0_ε and velocity u^1_ε. Here, the gradient $\partial I_{\varepsilon\delta}$ of the smooth energy $I_{\varepsilon\delta}$ is computed with respect to a suitable finite dimensional, atomistic, L^2-like topology with norm $\|\cdot\|_\varepsilon$, see (3.6) below. It corresponds to the system of conservative forces acting on the discrete state. The constant $\nu > 0$ represents a friction coefficient, whereas $\rho > 0$ denotes the atomic mass. The case $\rho = 0$, corresponding to the purely viscous setting, is covered by our analysis, as well. In particular, $\nu \dot{u}_{\varepsilon\delta}$ is a linear friction term, modeling the interaction of the discrete system with the environment. System (3.1) corresponds to the time evolution of an elastic body under viscous damping. In one and two space dimensions, such damping may arise from some friction

effect, see [19, 82, 88] and the references therein. Note that (3.1) can be easily complemented with forces, which we however neglect for the sake of notational simplicity. In particular, the smooth Cauchy problem (3.1) for ODEs has a unique global solution $u_{\varepsilon\delta}$, cf. Remark 3.2.1.

We will prove that (suitable interpolations of) the atomistic trajectories $u_{\varepsilon\delta}$ converge as ε, $\delta \to 0$ to the unique weak solution $w\colon (0,T)\times\Omega \to \mathbb{R}^d$ of

$$\begin{cases} \rho\partial_{tt} w + \nu\partial_t w - \operatorname{div}(\mathbb{C} : \nabla^s w) = 0 & \text{in } (0,T)\times\Omega, \quad (3.2a)\\ w = 0 & \text{on } (0,T)\times\partial\Omega, \quad (3.2b)\\ w(0,\cdot) = w^0 & \text{in } \Omega, \quad (3.2c)\\ \partial_t w(0,\cdot) = w^1 & \text{in } \Omega, \quad (3.2d) \end{cases}$$

where w^0 and w^1 are suitable limits of u_ε^0 and u_ε^1, respectively. Due to the volume scaling in the energy, $\nu > 0$ is now interpreted as a friction coefficient, $\rho > 0$ is the mass density, whereas the case $\rho = 0$ corresponds to a purely viscous flow.

In order to prove convergence of solutions, we pass to the limit directly in the atomistic equation of motion (3.1a). To this end, we reformulate (3.1a) in terms of an energy-dissipation-inertia equality [120], namely,

$$\begin{aligned} &\frac{\rho}{2}\|\dot u_{\varepsilon\delta}(t)\|_\varepsilon^2 + I_{\varepsilon\delta}(u_{\varepsilon\delta}(t)) + \frac{1}{2\nu}\int_0^t \|\rho\ddot u_{\varepsilon\delta} + \partial I_{\varepsilon\delta}(u_{\varepsilon\delta})\|_\varepsilon^2 \,\mathrm{d}s + \frac{\nu}{2}\int_0^t \|\dot u_{\varepsilon\delta}\|_\varepsilon^2 \,\mathrm{d}s \\ &= \frac{\rho}{2}\|\dot u_{\varepsilon\delta}(0)\|_\varepsilon^2 + I_{\varepsilon\delta}(u_{\varepsilon\delta}(0)) \qquad \forall t\in[0,T]. \end{aligned} \tag{3.3}$$

From this we deduce uniform bounds, allowing to extract a weakly converging subsequence by compactness. The main work will then be that of identifying the limit. The crucial point is the discussion of the convergence of the terms $\rho\ddot u_{\varepsilon\delta}$ and $\partial I_{\varepsilon\delta}(u_{\varepsilon\delta})$, where the discrete structure of the atomistic problem comes into play. We will see that in the purely viscous case the analysis is simplified in several respects.

For proving energy convergence of solutions, and thus also strong convergence of gradients, we follow the classical evolutionary Γ-convergence approach pioneered by Sandier and Serfaty [119]. The energy-dissipation-inertia equation (3.3) is passed to the limit to obtain the corresponding equality for the momentum equation at the continuum level. This in turn hinges on the validity of some lim inf-inequalities, chain rules for the energies $I_{\varepsilon\delta}$ and I, and the so-called *well-preparedness* of initial data. For the validity of the chain rule, we require slightly stronger assumptions on the initial data, compared to the proof of convergence of solutions. Taking advantage of the Γ-convergence theory in [123], the main point will be that of checking

$$\begin{aligned} &\int_0^t \|\rho\partial_{tt} w(s,\cdot) + \partial I(w(s,\cdot))\|_{L^2(\Omega)}^2 \,\mathrm{d}s \\ &\le \liminf_{\varepsilon,\delta\to 0} \int_0^t \|\rho\ddot u_{\varepsilon\delta}(s,\cdot) + \partial I_{\varepsilon\delta}(u_{\varepsilon\delta}(s,\cdot))\|_\varepsilon^2 \,\mathrm{d}s \qquad \forall t\in[0,T], \end{aligned} \tag{3.4}$$

see inequality (3.16d) below.

The energy convergence entails the strong convergence of gradients and prevents oscillations in the sequence of atomistic solutions. This absence of oscillations can be mechanically interpreted as evidence for the validity of the classical Cauchy-Born hypothesis. In particular, microstructures are not expected to develop.

The chapter is organized as follows. In Section 3.2, we specify the lattice model and state the main result, namely the convergence of solutions and the evolutionary Γ-convergence, see Theorem 3.2.2. Section 3.3 is then devoted to the proof of the first part of Theorem 3.2.2, which is the convergence of solutions. We first recall some crucial results from [123] in Section 3.3.1 and then prove the convergence of solutions in Sections 3.3.2–3.3.6. In Section 3.4, we address the second part of Theorem 3.2.2, namely energy convergence. In Section 3.4.1, we establish the lim inf-inequalities, including (3.4), which are then used in Section 3.4.2 to conclude the argument.

3.2 Setting of the problem and main result

In this section, we introduce notation, present preliminaries, and state our main convergence result, namely Theorem 3.2.2. At first, we introduce the atomistic energy. We follow the setting of [123], upon restricting to the choice of homogeneous Dirichlet boundary conditions for simplicity.

Throughout the chapter, we denote the single contraction among vectors and tensors as $a \cdot b := a_i b_i$, $(A \cdot b)_i = A_{ij} b_j$, $(A \cdot B)_{ij} := A_{ik} B_{kj}$, $(\mathbb{C} \cdot A)_{ijkl} := \mathbb{C}_{ijkp} A_{pl}$, and $(A \cdot \mathbb{C})_{ijkl} := A_{ip} \mathbb{C}_{pjkl}$, where we employ Einstein's summation convention over repeated indices and tacitly assume that the dimension of the contracting index matches. The double contraction is denoted by $A : B := A_{ij} B_{ij}$, $(\mathbb{C} : A)_{ij} := \mathbb{C}_{ijkl} A_{kl}$, and $(A : \mathbb{C})_{ij} := A_{kl} \mathbb{C}_{klij}$ instead, again under the assumption that the dimensions of the contracting indices agree.

The transposed of the two-tensor A is classically denoted by $A^\top$, whereas we use the notation $\mathbb{C}^t$ to indicate the minor transposition of the four-tensor $\mathbb{C}$, in components $(\mathbb{C}^t)_{ijkl} = \mathbb{C}_{jikl}$. A four-tensor is called *(left) minor symmetric* if $\mathbb{C}^t = \mathbb{C}$, i.e., $\mathbb{C}_{ijkl} = \mathbb{C}_{jikl}$, and *major symmetric* if $\mathbb{C}_{ijkl} = \mathbb{C}_{klij}$.

3.2.1 Lattice model

Let $v_1, \dots, v_d \subset \mathbb{R}^d$, $d \geq 1$, be linearly independent vectors. Define the *Bravais lattice*

$$\mathcal{L} := A \cdot \mathbb{Z}^d := \{\lambda_1 v_1 + \dots + \lambda_d v_d : \lambda_1, \dots, \lambda_d \in \mathbb{Z}\}.$$

Here, the columns of the matrix $A = (v_1, \dots, v_d)$ consist of the vectors v_i, which we assume with no loss of generality to be ordered in such a way that $\det A > 0$. Let the small parameter $\varepsilon > 0$ measure the interatomic distance (see Figure 3.1) and define the *scaled* Bravais lattice $\mathcal{L}_\varepsilon := \varepsilon A \cdot \mathbb{Z}^d$. An *ε-cell* of the scaled lattice is a set of the form $\varepsilon A \cdot (\lambda + [0,1)^d)$ for some $\lambda \in \mathbb{Z}^d$. We denote the set of *barycenters of ε-cells* by $\mathcal{L}'_\varepsilon := \varepsilon A \cdot \big((1/2, \dots, 1/2) + \mathbb{Z}^d\big)$. Moreover, we indicate by $Z = (z_1, \dots, z_{2^d}) \in \mathbb{R}^{d \times 2^d}$

a fixed *labeling* of the 2^d corner points of the *reference cell* $A \cdot \{-1/2, 1/2\}^d$, so that $\mathcal{L}_\varepsilon = \mathcal{L}'_\varepsilon + \varepsilon\{z_1, \dots, z_{2^d}\}$.

Let $\Omega \subset \mathbb{R}^d$ be a bounded domain with $C^{1,1}$ boundary. For every $x \in \Omega$, we denote by $\overline{x}(x,\varepsilon) \in \mathcal{L}'_\varepsilon$ the barycenter of the ε-cell containing x and correspondingly by $Q_\varepsilon(x) := \overline{x}(x,\varepsilon) + A \cdot [-\varepsilon/2, \varepsilon/2)^d$ the ε-cell containing x, see Figure 3.1. In particular, for $\bar{x} \in \mathcal{L}'_\varepsilon$, we have $Q_\varepsilon(\overline{x}) = \overline{x} + A \cdot [-\varepsilon/2, \varepsilon/2)^d$ and for $x \in \mathcal{L}_\varepsilon$, we have $Q_\varepsilon(x) = x + A \cdot [0, \varepsilon)^d$.

At the atomistic level, the central objects are *lattice deformations* $y\colon \mathcal{L}_\varepsilon \cap \Omega \to \mathbb{R}^d$, describing the response of each lattice point in Ω to mechanical actions. We impose homogeneous Dirichlet conditions on the whole boundary in the following sense: let $\widetilde{\Omega} \subset \mathbb{R}^d$ be a bounded open set with $\Omega \subset\subset \widetilde{\Omega}$ (compactly contained). Given a lattice deformation $y\colon \mathcal{L}_\varepsilon \cap \Omega \to \mathbb{R}^d$, we extend it to $\mathcal{L}_\varepsilon \cap \widetilde{\Omega}$ by setting $y(x) = x$ for $x \in \mathcal{L}_\varepsilon \cap (\widetilde{\Omega} \setminus \Omega)$. This choice of boundary conditions is meant to simplify notations. It is possible to also consider nonhomogeneous Dirichlet conditions or even Neumann-like conditions, see [123]. This would however require some additional modeling choice and a more technical treatment.

We denote the set of *barycenters of ε-cells inside* $\widetilde{\Omega}$ by $\mathcal{L}'_\varepsilon(\widetilde{\Omega}) := \{\overline{x} \in \mathcal{L}'_\varepsilon\colon \overline{Q_\varepsilon(\overline{x})} \subset \widetilde{\Omega}\}$ and abbreviate the union of cells which are fully contained in $\widetilde{\Omega}$ by $\bigcup Q_\varepsilon := \bigcup_{\overline{x} \in \mathcal{L}'_\varepsilon(\widetilde{\Omega})} Q_\varepsilon(\overline{x})$. For $y\colon \mathcal{L}_\varepsilon \cap \widetilde{\Omega} \to \mathbb{R}^d$ and $x \in Q_\varepsilon(\overline{x})$ with $\overline{x} \in \mathcal{L}'_\varepsilon(\widetilde{\Omega})$, we collect the deformations $y_i = y_i(x) := y(\overline{x} + \varepsilon z_i)$ of corner points, and define the *discrete gradient* $\bar{\nabla} y\colon \widetilde{\Omega} \to \mathbb{R}^{d \times 2^d}$ of y as

$$\bar{\nabla} y(x) := \varepsilon^{-1}(y_1 - \overline{y}, \dots, y_{2^d} - \overline{y}) \quad \text{with} \quad \overline{y} := \frac{1}{2^d} \sum_{i=1}^{2^d} y_i, \tag{3.5}$$

for $x \in \bigcup Q_\varepsilon$ and $\bar{\nabla} y(x) = 0$ for $x \in \widetilde{\Omega} \setminus \bigcup Q_\varepsilon$. As the discrete gradient is constant on individual cells, in the following we often indicate its argument simply by $\overline{x}$, that is, the barycenter of such a cell.

The energy is defined in terms of the *lattice displacement*, namely, $u := y - \mathrm{id}$, where id indicates the identity mapping on $\mathbb{R}^d$. In order to address the regime of small deformations, we consider the *scaled lattice displacement* $u = \delta^{-1}(y - \mathrm{id})$, where $\delta > 0$ is a small parameter, and define the set of *admissible (scaled lattice) displacements* as

$$\mathcal{A}_\varepsilon := \big\{u : \mathcal{L}_\varepsilon \cap \widetilde{\Omega} \to \mathbb{R}^d : u(x) = 0 \text{ for } x \notin \Omega\big\}.$$

Then, the *scaled atomistic energy* $I_{\varepsilon\delta} : \mathcal{A}_\varepsilon \to \mathbb{R}$ is defined as

$$I_{\varepsilon\delta}(u) := \frac{\varepsilon^d \det A}{\delta^2} \sum_{\overline{x} \in \mathcal{L}'_\varepsilon(\widetilde{\Omega})} W(Z + \delta \bar{\nabla} u(\overline{x})),$$

where the *elastic cell energy* W of the configuration only depends on the discrete gradient. The factor $\varepsilon^d \det A$ in the definition of $I_{\varepsilon\delta}$ corresponds to the volume of a single scaled cell, whereas the scaling δ^{-2} is instrumental for the setting of small displacements. Let $\mathrm{SO}(d) := \{Q \in \mathbb{R}^{d\times d}\colon Q^\top \cdot Q = \mathrm{Id}, \det Q = 1\}$ be the standard special orthogonal group.

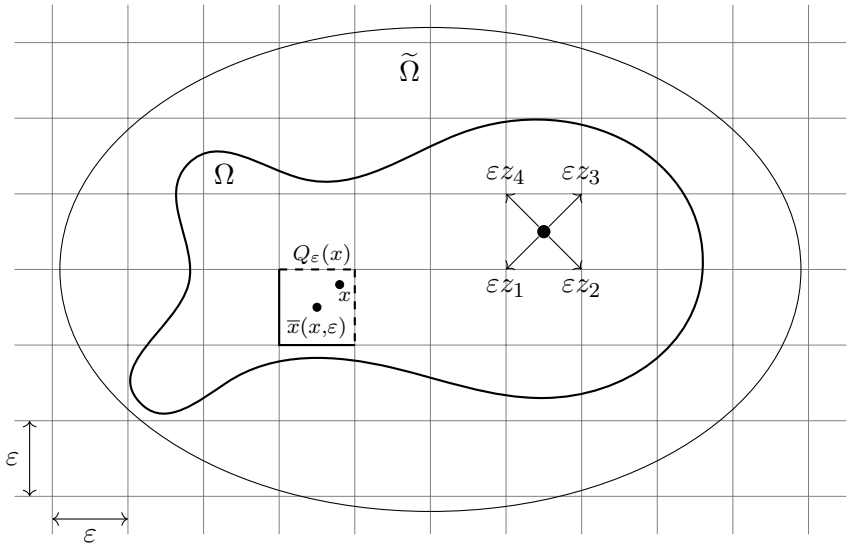

Figure 3.1: Scaled reference configuration of the atomistic system. Here, the lattice is $\mathcal{L}_\varepsilon = \varepsilon\mathbb{Z}^2$, i.e., A is the identity matrix. The labeling of the corner points of a scaled cell is indicated by the vectors εz_i, $i = 1, \dots, 4$.

Assumption 3.2.1. *We impose the following assumptions on the cell energy W.*

(i) *The cell energy $W\colon \mathbb{R}^{d\times 2^d} \to [0,\infty]$ is invariant under translations and rotations, that is, given $F \in \mathbb{R}^{d\times 2^d}$ we have that*

$$W\big(R\cdot F + \underbrace{(c,\dots,c)}_{2^d-\text{times}}\big) = W(F)$$

holds for all $R \in \mathrm{SO}(d)$ and $c \in \mathbb{R}^d$.

(ii) *$W(F) = 0$ if and only if there exists a rotation $R \in \mathrm{SO}(d)$ and a translation $c \in \mathbb{R}^d$ such that $F_i = R\cdot z_i + c$.*

(iii) *W is $\mathcal{C}^2$ and the Hessian $\mathbb{H} := D^2W(Z) \in \mathbb{R}^{d\times 2^d\times d\times 2^d}$ is positive definite on the orthogonal complement of the subspace spanned by infinitesimal translations $(x_1,\dots,x_{2^d}) \mapsto (c,\dots,c)$ and infinitesimal rotations $(x_1,\dots,x_{2^d}) \mapsto (S\cdot x_1,\dots,S\cdot x_{2^d})$, where $c \in \mathbb{R}^d$ and $S \in \mathbb{R}^{d\times d}_{\mathrm{skew}} := \{F \in \mathbb{R}^{d\times d}\colon F + F^\top = 0\}$.*

(iv) *W grows at infinity at least quadratically on the orthogonal complement of the subspace spanned by infinitesimal translations, i.e.,*

$$\liminf_{\substack{|F|\to\infty,\\ F\in V}} \frac{W(F)}{|F|^2} > 0,$$

with $V = \{F \in \mathbb{R}^{d\times 2^d}\colon F_1 + \dots + F_{2^d} = 0\}$.

(v) *The gradient of the cell energy grows at most quadratically, i.e.,* $|DW(F)| \leq c|F|^2 + c$ *for all* $F \in \mathbb{R}^{d\times 2^d}$ *for some constant* $c > 0$.

Assumptions 3.2.1 (i)–(iv) have already been considered by Schmidt [123] in the stationary setting and allow to characterize the Γ-limit of $I_{\varepsilon\delta}$ as $\varepsilon, \delta \to 0$. In this chapter, we strengthen the setting by additionally assuming Assumption 3.2.1 (v). This is needed for dealing with the gradients of the energies.

3.2.2 Main result

We start by defining the *atomistic* L^2*-inner product* $(\cdot,\cdot)_\varepsilon$ on the space of scaled lattice displacements. Given $u_\varepsilon, v_\varepsilon \colon \mathcal{L}_\varepsilon \cap \widetilde{\Omega} \to \mathbb{R}^d$, we define

$$(u_\varepsilon, v_\varepsilon)_\varepsilon := \varepsilon^d \det A \sum_{x\in\mathcal{L}_\varepsilon\cap\widetilde{\Omega}} u_\varepsilon(x)\cdot v_\varepsilon(x) \tag{3.6}$$

and denote the corresponding *atomistic* L^2*-norm* by $\|u_\varepsilon\|_\varepsilon := \sqrt{(u_\varepsilon,u_\varepsilon)_\varepsilon}$.

We look for a solution $u_{\varepsilon\delta}\colon [0,T]\times(\mathcal{L}_\varepsilon\cap\widetilde{\Omega}) \to \mathbb{R}^d$ with $u_{\varepsilon\delta}(\cdot,x) \in \mathcal{C}^2([0,T];\mathbb{R}^d)$ for all $x \in \mathcal{L}_\varepsilon\cap\widetilde{\Omega}$, and $u_{\varepsilon\delta}(t,\cdot) \in \mathcal{A}_\varepsilon$ for all $t\in[0,T]$ to the *atomistic equation of motion*

$$\begin{cases} \rho\ddot{u}_{\varepsilon\delta}(t,x) + \nu\dot{u}_{\varepsilon\delta}(t,x) + \partial I_{\varepsilon\delta}(u_{\varepsilon\delta}(t,x)) = 0 & \forall x\in\mathcal{L}_\varepsilon\cap\widetilde{\Omega},\ \forall t\in(0,T), \quad (3.7a)\\ u_{\varepsilon\delta}(0,x) = u_\varepsilon^0(x) & \forall x\in\mathcal{L}_\varepsilon\cap\widetilde{\Omega}, \quad (3.7b)\\ \dot{u}_{\varepsilon\delta}(0,x) = u_\varepsilon^1(x) & \forall x\in\mathcal{L}_\varepsilon\cap\widetilde{\Omega}, \quad (3.7c) \end{cases}$$

where $u_\varepsilon^0, u_\varepsilon^1 \in \mathcal{A}_\varepsilon$ are given *initial scaled lattice displacement* and *velocity*, respectively, $\rho > 0$ corresponds to the atomic mass, and $\nu > 0$ is a friction coefficient. The case $\rho = 0$ is also considered and corresponds to the purely viscous setting. Here, $\partial I_{\varepsilon\delta}(u_{\varepsilon\delta})$ indicates the first variation of $I_{\varepsilon\delta}$ in $\mathcal{A}_\varepsilon$ at $u_{\varepsilon\delta}$, that is,

$$\begin{aligned} &\partial I_{\varepsilon\delta} : (\mathcal{A}_\varepsilon, \|\cdot\|_\varepsilon) \to (\mathcal{A}_\varepsilon, \|\cdot\|_\varepsilon)^*\\ &u_{\varepsilon\delta} \mapsto \partial I_{\varepsilon\delta}(u_{\varepsilon\delta}), \end{aligned}$$

where, for each $v_\varepsilon \in \mathcal{A}_\varepsilon$,

$$\begin{aligned} \langle \partial I_{\varepsilon\delta}(u_{\varepsilon\delta}), v_\varepsilon\rangle :=& \frac{\mathrm{d}}{\mathrm{d}h} I_{\varepsilon\delta}(u_{\varepsilon\delta} + hv_\varepsilon)\big|_{h=0}\\ =& \varepsilon^d \det A \sum_{\overline{x}\in\mathcal{L}_\varepsilon'(\widetilde{\Omega})} \frac{1}{\delta} DW(Z + \delta\bar{\nabla}u_{\varepsilon\delta}(\overline{x})) : \bar{\nabla}v_\varepsilon(\overline{x}). \end{aligned} \tag{3.8}$$

The homogeneous Dirichlet boundary conditions entail the validity of a discrete divergence theorem, see Lemma 3.5.1. Hence, we can also interpret $\partial I_{\varepsilon\delta}(u_{\varepsilon\delta}) : \mathcal{L}_\varepsilon\cap\widetilde{\Omega} \to \mathbb{R}^d$ as the unique scaled lattice strain satisfying

$$\langle \partial I_{\varepsilon\delta}(u_{\varepsilon\delta}), v_\varepsilon\rangle = (\partial I_{\varepsilon\delta}(u_{\varepsilon\delta}), v_\varepsilon)_\varepsilon \qquad \text{for all } v_\varepsilon \in \mathcal{A}_\varepsilon. \tag{3.9}$$

As $\mathcal{L}_\varepsilon \cap \widetilde{\Omega}$ is a finite point set, problem (3.7) is nothing but a Cauchy problem for a smooth ODE system, see also Remark 3.2.1 below. It hence admits a unique global solution. Indeed, local well-posedness of (3.7) follows from the classical Picard-Lindelöf theorem. From the energy-dissipation-inertia equality (3.3) corresponding to the atomistic problem (3.7) one can derive bounds ensuring that $I_{\varepsilon\delta}(u_{\varepsilon\delta})$ remains bounded along the trajectories. From the coercivity in Assumption 3.2.1 (iv) one obtains that trajectories are bounded, see Theorem 3.3.1 below. Thus, the solution is global in time.

Remark 3.2.1. To clarify that the atomistic equation of motion (3.7) can indeed be interpreted as an ODE system, let N_ε be the number of atoms in $\mathcal{L}_\varepsilon \cap \Omega$ and $x_1, \dots, x_{N_\varepsilon}$ some corresponding labeling. Given a scaled lattice displacement $u_{\varepsilon\delta} \in \mathcal{A}_\varepsilon$, let $U_{\varepsilon\delta} := (u_1, \dots, u_{N_\varepsilon}) \in \mathbb{R}^{d\times N_\varepsilon}$ be the vector of the displaced atoms, where $u_i = u_{\varepsilon\delta}(x_i)$ for $i = 1, \dots, N_\varepsilon$. This defines a linear isomorphism $\iota\colon \mathcal{A}_\varepsilon \to \iota(\mathcal{A}_\varepsilon) \subset \mathbb{R}^{d\times N_\varepsilon}$.

The scaled atomistic energy can be equivalently rewritten as $\widetilde{I}_{\varepsilon\delta}(U_{\varepsilon\delta}) := I_{\varepsilon\delta}(\iota^{-1}(U_{\varepsilon\delta})) = I_{\varepsilon\delta}(u_{\varepsilon\delta})$. Then, problem (3.7) is equivalent to finding $U_{\varepsilon\delta}(t) = \iota(u_{\varepsilon\delta}(t))$ satisfying

$$\begin{cases} \rho\ddot{U}_{\varepsilon\delta}(t) + \nu\dot{U}_{\varepsilon\delta}(t) + \nabla\widetilde{I}_{\varepsilon\delta}(U_{\varepsilon\delta}(t)) = 0 \quad \forall t \in (0,T), \\ U_{\varepsilon\delta}(0) = U^0_\varepsilon, \\ \dot{U}_{\varepsilon\delta}(0) = U^1_\varepsilon, \end{cases}$$

where $U^0_\varepsilon = \iota(u^0_\varepsilon)$, $U^1_\varepsilon = \iota(u^1_\varepsilon)$, and $\nabla\widetilde{I}_{\varepsilon\delta} = \iota(\partial I_{\varepsilon\delta}(u_{\varepsilon\delta}))$.

The goal of this chapter is to show that solutions $u_{\varepsilon\delta}$ to the atomistic equation of motion (3.7) converge as $\varepsilon, \delta \to 0$ to the unique weak solution of the *linear continuum momentum balance*

$$\begin{cases} \rho\partial_{tt}w + \nu\partial_t w - \operatorname{div}(\mathbb{C} : \nabla^s w) = 0 & \text{in } (0,T)\times\Omega, & \text{(3.10a)} \\ w = 0 & \text{a.e. in } (0,T)\times\partial\Omega, & \text{(3.10b)} \\ w(0,\cdot) = w^0 & \text{a.e. in } \Omega, & \text{(3.10c)} \\ \partial_t w(0,\cdot) = w^1 & \text{a.e. in } \Omega, & \text{(3.10d)} \end{cases}$$

where $w^0 \in H^1_0(\Omega;\mathbb{R}^d)$ and $w^1 \in L^2(\Omega;\mathbb{R}^d)$ are the given *initial continuum displacement* and the *initial continuum velocity*, respectively. The fourth-order symmetric *elasticity tensor* $\mathbb{C}$ is defined as

$$\mathbb{C} := Z \cdot \mathbb{H}^t \cdot Z^\top = Z \cdot D^2W(Z)^t \cdot Z^\top \in \mathbb{R}^{d\times d\times d\times d}, \tag{3.11}$$

and we recall that $\nabla^s w := (\nabla w + \nabla w^\top)/2$ denotes the symmetrized gradient. In particular, $\mathbb{C}$ is solely determined by microscopic quantities and $\mathbb{C}$ is minor and major symmetric, see Assumptions 3.2.1 (iii) and Lemma 3.3.3 below.

We say that $w \in L^2(0,T;H^1_0(\Omega;\mathbb{R}^d)) \cap H^1(0,T;L^2(\Omega;\mathbb{R}^d)) \cap H^2(0,T;H^{-1}(\Omega;\mathbb{R}^d))$ is a *weak solution to* (3.10) if it satisfies $w(0) = w^0$, $\partial_t w(0) = w^1$, and

$$\langle\rho\partial_{tt}w, v\rangle_{H^1_0} + (\nu\partial_t w, v)_{L^2} + \int_\Omega \nabla^s w : \mathbb{C} : \nabla^s v \,\mathrm{d}x = 0 \quad \text{a.e. in } (0,T),$$

and for all $v \in H^1_0(\Omega;\mathbb{R}^d)$, where $(\cdot,\cdot)_{L^2}$ denotes the L^2-inner product and $\langle\cdot,\cdot\rangle_{H^1_0}$ the duality in H^1_0. In system (3.10), the term $-\operatorname{div}(\mathbb{C} : \nabla^s w)$ is hence interpreted in the weak H^1-sense and corresponds to the H^1-gradient ∂I of I, i.e., the Fréchet differential of the *linearized continuum energy* $I\colon H^1_0(\Omega;\mathbb{R}^d) \to \mathbb{R}$ given by

$$I(w) := \frac{1}{2}\int_\Omega (\nabla w \cdot Z) : \mathbb{H} : (\nabla w \cdot Z)\,\mathrm{d}x = \frac{1}{2}\int_\Omega \nabla^s w : \mathbb{C} : \nabla^s w\,\mathrm{d}x. \tag{3.12}$$

In particular, $\partial I : H^1_0(\Omega;\mathbb{R}^d) \to H^{-1}(\Omega;\mathbb{R}^d)$ is given by

$$\langle \partial I(w), v\rangle = \frac{\mathrm{d}}{\mathrm{d}h} I(w+hv)\big|_{h=0} = \int_\Omega (\nabla w \cdot Z) : \mathbb{H} : (\nabla v \cdot Z)\,\mathrm{d}x = \int_\Omega \nabla^s w : \mathbb{C} : \nabla^s v\,\mathrm{d}x.$$

We derive the formula above in Section 3.3.2 below, see (3.19).

In order to formulate our statement, we need to specify a notion of convergence for a sequence of scaled lattice displacements $u_\varepsilon\colon \mathcal{L}_\varepsilon \cap \widetilde{\Omega} \to \mathbb{R}^d$. Let $w \in L^2(\Omega;\mathbb{R}^d)$ be a continuum displacement and define its local mean on the lattice cells by

$$P_\varepsilon w(x) := \fint_{Q_\varepsilon(x)} \widetilde{w}(\xi)\,\mathrm{d}\xi \quad \forall x \in \mathcal{L}_\varepsilon \cap \widetilde{\Omega}, \tag{3.13}$$

where $\widetilde{w}\colon \widetilde{\Omega} \to \mathbb{R}^d$ is the trivial extension of w to $\widetilde{\Omega}$. We say that u_ε AC-*converges* to w and write $u_\varepsilon \overset{\mathrm{AC}}{\to} w$ (AC stands for *atomistic-to-continuum* convergence) as $\varepsilon \to 0$ if

$$\|u_\varepsilon - P_\varepsilon w\|_\varepsilon \to 0. \tag{3.14}$$

The main result of this chapter is the following.

Theorem 3.2.2 (Discrete-to-continuum linearization)**.** *Suppose that Assumption 3.2.1 holds and let ε_k and δ_k be such that $\varepsilon_k \to 0$ and $\delta_k \to 0$.*
Convergence of solutions: *Let $u^0_\varepsilon, u^1_\varepsilon \in \mathcal{A}_\varepsilon$ be an initial scaled lattice displacement and velocity, and let $w^0 \in H^1_0(\Omega;\mathbb{R}^d)$, $w^1 \in L^2(\Omega;\mathbb{R}^d)$ be an initial continuum displacement and velocity, respectively. If $u^0_{\varepsilon_k} \overset{\mathrm{AC}}{\to} w^0$, $u^1_{\varepsilon_k} \overset{\mathrm{AC}}{\to} w^1$ as $k \to \infty$ and $\sup_k I_{\varepsilon_k\delta_k}(u^0_{\varepsilon_k}) < +\infty$, then the solutions $(u_{\varepsilon_k\delta_k})_k$ to the atomistic equation of motion (3.7) AC-converge to w pointwise in time, where w is the unique weak solution to the continuum momentum equation (3.10).*
Energy convergence: *If, additionally, $w^0 \in H^2(\Omega;\mathbb{R}^d)$, $w^1 \in H^1(\Omega;\mathbb{R}^d)$, and $I_{\varepsilon_k\delta_k}(u^0_{\varepsilon_k}) \to I(w^0)$ as $k \to \infty$, then the solutions $(u_{\varepsilon_k\delta_k})_k$ to the atomistic equation of motion additionally satisfy the convergences $I_{\varepsilon_k\delta_k}(u_{\varepsilon_k\delta_k}(t)) \to I(w(t))$ for all $t \in [0,T]$ and $\bar{\nabla} u_{\varepsilon_k\delta_k}(t) \to \nabla w(t) \cdot Z$ strongly in $L^2(\Omega;\mathbb{R}^d)$ for all $t \in (0,T)$. Moreover, w is a strong solution of (3.10).*

In order to prove the first part of Theorem 3.2.2, i.e., the convergence of solutions, we pass to the limit in the atomistic equation of motion (3.7). To this end, we need to deduce uniform bounds on the individual terms of the atomistic equation of motion.

This is achieved by the energy-dissipation-inertia equality (3.3), which in the notation of Theorem 3.2.2 reads as

$$\frac{\rho}{2}\|\dot{u}_{\varepsilon_k\delta_k}(t)\|^2_{\varepsilon_k} + I_{\varepsilon_k\delta_k}(u_{\varepsilon_k\delta_k}(t)) + \frac{\nu}{2}\int_0^t \|\dot{u}_{\varepsilon_k\delta_k}(s)\|^2_{\varepsilon_k}\,\mathrm{d}s \\ + \frac{1}{2\nu}\int_0^t \|\rho\ddot{u}_{\varepsilon_k\delta_k}(s) + \partial I_{\varepsilon_k\delta_k}(u_{\varepsilon_k\delta_k}(s))\|^2_{\varepsilon_k}\,\mathrm{d}s = \frac{\rho}{2}\|u^1_{\varepsilon_k}\|^2_{\varepsilon_k} + I_{\varepsilon_k\delta_k}(u^0_{\varepsilon_k}) \tag{3.15}$$

for all $t \in [0,T]$, see Section 3.3.3 for its derivation.

On the contrary, we prove the second part of Theorem 3.2.2 by following the classical evolutive Γ-convergence approach pioneered by Sandier and Serfaty [119], see also [110, 115]. This hinges on the fact that the atomistic evolution problem (3.7) is actually equivalent to (3.15). One passes to the lim inf in the latter as $k \to \infty$. The right-hand side converges by assumption to $\frac{\rho}{2}\|w^1\|^2_{L^2(\Omega)} + I(w^0)$. As regards the terms in the left-hand side, we will check that, for each $t \in [0,T]$,

$$\|\partial_t w(t)\|^2_{L^2(\Omega)} \le \liminf_{k\to\infty} \|\dot{u}_{\varepsilon_k\delta_k}(t)\|^2_{\varepsilon_k}, \tag{3.16a}$$

$$\int_0^t \|\partial_t w(s)\|^2_{L^2(\Omega)}\,\mathrm{d}s \le \liminf_{k\to\infty} \int_0^t \|\dot{u}_{\varepsilon_k\delta_k}(s)\|^2_{\varepsilon_k}\,\mathrm{d}s, \tag{3.16b}$$

$$I(w(t)) \le \liminf_{k\to\infty} I_{\varepsilon_k\delta_k}(u_{\varepsilon_k\delta_k}(t)), \tag{3.16c}$$

$$\int_0^t \|\rho\partial_{tt} w(s) + \partial I(w(s))\|^2_{L^2(\Omega)}\,\mathrm{d}s \\ \le \liminf_{k\to\infty} \int_0^t \|\rho\ddot{u}_{\varepsilon_k\delta_k}(s) + \partial I_{\varepsilon_k\delta_k}(u_{\varepsilon_k\delta_k}(s))\|^2_{\varepsilon_k}\,\mathrm{d}s. \tag{3.16d}$$

Then, taking the lim inf as $k \to \infty$ in equality (3.15) will entail that the following energy-dissipation-inertia (in)equality holds

$$\frac{\rho}{2}\|\partial_t w(t)\|^2_{L^2(\Omega)} + I(w(t)) + \frac{\nu}{2}\int_0^t \|\partial_t w(s)\|^2_{L^2(\Omega)}\,\mathrm{d}s \\ + \frac{1}{2\nu}\int_0^t \|\rho\partial_{tt} w(s) + \partial I(w(s))\|^2_{L^2(\Omega)}\,\mathrm{d}s \le \frac{\rho}{2}\|w^1\|^2_{L^2(\Omega)} + I(w^0) \qquad \forall t \in [0,T].$$

As long as the initial conditions $w(0) = w^0$ and $\partial_t w(0) = w^1$ are satisfied, the latter is indeed equivalent to the corresponding equality, as well as to linear continuum momentum balance (3.10). We refer to Section 3.3.3 below where the precise argument is given for the discrete problem. This additionally implies that each lim inf in (3.16) is actually a limit. In particular, the energy $I_{\varepsilon_k\delta_k}(u_{\varepsilon_k\delta_k}(t))$ converges to $I(w(t))$ at all times, which eventually implies that $\bar{\nabla} u_{\varepsilon_k\delta_k}(t) \to \nabla w(t) \cdot Z$ strongly in $L^2(\Omega;\mathbb{R}^{d\times 2^d})$, as well.

Remark 3.2.3 (Purely viscous case). Theorem 3.2.2 above directly extends to the purely viscous setting of $\rho = 0$. In this case, the continuum problem (3.10) corresponds to a gradient flow and, assuming the milder regularity assumptions $w^0 \in H^1_0(\Omega;\mathbb{R}^d)$ and

$w^1 \in L^2(\Omega;\mathbb{R}^d)$, we can show that $\operatorname{div}(\mathbb{C} : \nabla^s w) \in L^2(0,T;L^2(\Omega;\mathbb{R}^d))$, see Remark 3.4.4 below. Hence, $-\operatorname{div}(\mathbb{C} : \nabla^s w)$ is the L^2-gradient of the elastic continuum energy I, given in (3.12). In particular, we obtain strong solutions for the continuum problem and strong convergence of gradients without the higher regularity assumption on the initial data. The proof can be simplified as inequality (3.16d) directly follows from Lemma 3.3.10 below. We refer to Remarks 3.4.1 and 3.4.4 for details.

3.3 Convergence of solutions

In this section, we prove the first part of Theorem 3.2.2, namely, the convergence of solutions. To this end, we derive uniform bounds from the energy-dissipation-inertia equality (3.15) and use compactness to obtain converging subsequences. The main focus is then on identifying limits.

For the reader's convenience, the argument is divided into steps. In Section 3.3.1, we start by recalling the compactness and Γ-convergence result of [123]. In Section 3.3.2, ∂I is computed and we further peruse properties of scaled lattice displacements. In Section 3.3.3, we derive (3.15) and state the resulting a priori estimates. Sections 3.3.4 and 3.3.5 are then devoted to computing the limits of $\nu\dot{u}_{\varepsilon_k\delta_k}$ and $\rho\ddot{u}_{\varepsilon_k\delta_k} + \partial I_{\varepsilon_k\delta_k}(u_{\varepsilon_k\delta_k})$, respectively. We conclude the proof in Section 3.3.6.

In the remainder of the chapter, given the sequences $\varepsilon_k, \delta_k \to 0$ with $k \to \infty$ from Theorem 3.2.2, we use the short-hand notation $I_k := I_{\varepsilon_k\delta_k}$, $u_k := u_{\varepsilon_k\delta_k}$, $(\cdot,\cdot)_k := (\cdot,\cdot)_{\varepsilon_k}$, and $\|\cdot\|_k := \|\cdot\|_{\varepsilon_k}$. Throughout this chapter, c denotes a positive constant, independent of k, but possibly varying from line to line. Moreover, we will denote the standard L^2-inner product by $(\cdot,\cdot)$ and denote duality pairings between the space X and its dual X^* by $\langle\cdot,\cdot\rangle_X : X^* \times X \to \mathbb{R}$. For $X = H^1_0(\Omega;\mathbb{R}^d)$, we will simply write $\langle\cdot,\cdot\rangle_{H^1_0} =: \langle\cdot,\cdot\rangle$.

3.3.1 Γ-convergence and compactness

In this section, we briefly summarize the Γ-convergence and compactness result by Schmidt [123], for these are crucial ingredients in the proof of Theorem 3.2.2.

Theorem 3.3.1 ([123, Theorem 2.6])**.** *Under Assumptions 3.2.1 we have the following:*

Compactness: *If $I_k(u_k)$ is equibounded for some sequence $(u_k)_k$ of scaled lattice displacements, then there exists a (not relabeled) subsequence such that $u_k \overset{\mathrm{AC}}{\to} w$ for some $w \in H^1_0(\Omega;\mathbb{R}^d)$. Moreover, $\bar{\nabla} u_k \rightharpoonup \nabla\widetilde{w} \cdot Z$ weakly in $L^2(\widetilde{\Omega};\mathbb{R}^{d\times 2^d})$, where $\widetilde{w}\colon \widetilde{\Omega} \to \mathbb{R}^d$ is the trivial extension of w to $\widetilde{\Omega}$.*

Γ-convergence: *The functionals I_k Γ-converge to the functional I in the sense of* AC*-convergence, i.e., the following is satisfied:*

(i) lim inf-inequality: *Every sequence $(u_k)_k$, $u_k \in \mathcal{A}_{\varepsilon_k}$,* AC*-converging to some $w \in H^1_0(\Omega;\mathbb{R}^d)$ satisfies the estimate*

$$\liminf_{k\to\infty} I_k(u_k) \geq I(w).$$

(ii) Recovery sequence: *For every* $w \in H^1_0(\Omega;\mathbb{R}^d)$ *there exists a sequence* $(u_k)_k$, $u_k \in \mathcal{A}_{\varepsilon_k}$, *such that* $u_k \overset{\mathrm{AC}}{\to} w$ *and*

$$\lim_{k\to\infty} I_k(u_k) = I(w).$$

Remark 3.3.2. The Γ-convergence and compactness result can be extended in various directions:

a) For recovery sequences, that are sequences $u_k \overset{\mathrm{AC}}{\to} w \in H^1_0(\Omega;\mathbb{R}^d)$ such that $I_k(u_k) \to I(w)$, one can also obtain strong convergence of discrete gradients, see [123, Theorem 2.7].

b) AC-convergence (3.14) is equivalent to the classical L^2-convergence for suitable interpolations, see for instance Lemma 3.3.6 below. The Γ-convergence result above could be equivalently reformulated to hold with respect to the strong L^2- or the weak H^1-topology for such interpolations.

c) The compactness statement in Theorem 3.3.1 hinges on the fact that Dirichlet boundary conditions are imposed on the whole $\partial\Omega$. By imposing Dirichlet conditions on a part of $\partial\Omega$ only, one could only conclude local weak L^2_{loc}-convergence of the discrete gradients. As already mentioned, other boundary conditions could be considered as well, by resorting to the theory in [123].

3.3.2 Gradients of the energy and auxiliary results

In order to prove convergence of solutions, we aim at showing the weak convergence of the Fréchet differential ∂I in a suitable dual space. Due to the varying underlying spaces, implementing this strategy requires some care. We show that, for a suitable sequence $v_k \overset{\mathrm{AC}}{\to} v$, the Gâteaux derivatives in direction v_k converge (Lemma 3.3.10 below). To this end, we introduce an approximation of test functions by scaled lattice displacements and study their properties.

We start by computing the Fréchet differential of I in Section 3.3.2. In Section 3.3.2, we address the approximation by scaled lattice displacements.

Fréchet differential of I

Recall that the Hessian of W evaluated at Z is $\mathbb{H} := D^2W(Z)$ and therefore $\mathbb{H}$ is major symmetric, namely, $\mathbb{H}_{ijkl} = \mathbb{H}_{klij}$.

Given $w \in H^1_0(\Omega;\mathbb{R}^d)$ and $v \in \mathcal{C}^\infty_{\mathrm{c}}(\Omega;\mathbb{R}^d)$, the variation of I in $H^1(\Omega;\mathbb{R}^d)$ at w in direction v can be classically computed as

$$\begin{aligned}\langle \partial I(w), v\rangle &= \frac{\mathrm{d}}{\mathrm{d}h} I(w+hv)\big|_{h=0}\\ &= \frac{1}{2}\int_\Omega \frac{\mathrm{d}}{\mathrm{d}h}\Big(\big((\nabla w + h\nabla v)\cdot Z\big)\colon \mathbb{H} \colon \big((\nabla w + h\nabla v)\cdot Z\big)\Big)\Big|_{h=0}\,\mathrm{d}x.\end{aligned}$$

Due to the major symmetry of $\mathbb{H}$, one readily checks that

$$\frac{\mathrm{d}}{\mathrm{d}h}\Big(\big((\nabla w + h\nabla v)\cdot Z\big)\colon \mathbb{H} \colon \big((\nabla w + h\nabla v)\cdot Z\big)\Big)\Big|_{h=0} = 2(\nabla w\cdot Z) : \mathbb{H} : (\nabla v \cdot Z).$$

Therefore, we deduce that

$$\langle \partial I(w), v\rangle = \int_\Omega (\nabla w \cdot Z) : \mathbb{H} : (\nabla v \cdot Z)\,\mathrm{d}x. \tag{3.17}$$

Arguing in components we get

$$\begin{aligned}(\nabla w \cdot Z) : \mathbb{H} : (\nabla v \cdot Z) &= (\nabla w)_{ip} Z_{pj} \mathbb{H}_{ijkl} (\nabla v)_{kq} Z_{ql} = (\nabla w)_{ip} Z_{pj} \mathbb{H}^t_{jikl} Z^\top_{lq} (\nabla v)_{kq} \\ &= (\nabla w)_{ip} ((Z \cdot \mathbb{H}^t)^t \cdot Z^\top)_{ipkq} (\nabla v)_{kq} = \nabla w : (Z \cdot \mathbb{H}^t \cdot Z^\top) : \nabla v,\end{aligned}$$

as $(Z \cdot \mathbb{H}^t)^t = Z \cdot \mathbb{H}^t$, see Lemma 3.3.3 below. Hence, by setting

$$\mathbb{C} = Z \cdot \mathbb{H}^t \cdot Z^\top,$$

we write

$$\langle \partial I(w), v\rangle = \int_\Omega \nabla w : \mathbb{C} : \nabla v\,\mathrm{d}x. \tag{3.18}$$

Note that major symmetry carries over from $\mathbb{H}$ to $\mathbb{C}$. We also have the following.

Lemma 3.3.3 (Symmetry of $\mathbb{C}$)**.** *The tensor $\mathbb{C}$ is minor symmetric, i.e., $\mathbb{C}^t = \mathbb{C}$, and it holds that $(Z \cdot \mathbb{H}^t)^t = Z \cdot \mathbb{H}^t$.*

Proof. Due to major symmetry of $\mathbb{H}$, it suffices to show that $\mathbb{C} : S = 0$ for all skew symmetric $S \in \mathbb{R}^{d\times d}_{\mathrm{skew}}$, i.e., $S^\top = -S$. Fix $S \in \mathbb{R}^{d\times d}_{\mathrm{skew}}$. Then, $e^{hS} \in \mathrm{SO}(d)$ for $h \in \mathbb{R}$ and by Assumption 3.2.1 (ii), we have that $0 = DW(e^{hS} \cdot Z)$. Thus,

$$\begin{aligned}0 &= \frac{\mathrm{d}}{\mathrm{d}h} DW(e^{hS} \cdot Z)|_{h=0} = D^2W(e^{hS} \cdot Z) : (e^{hS} \cdot S \cdot Z)|_{h=0} \\ &= \mathbb{H} : (S \cdot Z) = (\mathbb{H} \cdot Z^\top) : S.\end{aligned}$$

This shows $\mathbb{C} : S = Z \cdot \mathbb{H}^t \cdot Z^\top : S = 0$. To see the second statement, we use that $0 = (S \cdot Z) : \mathbb{H}$ by major symmetry of $\mathbb{H}$. Therefore, $0 = S : (Z \cdot \mathbb{H}^t)^t = S^\top : (Z \cdot \mathbb{H}^t)$ for all $S \in \mathbb{R}^{d\times d}_{\mathrm{skew}}$ which indeed yields $(Z \cdot \mathbb{H}^t)^t = Z \cdot \mathbb{H}^t$. □

Relations (3.17)–(3.18) eventually show

$$\langle \partial I(w), v\rangle = \int_\Omega (\nabla w \cdot Z) : \mathbb{H} : (\nabla v \cdot Z)\,\mathrm{d}x = \int_\Omega \nabla^s w : \mathbb{C} : \nabla^s v\,\mathrm{d}x. \tag{3.19}$$

Remark 3.3.4 (L^2-regularity of $\partial I(w)$). If $\partial I(w)$ is in $L^2(\Omega;\mathbb{R}^d)$, we have

$$(\partial I(w), v) = -\int_\Omega \mathrm{div}(\nabla w : \mathbb{C}) \cdot v\,\mathrm{d}x = -\int_\Omega \mathrm{div}(\mathbb{C} : \nabla^s w) \cdot v\,\mathrm{d}x, \tag{3.20}$$

that is, $-\mathrm{div}(\mathbb{C} : \nabla^s w) = \partial I(w)$ is the Fréchet differential of I with respect to the L^2-topology. Note that this L^2-regularity is available in the purely viscous setting $\rho = 0$, see Remark 3.4.1 below, or when assuming higher regularity on the initial data, see Lemma 3.4.2 below.

Approximation by scaled lattice displacements

We start by an auxiliary result which guarantees the existence of a sequence of scaled lattice displacements converging to a given smooth test function.

Lemma 3.3.5 (Approximation by scaled lattice displacements)**.** *For each $v \in C_c^\infty(\Omega;\mathbb{R}^d)$, there exists a sequence $(v_k)_k$ of admissible scaled lattice displacements $(v_k)_k$, $v_k \in \mathcal{A}_{\varepsilon_k}$, such that $v_k \overset{\mathrm{AC}}{\to} v$, $\|v_k\|_k \le \|v\|_{L^2(\Omega)}$, and*

$$\sup_k \|\bar\nabla v_k\|_{L^\infty(\widetilde\Omega)} \le c\|\nabla v\|_{L^\infty(\Omega)} < \infty, \tag{3.21}$$

where c depends on d and A only. Moreover, it holds that $\bar\nabla v_k \to \nabla v \cdot Z$ in $L^2(\Omega;\mathbb{R}^{d\times 2^d})$.

Proof. Extend v to an element of $C_c^\infty(\mathbb{R}^d;\mathbb{R}^d)$ and recall definition (3.13) of P_{ε_k}. By letting the sequence of scaled lattice displacements $v_k\colon \mathcal{L}_{\varepsilon_k}\cap\widetilde\Omega \to \mathbb{R}^d$ be defined by

$$v_k(x) := \begin{cases} P_{\varepsilon_k} v(x) & \text{for} \quad x \in \mathcal{L}_{\varepsilon_k}\cap\Omega, \\ 0 & \text{for} \quad x \in \mathcal{L}_{\varepsilon_k}\cap(\widetilde\Omega\setminus\Omega), \end{cases}$$

the convergence $v_k \overset{\mathrm{AC}}{\to} v$ follows directly by definition (3.14). Moreover, $\|v_k\|_k \le \|v\|_{L^2(\Omega)}$ is a consequence of the definition of v_k, (3.6), and Jensen's inequality.

We now show (3.21). We fix $\bar x \in \mathcal{L}'_{\varepsilon_k}\cap\widetilde\Omega$ and write $v_k^i = v_k^i(\bar x) = v_k(\bar x + \varepsilon_k z_i)$, $i = 1,\dots,2^d$, and $\bar v_k = \bar v_k(\bar x) = 2^{-d}\sum_{i=1}^{2^d} v_k^i$. Let $j_0 \in \{1,\dots,2^d\}$ be such that $\max_{j=1,\dots,2^d}|v_k^i(x) - v_k^j(x)| = |v_k^i(x) - v_k^{j_0}(x)|$. To obtain an L^∞-bound on the discrete gradient, we use the Mean-Value Theorem to compute

$$|v_k^i - \bar v_k| \le |v_k^i - v_k^{j_0}| \le c\varepsilon_k\|\nabla v\|_{L^\infty(\widetilde\Omega)} \le c\varepsilon_k\|\nabla v\|_{L^\infty(\Omega)},$$

where $c = c(d,A)$ is the diameter of $\varepsilon_k^{-1}A[\bar x - \frac{3}{2}\varepsilon_k, \bar x + \frac{3}{2}\varepsilon_k]^d$, noting that $Q_\varepsilon(\overline{x}+\varepsilon_k z_i) \subset A[\bar x - \frac{3}{2}\varepsilon_k, \bar x + \frac{3}{2}\varepsilon_k]^d$ for all $i = 1,\dots,2^d$. As the discrete gradient is constant on individual scaled cells, we obtain

$$\|\bar\nabla v_k\|_{L^\infty(\widetilde\Omega)} = \sup_{\bar x\in\mathcal{L}'_{\varepsilon_k}(\widetilde\Omega)} \Big(\sum_{i=1}^{2^d}\frac{1}{\varepsilon_k^2}|v_k^i(\bar x) - \bar v_k(\bar x)|^2\Big)^{1/2} \le \big(2^d c^2\|\nabla v\|^2_{L^\infty(\Omega)}\big)^{1/2} < \infty.$$

For the proof of $\bar\nabla v_k \to \nabla v \cdot Z$ in $L^2(\Omega;\mathbb{R}^{d\times 2^d})$, we refer to [123, Lemma 4.4]. □

Let us now introduce the *piecewise constant interpolation* $\widetilde u_k$ on scaled cells of an admissible scaled lattice displacement $u_k \in \mathcal{A}_{\varepsilon_k}$. To this end, recall the notation $\bigcup Q_{\varepsilon_k} = \bigcup_{\bar x\in\mathcal{L}'_{\varepsilon_k}(\widetilde\Omega)} Q_{\varepsilon_k}(\bar x)$. For $\xi \in \bigcup Q_{\varepsilon_k}$, let $x \in \mathcal{L}_{\varepsilon_k}\cap\widetilde\Omega$ be such that $\xi \in Q_{\varepsilon_k}(x)$. Then, the piecewise constant interpolation is defined as

$$\widetilde u_k(\xi) := \begin{cases} u_k(x) & \text{if} \quad Q_{\varepsilon_k}(x)\cap\Omega \neq \emptyset \\ 0 & \text{if} \quad Q_{\varepsilon_k}(x)\cap\Omega = \emptyset. \end{cases} \tag{3.22}$$

Moreover, we trivially extend $\widetilde{u}_k$ to the whole of $\widetilde{\Omega}$ without changing notation. We thus get for $\varepsilon_k > 0$ small enough that

$$\begin{aligned}\varepsilon_k^d \det A \sum_{x\in\mathcal{L}_{\varepsilon_k}\cap\widetilde{\Omega}} u_k(x) &= \varepsilon_k^d \det A \sum_{x\in\mathcal{L}_{\varepsilon_k}\cap\widetilde{\Omega}} \fint_{Q_{\varepsilon_k}(x)} \widetilde{u}_k(\xi)\,\mathrm{d}\xi \\ &= \int_{\bigcup Q_{\varepsilon_k}} \widetilde{u}_k(\xi)\,\mathrm{d}\xi = \int_{\widetilde{\Omega}} \widetilde{u}_k(\xi)\,\mathrm{d}\xi. \end{aligned} \tag{3.23}$$

In particular, by a similar argument we also have that

$$\|u_k\|_k = \|\widetilde{u}_k\|_{L^2(\widetilde{\Omega})}. \tag{3.24}$$

The above interpolation is motivated by the following properties.

Lemma 3.3.6 (Equivalence of atomistic and L^2-convergence)**.** *Letting $(u_k)_k$, $u_k \in \mathcal{A}_{\varepsilon_k}$, be a sequence of admissible scaled lattice displacements and $u \in L^2(\Omega;\mathbb{R}^d)$, then*

$$u_k \overset{\mathrm{AC}}{\to} u \quad \Longleftrightarrow \quad \int_{\widetilde{\Omega}} |\widetilde{u}_k - \widetilde{u}|^2 \to 0,$$

where $\widetilde{u}$ is the trivial extension of u to $\widetilde{\Omega}$. Moreover, for $u, v \in L^2(\Omega;\mathbb{R}^d)$ and $(u_k)_k$, $(v_k)_k$ with $u_k, v_k \in \mathcal{A}_{\varepsilon_k}$ such that $u_k \overset{\mathrm{AC}}{\to} u$ and $v_k \overset{\mathrm{AC}}{\to} v$, it holds that

$$(u_k, v_k)_k \to (u, v).$$

In particular, we have that $\|u_k\|_k \to \|u\|_{L^2(\Omega)}$ for $k \to \infty$.

Proof. At first, note that AC-convergence implies strong L^2-convergence of piecewise constant interpolations. Indeed, let $\widetilde{u}_k$ and $\widetilde{P}_{\varepsilon_k} u$ be the piecewise constant interpolations of u_k and $P_{\varepsilon_k} u$, respectively. Then, extending u trivially as $\widetilde{u}$ to $\widetilde{\Omega}$, we obtain

$$\begin{aligned}\int_{\widetilde{\Omega}} |\widetilde{u}_k(\xi) - \widetilde{u}(\xi)|^2\,\mathrm{d}\xi &\le 2\int_{\widetilde{\Omega}} |\widetilde{u}_k(\xi) - \widetilde{P}_{\varepsilon_k} u(\xi)|^2\,\mathrm{d}\xi + 2\int_{\widetilde{\Omega}} |\widetilde{P}_{\varepsilon_k} u(\xi) - \widetilde{u}(\xi)|^2\,\mathrm{d}\xi \\ &= 2\varepsilon_k^d \det A \sum_{x\in\mathcal{L}_{\varepsilon_k}\cap\widetilde{\Omega}} |u_k(x) - P_{\varepsilon_k} u(x)|^2 + 2\int_{\widetilde{\Omega}} |\widetilde{P}_{\varepsilon_k} u(\xi) - \widetilde{u}(\xi)|^2\,\mathrm{d}\xi \to 0. \end{aligned}$$

Here, we used that $\widetilde{P}_{\varepsilon_k} u \to \widetilde{u}$ strongly in $L^2(\widetilde{\Omega};\mathbb{R}^d)$. Conversely, strong L^2-convergence of piecewise constant interpolations implies AC-convergence as

$$\begin{aligned}\varepsilon_k^d \det A \sum_{x\in\mathcal{L}_{\varepsilon_k}\cap\widetilde{\Omega}} |u_k(x) - P_{\varepsilon_k} u(x)|^2 &= \int_{\widetilde{\Omega}} |\widetilde{u}_k - \widetilde{P}_{\varepsilon_k} u|^2 \\ &\le 2\int_{\widetilde{\Omega}} |\widetilde{u}_k - \widetilde{u}|^2 + 2\int_{\widetilde{\Omega}} |\widetilde{u} - \widetilde{P}_{\varepsilon_k} u|^2 \to 0. \end{aligned}$$

Eventually, due to $\widetilde{u}_k \to u$ and $\widetilde{v}_k \to v$ in $L^2(\widetilde{\Omega};\mathbb{R}^d)$, we get that

$$\begin{aligned}(u_k, v_k)_k &= \varepsilon_k^d \det A \sum_{x\in\mathcal{L}_{\varepsilon_k}\cap\widetilde{\Omega}} u_k(x)\cdot v_k(x) \\ &= \int_{\widetilde{\Omega}} \widetilde{u}_k(\xi)\cdot\widetilde{v}_k(\xi)\,\mathrm{d}\xi \to \int_{\Omega} u(\xi)\cdot v(\xi)\,\mathrm{d}\xi = (u, v). \end{aligned}$$

□

3.3.3 A priori estimates

Let u_k be the solution of the atomistic equation of motion (3.7). By using the chain rule, for all $t \in [0,T]$ we get

$$\begin{aligned}
0 &= \frac{1}{2\nu}\int_0^t \|\rho\ddot{u}_k(s) + \nu\dot{u}_k(s) + \partial I_k(u_k(s))\|_k^2 \,\mathrm{d}s \\
&= \int_0^t \left(\big(\rho\ddot{u}_k(s) + \partial I_k(u_k(s)), \dot{u}_k(s)\big)_k + \frac{\nu}{2}\|\dot{u}_k(s)\|_k^2 + \frac{1}{2\nu}\|\rho\ddot{u}_k(s) + \partial I_k(u_k(s))\|_k^2 \right) \mathrm{d}s \\
&= \frac{\rho}{2}\|\dot{u}_k(t)\|_k^2 + I_k(u_k(t)) - \frac{\rho}{2}\|\dot{u}_k(0)\|_k^2 - I_k(u_k(0)) \\
&\quad + \frac{\nu}{2}\int_0^t \|\dot{u}_k(s)\|_k^2 \,\mathrm{d}s + \frac{1}{2\nu}\int_0^t \|\rho\ddot{u}_k(s) + \partial I_k(u_k(s))\|_k^2 \,\mathrm{d}s,
\end{aligned}$$

where $\partial I_k(u_k(t))$ denotes the scaled lattice strain given in (3.9). In particular, given the initial conditions $u_k(0) = u_k^0 := u_{\varepsilon_k}^0$ and $\dot{u}_k(0) = u_k^1 := u_{\varepsilon_k}^1$, system (3.7) is equivalent to the energy-dissipation-inertia equation

$$\begin{aligned}
&\frac{\rho}{2}\|\dot{u}_k(t)\|_k^2 + I_k(u_k(t)) + \frac{\nu}{2}\int_0^t \|\dot{u}_k(s)\|_k^2 \,\mathrm{d}s + \frac{1}{2\nu}\int_0^t \|\rho\ddot{u}_k(s) + \partial I_k(u_k(s))\|_k^2 \,\mathrm{d}s \\
&\quad = \frac{\rho}{2}\|u_k^1\|_k^2 + I_k(u_k^0) \quad \forall t \in [0,T],
\end{aligned} \tag{3.25}$$

or, equivalently, for $t = T$. As we are assuming that $u_k^1 \overset{\text{AC}}{\to} w^1 \in L^2(\Omega;\mathbb{R}^d)$ and that $I_k(u_k^0)$ is bounded, from the energy-dissipation-inertia equation we obtain the following.

Lemma 3.3.7 (A priori estimates)**.** *Let u_k be the solution of the atomistic equation of motion (3.7). Then,*

$$\sqrt{\rho}\max_{t\in[0,T]}\|\dot{u}_k(t)\|_k \le c, \tag{3.26}$$

$$\max_{t\in[0,T]} I_k(u_k(t)) \le c, \tag{3.27}$$

$$\int_0^T \|\dot{u}_k(s)\|_k^2 \,\mathrm{d}s \le c, \tag{3.28}$$

$$\int_0^T \|\rho\ddot{u}_k(s) + \partial I_k(u_k(s))\|_k^2 \,\mathrm{d}s \le c, \tag{3.29}$$

where $c > 0$ depends only on $\rho\sup_k \|u_k^1\|_k^2$, $\sup_k I_k(u_k^0))$, and ν.

3.3.4 Compactness and limit of $\nu\dot{u}_k$

In this section, we show that the sequence $(u_k)_k$ of solutions to the atomistic problem (3.7) admits an AC-converging subsequence $u_k(t) \overset{\text{AC}}{\to} w(t) \in L^2(\Omega;\mathbb{R}^d)$ for all $t \in [0,T]$. Moreover, as a first step towards showing that the limit w solves the continuum problem, we also prove that $\nu\dot{u}_k \rightharpoonup \nu\partial_t w$ in a weak $L^2(0,T;L^2(\Omega;\mathbb{R}^d))$-sense made precise below.

From (3.28) we obtain that $\dot{u}_k$ is uniformly bounded in $L^2(0,T;(\mathcal{A}_{\varepsilon_k},\|\cdot\|_k))$. Let now $\partial_t\widetilde{u}_k$ indicate the piecewise constant interpolants of $\dot{u}_k$ from (3.22). In view of (3.24), we get

$$\int_0^T \|\dot{u}_k(s,\cdot)\|_k^2\,\mathrm{d}s = \int_0^T \|\partial_t\widetilde{u}_k(s,\cdot)\|_{L^2(\widetilde{\Omega})}^2\,\mathrm{d}s \le c. \tag{3.30}$$

This along with the compactness result in Theorem 3.3.1 yields that the solution u_k to the atomistic problem (3.7) satisfies that $(\widetilde{u}_k(t))_k$ is compact in $L^2(\widetilde{\Omega};\mathbb{R}^d)$ for all $t\in(0,T)$. This leads to the following.

Lemma 3.3.8 (Compactness)**.** *Let $(u_k)_k$ be a sequence of solutions to the atomistic problem (3.7). Then, there exists $w\in C([0,T],L^2(\Omega;\mathbb{R}^d))\cap L^\infty(0,T;H^1_0(\Omega;\mathbb{R}^d))$ and a (non relabeled) subsequence of $(u_k)_k$ such that*

$$\widetilde{u}_k\to\widetilde{w}\quad \text{in } C([0,T],L^2(\widetilde{\Omega};\mathbb{R}^d)),$$

where $\widetilde{u}_k$ is the piecewise constant interpolation of u_k and $\widetilde{w}$ denotes the trivial extension of w to $\widetilde{\Omega}$.

Proof. The proof relies on a variant of the Aubin-Lions Theorem. However, due to the discrete nature of our spaces, it is more convenient to directly resort to the Arzelà-Ascoli Theorem. First, note that due to (3.27) and Theorem 3.3.1 the set $\{\widetilde{u}_k(t):k\in\mathbb{N}\}$ is relatively compact in $L^2(\widetilde{\Omega};\mathbb{R}^d)$ for each $t\in[0,T]$. Equi-continuity of $(\widetilde{u}_k)_k$ follows from (3.30). Indeed, (3.30) implies that $(\widetilde{u}_k)_k\subset H^1(0,T;L^2(\widetilde{\Omega};\mathbb{R}^d))\subset C([0,T],L^2(\widetilde{\Omega};\mathbb{R}^d))$ and for each $0<s\le t<T$

$$\|\widetilde{u}_k(t)-\widetilde{u}_k(s)\|_{L^2(\widetilde{\Omega})}\le\int_s^t\|\partial_t\widetilde{u}_k(\tau)\|_{L^2(\widetilde{\Omega})}\,\mathrm{d}\tau\le\sqrt{t-s}\|\partial_t\widetilde{u}_k\|_{L^2(0,T;L^2(\widetilde{\Omega};\mathbb{R}^d))}\le c\sqrt{t-s}.$$

Thus, $(\widetilde{u}_k)_k$ is equi-continuous and the convergence to a limit $w\in C([0,T],L^2(\widetilde{\Omega};\mathbb{R}^d))$ follows from the Arzelà-Ascoli Theorem. Since u_k is extended by 0 on $\mathcal{L}_{\varepsilon_k}\cap(\widetilde{\Omega}\setminus\Omega)$, the limit w is indeed supported on Ω. Eventually, applying again (3.27) and Theorem 3.3.1 we find that $w(t)\in H^1_0(\Omega)$ for all $t\in[0,T]$ with uniformly controlled $H^1_0(\Omega)$-norm. □

The lemma above implies that $u_k(t)\overset{\mathrm{AC}}{\to}w(t)$ for all $t\in[0,T]$ as L^2- and AC-convergence are equivalent due to Lemma 3.3.6.

We now prove that w is indeed a solution to the continuum problem (3.10). As a first step, we show that the piecewise constant interpolations of $\nu\dot{u}_k$ converge weakly to $\partial_t w$ in $L^2(0,T;L^2(\widetilde{\Omega};\mathbb{R}^d))$. Indeed, from (3.30) we can extract a (not relabeled) subsequence of u_k such that $\partial_t\widetilde{u}_k\rightharpoonup f$ in $L^2(0,T;L^2(\widetilde{\Omega};\mathbb{R}^d))$. From the linearity of the time derivative we deduce that $f=\partial_t\widetilde{w}$, where $\widetilde{w}$ again denotes the trivial extension of w to $\widetilde{\Omega}$. Thus, we have shown

$$\partial_t\widetilde{u}_k\rightharpoonup\partial_t\widetilde{w}\quad\text{ in } L^2(0,T;L^2(\widetilde{\Omega};\mathbb{R}^d)). \tag{3.31}$$

Remark 3.3.9 (Purely viscous case $\rho=0$). Note that the results of this section stay valid when considering the purely viscous case of $\rho=0$. Indeed, as also the energy-dissipation equality (3.25) holds (along with the obvious modifications), Lemmas 3.3.7 and 3.3.8 remain true, where (3.26) becomes trivial.

3.3.5 Limit of $\rho\ddot{u}_k + \partial I_k(u_k)$

In this section, we prove that, given the pointwise in time AC-converging sequence $u_k \overset{\mathrm{AC}}{\to} w$ from Lemma 3.3.8, we also have that the piecewise constant interpolants of $\rho\ddot{u}_k + \partial I_k(u_k)$ converge weakly to $\rho\partial_{tt}w + \partial I(w)$ in $L^2(0,T;L^2(\Omega;\mathbb{R}^d))$.

Denoting by $(\rho\ddot{u}_k + \partial I_k(u_k))^\sim$ the interpolation of $\rho\ddot{u}_k + \partial I_k(u_k)$ introduced in (3.22), (3.29) together with (3.24) implies that there exists $\alpha \in L^2(0,T;L^2(\widetilde{\Omega};\mathbb{R}^d))$ such that

$$(\rho\ddot{u}_k + \partial I_k(u_k))^\sim \rightharpoonup \alpha \quad \text{weakly in } L^2(0,T;L^2(\widetilde{\Omega};\mathbb{R}^d)). \tag{3.32}$$

We are left with showing that $\alpha = \rho\partial_{tt}\widetilde{w} + \partial I(\widetilde{w})$ in $L^2(0,T;L^2(\widetilde{\Omega};\mathbb{R}^d))$, where $\widetilde{w}$ is the trivial extension of w. For the identification of the limit, we separately investigate the limits of $\rho\partial_{tt}\widetilde{u}_k(t)$ and $(\partial I_k(u_k(t)))^\sim$, i.e., the limits of the piecewise constant interpolations of $\rho\ddot{u}_k$ and $\partial I_k(u_k)$. This is a delicate issue, for $\partial I_k(u_k)$ is defined on a space which depends on k. As an important ingredient, we deduce separate uniform bounds on $\rho\partial_{tt}\widetilde{u}_k(t)$ and $(\partial I_k(u_k(t)))^\sim$, respectively, by resorting to a sufficiently weak topology. We treat the respective limits separately in Sections 3.3.5–3.3.5, and identify α in Section 3.3.5.

Limit of $\partial I_k(u_k)$

Here, we prove convergence of $\partial I_k(u_k)$ to $\partial I(w)$ in the sense of Gâteaux derivatives. The analysis of this section is carried out for $t \in (0,T)$ arbitrary but fixed. Correspondingly, we omit to indicate the dependence on t for brevity. We start by computing the variation of I_k at u_k in direction v_k as

$$\frac{\mathrm{d}}{\mathrm{d}h} I_k(u_k + hv_k)\big|_{h=0} = \varepsilon_k^d \det A \sum_{\overline{x}\in\mathcal{L}'_{\varepsilon_k}(\widetilde{\Omega})} \frac{1}{\delta_k} DW(Z + \delta_k\bar{\nabla}u_k(\overline{x})) \cdot \bar{\nabla}v_k(\overline{x}).$$

We have the following.

Lemma 3.3.10 (Convergence of Gâteaux derivatives)**.** *Let $(u_k)_k$ be a sequence of admissible scaled lattice displacements, $u_k \in \mathcal{A}_{\varepsilon_k}$, with equibounded atomistic energy, i.e., $\sup_k I_k(u_k) < \infty$. Suppose that $u_k \overset{\mathrm{AC}}{\to} w$ with $w \in H^1_0(\Omega;\mathbb{R}^d)$. Assuming $v \in \mathcal{C}^\infty_{\mathrm{c}}(\Omega;\mathbb{R}^d)$ with v_k being the corresponding scaled lattice displacements from Lemma 3.3.5, we have*

$$\varepsilon_k^d \det A \sum_{\overline{x}\in\mathcal{L}'_{\varepsilon_k}(\widetilde{\Omega})} \frac{1}{\delta_k} DW(Z + \delta_k\bar{\nabla}u_k(\overline{x})) : \bar{\nabla}v_k(\overline{x}) \to \int_\Omega (\nabla w \cdot Z) : \mathbb{H} : (\nabla v \cdot Z)\,\mathrm{d}x$$

as $k \to \infty$, where we recall that the right-hand side coincides with $\langle \partial I(w), v\rangle$, see (3.17).

Proof. We compute the Taylor expansion of DW at Z. This calls for $\delta_k\bar{\nabla}u_k$ to be small. We hence define *good sets* G_k and *bad sets* B_k as

$$G_k := \left\{\overline{x} \in \mathcal{L}'_{\varepsilon_k}(\widetilde{\Omega}) : |\delta_k\bar{\nabla}u_k(\overline{x})| < \beta_k^{-1}\right\},$$
$$B_k := \left\{\overline{x} \in \mathcal{L}'_{\varepsilon_k}(\widetilde{\Omega}) : |\delta_k\bar{\nabla}u_k(\overline{x})| \geq \beta_k^{-1}\right\},$$

where β_k is chosen in such a way that $\beta_k \to \infty$, and $\beta_k^2 \delta_k \to 0$ as $k \to \infty$. Denoting by $\#B_k$ the cardinality of B_k, a Chebyshev argument ensures that $\delta_k^{-1}\varepsilon_k^d \#B_k \to 0$ for $k \to \infty$. Indeed, by relation (3.24) we estimate

$$\frac{\varepsilon_k^d}{\delta_k}\#B_k = \frac{\varepsilon_k^d \beta_k^2}{\delta_k} \sum_{\overline{x}\in B_k} \frac{1}{\beta_k^2} \le \frac{\varepsilon_k^d \beta_k^2}{\delta_k} \sum_{\overline{x}\in B_k} \delta_k^2 |\bar{\nabla} u_k(\overline{x})|^2 \le \frac{\beta_k^2 \delta_k}{\det A} \|\bar{\nabla} u_k\|^2_{L^2(\widetilde{\Omega})} \to 0, \tag{3.33}$$

where we have used $\sup_k \|\bar{\nabla} u_k\|_{L^2(\widetilde{\Omega})} < \infty$, which follows from the compactness result of Theorem 3.3.1. A fortiori, we have $\varepsilon_k^d \#B_k \to 0$ as $k \to \infty$.

Now, we Taylor-expand DW at Z for $\overline{x} \in G_k$ obtaining

$$\begin{aligned} DW(Z + \delta_k \bar{\nabla} u_k(\overline{x})) &= D^2 W(Z) : (\delta_k \bar{\nabla} u_k(\overline{x})) + R(\delta_k \bar{\nabla} u_k(\overline{x})) \\ &= \delta_k \mathbb{H} : \bar{\nabla} u_k(\overline{x}) + R(\delta_k \bar{\nabla} u_k(\overline{x})), \end{aligned}$$

where the *remainder term* $R\colon \mathbb{R}^{d\times 2^d} \to \mathbb{R}^{d\times 2^d}$ satisfies

$$\sup\left\{ \frac{|R(F)|}{|F|} \,:\, |F| \le \rho \right\} \to 0 \quad \text{as } \rho \to 0.$$

Considering only the energy of cells in G_k, due to the major symmetry of $\mathbb{H}$, we arrive at

$$\begin{aligned} &\varepsilon_k^d \det A \sum_{\overline{x}\in \mathcal{L}'_{\varepsilon_k}(\widetilde{\Omega})\cap G_k} \frac{1}{\delta_k} DW(Z + \delta_k \bar{\nabla} u_k(\overline{x})) : \bar{\nabla} v_k(\overline{x}) \\ &= \varepsilon_k^d \det A \sum_{\overline{x}\in \mathcal{L}'_{\varepsilon_k}(\widetilde{\Omega})\cap G_k} \left(\bar{\nabla} u_k(\overline{x}) : \mathbb{H} : \bar{\nabla} v_k(\overline{x}) + \delta_k^{-1} \bar{\nabla} v_k(\overline{x}) : R(\delta_k \bar{\nabla} u_k(\overline{x})) \right). \end{aligned} \tag{3.34}$$

The next step is to control $\delta_k^{-1} \bar{\nabla} v_k : R(\delta_k \bar{\nabla} u_k)$ on G_k. Note that, as $\bar{\nabla} u_k(\overline{x})$ is constant on scaled cells $Q_{\varepsilon_k}(\overline{x})$, we have, analogously to (3.23), $\int_{Q_{\varepsilon_k}(\overline{x})} \bar{\nabla} u_k(x)\,\mathrm{d}x = \varepsilon_k^d \det A\, \bar{\nabla} u_k(\overline{x})$, and thus,

$$\int_{\bigcup Q_{\varepsilon_k}} \bar{\nabla} u_k(x)\,\mathrm{d}x = \varepsilon_k^d \det A \sum_{\overline{x}\in \mathcal{L}'_{\varepsilon_k}(\widetilde{\Omega})} \bar{\nabla} u_k(\overline{x}), \tag{3.35}$$

where we recall that $\bigcup Q_{\varepsilon_k} = \bigcup_{\overline{x}\in \mathcal{L}'_{\varepsilon_k}(\widetilde{\Omega})} Q_{\varepsilon_k}(\overline{x})$. Therefore, letting $k \to \infty$, by Hölder's inequality we get

$$\begin{aligned} &\varepsilon_k^d \det A \left| \sum_{\overline{x}\in \mathcal{L}'_{\varepsilon_k}(\widetilde{\Omega})\cap G_k} \delta_k^{-1} \bar{\nabla} v_k(\overline{x}) : R(\delta_k \bar{\nabla} u_k(\overline{x})) \right| \\ &\le \int_{\bigcup_{G_k} Q_{\varepsilon_k}} |\bar{\nabla} v_k(x)|\, |\bar{\nabla} u_k(x)| \frac{|R(\delta_k \bar{\nabla} u_k(x))|}{|\delta_k \bar{\nabla} u_k(x)|}\,\mathrm{d}x \\ &\le \sup_{\bigcup_{G_k} Q_{\varepsilon_k}} \left(\frac{|R(\delta_k \bar{\nabla} u_k)|}{\delta_k |\bar{\nabla} u_k|} \right) \|\bar{\nabla} v_k\|_{L^2(\widetilde{\Omega})} \|\bar{\nabla} u_k\|_{L^2(\widetilde{\Omega})} \to 0, \end{aligned} \tag{3.36}$$

where we set $\bigcup_{G_k} Q_{\varepsilon_k} := \bigcup_{\overline{x}\in G_k\cap\mathcal{L}'_{\varepsilon_k}(\widetilde{\Omega})} Q_{\varepsilon_k}(\overline{x})$. Convergence (3.36) follows as $|\delta_k\bar{\nabla}u_k| < \beta_k^{-1}$ uniformly on G_k with $\beta_k^{-1}\to 0$. Hence, the above supremum over $\bigcup_{G_k} Q_{\varepsilon_k}$ converges to 0. Recall also that $\|\bar{\nabla}v_k\|_{L^2(\widetilde{\Omega})}$ and $\|\bar{\nabla}u_k\|_{L^2(\widetilde{\Omega})}$ are uniformly bounded by Lemma 3.3.5 and Theorem 3.3.1, respectively.

On the bad sets B_k, we use Assumption 3.2.1 (v) and the fact that $\|\bar{\nabla}v_k\|_{L^\infty(\widetilde{\Omega})}\le c$, see Lemma 3.3.5, to obtain

$$\begin{aligned}
&\frac{\varepsilon_k^d\det A}{\delta_k}\sum_{\overline{x}\in\mathcal{L}'_{\varepsilon_k}(\widetilde{\Omega})\cap B_k} DW(Z+\delta_k\bar{\nabla}u_k):\bar{\nabla}v_k \le \frac{1}{\delta_k}\int_{\bigcup_{B_k}Q_{\varepsilon_k}} |DW(Z+\delta_k\bar{\nabla}u_k)|\,|\bar{\nabla}v_k|\,\mathrm{d}x\\
&\le \frac{c}{\delta_k}\|\bar{\nabla}v_k\|_{L^\infty(\widetilde{\Omega})}\int_{\bigcup_{B_k}Q_{\varepsilon_k}}|Z+\delta_k\bar{\nabla}u_k|^2\,\mathrm{d}x + \frac{c}{\delta_k}\det A\,\varepsilon_k^d\|\bar{\nabla}v_k\|_{L^\infty(\widetilde{\Omega})}\#B_k\\
&\le \frac{c}{\delta_k}\int_{\bigcup_{B_k}Q_{\varepsilon_k}}\big(|Z|^2+\delta_k^2|\bar{\nabla}u_k|^2\big)\,\mathrm{d}x + \frac{c}{\delta_k}\det A\,\varepsilon_k^d\#B_k\\
&\le \frac{c}{\delta_k}\det A\,\varepsilon_k^d\#B_k|Z|^2 + c\delta_k\|\bar{\nabla}u_k\|^2_{L^2(\widetilde{\Omega})} + \frac{c}{\delta_k}\det A\,\varepsilon_k^d\#B_k\to 0,
\end{aligned}\tag{3.37}$$

where we set $\bigcup_{B_k} Q_{\varepsilon_k} := \bigcup_{\overline{x}\in B_k\cap\mathcal{L}'_{\varepsilon_k}(\widetilde{\Omega})} Q_{\varepsilon_k}(\overline{x})$ and used the fact that $\delta_k^{-1}\varepsilon_k^d\#B_k\to 0$ due to (3.33). Here, we again employed Theorem 3.3.1 to bound $\sup_k\|\bar{\nabla}u_k\|^2_{L^2(\widetilde{\Omega})}\le c$.

By Lemma 3.3.5 we have that $\bar{\nabla}v_k\to\nabla v\cdot Z$ strongly in $L^2(\widetilde{\Omega};\mathbb{R}^{d\times 2^d})$. Indicating by $\chi_{\bigcup_{G_k}Q_{\varepsilon_k}}$ the characteristic function of the set $\bigcup_{G_k}Q_{\varepsilon_k}$, we observe that $\chi_{\bigcup_{G_k}Q_{\varepsilon_k}}\to 1$ in measure. Recall that $\bar{\nabla}u_k\rightharpoonup\nabla\widetilde{w}\cdot Z$ weakly in $L^2(\widetilde{\Omega};\mathbb{R}^{d\times 2^d})$ by Theorem 3.3.1. By the linearity of $F\mapsto\mathbb{H}:F$, we obtain

$$\chi_{\bigcup_{G_k}Q_{\varepsilon_k}}\,\mathbb{H}:(\bar{\nabla}u_k)\rightharpoonup\mathbb{H}:(\nabla w\cdot Z)\text{ weakly in }L^2(\widetilde{\Omega};\mathbb{R}^{d\times 2^d}).$$

This, together with (3.35) and (3.36), implies

$$\begin{aligned}
&\varepsilon_k^d\det A\sum_{\overline{x}\in\mathcal{L}'_{\varepsilon_k}(\widetilde{\Omega})\cap G_k}\big(\bar{\nabla}u_k:\mathbb{H}:\bar{\nabla}v_k+\delta_k^{-1}\bar{\nabla}v_k:R(\delta_k\bar{\nabla}u_k)\big)\\
&\to\int_\Omega(\nabla w\cdot Z):\mathbb{H}:(\nabla v\cdot Z)\,\mathrm{d}x
\end{aligned}$$

which, along with (3.34) and (3.37), concludes the proof. □

Limit of $\rho\ddot{u}_k$

We now show that $\rho\ddot{u}_k$ converges suitably to $\rho\partial_{tt}w$. To this end, we uniformly bound $\rho\ddot{u}_k$ in a weaker topology to obtain compactness and then identify the corresponding limit.

Let $\ell>\frac{d}{2}+1$, so that $H_0^\ell(\Omega;\mathbb{R}^d)\subset W^{1,\infty}(\Omega;\mathbb{R}^d)$, see, e.g., [1, Theorem 4.12]. We define $\overline{\ddot{u}_k}\in L^2(0,T;H^{-\ell}(\Omega;\mathbb{R}^d))$ almost everywhere in time as

$$\langle\overline{\ddot{u}_k(t)},v\rangle_{H_0^\ell(\Omega)} := (\ddot{u}_k(t),v_k)_k\qquad\text{for all }v\in H_0^\ell(\Omega;\mathbb{R}^d),\tag{3.38}$$

where v_k are the scaled lattice displacements of v from Lemma 3.3.5. Note that, strictly speaking, we define (3.38) for $v \in C_c^\infty(\Omega;\mathbb{R}^d)$ only and argue by density, as the approximation by scaled lattice displacements from Lemma 3.3.5 has only been introduced for smooth functions with compact support.

Analogously to $\overline{\ddot{u}_k}$ in (3.38), we define $\overline{\partial I_k(u_k)} \in L^2(0,T;H^{-\ell}(\Omega;\mathbb{R}^d))$ by setting, again almost everywhere in time,

$$\langle \overline{\partial I_k(u_k(t))}, v\rangle_{H_0^\ell(\Omega)} := \langle \partial I_k(u_k(t)), v_k\rangle \qquad \text{for all } v \in H_0^\ell(\Omega;\mathbb{R}^d), \tag{3.39}$$

where the right-hand side of (3.39) is defined by (3.8). We now prove that $\overline{\ddot{u}_k(t)}$ and $\overline{\partial I_k(u_k(t))}$ have L^2-regularity in time uniformly in k.

Lemma 3.3.11 (Uniform bound)**.** *The functions $\rho\overline{\ddot{u}_k}$ and $\overline{\partial I_k(u_k)}$ are uniformly bounded in $L^2(0,T;H^{-\ell}(\Omega;\mathbb{R}^d))$, i.e.,*

$$\textit{(i)}\quad \sup_k \int_0^T \Big\|\overline{\partial I_k(u_k(t))}\Big\|_{H^{-\ell}(\Omega)}^2 \,\mathrm{d}t \le c, \qquad \textit{(ii)}\quad \sup_k \int_0^T \Big\|\rho\overline{\ddot{u}_k(t)}\Big\|_{H^{-\ell}(\Omega)}^2 \,\mathrm{d}t \le c.$$

Proof. We start by checking (i). Let $t \in (0,T)$ be fixed and recall by (3.8) that

$$\begin{aligned}\langle \overline{\partial I_k(u_k(t))}, v\rangle_{H_0^\ell(\Omega)} &= \langle \partial I_k(u_k(t,\cdot)), v_k\rangle \\ &= \varepsilon_k^d \det A \sum_{\overline{x}\in\mathcal{L}_\varepsilon'(\widetilde{\Omega})} \frac{1}{\delta_k} DW(Z+\delta_k\bar\nabla u_k(t,\overline{x})) : \bar\nabla v_k(\overline{x}).\end{aligned}$$

We argue as in Lemma 3.3.10. By Assumption 3.2.1 (ii) and (iii) the energy density W is quadratic near Z, i.e., there exists $\eta > 0$ such that $|DW(Z+F)| \le c|F|$ for all $F \in \mathbb{R}^{d\times 2^d}$ with $|F| \le \eta$. On the other hand, given $F \in \mathbb{R}^{d\times 2^d}$ with $|F| > \eta$, by Assumption 3.2.1 (v) we can bound $|DW(Z+F)| \le c|F|^2 + c \le c(1+1/\eta^2)|F|^2$. Combining both estimates, we conclude the existence of a constant $c > 0$ such that

$$\frac{1}{\delta_k} DW(Z+\delta_k\bar\nabla u_k(t,\cdot)) \le \frac{1}{\delta_k}\big(c\delta_k|\bar\nabla u_k(t,\cdot)| + c\delta_k^2|\bar\nabla u_k(t,\cdot)|^2\big) \le c(1+|\bar\nabla u_k(t,\cdot)|^2)$$

a.e. for almost every $t \in (0,T)$. Here, the last step follows from Young's inequality. Since the discrete gradient is defined everywhere in $\widetilde{\Omega}$, we can replace the sum by the integral as in (3.23) and hence obtain

$$\begin{aligned}&\varepsilon_k^d \det A \sum_{\overline{x}\in\mathcal{L}_\varepsilon'(\widetilde{\Omega})} \frac{1}{\delta_k} DW(Z+\delta_k\bar\nabla u_k(t,\overline{x})) : \bar\nabla v_k(\overline{x}) \\ &\le c\big(1+\|\bar\nabla u_k(t,\cdot)\|_{L^2(\widetilde{\Omega})}^2\big)\|\bar\nabla v_k\|_{L^\infty(\widetilde{\Omega})}.\end{aligned}$$

Now, using (3.21), $H_0^\ell(\Omega;\mathbb{R}^d) \subset W^{1,\infty}(\Omega;\mathbb{R}^d)$, $\sup_k \|\bar\nabla u_k(t,\cdot)\|_{L^2(\widetilde{\Omega})} \le c$ (uniformly in t) by (3.27) and the compactness from Theorem 3.3.1, we arrive at

$$\langle \overline{\partial I_k(u_k(t))}, v\rangle_{H_0^\ell(\Omega)} \le c\|\nabla v\|_{L^\infty(\Omega)} \le c\|v\|_{H_0^\ell(\Omega)} \quad \text{for almost every } t \in (0,T).$$

In particular, by integrating in time we obtain (i).

We now address (ii). Due to

$$\int_0^T \left\|\rho\overline{\ddot{u}_k(t)}\right\|^2_{H^{-\ell}(\Omega)} \mathrm{d}t \le 2\int_0^T \left\|\rho\overline{\ddot{u}_k(t)} + \overline{\partial I_k(u_k(t))}\right\|^2_{H^{-\ell}(\Omega)} + 2\int_0^T \left\|\overline{\partial I_k(u_k(t))}\right\|^2_{H^{-\ell}(\Omega)}$$

and (i), it suffices to bound the first term on the right-hand side. To this aim, for fixed $t \in (0,T)$, by definitions (3.38)–(3.39) and the interpretation of $\partial I_k(u_k)$ as scaled lattice strain (3.9), we get

$$\begin{aligned}\left|\langle\rho\overline{\ddot{u}_k(t)} + \overline{\partial I_k(u_k(t))}, v\rangle_{H^\ell_0(\Omega)}\right|^2 &= |(\rho\ddot{u}_k(t) + \partial I_k(u_k(t)), v_k)_k|^2 \\ &\le \|v_k\|_k^2 \, \|\rho\ddot{u}_k(t) + \partial I_k(u_k(t))\|_k^2.\end{aligned}$$

Since $\|v_k\|_k \le \|v\|_{L^2(\Omega)}$ by Lemma 3.3.5 and $H^\ell_0(\Omega;\mathbb{R}^d) \subset L^2(\Omega;\mathbb{R}^d)$, we deduce

$$\|\rho\overline{\ddot{u}_k(t)} + \overline{\partial I_k(u_k(t))}\|^2_{H^{-\ell}(\Omega)} \le c\|\rho\ddot{u}_k(t) + \partial I_k(u_k(t))\|_k^2$$

for a.e. $t \in (0,T)$. Then, by (3.29) we conclude. □

The lemma above implies the existence of $\xi \in L^2(0,T;H^{-\ell}(\Omega;\mathbb{R}^d))$ such that $\overline{\partial I_k(u_k)} \rightharpoonup \xi$ in $L^2(0,T;H^{-\ell}(\Omega;\mathbb{R}^d))$. Lemma 3.3.10 and strong convergence pointwise in time from Lemma 3.3.8 allows us to identify $\xi = \partial I(w)$. Moreover, there exists $\lambda \in L^2(0,T;H^{-\ell}(\Omega;\mathbb{R}^d))$ such that

$$\rho\overline{\ddot{u}_k} \rightharpoonup \lambda \quad \text{in } L^2(0,T;H^{-\ell}(\Omega;\mathbb{R}^d)). \tag{3.40}$$

It remains to identify $\lambda = \rho\partial_{tt}w$. To this end, let $\varphi \in C^\infty_c([0,T]\times\Omega;\mathbb{R}^d)$ be of the form $\varphi(t,x) = \psi(t)v(x)$ for $\psi \in C^\infty_c([0,T])$ and $v \in C^\infty_c(\Omega;\mathbb{R}^d)$. By (3.40) we obtain

$$\int_0^T \langle\rho\overline{\ddot{u}_k(t)}, \varphi(t)\rangle_{H^\ell_0(\Omega)} \,\mathrm{d}t \to \int_0^T \langle\lambda(t), \varphi(t)\rangle_{H^\ell_0(\Omega)} \,\mathrm{d}t. \tag{3.41}$$

On the other hand, writing $\varphi_k(t) = \psi(t)v_k$ for each $t \in [0,T]$, where v_k are the scaled lattice displacements from Lemma 3.3.5, we have by (3.38) that

$$\begin{aligned}&\int_0^T \langle\rho\overline{\ddot{u}_k(t)}, \varphi(t)\rangle_{H^\ell_0(\Omega)} \,\mathrm{d}t = \int_0^T \big(\rho\ddot{u}_k(t), \varphi_k(t)\big)_k \,\mathrm{d}t = \int_0^T \ddot{\psi}(t)(\rho u_k(t), v_k)_k \,\mathrm{d}t \\ &\to \int_0^T \ddot{\psi}(t)(\rho w(t), v)\,\mathrm{d}t = \int_0^T (\rho w(t), \ddot{\varphi}(t))\,\mathrm{d}t,\end{aligned} \tag{3.42}$$

where the convergence follows from Lemma 3.3.6 and Lemma 3.3.8. By the density of linear combinations of test functions of the above form and (3.41)–(3.42) we get $\lambda = \rho\partial_{tt}w$ in $L^2(0,T;H^{-\ell}(\Omega;\mathbb{R}^d))$. From (3.41) we can also deduce pointwise convergence of $\partial_t\widetilde{u}_k(t)$ for all $t \in [0,T]$. We formulate and prove this property here for later purposes.

Lemma 3.3.12 (Convergence of $\partial_t \widetilde{u}_k$)**.** *Let $(u_k)_k$ be a sequence of solutions to the atomistic problem (3.7) and let $\widetilde{w}$ be its limit from Lemma 3.3.8. Then*

$$\partial_t \widetilde{u}_k(t) \rightharpoonup \partial_t \widetilde{w}(t) \text{ weakly in } L^2(\widetilde{\Omega};\mathbb{R}^d) \text{ for all } t \in [0,T].$$

Proof. Similarly to (3.41)–(3.42), we consider a test function $\varphi \in C^\infty([0,T]\times\Omega;\mathbb{R}^d)$ of the form $\varphi(t,x) = \psi(t)v(x)$, now for $v \in C_c^\infty(\Omega;\mathbb{R}^d)$ and $\psi \in C^\infty([0,T])$ with $\psi(T) = 0$. As $\partial_{tt} w \in L^2(0,T;H^{-\ell}(\Omega;\mathbb{R}^d))$, we get $\partial_t w \in C([0,T];H^{-\ell}(\Omega;\mathbb{R}^d))$ and, for fixed $t \in [0,T]$, we obtain by integration by parts

$$\int_t^T \langle \partial_{tt} w(s), \varphi(s)\rangle_{H_0^\ell(\Omega)} \,\mathrm{d}s = -\int_t^T \big(\partial_t w(s), \partial_t\varphi(s)\big)\,\mathrm{d}s - (\partial_t w(t), \varphi(t)) \tag{3.43}$$

where we also used $\partial_t \widetilde{w} \in L^2(0,T;L^2(\widetilde{\Omega};\mathbb{R}^d))$, see (3.31). In a similar fashion, we get

$$\int_t^T \langle \overline{\ddot{u}_k(s)}, \varphi(s)\rangle_{H_0^\ell(\Omega)} \,\mathrm{d}s = -\int_t^T \big(\dot{u}_k(s), (\partial_t\varphi)_k(s)\big)_k \,\mathrm{d}s - (\dot{u}_k(t), \psi(t)v_k)_k, \tag{3.44}$$

where $(\partial_t\varphi)_k(s) = \partial_t\psi(s)v_k$ for each $s \in [0,T]$. By using (3.26) and (3.24), we find a (not relabeled) subsequence and $z(t) \in L^2(\widetilde{\Omega};\mathbb{R}^d)$ such that $\partial_t \widetilde{u}_k(t) \rightharpoonup z(t)$ in $L^2(\widetilde{\Omega};\mathbb{R}^d)$. Then, by (3.31), (3.41) (with $\lambda = \rho\partial_{tt} w$), and Lemma 3.3.6, we pass to the limit in (3.44), and we compare with (3.43) to find $(\partial_t w(t), \varphi(t)) = (z(t), \varphi(t))$. By the arbitrariness of the test function, we get $z(t) = \partial_t \widetilde{w}(t)$. Uniqueness of the limit eventually shows that the whole sequence $\partial_t \widetilde{u}_k(t)$ converges to $\partial_t \widetilde{w}(t)$. This concludes the proof. □

Joint limit

From definitions (3.38)–(3.39) and the interpretation of $\partial I_k(u_k)$ as scaled lattice strain, see (3.9), we get $\langle \overline{\rho\ddot{u}_k(t)} + \overline{\partial I_k(u_k(t))}, v\rangle_{H_0^\ell(\Omega)} = (\rho\ddot{u}_k(t) + \partial I_k(u_k(t)), v_k)_k$ for $v \in C_c^\infty(\Omega)$. Moreover, for test functions $\varphi \in C_c^\infty([0,T]\times\Omega;\mathbb{R}^d)$ of the form $\varphi(t,x) = \psi(t)v(x)$, with $v \in C_c^\infty(\Omega;\mathbb{R}^d)$ and $\psi \in C_c^\infty([0,T])$, we have

$$\begin{aligned}\int_0^T \big|((\rho\ddot{u}_k + \partial I_k(u_k))^\sim(t), \psi(t)v) - (\rho\ddot{u}_k(t) + \partial I_k(u_k(t)), \psi(t)v_k)_k\big|^2 \,\mathrm{d}t \\ \le \|\widetilde{v}_k - v\|^2_{L^2(\widetilde{\Omega})} \|\psi\|_{L^\infty(0,T)} \int_0^T \|(\rho\ddot{u}_k + \partial I_k(u_k))^\sim(t)\|^2_{L^2(\widetilde{\Omega})} \,\mathrm{d}t \to 0\end{aligned}$$

by (3.24), (3.29), Lemmas 3.3.5–3.3.6, and Hölder's inequality. Hence, recalling (3.32) and the convergences established in Sections 3.3.5–3.3.5, by uniqueness of weak limits we conclude that

$$\alpha = \rho\partial_{tt}\widetilde{w} + \partial I(\widetilde{w}) \quad \text{in } L^2(0,T;L^2(\widetilde{\Omega};\mathbb{R}^d)). \tag{3.45}$$

3.3.6 Proof of the first part of Theorem 3.2.2: convergence of solutions

Collecting the results from Lemma 3.3.8, (3.31), (3.32), and (3.45) we conclude the existence of a (non relabeled) subsequence of solutions $(u_k)_k$ to the atomistic equation of motion (3.7), satisfying

$$\widetilde{u}_k(t) \to \widetilde{w}(t) \qquad \text{in } L^2(\widetilde{\Omega};\mathbb{R}^d) \text{ for all } t \in [0,T], \tag{3.46}$$

$$\nu\partial_t\widetilde{u}_k \rightharpoonup \nu\partial_t\widetilde{w} \qquad \text{in } L^2(0,T;L^2(\widetilde{\Omega};\mathbb{R}^d)), \tag{3.47}$$

$$\rho\partial_{tt}\widetilde{u}_k + (\partial I_k(u_k))^{\sim} \rightharpoonup \rho\partial_{tt}\widetilde{w} + \partial I(\widetilde{w}) \qquad \text{in } L^2(0,T;L^2(\widetilde{\Omega};\mathbb{R}^d)). \tag{3.48}$$

In particular, testing (3.7) with $\psi(t)v_k$, where $\psi \in C^\infty([0,T])$ and v_k is the associated scaled lattice displacements for some $v \in C_c^\infty(\Omega)$, and passing to the limit $k \to \infty$, we find that w is a weak solution of the continuum momentum equation. Moreover, the initial conditions are satisfied. In fact, by Lemma 3.3.8 we have $u_k(0) \to w(0)$ in $L^2(\widetilde{\Omega};\mathbb{R}^d)$, and Lemma 3.3.12 implies $\partial_t\widetilde{u}_k(0) \rightharpoonup \partial_t w(0)$ in $L^2(\widetilde{\Omega};\mathbb{R}^d)$. This along with $\widetilde{u}_k(0,\cdot) \to w^0$ and $\partial_t\widetilde{u}_k(0,\cdot) \to w^1$ in $L^2(\widetilde{\Omega};\mathbb{R}^d)$ by assumption yields the claim. By $w \in L^\infty(0,T;H_0^1(\Omega;\mathbb{R}^d))$ (see Lemma 3.3.8), (3.19), and comparison, we have $\partial_{tt}w \in L^2(0,T;H^{-1}(\Omega;\mathbb{R}^d))$.

As the continuum problem (3.10) admits a unique weak solution w, the entire sequence $(u_k)_k$ of solutions to the atomistic problem AC-converges. □

The convergence given in (3.47) and (3.48) can be improved under the stronger assumption on the initial data in the second part of Theorem 3.2.2, see Corollary 3.4.3 below for details.

3.4 Energy convergence

We devote this section to the proof the energy-convergence statement in Theorem 3.2.2. In Section 3.4.1, we prove inequalities (3.16a)–(3.16d). The proof of Theorem 3.2.2 is then concluded in Section 3.4.2.

3.4.1 lim inf-inequalities

Having already established the convergences (3.46)–(3.48), we now simply use the weak lower semicontinuity of norms to establish the inequalities.

Inequality (3.16a) follows from Lemma 3.3.12, (3.24), and the weak lower semicontinuity of norms. Then, (3.16b) follows by integration and Fatou's Lemma.

For (3.16c), we use (3.46), Lemma 3.3.6, and the Γ-lim inf inequality of Theorem 3.3.1.

Eventually, inequality (3.16d) follows from (3.32), (3.45), and weak lower semicontinuity of norms, again recalling relation (3.24).

Remark 3.4.1 (Purely viscous case $\rho = 0$). Let us address the analog of the inequalities (3.16a)–(3.16d) in the purely viscous setting. First, (3.16a) is not needed and (3.16c) remains unchanged. Inequality (3.16b) still holds, but for its derivation we do not resort to (3.16a), but simply use (3.31), lower semicontinuity of norms, and (3.24).

The only inequality which essentially changes is (3.16d): it is replaced by

$$\|\operatorname{div}(\mathbb{C} : \nabla^s w(t,\cdot))\|_{L^2(\Omega)} \le \liminf_{k\to\infty} \|\partial I_k(u_k(t,\cdot))\|_k \quad \text{for a.e. } t \in (0,T). \tag{3.49}$$

Once (3.49) is shown, we can use the uniform bound on $\int_0^T \|\partial I_k(u_k(s))\|_k^2 \,\mathrm{d}s$, see (3.25) (for $\rho = 0$) and Fatou's Lemma to conclude that $\partial I(w) \in L^2(0,T;L^2(\Omega;\mathbb{R}^d))$, cf. (3.20).

Let us show (3.49). By summation by parts, see Lemma 3.5.1, $\langle \partial I_k(u_k(t)), v_k\rangle$ can be expressed via the atomistic inner product $(\cdot,\cdot)_k$ as

$$\varepsilon_k^d \det A \sum_{\overline{x}\in\mathcal{L}'_{\varepsilon_k}(\widetilde{\Omega})} \frac{1}{\delta_k} DW(Z + \delta_k \bar{\nabla} u_k(t,\overline{x})) \cdot \bar{\nabla} v_k(\overline{x}) = (f_k(t), v_k)_k$$

for any $v \in C_c^\infty(\Omega;\mathbb{R}^d)$ and the corresponding v_k from Lemma 3.3.5, where the specific form of $f_k(t)$ can be found in (3.56) below. It is not restrictive to assume that $\liminf_{k\to\infty} \|f_k(t)\|_k < \infty$ as otherwise (3.49) is trivial. Then, by Lemma 3.3.5 we get

$$\liminf_{k\to\infty} (f_k(t), v_k)_k \le \liminf_{k\to\infty} \|f_k(t)\|_k \|v_k\|_k \le c\|v\|_{L^2(\Omega)}.$$

As Lemma 3.3.10 implies

$$\langle \partial I(w(t)), v\rangle = \int_\Omega (\nabla w(t) \cdot Z) : \mathbb{H} : (\nabla v \cdot Z)\,\mathrm{d}x = \lim_{k\to\infty} (f_k(t), v_k)_k,$$

we get that $\partial I(w(t))$ is bounded in $L^2(\Omega;\mathbb{R}^d)$. Then, (3.20) yields

$$(f_k(t), v_k)_k \to (\partial I(w(t)), v) = -\int_\Omega \operatorname{div}(\mathbb{C} : \nabla^s w(t)) \cdot v \,\mathrm{d}x = (f(t), v),$$

where $f(t) := -\operatorname{div}(\mathbb{C} : \nabla^s w(t))$. Denoting by $\widetilde{f}_k(t)$ the piecewise constant interpolation of $f_k(t)$ introduced in (3.22), we claim $\widetilde{f}_k(t) \rightharpoonup f(t)$ weakly in $L^2(\Omega;\mathbb{R}^d)$. This would then show $\|f(t)\|_{L^2(\Omega)} \le \liminf_{k\to\infty} \|\widetilde{f}_k(t)\|_{L^2(\widetilde{\Omega})}$ which, along with (3.24), concludes the proof of (3.49).

We are left with proving that $\widetilde{f}_k(t) \rightharpoonup f(t)$ weakly in $L^2(\widetilde{\Omega};\mathbb{R}^d)$. Given $v \in C_c^\infty(\Omega)$, we note that $|(\widetilde{f}_k(t), v) - (\partial I(w(t)), v)| \le |(\widetilde{f}_k(t), v) - (f_k(t), v_k)_k| + |(f_k(t), v_k)_k - (\partial I(w(t)), v)|$ and hence by (3.23) it is enough to check that $|(\widetilde{f}_k(t), v) - (\widetilde{f}_k(t), \widetilde{v}_k)|$ vanishes as $k \to \infty$. Indeed, by Hölder's inequality and (3.24) we have

$$|(\widetilde{f}_k(t), v) - (\widetilde{f}_k(t), \widetilde{v}_k)|^2 \le \|v - \widetilde{v}_k\|^2_{L^2(\widetilde{\Omega})} \|f_k\|_k^2 = \|v - \widetilde{v}_k\|^2_{L^2(\widetilde{\Omega})} \|\partial I_k(u_k(s))\|_k^2 \to 0,$$

where the convergence follows from $\liminf_{k\to\infty} \|f_k(t)\|_k < \infty$ and Lemma 3.3.6.

3.4.2 Conclusion of the proof of Theorem 3.2.2

In order to follow the evolutionary Γ-convergence approach, the chain rule for $\rho\partial_{tt} w + \partial I(w)$ is needed. For our weak solutions, however, with regularity $\partial_{tt} w \in$

$L^2(0,T;H^{-1}(\Omega;\mathbb{R}^d))$ and $\partial_t w \in L^2(0,T;L^2(\Omega;\mathbb{R}^d))$, the required chain rule in L^2 is not available. By assuming additional regularity on the initial data, we can prove the existence of strong solutions to the continuum momentum equation (3.10), which are sufficiently regular such that a chain rule in L^2 holds.

Indeed, standard arguments, see, e.g., [87, Prop. 6.3.2 on p. 204], give the following.

Lemma 3.4.2 (Strong solutions to (3.10) and the chain rule)**.** *Let $w^0 \in H^2(\Omega;\mathbb{R}^d)$ and $w^1 \in H^1(\Omega;\mathbb{R}^d)$. Then, the unique weak solution w to the continuum momentum equation (3.10) is a strong solution with*

$$\begin{aligned} w &\in L^\infty(0,T;H^2(\Omega;\mathbb{R}^d)),\\ \partial_t w &\in L^\infty(0,T;H^1_0(\Omega;\mathbb{R}^d)),\\ \partial_{tt} w &\in L^\infty(0,T;L^2(\Omega;\mathbb{R}^d)). \end{aligned}$$

In particular, $\partial I(w) \in L^2(0,T;L^2(\Omega;\mathbb{R}^d))$ by comparison and the chain rule

$$\frac{\mathrm{d}}{\mathrm{d}s}\Big(\frac{\rho}{2}\|\partial_t w(s,\cdot)\|^2_{L^2(\Omega)} + I(w(s))\Big) = \big(\rho\partial_{tt} w(s,\cdot) + \partial I(w(s,\cdot)), \partial_t w(s,\cdot)\big) \tag{3.50}$$

holds for almost every $s \in (0,T)$.

Proof of Theorem 3.2.2. To obtain energy convergence, our idea is to pass to the limit in the atomistic energy-dissipation inertia equalities by arguing along the lines of Sandier & Serfaty [119]. As u_k is a solution to the atomistic equation of motion (3.7), (3.25) holds, i.e.,

$$\begin{aligned} &I_k(u_k(0)) - I_k(u_k(t)) + \frac{\rho}{2}\|\dot u_k(0)\|_k^2 - \frac{\rho}{2}\|\dot u_k(t)\|_k^2\\ &\quad= \frac{\nu}{2}\int_0^t \|\dot u_k(s,\cdot)\|_k^2 \,\mathrm{d}s + \frac{1}{2\nu}\int_0^t \|\rho\ddot u_k(s,\cdot) + \partial I_k(u_k(s,\cdot))\|_k^2 \,\mathrm{d}s \quad \forall t \in [0,T]. \end{aligned} \tag{3.51}$$

By Lemma 3.3.8 we find $w(t,\cdot) \in H^1_0(\Omega;\mathbb{R}^d)$ such that $u_k(t,\cdot) \overset{\mathrm{AC}}{\to} w(t,\cdot)$ for all $t \in [0,T]$. Therefore, by means of inequalities (3.16a)–(3.16d), $I_k(u_k) \to I(w^0)$, and $\dot u_k(0) \overset{\mathrm{AC}}{\to} \partial_t w(0)$, we get

$$\begin{aligned} &I(w(0)) - I(w(t)) + \frac{\rho}{2}\|\partial_t w(0,\cdot)\|^2_{L^2(\Omega)} - \frac{\rho}{2}\|\partial_t w(t,\cdot)\|^2_{L^2(\Omega)}\\ &\geq \liminf_{k\to\infty}\big(I_k(u_k(0)) - I_k(u_k(t))\big) + \liminf_{k\to\infty}\Big(\frac{\rho}{2}\|\dot u_k(0)\|_k^2 - \frac{\rho}{2}\|\dot u_k(t)\|_k^2\Big)\\ &\geq \liminf_{k\to\infty}\frac{\nu}{2}\int_0^t \|\dot u_k(s,\cdot)\|_k^2 \,\mathrm{d}s + \liminf_{k\to\infty}\frac{1}{2\nu}\int_0^t \|\rho\ddot u_k(s,\cdot) + \partial I_k(u_k(s,\cdot))\|_k^2 \,\mathrm{d}s\\ &\geq \frac{\nu}{2}\int_0^t \|\partial_t w(s,\cdot)\|^2_{L^2(\Omega)} \,\mathrm{d}s + \frac{1}{2\nu}\int_0^t \|\rho\partial_{tt} w(s,\cdot) + \partial I(w(s,\cdot))\|^2_{L^2(\Omega)} \,\mathrm{d}s. \end{aligned} \tag{3.52}$$

Using Young's inequality we can further estimate

$$\begin{aligned} &\frac{\nu}{2}\int_0^t \|\partial_t w(s,\cdot)\|^2_{L^2(\Omega)} \,\mathrm{d}s + \frac{1}{2\nu}\int_0^t \|\rho\partial_{tt} w(s,\cdot) + \partial I(w(s,\cdot))\|^2_{L^2(\Omega)} \,\mathrm{d}s\\ &\geq -\int_0^t (\rho\partial_{tt} w(s,\cdot) + \partial I(w(s,\cdot)), \partial_t w(s,\cdot)) \,\mathrm{d}s. \end{aligned} \tag{3.53}$$

Hence, from the chain rule (3.50), the right-hand side of (3.53) equals

$$
\begin{aligned}
&-\int_0^t \frac{\mathrm{d}}{\mathrm{d}s}\left(\frac{\rho}{2}\|\partial_t w(s,\cdot)\|_{L^2(\Omega)}^2 + I(w(s))\right)\mathrm{d}s \\
&\quad = I(w(0)) - I(w(t)) + \frac{\rho}{2}\|\partial_t w(0,\cdot)\|_{L^2(\Omega)}^2 - \frac{\rho}{2}\|\partial_t w(t,\cdot)\|_{L^2(\Omega)}^2. \qquad (3.54)
\end{aligned}
$$

Collecting (3.52)–(3.54) we thus conclude that all inequalities above are actually equalities. This is exactly the energy-dissipation-inertia equality corresponding to the continuum equation of motion (3.10), i.e., we have rederived that w is a solution to (3.10). In contrast to the reasoning in Section 3.3.6, the present approach has the advantage of yielding energy convergence $I_k(u_k(t)) \to I(w(t))$ for all $t \in (0,T)$. Eventually, energy convergence entails the strong convergence of gradients, namely $\bar{\nabla} u_k(t) \to \nabla w(t) \cdot Z$ strongly in $L^2(\Omega;\mathbb{R}^d)$ for all $t \in (0,T)$, see Remark 3.3.2. □

By inspecting the above argument, the convergence can be strengthened as follows.

Corollary 3.4.3 (Enhanced convergence)**.** *Let u_k and w solve (3.7) and (3.10) respectively. Under the assumptions of the second part of Theorem 3.2.2, we have*

$$
\begin{aligned}
&\text{(i)} && \int_0^T \|\partial_t \widetilde{u}_k(t,\cdot) - \partial_t \widetilde{w}(t,\cdot)\|_{L^2(\widetilde{\Omega})}^2 \,\mathrm{d}t \to 0, \\
&\text{(ii)} && \int_0^T \|(\rho \ddot{u}_k(t) + \partial I_k(u_k(t)))^{\sim} - (\rho \partial_{tt}\widetilde{w}(t,\cdot) + \partial I(\widetilde{w}))(t,\cdot)\|_{L^2(\widetilde{\Omega})}^2 \,\mathrm{d}t \to 0.
\end{aligned}
$$

Proof. Observe that weak convergence has already been established in (3.47)–(3.48). Strong convergence in $L^2(0,T;L^2(\widetilde{\Omega};\mathbb{R}^d))$ then follows by checking that also the norms convergence. The latter is a consequence of (3.24) and the evolutive Γ-convergence in proof of Theorem 3.2.2, again observing that all inequalities are actually equalities. □

Remark 3.4.4 (Purely viscous case $\rho = 0$). In the case $\rho = 0$, we first note that we still can identify a limit w, see Remark 3.3.9. Remark 3.4.1 yields $\mathrm{div}(\mathbb{C} : \nabla^s w) \in L^2(0,T;L^2(\Omega;\mathbb{R}^d))$. This ensures the validity of the L^2 chain rule under no additional regularity assumption on the initial data. Therefore, existence of solutions needs not be proven beforehand, but follows from passing to the limit in the energy-dissipation equation (3.51) for $\rho = 0$, by resorting to the inequalities (3.16b), (3.16c), (3.49), and using Fatou's Lemma. Eventually, standard elliptic regularity also implies $w \in L^2(0,T;H^2(\Omega;\mathbb{R}^d))$, i.e., w is the unique strong solutions of the continuum momentum equation.

3.5 Summation by parts

Lemma 3.5.1 (Summation by parts)**.** *Let $g = (g_1,\dots,g_{2^d})\colon \mathcal{L}'_\varepsilon(\Omega) \to \mathbb{R}^{d\times 2^d}$, i.e., $g_i(\overline{x}) \in \mathbb{R}^d$ for $i = 1,\dots,2^d$, $\bar{x} \in \mathcal{L}'_\varepsilon(\Omega)$, and let $v \in \mathcal{A}_\varepsilon$ for $\varepsilon > 0$ small enough. Then,*

the following summation by parts formula holds

$$\sum_{\overline{x}\in\mathcal{L}'_\varepsilon(\widetilde{\Omega})} g(\overline{x})\colon \bar{\nabla} v(\overline{x}) = -\sum_{x\in\mathcal{L}_\varepsilon\cap\Omega} \bar{\nabla}^* g(x)\cdot v(x), \tag{3.55}$$

where $\bar{\nabla} v$ is the discrete gradient defined in (3.5) and $\bar{\nabla}^*$ denotes the conjugate operator to $\bar{\nabla}$ given by

$$\bar{\nabla}^* g(x) = \frac{1}{\varepsilon}\sum_{i=1}^{2^d}\left(-g_i(x-\varepsilon z_i) + \frac{1}{2^d}\sum_{j=1}^{2^d} g_i(x-\varepsilon z_j)\right) \quad \forall\, x\in\mathcal{L}_\varepsilon\cap\Omega. \tag{3.56}$$

Proof. Recall the definition of $\bar{\nabla} v(\overline{x}) = \frac{1}{\varepsilon}\big(v(\overline{x}+\varepsilon z_1)-\bar{v}(\overline{x}),\dots,v(\overline{x}+\varepsilon z_{2^d})-\bar{v}(\overline{x})\big)$, where $\bar{v}(\overline{x}) = \frac{1}{2^d}\sum_{j=1}^{2^d} v(\overline{x}+\varepsilon z_j)$. We abbreviate $v_i(\overline{x}) := v(\overline{x}+\varepsilon z_i)$ in the following. We split the left hand side of (3.55) as

$$\sum_{\overline{x}\in\mathcal{L}'_\varepsilon(\widetilde{\Omega})} g(\overline{x})\colon \bar{\nabla} v(\overline{x}) = I - II$$

with

$$\begin{aligned} I &:= \frac{1}{\varepsilon}\sum_{\overline{x}\in\mathcal{L}'_\varepsilon(\widetilde{\Omega})} g(\overline{x})\colon (v_1(\overline{x}),\dots,v_{2^d}(\overline{x})),\\ II &:= \frac{1}{\varepsilon}\sum_{\overline{x}\in\mathcal{L}'_\varepsilon(\widetilde{\Omega})} g(\overline{x})\colon (\bar{v}(\overline{x}),\dots,\bar{v}(\overline{x})). \end{aligned}$$

For the first term we obtain

$$I = \frac{1}{\varepsilon}\sum_{\overline{x}\in\mathcal{L}'_\varepsilon(\widetilde{\Omega})}\sum_{i=1}^{2^d} g_i(\overline{x})\cdot v(\overline{x}+\varepsilon z_i) = \frac{1}{\varepsilon}\sum_{x\in\mathcal{L}_\varepsilon\cap\Omega} v(x)\cdot\left(\sum_{i=1}^{2^d} g_i(x-\varepsilon z_i)\right),$$

which follows by the change of variables $\overline{x}+\varepsilon z_i = x$ and by noting that $v(x)=0$ for $x\notin\Omega$. The second term can be handled analogously as

$$\begin{aligned} II &= \frac{1}{\varepsilon}\sum_{\overline{x}\in\mathcal{L}'_\varepsilon(\widetilde{\Omega})}\sum_{i=1}^{2^d} g_i(\overline{x})\cdot\bar{v}(\overline{x}) = \frac{1}{\varepsilon}\sum_{\overline{x}\in\mathcal{L}'_\varepsilon(\widetilde{\Omega})}\sum_{i=1}^{2^d} g_i(\overline{x})\cdot\left(\frac{1}{2^d}\sum_{j=1}^{2^d} v(\overline{x}+\varepsilon z_j)\right)\\ &= \frac{1}{\varepsilon}\sum_{x\in\mathcal{L}_\varepsilon\cap\Omega} v(x)\cdot\left(\sum_{i=1}^{2^d}\frac{1}{2^d}\sum_{j=1}^{2^d} g_i(x-\varepsilon z_j)\right), \end{aligned}$$

with the change of variables as above. □

Acknowledgments

This work was supported by the DFG project FR 4083/3-1, by the Deutsche Forschungsgemeinschaft (DFG, German Research Foundation) under Germany's Excellence Strategy EXC 2044 -390685587, Mathematics Münster: Dynamics–Geometry–Structure, by the Austrian Science Fund (FWF) projects 10.55776/F65, 10.55776/I4354, 10.55776/I5149, and 10.55776/P32788. The authors would like to thank Marco Cicalese, Mark Peletier, and Florian Theil for some interesting comments on a previous version of [71].

4 Nonlocal-to-local limit in linearized viscoelasticity

This chapter consists of the paper [72] in collaboration with Manuel Friedrich and Ulisse Stefanelli.

Abstract

We study the quasistatic evolution of a linear peridynamic Kelvin-Voigt viscoelastic material. More specifically, we consider the gradient flow of a nonlocal elastic energy with respect to a nonlocal viscous dissipation. Following an evolutionary Γ-convergence approach, we prove that the solutions of the nonlocal problem converge to the solution of the local problem, when the peridynamic horizon tends to 0, that is, in the nonlocal-to-local limit.

4.1 Introduction

The model. In this chapter, we are interested in the quasistatic evolution of linear peridynamic Kelvin–Voigt viscoelastic materials. Let $\Omega \subset \mathbb{R}^d$ ($d \geq 2$) be a bounded reference domain and indicate by $u\colon [0,T] \times \Omega \to \mathbb{R}^d$ the *time dependent displacement*. To prescribe nonlocal homogeneous Dirichlet boundary values, we fix $\widetilde{\Omega} \in \mathbb{R}^d$ such that $\Omega \subset\subset \widetilde{\Omega}$ (compactly contained) and extend u by setting $u(x) = 0$ for $x \in \widetilde{\Omega} \setminus \Omega$. Following [101] and moving within the framework of (state-based) peridynamics, we define the *nonlocal elastic energy* of a homogeneous, isotropic material as

$$\begin{aligned} E_\rho(u) =& \frac{\beta}{2} \int_{\widetilde{\Omega}} (\mathfrak{D}_\rho(u)(x))^2 \,\mathrm{d}x \\ &+ \frac{\alpha}{2} \int_{\widetilde{\Omega}} \int_{\widetilde{\Omega}} \rho(x'-x) \left(\mathscr{D}(u)(x',x) - \frac{1}{d} \mathfrak{D}_\rho(u)(x) \right)^2 \mathrm{d}x' \,\mathrm{d}x. \end{aligned} \tag{4.1}$$

Here, $\rho : \mathbb{R}^d \to [0,\infty)$ is a radially symmetric kernel, weighting the strength of nonlocal interactions. We assume that $\rho(\xi) = 0$ for $|\xi| > h$, where h is the so-called *peridynamic horizon*. Furthermore, we let

$$\mathscr{D}(u)(x',x) := \frac{(u(x') - u(x)) \cdot (x'-x)}{|x'-x|^2} \tag{4.2}$$

indicate the *nonlocal strain* in the direction $(x'-x)/|x'-x|$. The weighted nonlocal strain, called *nonlocal divergence*, is given by

$$\mathfrak{D}_\rho(u)(x) = \text{pv-}\int_{\widetilde{\Omega}} \rho(x'-x) \mathscr{D}(u)(x',x) \,\mathrm{d}x', \tag{4.3}$$

where 'pv' indicates the Cauchy principle value. In fact, it can be shown that $\mathfrak{D}_\rho(u) \to \operatorname{div} u$ as $\rho \to \delta_0$ (Dirac delta in 0) suitably, see Lemma 4.5.1 below. The constants $\alpha, \beta > 0$ are material parameters related to the shear and bulk modulus, respectively.

Under suitable assumptions on the kernel ρ, Mengesha and Du showed that E_ρ admits a unique minimizer [101, Theorem 1.1]. Moreover, they proved that E_ρ Γ-converges [47] with respect to the strong L^2-topology to the *local elastic energy*

$$E(u) = \frac{\lambda}{2} \int_\Omega \operatorname{div} u(x)^2 \,\mathrm{d}x + \frac{\mu}{2} \int_\Omega |\varepsilon(u(x))|^2 \,\mathrm{d}x \tag{4.4}$$

when passing from the nonlocal to the local problem, that is, when $\rho \to \delta_0$ suitably [101, Theorem 1.2]. Here $\varepsilon(u) = (\nabla u + \nabla u^\top)/2$ denotes the *symmetric gradient of* u. The *Lamé coefficients* λ and μ can be expressed in terms of α, β and the dimension d, see (4.8) below or [101, Appendix A]. Note that the integration domain in (4.4) is merely Ω, for admissible configurations for E will be considered as belonging to $H^1_0(\Omega;\mathbb{R}^d)$.

In order to incorporate viscous dissipation in the model, we introduce the *nonlocal potential of viscous forces* given by

$$D_\rho(\dot{u}) = \frac{1}{2} \int_{\widetilde{\Omega}} \int_{\widetilde{\Omega}} \rho(x' - x) |\mathscr{D}(\dot{u})(x', x)|^2 \,\mathrm{d}x' \,\mathrm{d}x, \tag{4.5}$$

where, here and in the following, the symbol $\dot{u}$ denotes the time-derivative of u.

As it turns out, the energy E_ρ is finite if and only if

$$|u|_\rho^2 := \int_{\widetilde{\Omega}} \int_{\widetilde{\Omega}} \rho(x' - x) |\mathscr{D}(u)(x', x)|^2 \,\mathrm{d}x' \,\mathrm{d}x$$

is finite. This motivates the definition of the following *nonlocal energy space*

$$\mathcal{S}_\rho(\widetilde{\Omega};\mathbb{R}^d) := \left\{ u \in L^2(\widetilde{\Omega};\mathbb{R}^d) : |u|_\rho < \infty \text{ and } u = 0 \text{ on } \widetilde{\Omega} \setminus \Omega \right\}.$$

Due to the nonlocal boundary values, a Poincaré inequality is available, and thus $\mathcal{S}_\rho(\widetilde{\Omega};\mathbb{R}^d)$ is a Hilbert space when endowed with the inner product

$$(u, v)_\rho := \int_{\widetilde{\Omega}} \int_{\widetilde{\Omega}} \rho(x' - x) \mathscr{D}(u)(x', x) \mathscr{D}(v)(x', x) \,\mathrm{d}x' \,\mathrm{d}x.$$

Our result. Given some *initial displacement* $u_{\rho,0} \in \mathcal{S}_\rho(\widetilde{\Omega};\mathbb{R}^d)$, we look for a solution $u_\rho \in H^1(0,T;\mathcal{S}_\rho(\widetilde{\Omega};\mathbb{R}^d))$ to the *nonlocal viscoelastic problem* given by

$$\begin{cases} \mathrm{d}_\rho D_\rho(\dot{u}_\rho) + \mathrm{d}_\rho E_\rho(u_\rho) = 0 & \text{in } \mathcal{S}_\rho(\widetilde{\Omega};\mathbb{R}^d)^* \quad \text{for almost every } t \in [0,T], \quad (4.6a) \\ u_\rho(0,\cdot) = u_{\rho,0} & \text{in } \widetilde{\Omega}. \quad (4.6b) \end{cases}$$

Here, $\mathrm{d}_\rho D_\rho$, $\mathrm{d}_\rho E_\rho \colon \mathcal{S}_\rho(\widetilde{\Omega};\mathbb{R}^d) \to \mathcal{S}_\rho(\widetilde{\Omega};\mathbb{R}^d)^*$ (dual space) are the Fréchet differentials of the quadratic functionals D_ρ and E_ρ, see Corollary 4.3.2.

In particular, $\mathrm{d}_\rho D_\rho$ and $\mathrm{d}_\rho E_\rho$ are linear, and existence and uniqueness of solutions to the nonlocal viscoelastic problem follow from classical theory, see, e.g., [87, Section 6.4] or [125, Section III. 2].

The main goal of the chapter is to show that the solutions to the nonlocal viscoelastic problem converge to a solution of the *local viscoelastic problem* in the nonlocal-to-local limit, that is, when the kernels ρ converge to δ_0 in a suitable sense. The *local viscoelastic problem* is that of finding a weak solution $u \in H^1(0,T;H^1_0(\Omega;\mathbb{R}^d))$ of

$$\begin{cases} -\nabla\cdot(\mathbb{D}\varepsilon(\dot u)+\mathbb{C}\varepsilon(u))=0 & \text{a.e. in } (0,T)\times\Omega, \qquad (4.7a)\\ u(0,\cdot)=u_0 & \text{in } \Omega, \qquad (4.7b)\end{cases}$$

where $u_0 \in H^1_0(\Omega;\mathbb{R}^d)$ is a given initial displacement. Here, $\mathbb{C}$ and $\mathbb{D}$ are the *elasticity tensor* and the *viscosity tensor*, respectively, given by

$$\mathbb{C}_{ijkl} = \frac{2\alpha}{d+2}\delta_{ik}\delta_{jl} + \left(\beta - \frac{2\alpha}{d(d+2)}\right)\delta_{ij}\delta_{kl} = \mu\delta_{ik}\delta_{jl} + \lambda\delta_{ij}\delta_{kl}, \qquad (4.8)$$

$$\mathbb{D}_{ijkl} = \frac{2}{d+2}\delta_{ik}\delta_{jl} + \frac{1}{d+2}\delta_{ij}\delta_{kl}, \qquad (4.9)$$

for $i,j,k,l = 1,\dots,d$, where δ_{ij} is the Kronecker delta. Note that we can rewrite the local elastic energy (4.4) as

$$E(u) = \frac{1}{2}\int_\Omega \mathbb{C}\varepsilon(u(x)) : \varepsilon(u(x))\,\mathrm{d}x, \qquad (4.10)$$

see Lemma 4.7.5 below. Moreover, we set

$$D(\dot u) = \frac{1}{2}\int_\Omega \mathbb{D}\varepsilon(\dot u(x)) : \varepsilon(\dot u(x))\,\mathrm{d}x \qquad (4.11)$$

to be the *local viscous potential*, which corresponds to the nonlocal-to-local limit of D_ρ defined in (4.5), see Lemma 4.6.2. The local viscoelastic problem (4.7) models the quasistatic evolution for a linear Kelvin-Voigt viscoelastic material in classical rheology.

The energy (4.1) could easily be complemented with the contribution of body forces. As this does not add difficulties, we prefer to stay with the current, force-free situation, for the sake of notational brevity.

Proof strategy. Problem (4.7) is a gradient flow with respect to the metric defined via the viscous potential as

$$(u,\bar u) \mapsto \int_\Omega \mathbb{D}\varepsilon(u-\bar u) : \varepsilon(u-\bar u).$$

We will tackle the nonlocal-to-local limit of (4.6) as $\rho \to \delta_0$ by resorting to an evolutionary Γ-convergence approach [110, 119]. To this aim, the gradient flow (4.6) is

reformulated in terms of an *energy dissipation equality* (also called *Energy Dissipation Principle* or *De Giorgi's Principle* [120]), which reads as

$$E_\rho\left(u_\rho(s)\right)\Big|_0^t + \int_0^t D_\rho\left(\dot{u}_\rho(s)\right)\mathrm{d}s + \int_0^t D_\rho^*\big(-\mathrm{d}_\rho E_\rho(\dot{u}_\rho(s))\big)\,\mathrm{d}s = 0 \quad \forall t\in[0,T]. \tag{4.12}$$

Here, D_ρ^* denotes the convex conjugate of the nonlocal potential of viscous forces D_ρ.

Passing to the liminf in equation (4.12) and using the inequalities

$$\liminf_{\rho\to\delta_0} E_\rho(u_\rho(t)) \geq E(u(t)), \tag{4.13}$$

$$\liminf_{\rho\to\delta_0} \int_0^t D_\rho(\dot{u}_\rho(s))\,\mathrm{d}s \geq \int_0^t D(\dot{u}(s))\,\mathrm{d}s, \tag{4.14}$$

$$\liminf_{\rho\to\delta_0} \int_0^t D_\rho^*\big(-\mathrm{d}_\rho E_\rho(u_\rho(s))\big)\,\mathrm{d}s \geq \int_0^t D^*\big(-\mathrm{d}E(u(s))\big)\,\mathrm{d}s \tag{4.15}$$

as well as assuming well-preparedness of initial data (namely, $u_\rho(0)\to u(0)$ and $E_\rho(u_\rho(0))\to E(u(0))$), we deduce the corresponding energy dissipation inequality for the (local) limiting problem

$$E(u(t)) - E(u(0)) + \int_0^t D(\dot{u}(s))\,\mathrm{d}s + \int_0^t D^*\big(-\mathrm{d}E(u(s))\big)\,\mathrm{d}s \leq 0. \tag{4.16}$$

In (4.15) and (4.16), $\mathrm{d}E(u)$ denotes the Fréchet derivative in $H^1(\Omega;\mathbb{R}^d)$ of the local energy E (4.10) at u. From the definition of the Fenchel-Legendre transform and the chain rule, we obtain equality in (4.16). This is eventually equivalent to u being a (weak) solution to the local viscoelastic problem (4.7).

This chapter is devoted to make the above argument rigorous, see Theorem 4.2.1 below. In order to achieve this, we prove compactness and the above liminf-inequalities (4.13)–(4.15). In fact, inequality (4.13) has already been established in [101] as part of the Γ-convergence result. The other two liminf-inequalities (4.14) and (4.15) are proved in Section 4.6. Crucial for proving both inequalities is the nonlocal-to-local convergence of $\mathrm{d}_\rho D_\rho$ and $\mathrm{d}_\rho E_\rho$. Note that here also the arguments depend on ρ, which adds some difficulties if compared to the analysis in [101].

Passing to the limit directly in the equations, namely, without reasoning to the equivalent energy-dissipation-inequality formulation, would also be possible. Still, it would require to cope with ρ-dependent spaces, resulting in a more involved argument. The variational perspective has the advantage of additionally providing convergence of the nonlocal elastic energies along the evolution, see Corollary 4.6.4.

Literature. Let us now put our result in the context of the available literature. Since the introduction of peridynamics by Silling [127], the dynamic peridynamic model has already attracted some attention, see [60, 61] and the references therein for an overview on dynamic problems and [85] for a survey of the general peridynamic literature. In [62], the authors prove well-posedness of a linear peridynamic momentum balance by using the Duhamel principle. Moreover, in the nonlocal-to-local limit they recover the Navier

equation of classical elasticity in a perturbative fashion, similar to that of [8, 58] in the case of atomistic-to-continuum limits. This result has then been generalized in various directions, e.g., allowing for less regular solutions [56], or rotational variant kernels [104]. Also the nonlinear case has been studied [44].

For the static case, in [102] it has been shown well-posedness of a bond-based peridynamic boundary value problem, namely, $\mathcal{L}_\rho u = b$, where $\mathcal{L}_\rho$ is a nonlocal operator (similar to $v \mapsto (u, v)_\rho$) and b models body forces. Moreover, its nonlocal-to-local limit to the classical Navier equation has been derived.

Various viscoelastic models have already been used successfully by the engineering community to model and simulate rate-dependent phenomena involving discontinuities [51, 79, 97, 112, 135, 137]. Rigorous mathematical results involving viscosity are however still not available.

A nonlocal parabolic equation related to peridynamics has been investigated in [141]. Existence and uniqueness of solutions to the nonlocal problem are proved by a Galerkin method. However, nonlocal-to-local convergence has not been treated. In a recent work Yang, Zhang, and Nie [140] considered a linearized bond-based peridynamic dynamic problem incorporating a nonlocal damping term. They establish well-posedness of the nonlocal problem by resorting to a Galerkin method, as well. Passing to the limit in the equation, they show that solutions to the nonlocal problem converge to weak solutions of the local problem, which turns out to be the elastodynamic equation of motion. In fact, due to their choice of the nonlocal kernel in the damping operator, the viscous effects vanish when passing to the limit and the bond-based peridynamic approach gives rise to the Laplacian in the limit (see also [14, 127] for a discussion on the limitations of the bond-based approach). Although their result is similar to ours, the techniques are fundamentally different. Their result applies to a bond-based peridynamic model only and it does not allow to recover viscous effects in the small-horizon limit.

A paper more closely to this chapter in spirit is [86]. There, the authors investigate a peridynamic model related to elastoplasticity in the small strain regime. They prove well-posedness of the nonlocal problem via a time discretization scheme. Then, they pass to the limit via an evolutionary Γ-convergence approach for rate-independent systems [111]. As the viscosity potential D_ρ (4.5) considered here is quadratic, we are not in the setting of rate-independent systems.

Organization of the chapter. This chapter is organized as follows. We introduce the model and state the main result on the evolutionary Γ-convergence in Section 4.2. In Section 4.3, we compute the derivatives of the energy and the viscous potential and collect some of their properties. These will then be used in Section 4.4, where existence of solutions to the nonlocal problem, a priori estimates, and compactness are proved. In Section 4.5, we collect several nonlocal-to-local convergence results and in particular establish the convergence of the derivatives of D_ρ and E_ρ. The last part, Section 4.6, is then devoted to the proof of our main result.

4.2 The model and main result

4.2.1 Notation

We denote the Euclidean inner product in $\mathbb{R}^d$ by $a \cdot b := a_i b_i$ and the contraction of two-tensors by $A : B := A_{ij} B_{ij}$.

Given a smooth function $u \colon \Omega \subset \mathbb{R}^d \to \mathbb{R}^d$, we abbreviate the partial derivative with respect to the j-th spatial coordinate with ∂_j and write $\nabla u(x) \in \mathbb{R}^{d\times d}$ with $(\nabla u(x))_{ij} = \partial_j u_i(x)$ for its Jacobian. Moreover, we denote the *symmetric gradient of* u by $\varepsilon(u) := (\nabla u + (\nabla u)^\top)/2$. We let $⨍_{S^{d-1}} f(s)\,\mathrm{d}\mathcal{H}^{d-1}(s) := \big(\mathcal{H}^{d-1}(S^{d-1})\big)^{-1} \int_{S^{d-1}} f(s)\,\mathrm{d}\mathcal{H}^{d-1}(s)$, where $\mathcal{H}^{d-1}$ is the $(d-1)$-dimensional Hausdorff-measure and S^{d-1} the $(d-1)$-dimensional unit sphere.

We follow the convention to abbreviate the L^2-inner product by $(u, v) := \int_\Omega u(x) \cdot v(x)\,\mathrm{d}x$ for $u, v \in L^2(\Omega;\mathbb{R}^d)$. Moreover, the $L^p(\Omega;\mathbb{R}^N)$-norm will be denoted by $\|\cdot\|_{L^p(\Omega)^N}$, where we omit N if $N = 1$. Furthermore, c denotes a generic positive constant, only depending on data and the dimension d, and possibly varying from line to line.

4.2.2 The model

Let $\Omega \subset \mathbb{R}^d$ ($d \geq 2$) be a bounded domain with Lipschitz boundary representing the reference configuration of the elastic body. The deformation of the body is described by a *time-dependent displacement* $u \colon [0, T] \times \Omega \to \mathbb{R}^d$, where $T > 0$ is a *final reference time*.

To introduce *nonlocal homogeneous Dirichlet boundary values* (or nonlocal volumetric constraints), see, e.g., [53, 54], we fix $\widetilde{\Omega} \subset \mathbb{R}^d$ open such that $\Omega \subset\subset \widetilde{\Omega}$ (compactly contained). We then extend deformations from Ω to $\widetilde{\Omega}$ by 0, that is, we set

$$V := \left\{ u \in L^2(\widetilde{\Omega};\mathbb{R}^d) : u = 0 \text{ on } \widetilde{\Omega} \setminus \Omega \right\}.$$

We recall that the nonlocal strain $\mathscr{D}(u)$ and the nonlocal divergence $\mathfrak{D}_\rho(u)$ are given by

$$\begin{aligned} \mathscr{D}(u)(x', x) &= \frac{(u(x') - u(x)) \cdot (x' - x)}{|x' - x|^2}, \\ \mathfrak{D}_\rho(u)(x) &= \text{pv-}\!\int_{\widetilde{\Omega}} \rho(x' - x)\mathscr{D}(u)(x', x)\,\mathrm{d}x', \end{aligned}$$

where ρ is a positive and integrable kernel, see Assumption 4.2.1 below. Moreover, we recall the notation

$$|u|_\rho^2 = \int_{\widetilde{\Omega}} \int_{\widetilde{\Omega}} \rho(x' - x)|\mathscr{D}(u)(x', x)|^2\,\mathrm{d}x'\,\mathrm{d}x \tag{4.17}$$

and the definition of the *nonlocal energy space*

$$\mathcal{S}_\rho(\widetilde{\Omega};\mathbb{R}^d) = \left\{ u \in V : |u|_\rho^2 < \infty \right\}.$$

Fixing the displacement on $\widetilde{\Omega}\setminus\Omega$ allows us to employ a nonlocal Korn-type inequality on $\mathcal{S}_\rho(\widetilde{\Omega};\mathbb{R}^d)$ [99], see Proposition 4.4.2 below, which entails that the seminorm in (4.17) is actually a norm. Therefore, $\mathcal{S}_\rho(\widetilde{\Omega};\mathbb{R}^d)$ is a Hilbert space when equipped with the inner product

$$(u,v)_\rho := \int_{\widetilde{\Omega}}\int_{\widetilde{\Omega}} \rho(x'-x)\mathscr{D}(u)(x',x)\mathscr{D}(v)(x',x)\,\mathrm{d}x'\,\mathrm{d}x,$$

see [101, Theorem 2.1].

Recalling the definition of the nonlocal elastic energy (4.1), we have

$$E_\rho(u)<\infty \iff |u|_\rho<\infty. \tag{4.18}$$

Indeed, by Hölder's inequality we have that $\mathfrak{D}_\rho(u)\in L^2(\widetilde{\Omega};\mathbb{R}^d)$ if $|u|_\rho\le c$, and thus $E_\rho(u)\le c$ for $u\in\mathcal{S}_\rho(\widetilde{\Omega};\mathbb{R}^d)$. The converse also holds true: If $E_\rho(u)<\infty$, then also $|u|_\rho<\infty$, see [100, Proposition 1].

We extend the energy E_ρ from $\mathcal{S}_\rho(\widetilde{\Omega};\mathbb{R}^d)$ to all of V by setting $E_\rho(u)=\infty$ whenever $u\in V\setminus\mathcal{S}_\rho(\widetilde{\Omega};\mathbb{R}^d)$.

To study the passage from the nonlocal to the local model, we introduce a family of radial kernels $\rho_n:\mathbb{R}^d\to[0,\infty]$ suitably converging to the Dirac δ_0. More precisely, we require $(\rho_n)_n$ to satisfy the following.

Assumption 4.2.1. *Let $\rho_n:\mathbb{R}^d\to[0,\infty)$ $(n\ge1)$ be a family of radially symmetric kernels, i.e., $\tilde\rho_n(|\xi|)=\rho_n(\xi)$ for some $\tilde\rho_n\colon[0,\infty)\to[0,\infty)$. We assume that $(\rho_n)_n$ satisfies the following*

$$\begin{aligned}
&\text{(i)} && r\mapsto r^{-2}\tilde\rho_n(r) \text{ is nonincreasing in } r,\\
&\text{(ii)} && \int_{\mathbb{R}^d}\rho_n(\xi)\,\mathrm{d}\xi = d,\\
&\text{(iii)} && \lim_{n\to\infty}\int_{\{|\xi|\ge r_0\}}\rho_n(\xi)\,\mathrm{d}\xi=0 \qquad \forall r_0>0.
\end{aligned} \tag{4.19}$$

These assumptions have already been considered in [101] for the proof of the Γ-convergence of $(E_{\rho_n})_n$. In the following, in order to simply notation, we set

$$E_n := E_{\rho_n},\quad D_n := D_{\rho_n},\quad \mathcal{S}_n(\widetilde{\Omega};\mathbb{R}^d) := \mathcal{S}_{\rho_n}(\widetilde{\Omega};\mathbb{R}^d),\quad \mathfrak{D}_n := \mathfrak{D}_{\rho_n},\quad |\cdot|_n := |\cdot|_{\rho_n}.$$

As $n\to\infty$, one expects the nonlocal energy spaces $\mathcal{S}_n(\widetilde{\Omega};\mathbb{R}^d)$ to approach the set $\{u\in H^1(\widetilde{\Omega};\mathbb{R}^d) : u=0 \text{ on } \widetilde{\Omega}\setminus\Omega\}$, which can be identified with

$$H^1_0(\Omega;\mathbb{R}^d) := \left\{H^1(\Omega;\mathbb{R}^d) : u|_{\partial\Omega}=0\right\},$$

where $u|_{\partial\Omega}$ has to be interpreted in the usual trace sense.

4.2.3 Main result

Given some *initial nonlocal displacement* $u_n^0 \in \mathcal{S}_n(\widetilde{\Omega};\mathbb{R}^d)$, we consider the solution u_n to the *nonlocal viscoelastic problem* given by

$$\begin{cases} \mathrm{d}_n D_n(\dot{u}_n) + \mathrm{d}_n E_n(u_n) = 0 & \text{in } \mathcal{S}_n(\widetilde{\Omega};\mathbb{R}^d)^* \quad \text{for almost all } t \in [0,T], \qquad (4.20a) \\ u_n(0,\cdot) = u_n^0 & \text{in } \widetilde{\Omega}. \qquad (4.20b) \end{cases}$$

Here, $\mathrm{d}_n F(x)$ denotes the Fréchet differential of F evaluated at x in the space $\mathcal{S}_n(\widetilde{\Omega};\mathbb{R}^d)$ and $(\mathcal{S}_n(\widetilde{\Omega};\mathbb{R}^d))^*$ denotes the dual space of $\mathcal{S}_n(\widetilde{\Omega};\mathbb{R}^d)$. We say that $u_n \in H^1(0,T;\mathcal{S}_n(\widetilde{\Omega};\mathbb{R}^d))$ is a solution to (4.20) if it satisfies the initial condition and

$$\mathrm{d}_n D_n(\dot{u}_n)(v) + \mathrm{d}_n E_n(u_n)(v) = 0$$

for all $v \in \mathcal{S}_n(\widetilde{\Omega};\mathbb{R}^d)$ and almost every $t \in [0,T]$, where $\mathrm{d}_n F(x)(v) = \lim_{\eta\to 0} \frac{F(x+\eta v)-F(x)}{\eta}$ is the Gâteaux derivative of F at $x \in \mathcal{S}_n(\widetilde{\Omega};\mathbb{R}^d)$ in direction $v \in \mathcal{S}_n(\widetilde{\Omega};\mathbb{R}^d)$.

The *local viscoelastic problem* is to find $u \in H^1(0,T;H_0^1(\Omega;\mathbb{R}^d))$ solving, in the weak sense, the system

$$\begin{cases} \mathrm{d}D(\dot{u}(t)) + \mathrm{d}E(u(t)) = 0 & \text{in } (H_0^1(\Omega;\mathbb{R}^d))^* \quad \text{for almost every } t \in [0,T], \qquad (4.21a) \\ u(0,\cdot) = u^0 & \text{in } \Omega. \qquad (4.21b) \end{cases}$$

Here, $u^0 \in H_0^1(\Omega;\mathbb{R}^d)$ is a given *initial local displacement*. Moreover, $\mathrm{d}F(x)$ denotes the Fréchet differential of F evaluated at x in the space $H_0^1(\Omega;\mathbb{R}^d)$. Owing to the explicit form of $\mathrm{d}E$ and $\mathrm{d}D$, see (4.26) and (4.27) below, a weak solution $u \in H^1(0,T;H_0^1(\Omega;\mathbb{R}^d))$ to (4.21) equivalently satisfies

$$\int_\Omega \mathbb{D}\varepsilon(\dot{u}(x)) : \varepsilon(v(x)) + \mathbb{C}\varepsilon(u(x)) : \varepsilon(v(x))\,\mathrm{d}x = 0$$

for all $v \in H_0^1(\Omega;\mathbb{R}^d)$ and almost every $t \in [0,T]$. Here, recall that $\mathbb{C}$ is the elasticity tensor and $\mathbb{D}$ is the viscosity tensor defined in (4.8) and (4.9), respectively.

Our main result reads as follows.

Theorem 4.2.1 (Evolutionary Γ-convergence)**.** *Under Assumptions 4.2.1, let a sequence of initial conditions $u_n^0 \in \mathcal{S}_n(\widetilde{\Omega};\mathbb{R}^d)$ and $u^0 \in H_0^1(\Omega;\mathbb{R}^d)$ be given such that $u_n^0 \to u^0$ strongly in $L^2(\widetilde{\Omega};\mathbb{R}^d)$ and $E_n(u_n^0) \to E(u^0)$ as $n \to \infty$. Then, for all $n \in \mathbb{N}$, the nonlocal viscoelastic problem (4.20) admits a unique solution $u_n \in H^1(0,T;\mathcal{S}_n(\widetilde{\Omega};\mathbb{R}^d))$ and $u_n \to u$ in $C([0,T];L^2(\widetilde{\Omega};\mathbb{R}^d))$, where $u \in H^1(0,T;H_0^1(\Omega;\mathbb{R}^d))$ is the unique weak solution to the local viscoelastic problem (4.21).*

The convergence of $u_n \to u$ and $u_n^0 \to u^0$ in the theorem above, has to be interpreted as convergence of u_n and u_n^0 to the extensions of u and u^0 to $\widetilde{\Omega}$ by 0, i.e., as convergence on $\widetilde{\Omega}$. From now on, we will understand all limits of elements of $\mathcal{S}_n(\widetilde{\Omega},\mathbb{R}^d)$ in this sense without changing the notation, and identify $u \in H_0^1(\Omega;\mathbb{R}^d)$ with its trivial extension to $\widetilde{\Omega}$, whenever convenient.

Remark 4.2.2 (Regularity). (i) As we are in the force-free setting, the solution u to (4.21) actually satisfies $u \in C^\infty(0,T;H^1_0(\Omega;\mathbb{R}^d))$. Indeed, as $u \in H^1(0,T;H^1_0(\Omega;\mathbb{R}^d))$, also $\mathrm{d}E(u) \in H^1(0,T;(H^1_0(\Omega;\mathbb{R}^d))^*)$ by (4.26) below. Comparison in equation (4.21) yields that also $\mathrm{d}D(\dot{u}) \in H^1(0,T;(H^1_0(\Omega;\mathbb{R}^d))^*)$, and hence by (4.27) and Korn's inequality (see Lemma 4.4.4 below) we deduce $\dot{u} \in H^1(0,T;H^1_0(\Omega;\mathbb{R}^d))$. An induction argument yields the claim.

(ii) Analogously to (i), if u_n is a solution to the nonlocal viscoelastic problem (4.20), then $u_n \in C^\infty(0,T;\mathcal{S}_n(\widetilde{\Omega};\mathbb{R}^d))$ (replacing (4.26)–(4.27) by (4.22)–(4.23) in the argument above).

(iii) Note that in the case with body forces $f \in L^2(0,T;L^2(\Omega;\mathbb{R}^d))$, the solution to the local viscoelastic problem (4.21) satisfies (only) $u \in H^1(0,T;H^1_0(\Omega;\mathbb{R}^d))$ and analogously a solution to the nonlocal viscoelastic problem would be in $H^1(0,T;\mathcal{S}_n(\widetilde{\Omega};\mathbb{R}^d))$.

4.3 Differentials of the potentials

4.3.1 Nonlocal potentials

In this section, we calculate the directional derivatives of the nonlocal elastic energy (4.1) and the nonlocal viscous potential (4.5). Based on this, we also get that D_n and E_n are Fréchet differentiable, as the Gâteaux derivatives are linear and continuous.

Lemma 4.3.1 (Gâteaux derivatives)**.** *Let u, $v \in \mathcal{S}_n(\widetilde{\Omega};\mathbb{R}^d)$. Then,*

$$\begin{aligned}\mathrm{d}_n E_n(u)(v) &= \beta \int_{\widetilde{\Omega}} (\mathfrak{D}_n(u)(x))(\mathfrak{D}_n(v)(x))\,\mathrm{d}x + \alpha \int_{\widetilde{\Omega}}\int_{\widetilde{\Omega}} \rho_n(x'-x) \\ &\quad \times \left(\mathscr{D}(u)(x',x) - \frac{1}{d}\mathfrak{D}_n(u)(x)\right)\left(\mathscr{D}(v)(x',x) - \frac{1}{d}\mathfrak{D}_n(v)(x)\right)\mathrm{d}x'\,\mathrm{d}x, \quad (4.22)\\ \mathrm{d}_n D_n(u)(v) &= \int_{\widetilde{\Omega}}\int_{\widetilde{\Omega}} \rho_n(x'-x)\mathscr{D}(u)(x',x)\mathscr{D}(v)(x',x)\,\mathrm{d}x'\,\mathrm{d}x. \quad (4.23)\end{aligned}$$

In particular, the Gâteaux derivatives are linear.

Proof. We split the energy E_n into the dilatational part and the deviatoric part as $E_n = E_\beta + E_\alpha$ with

$$\begin{aligned}E_\beta(u) &= \frac{\beta}{2}\int_{\widetilde{\Omega}} (\mathfrak{D}_n(u)(x))^2\,\mathrm{d}x,\\ E_\alpha(u) &= \frac{\alpha}{2}\int_{\widetilde{\Omega}}\int_{\widetilde{\Omega}} \rho_n(x'-x)\left(\mathscr{D}(u)(x',x) - \frac{1}{d}\,\mathfrak{D}_n(u)(x)\right)^2\mathrm{d}x'\,\mathrm{d}x.\end{aligned}$$

Recall the definition of the nonlocal strain from (4.2). As $u \mapsto \mathscr{D}(u)$ is linear, its Gâteaux derivative in direction $v \in \mathcal{S}_n(\widetilde{\Omega};\mathbb{R}^d)$ is

$$\frac{\mathrm{d}}{\mathrm{d}h}\mathscr{D}(u+hv)(x',x)\big|_{h=0} = \mathscr{D}(v)(x',x). \quad (4.24)$$

By (4.24), for the nonlocal divergence (4.3) we get

$$\frac{\mathrm{d}}{\mathrm{d}h}\mathfrak{D}_n(u+hv)(x)|_{h=0} = \text{pv-}\int_{\widetilde{\Omega}} \rho_n(x'-x)\mathscr{D}(v)(x',x)\,\mathrm{d}x' = \mathfrak{D}_n(v)(x),$$

and consequently

$$\frac{\mathrm{d}}{\mathrm{d}h}E_\beta(u+hv)|_{h=0} = \frac{\beta}{2}\int_{\widetilde{\Omega}} \frac{\mathrm{d}}{\mathrm{d}h}(\mathfrak{D}_n(u+hv)(x))^2\big|_{h=0}\,\mathrm{d}x = \beta\int_{\widetilde{\Omega}}(\mathfrak{D}_n(u)(x))(\mathfrak{D}_n(v)(x))\,\mathrm{d}x.$$

For the deviatoric energy term, we compute

$$\begin{aligned}
&\frac{\mathrm{d}}{\mathrm{d}h}E_\alpha(u+hv)\big|_{h=0}\\
&= \frac{\mathrm{d}}{\mathrm{d}h}\frac{\alpha}{2}\int_{\widetilde{\Omega}}\int_{\widetilde{\Omega}} \rho_n(x'-x)\left(\mathscr{D}(u+hv)(x',x) - \frac{1}{d}\mathfrak{D}_n(u+hv)(x)\right)^2 \mathrm{d}x'\,\mathrm{d}x\big|_{h=0}\\
&= \alpha\int_{\widetilde{\Omega}}\int_{\widetilde{\Omega}} \rho_n(x'-x)\left(\mathscr{D}(u)(x',x) - \frac{1}{d}\mathfrak{D}_n(u)(x)\right)\left(\mathscr{D}(v)(x',x) - \frac{1}{d}\mathfrak{D}_n(v)(x)\right)\mathrm{d}x'\,\mathrm{d}x,
\end{aligned}$$

giving (4.22).

Finally, we calculate the directional derivative of D_n at u in direction v. By (4.24) we readily get

$$\frac{\mathrm{d}}{\mathrm{d}h}D_n(u+hv)\big|_{h=0} = \int_{\widetilde{\Omega}}\int_{\widetilde{\Omega}} \rho_n(x'-x)\mathscr{D}(u)(x',x)\mathscr{D}(v)(x',x)\,\mathrm{d}x'\,\mathrm{d}x,$$

which concludes the proof. □

Recall the definition of the nonlocal seminorm (4.17).

Corollary 4.3.2. *For $u, v \in \mathcal{S}_n(\widetilde{\Omega};\mathbb{R}^d)$, we have*

$$\begin{aligned}
|\,\mathrm{d}_n E_n(u)(v)| &\le c|u|_n|v|_n,\\
|\,\mathrm{d}_n D_n(u)(v)| &\le c|u|_n|v|_n.
\end{aligned}$$

In particular, E_n and D_n are Fréchet differentiable in $\mathcal{S}_n(\widetilde{\Omega};\mathbb{R}^d)$.

Proof. Linearity is clear from Lemma 4.3.1, so we focus on boundedness. Writing $\rho_n = \sqrt{\rho_n}\sqrt{\rho_n}$, by Hölder's inequality we have

$$|\mathfrak{D}_n(u)(x)|^2 \le \int_{\widetilde{\Omega}} \rho_n(x'-x)\,\mathrm{d}x' \int_{\widetilde{\Omega}} \rho_n(x'-x)\left(\mathscr{D}(u)(x',x)\right)^2\mathrm{d}x',$$

and consequently, (4.19) yields

$$\|\mathfrak{D}_n(u)\|_{L^2(\widetilde{\Omega})} \le \|\rho_n\|^{1/2}_{L^1(\mathbb{R}^d)}|u|_n = d^{1/2}|u|_n.$$

In a similar fashion, we also get

$$\int_{\widetilde{\Omega}} (\mathfrak{D}_n(u)(x))(\mathfrak{D}_n(v)(x))\,\mathrm{d}x \leq \|\rho_n\|_{L^1(\mathbb{R}^d)}^{1/2} |u|_n |v|_n = d|u|_n|v|_n. \tag{4.25}$$

Expanding the product in

$$\int_{\widetilde{\Omega}}\int_{\widetilde{\Omega}} \rho_n(x'-x)\left(\mathscr{D}(u)(x',x) - \frac{1}{d}\mathfrak{D}_n(u)(x)\right)\left(\mathscr{D}(v)(x',x) - \frac{1}{d}\mathfrak{D}_n(v)(x)\right)\mathrm{d}x'\,\mathrm{d}x,$$

and noting that the mixed terms are of the form $\int_{\widetilde{\Omega}} \mathfrak{D}_n(u)(x)\mathfrak{D}_n(v)(x)\,\mathrm{d}x$, one realizes that, due to (4.25), we just need to bound the term

$$\int_{\widetilde{\Omega}}\int_{\widetilde{\Omega}} \rho_n(x'-x)\mathscr{D}(u)(x',x)\mathscr{D}(v)(x',x)\,\mathrm{d}x'\,\mathrm{d}x.$$

Applying Hölder's inequality, we have

$$\begin{aligned}
&\int_{\widetilde{\Omega}} \rho_n(x'-x)\mathscr{D}(u)(x',x)\mathscr{D}(v)(x',x)\,\mathrm{d}x' \\
&\leq \left(\int_{\widetilde{\Omega}} \rho_n(x'-x)\left(\mathscr{D}(u)(x',x)\right)^2\mathrm{d}x'\right)^{1/2}\left(\int_{\widetilde{\Omega}} \rho_n(x'-x)\left(\mathscr{D}(v)(x',x)\right)^2\mathrm{d}x'\right)^{1/2}
\end{aligned}$$

and therefore also

$$\int_{\widetilde{\Omega}}\int_{\widetilde{\Omega}} \rho_n(x'-x)\mathscr{D}(u)(x',x)\mathscr{D}(v)(x',x)\,\mathrm{d}x'\,\mathrm{d}x \leq c|u|_n|v|_n. \qquad \square$$

4.3.2 Local potentials

Let us recall the definition of the tensors (4.8) and (4.9), as well as the local elastic energy (4.10) and the local viscous potential (4.11). As the tensors $\mathbb{C}$ and $\mathbb{D}$ are major-symmetric, i.e., $\mathbb{C}_{ijkl} = \mathbb{C}_{klij}$ and $\mathbb{D}_{ijkl} = \mathbb{D}_{klij}$, we can compute the Gâteaux derivatives of E and D in $H^1(\Omega;\mathbb{R}^d)$ as

$$\mathrm{d}E(u)(v) = \int_\Omega \mathbb{C}\varepsilon(u(x)) : \varepsilon(v(x))\,\mathrm{d}x, \tag{4.26}$$

$$\mathrm{d}D(u)(v) = \int_\Omega \mathbb{D}\varepsilon(u(x)) : \varepsilon(v(x))\,\mathrm{d}x, \tag{4.27}$$

for all $u, v \in H^1(\Omega;\mathbb{R}^d)$.

4.4 Nonlocal well-posedness and energy-dissipation-equality

In this section, we prove the well-posedness of the nonlocal viscoelastic problem (4.20), derive the energy-dissipation equality, and prove compactness. To this end, we start with a short preliminary section, recalling some related results from the literature.

4.4.1 Preliminary results

To start with, let us recall the following useful result.

Lemma 4.4.1 ([99, Lemma 2.1]). *For any $u \in H^1(\widetilde{\Omega};\mathbb{R}^d)$, we have*

$$|u|_n \leq c\|\varepsilon(u)\|_{L^2(\widetilde{\Omega})^{d\times d}},$$

where c only depends on $\widetilde{\Omega}$ and d.

Next, we consider a nonlocal Poincaré-Korn inequality. To this end, note that $|u|_n = 0$ if and only if u is an infinitesimal rigid displacement, i.e.,

$$u \in \mathcal{R} := \left\{ x \mapsto Ax + t : A \in \mathbb{R}^{d\times d},\ A^\top = -A,\ t \in \mathbb{R}^d \right\},$$

see [100, Lemma 1]. In particular, $\mathcal{S}_n(\widetilde{\Omega};\mathbb{R}^d) \cap \mathcal{R} = \{0\}$, which is necessary for the following.

Proposition 4.4.2 (Nonlocal Poincaré-Korn inequality, [101, Proposition 2.7]). *There exists a positive constant $c = c(\widetilde{\Omega}, \rho_n)$ such that*

$$\|u\|^2_{L^2(\widetilde{\Omega})^d} \leq c|u|^2_n \qquad \forall u \in \mathcal{S}_n(\widetilde{\Omega};\mathbb{R}^d). \tag{4.28}$$

Note that in principle the constant may depend on n. Yet, the following compactness result and a standard compactness-contradiction argument show that the constant in (4.28) can in fact be chosen independently of n.

Proposition 4.4.3 (Compactness, [101, Proposition 4.2]). *Assume that ρ_n satisfy Assumption 4.2.1. If u_n is a bounded sequence in V satisfying the uniform bound*

$$\sup_{n\in\mathbb{N}} |u_n|_n \leq c,$$

there exists $u \in H^1_0(\Omega;\mathbb{R}^d)$ and a (not relabeled) subsequence such that $u_n \to u$ strongly in $L^2(\widetilde{\Omega};\mathbb{R}^d)$.

To be precise, the fact that u has zero trace is not inferred from [101, Proposition 4.2], but comes from the almost everywhere pointwise convergence of $u_n \in V$, which is 0 on $\widetilde{\Omega} \setminus \Omega$.

In particular, the estimate (4.28) entails that $|\cdot|_n$ is a norm on $\mathcal{S}_n(\widetilde{\Omega};\mathbb{R}^d)$ and thus $(\cdot,\cdot)_n$ constitutes an inner product. Note that relation (4.23) implies that $\mathrm{d}_n D_n$ is the Riesz isomorphism, as $\mathrm{d}_n D_n(u)(v) = (u,v)_n$.

We recall the classical Korn inequality, see, e.g., [76, Proposition 1].

Lemma 4.4.4 (Korn inequality). *There is a constant $c > 0$ with*

$$\|u\|_{H^1(\Omega)^d} \leq c\|\varepsilon(u)\|_{L^2(\Omega)^{d\times d}} \qquad \forall u \in H^1_0(\Omega;\mathbb{R}^d).$$

Next, we recall the following Γ-convergence result, which is crucial for our analysis.

Theorem 4.4.5 (Γ-convergence, [101, Theorem 1.2]). *The sequence E_n Γ-converges in the strong L^2-topology to E, defined in (4.4), which can be equivalently rewritten as*

$$\begin{aligned} E(u) =& \frac{1}{2}\int_\Omega \mathbb{C}\varepsilon(u(x)) : \varepsilon(u(x))\,\mathrm{d}x \\ =& \frac{\beta}{2}\int_\Omega \operatorname{div}^2 u(x)\,\mathrm{d}x + \frac{\alpha}{2}d\int_\Omega \fint_{S^{d-1}} \left(s\cdot\nabla u(x)s - \frac{1}{d}\operatorname{div} u(x)\right)^2 \mathrm{d}\mathcal{H}^{d-1}(s)\,\mathrm{d}x \\ =& \frac{\mu}{2}\int_\Omega |\varepsilon(u(x))|^2\,\mathrm{d}x + \frac{\lambda}{2}\int_\Omega (\operatorname{div} u(x))^2\,\mathrm{d}x, \end{aligned} \tag{4.29}$$

with $\mu = \frac{2\alpha}{d+2}$ and $\lambda = \beta - \frac{2\alpha}{d(d+2)}$.

A proof of the claim that the different representations (4.10) and (4.29) of the energy E are indeed equivalent can be found in the Appendix 4.7, Lemmas 4.7.4 and 4.7.5.

We close this section with a representation of the viscous potential D which follows from Lemma 4.7.3 and a computation analogous to the one of Lemma 4.7.5 (by just replacing λ and μ there by $\frac{1}{d+2}$ and $\frac{2}{d+2}$, respectively).

Lemma 4.4.6. *The local viscous potential, defined in (4.11) can be equivalently written as*

$$\begin{aligned} D(w) &= \frac{1}{2}\int_\Omega \mathbb{D}\varepsilon(w(x)) : \varepsilon(w(x))\,\mathrm{d}x \\ &= \frac{1}{d+2}\int_\Omega |\varepsilon(w(x))|^2\,\mathrm{d}x + \frac{1}{2(d+2)}\int_\Omega (\operatorname{div} w(x))^2\,\mathrm{d}x \\ &= \frac{d}{2}\int_\Omega \fint_{S^{d-1}} (s\cdot\nabla w(x)s)^2\,\mathrm{d}\mathcal{H}^{d-1}(s)\,\mathrm{d}x \end{aligned}$$

for all $w \in H^1(\Omega;\mathbb{R}^d)$.

4.4.2 Solutions to the nonlocal viscoelastic problem

Here, we prove the well-posedness of the nonlocal viscoelastic problem (4.20). As $\mathrm{d}_n D_n$ and $\mathrm{d}_n E_n$ are linear, the nonlocal viscoelastic problem is nothing but a linear Cauchy problem on the Hilbert space $\mathcal{S}_n(\widetilde{\Omega};\mathbb{R}^d)$. Therefore, well-posedness is classical.

Proposition 4.4.7 (Well-posedness of nonlocal viscoelastic problem). *The nonlocal viscoelastic problem (4.20) has a unique solution $u_n \in H^1(0,T;\mathcal{S}_n(\widetilde{\Omega};\mathbb{R}^d))$.*

Proof. As $\mathrm{d}_n D_n(\dot{u}_n)(v_n) = (\dot{u}_n, v_n)_n$ by Lemma 4.3.1, $\mathrm{d}_n D_n$ is nothing but the Riesz isomorphism. In particular, (4.20) is equivalent to

$$\frac{\mathrm{d}}{\mathrm{d}t}u_n(t) + ((\mathrm{d}_n D_n)^{-1}\circ \mathrm{d}_n E_n)(u_n) = 0.$$

Moreover, as $\mathrm{d}_n D_n$ is the Riesz isomorphism, Corollary 4.3.2 implies that $(\mathrm{d}_n D_n)^{-1}\circ \mathrm{d}_n E_n$ is a Lipschitz map. Therefore, the classical Picard Theorem for Banach spaces applies, see, e.g., [95, Theorem 6]. □

4.4.3 Energy dissipation equality and a priori estimates

In this section, we derive the energy dissipation equality and, as a consequence, the a priori estimates. As a crucial ingredient, we first check that the chain rule holds in the nonlocal setting.

Lemma 4.4.8 (Chain rule)**.** *Let u_n be the solution to the nonlocal viscoelastic problem (4.20). Then, the chain rule holds, i.e., we have, for almost all $t \in (0,T)$,*

$$\frac{\mathrm{d}}{\mathrm{d}t} E_n(u_n(t,\cdot)) = \mathrm{d}_n E_n(u_n(t))(\dot{u}_n(t)).$$

Proof. By Proposition 4.4.7, we have that $\dot{u}_n \in L^2(0,T;\mathcal{S}_n(\widetilde{\Omega};\mathbb{R}^d))$. Corollary 4.3.2 implies that $\mathrm{d}_n D_n(\dot{u}_n) \in L^2(0,T;(\mathcal{S}_n(\widetilde{\Omega};\mathbb{R}^d))^*)$ and hence by comparison in equation (4.20), also $\mathrm{d}_n E_n(u_n) \in L^2(0,T;(\mathcal{S}_n(\widetilde{\Omega};\mathbb{R}^d))^*)$. The assertion now follows from [130, Proposition 2.2], after noting that E_n is quadratic and therefore also proper, convex, and lower semicontinuous. □

Let u_n be the solution to the nonlocal viscoelastic problem (4.20), see Proposition 4.4.7. Testing the nonlocal viscoelastic problem (4.20) against $\dot{u}_n$, we obtain

$$0 = \mathrm{d}_n E_n(u_n)(\dot{u}_n) + \mathrm{d}_n D_n(\dot{u}_n)(\dot{u}_n).$$

As equality in the Fenchel-Young inequality holds, using the chain rule Lemma 4.4.8, integration in time yields, for all $t \in [0,T]$,

$$E_n(u_n(s,\cdot))\Big|_0^t + \int_0^t D_n(\dot{u}_n(s,\cdot))\,\mathrm{d}s + \int_0^t D_n^*\big(-\mathrm{d}_n E_n(u_n(s,\cdot))\big)\,\mathrm{d}s = 0, \tag{4.30}$$

where D_n^* denotes the Fenchel-Legendre transform of D_n, namely,

$$D_n^*(v^*) = \sup\left\{\langle v^*, w\rangle_n - D_n(w) : w \in \mathcal{S}_n(\widetilde{\Omega};\mathbb{R}^d)\right\}. \tag{4.31}$$

Here, $\langle\cdot,\cdot\rangle_n$ denotes the dual pairing between $\mathcal{S}_n(\widetilde{\Omega};\mathbb{R}^d)^*$ and $\mathcal{S}_n(\widetilde{\Omega};\mathbb{R}^d)$. From (4.30) and the assumption that $\sup_n E_n(u_n(0)) < \infty$, see the statement of Theorem 4.2.1, we immediately get the following lemma.

Lemma 4.4.9 (A priori estimates)**.** *Let u_n be the solution to the nonlocal viscoelastic problem (4.20). Then, for all $t \in [0,T]$ we have*

$$E_n(u_n(t,\cdot)) \le c, \tag{4.32}$$

$$\int_0^t D_n(\dot{u}_n(s,\cdot))\,\mathrm{d}s \le c, \tag{4.33}$$

$$\int_0^t D_n^*\big(-\mathrm{d}_n E_n(u_n(s,\cdot))\big)\,\mathrm{d}s \le c, \tag{4.34}$$

where c only depends on $\sup_n E_n(u_n(0,\cdot))$.

Here, we use that $D_n^*(v_n^*) \geq 0$ for all $v_n^* \in (\mathcal{S}_n(\widetilde{\Omega};\mathbb{R}^d))^*$ as $D_n(0) = 0$. Furthermore, by the definition of D_n, (4.33) is nothing else but

$$\int_0^t |\dot{u}_n(s,\cdot)|_n^2 \,\mathrm{d}s \leq c. \tag{4.35}$$

4.4.4 Compactness

Recall the static compactness result Proposition 4.4.3, which allows us to prove an Aubin-Lions-type result.

Proposition 4.4.10 (Aubin-Lions-type compactness)**.** *Let $(u_n)_n$ be a sequence of solutions to the nonlocal viscoelastic problem (4.20). Then, there exists $u \in C([0,T];L^2(\widetilde{\Omega};\mathbb{R}^d))$ and a (non relabeled) subsequence $(u_n)_n$ such that*

$$u_n \to u \quad \text{in } C([0,T];L^2(\widetilde{\Omega};\mathbb{R}^d)).$$

Proof. We use the Arzelà-Ascoli Theorem. First, note that (4.18) and (4.32) imply that the set $\{u_n(t) : n \in \mathbb{N}\}$ is bounded in $\mathcal{S}_n(\widetilde{\Omega};\mathbb{R}^d)$. Thus, by Proposition 4.4.3 it is relatively compact in $L^2(\widetilde{\Omega};\mathbb{R}^d)$. Equicontinuity follows from (4.33). Indeed, from (4.35) and the nonlocal Poincaré inequality, Proposition 4.4.2, we have that $\sup_n \|\dot{u}_n\|_{L^2(0,T;L^2(\widetilde{\Omega};\mathbb{R}^d))} \leq c$. Thus,

$$\|u_n(t) - u_n(s)\|_{L^2(\widetilde{\Omega})^d} \leq \int_s^t \|\dot{u}_n(\tau)\|_{L^2(\widetilde{\Omega})^d} \,\mathrm{d}\tau \leq \sqrt{t-s}\|\dot{u}_n\|_{L^2(0,T;L^2(\widetilde{\Omega};\mathbb{R}^d))} \leq c\sqrt{t-s}.$$

Therefore, the Arzelà-Ascoli Theorem is applicable and yields the claim. □

Note that $u(t) \in H_0^1(\Omega,\mathbb{R}^d)$ for all $t \in [0,T]$ from Proposition 4.4.3.

4.5 Nonlocal-to-local convergence of derivatives

4.5.1 General nonlocal-to-local convergence results

In this section, we collect several results, which will be used in the following.

Lemma 4.5.1 (Divergence)**.** *For $u \in H_0^1(\Omega;\mathbb{R}^d)$ we have*

$$\text{pv-}\int_{\widetilde{\Omega}} \rho_n(x'-\cdot)\mathscr{D}(u)(x',\cdot)\,\mathrm{d}x' \to d \fint_{S^{d-1}} s\cdot\nabla u s \,\mathrm{d}\mathcal{H}^{d-1}(s) = \operatorname{div} u$$

strongly in $L^2(\widetilde{\Omega};\mathbb{R}^d)$.

A proof of the above lemma can be found in [101, Lemma 3.1], where the second identity follows from Lemma 4.7.2.

A similar result holds true if the function u is replaced by a sequence of functions $(u_n)_n$, up to resorting to weak convergence.

Lemma 4.5.2 ([101, Lemma 3.6]). *For $u \in H^1_0(\Omega;\mathbb{R}^d)$ and a sequence $u_n \in \mathcal{S}_n(\widetilde{\Omega};\mathbb{R}^d)$ such that $u_n \to u$ in $L^2(\widetilde{\Omega};\mathbb{R}^d)$ and $\sup_n |u_n|_n \le c$ we have*

$$\text{pv-}\int_{\widetilde{\Omega}} \rho_n(x'-\cdot)\mathscr{D}(u_n)(x',\cdot)\,\mathrm{d}x' \rightharpoonup d \fint_{S^{d-1}} s\cdot\nabla u s\,\mathrm{d}\mathcal{H}^{d-1}(s)$$

weakly in $L^2(\widetilde{\Omega};\mathbb{R}^d)$.

The proof in [101] is based on a nonlocal integration by parts formula. Note that Lemmas 4.5.1 and 4.5.2 immediately imply the following result.

Corollary 4.5.3. *Let $u, v \in H^1_0(\Omega;\mathbb{R}^d)$ and $u_n \in \mathcal{S}_n(\widetilde{\Omega};\mathbb{R}^d)$ with $u_n \to u$ in $L^2(\widetilde{\Omega};\mathbb{R}^d)$ and $\sup_n |u_n|_n \le c$. Then,*

$$\int_{\widetilde{\Omega}} \mathfrak{D}_n(u_n(x))\,\mathfrak{D}_n(v(x))\,\mathrm{d}x \to \int_{\Omega} \operatorname{div} u(x) \operatorname{div} v(x)\,\mathrm{d}x.$$

Next, we investigate the limit of $(u_n, v_n)_n$. As $(\cdot,\cdot)_n$ can be interpreted as a nonlocal H^1-inner product, one can only expect convergence under strong convergence assumptions on u_n and v_n. We will therefore first prove the result in the smooth case. Based on this, we can then compute the limit of $(u_n, v)_n$ for a weakly convergent sequence $u_n \rightharpoonup u$ in $L^2(\widetilde{\Omega};\mathbb{R}^d)$ and v fixed, by resorting to mollification. As the nonlocal operator considered in [102] resembles the nonlocal inner product, the following lemma is reminiscent of the results in [102].

Lemma 4.5.4. *Let $u_n, v_n \in C^2(\widetilde{\Omega};\mathbb{R}^d)$ and $u, v \in H^1_0(\Omega;\mathbb{R}^d)$ be such that $\nabla u_n \to \nabla u$ and $\nabla v_n \to \nabla v$ strongly in $L^2(\widetilde{\Omega};\mathbb{R}^{d\times d})$. Moreover, assume that $\sup_n \|u_n\|_{W^{2,\infty}(\widetilde{\Omega})^d} + \|v_n\|_{W^{2,\infty}(\widetilde{\Omega})^d} \le c$. Then,*

$$\begin{aligned}&\lim_{n\to\infty} \int_{\widetilde{\Omega}} \int_{\widetilde{\Omega}} \rho_n(x'-x)\mathscr{D}(u_n)(x',x)\mathscr{D}(v_n)(x',x)\,\mathrm{d}x'\,\mathrm{d}x\\ &= d\int_{\widetilde{\Omega}} \fint_{S^{d-1}} (s\cdot\nabla u(x)s)\,(s\cdot\nabla v(x)s)\,\mathrm{d}\mathcal{H}^{d-1}(s)\,\mathrm{d}x.\end{aligned}$$

Proof. Fix $x \in \widetilde{\Omega}$. Since the kernels localize around x, we split the integral into two parts. To this end let $R := \operatorname{dist}(x, \partial\widetilde{\Omega})$ and $B(x,R)$ be the ball with radius R centered at x. Then we have

$$\begin{aligned}&\int_{\widetilde{\Omega}} \rho_n(x'-x)\mathscr{D}(u_n)(x',x)\mathscr{D}(v_n)(x',x)\,\mathrm{d}x'\\ &= \left[\int_{B(x,R)} + \int_{\widetilde{\Omega}\setminus B(x,R)}\right] \rho_n(x'-x)\mathscr{D}(u_n)(x',x)\mathscr{D}(v_n)(x',x)\,\mathrm{d}x'. \qquad (4.36)\end{aligned}$$

Note that, by Assumption 4.2.1 on the kernels, the second integral vanishes as $n \to \infty$, because

$$\begin{aligned}&\int_{\widetilde{\Omega}\setminus B(x,R)} \rho_n(x'-x)\mathscr{D}(u_n)(x',x)\mathscr{D}(v_n)(x',x)\,\mathrm{d}x'\\ &\le c(x)\|u_n\|_{L^\infty(\widetilde{\Omega})^d}\|v_n\|_{L^\infty(\widetilde{\Omega})^d} \int_{\widetilde{\Omega}\setminus B(x,R)} \rho_n(x'-x)\,\mathrm{d}x' \to 0.\end{aligned}$$

We therefore restrict the analysis to the integral over $B(x,R)$, where we use a Taylor expansion for $\mathscr{D}(u_n)$ and $\mathscr{D}(v_n)$. There exist $z = z(x',x,u_n) \in B(x,R)$ and $z' = z'(x',x,v_n) \in B(x,R)$ such that

$$\mathscr{D}(u_n)(x',x) = \frac{x'-x}{|x'-x|}\cdot\nabla u_n(x)\frac{x'-x}{|x'-x|} + \frac{1}{2}(x'-x)\cdot\nabla^2 u_n(z) : \left(\frac{x'-x}{|x'-x|}\otimes\frac{x'-x}{|x'-x|}\right),$$
$$\mathscr{D}(v_n)(x',x) = \frac{x'-x}{|x'-x|}\cdot\nabla v_n(x)\frac{x'-x}{|x'-x|} + \frac{1}{2}(x'-x)\cdot\nabla^2 v_n(z') : \left(\frac{x'-x}{|x'-x|}\otimes\frac{x'-x}{|x'-x|}\right),$$

where $\nabla^2 u_n$ and $\nabla^2 v_n$ are the third order tensors of second derivatives. Using the above expressions, by expanding the product $\mathscr{D}(u_n)(x',x)\mathscr{D}(v_n)(x',x)$ in the integral, we obtain four summands, namely,

$$\int_{B(x,R)} \rho_n(x'-x)\mathscr{D}(u_n)(x',x)\mathscr{D}(v_n)(x',x)\,\mathrm{d}x' = I_1 + I_2(u_n,v_n) + I_2(v_n,u_n) + I_3,$$

where, setting $\xi = x'-x$,

$$I_1 = \int_{B(0,R)} \rho_n(\xi)\left(\frac{\xi}{|\xi|}\cdot\nabla u_n(x)\frac{\xi}{|\xi|}\right)\left(\frac{\xi}{|\xi|}\cdot\nabla v_n(x)\frac{\xi}{|\xi|}\right)\mathrm{d}\xi, \tag{4.37}$$
$$I_2(u_n,v_n) = \int_{B(0,R)} \rho_n(\xi)\left(\frac{\xi}{|\xi|}\cdot\nabla u_n(x)\frac{\xi}{|\xi|}\right)\left(\frac{\xi}{2}\cdot\nabla^2 v_n(z') : \left(\frac{\xi}{|\xi|}\otimes\frac{\xi}{|\xi|}\right)\right)\mathrm{d}\xi, \tag{4.38}$$
$$I_3 = \int_{B(0,R)} \rho_n(\xi)\left(\frac{\xi}{2}\cdot\nabla^2 u_n(z) : \left(\frac{\xi}{|\xi|}\otimes\frac{\xi}{|\xi|}\right)\right)\left(\frac{\xi}{2}\cdot\nabla^2 v_n(z') : \left(\frac{\xi}{|\xi|}\otimes\frac{\xi}{|\xi|}\right)\right)\mathrm{d}\xi. \tag{4.39}$$

To calculate the limit of I_1, note that $\xi \mapsto \left(\frac{\xi}{|\xi|}\cdot\nabla u_n(x)\frac{\xi}{|\xi|}\right)\left(\frac{\xi}{|\xi|}\cdot\nabla v_n(x)\frac{\xi}{|\xi|}\right)$ is positively homogeneous of degree 0. Hence, as the kernels are radially symmetric by Assumption 4.2.1, we can write

$$I_1 = \int_{B(0,R)} \rho_n(\xi)\,\mathrm{d}\xi \fint_{S^{d-1}} (s\cdot\nabla u_n(x)s)(s\cdot\nabla v_n(x)s)\,\mathrm{d}\mathcal{H}^{d-1}(s), \tag{4.40}$$

see, e.g., [86, Lemma A.2]. As $\nabla u_n \to \nabla u$ and $\nabla v_n \to \nabla v$ strongly in $L^2(\widetilde{\Omega};\mathbb{R}^{d\times d})$, by using Assumption 4.2.1 (ii), (iii), we therefore obtain

$$I_1 \to d \fint_{S^{d-1}} (s\cdot\nabla u(x)s)(s\cdot\nabla v(x)s)\,\mathrm{d}\mathcal{H}^{d-1}(s),$$

as $n\to\infty$.

The mixed terms $I_2(u_n,v_n)$ and $I_2(v_n,u_n)$ vanish as $n\to\infty$. Indeed,

$$I_2(u_n,v_n) \le c\|\nabla u_n\|_{L^\infty(\widetilde{\Omega})^{d\times d}}\|\nabla^2 v_n\|_{L^\infty(\widetilde{\Omega})^{d\times d\times d}}\int_{B(0,R)}\rho_n(\xi)|\xi|\,\mathrm{d}\xi. \tag{4.41}$$

Given $0 < \varepsilon < R$, we split the domain of integration and obtain

$$\begin{aligned}\int_{B(0,R)} \rho_n(\xi)|\xi| \,\mathrm{d}\xi &= \int_{B(0,\varepsilon)} \rho_n(\xi)|\xi| \,\mathrm{d}\xi + \int_{\varepsilon<|\xi|<R} \rho_n(\xi)|\xi| \,\mathrm{d}\xi \\ &\leq \varepsilon d + R \int_{\varepsilon<|\xi|<R} \rho_n(|\xi|) \,\mathrm{d}\xi.\end{aligned}$$

The second term vanishes by Assumption 4.2.1 and hence by (4.41) we conclude the claim as $\varepsilon > 0$ is arbitrary and the norms of u_n and v_n are uniformly bounded. The analogous statement holds when exchanging the roles of u_n and v_n, and hence $I_2(v_n, u_n) \to 0$ as $n \to \infty$, as well. Moreover, the argument above also implies that $I_3 \to 0$ as $n \to \infty$.

We thus conclude that

$$\int_{\widetilde{\Omega}} \rho_n(x' - x)\mathscr{D}(u_n)(x', x)\mathscr{D}(v_n)(x', x) \,\mathrm{d}x' \to d \fint_{S^{d-1}} (s \cdot \nabla u(x)s)\,(s \cdot \nabla v(x)s) \,\mathrm{d}\mathcal{H}^{d-1}(s)$$

pointwise in x as $n \to \infty$. By the Dominated Convergence Theorem this also holds in $L^1(\widetilde{\Omega}; \mathbb{R}^d)$. Indeed, as u_n and v_n are smooth and their gradients are uniformly bounded, we can find $M > 0$ such that

$$\left|(u_n(x') - u_n(x)) \cdot \frac{x' - x}{|x' - x|^2}\right| \leq M \quad \text{and} \quad \left|(v_n(x') - v_n(x)) \cdot \frac{x' - x}{|x' - x|^2}\right| \leq M,$$

and thus

$$\int_{\widetilde{\Omega}} \rho_n(x' - x)|\mathscr{D}(u_n)(x', x)||\mathscr{D}(v_n)(x', x)| \,\mathrm{d}x' \leq M^2 \int_{\widetilde{\Omega}} \rho_n(x' - x) \,\mathrm{d}x' \leq M^2 d. \qquad \square$$

We now formulate two consequences of the above lemma.

Lemma 4.5.5. *Let $w_n, w \in L^2(0,T; H^1(\widetilde{\Omega}; \mathbb{R}^d))$ be such that $w_n(t) \in C^2(\widetilde{\Omega}; \mathbb{R}^d)$ for almost all $t \in [0,T]$. Moreover, assume that $w_n|_\Omega \rightharpoonup w|_\Omega$ weakly in $L^2(0,T; H^1(\Omega; \mathbb{R}^d))$ and that $\sup_n \int_0^T \|w_n(t)\|^2_{W^{2,\infty}(\widetilde{\Omega})^d} \,\mathrm{d}t \leq c$. Then, we have*

$$\begin{aligned}&\liminf_{n\to\infty} \int_0^T \int_\Omega \int_\Omega \rho_n(x' - x)\mathscr{D}(w_n)^2(x', x) \,\mathrm{d}x' \,\mathrm{d}x \,\mathrm{d}t \\ &\geq d \int_0^T \int_\Omega \fint_{S^{d-1}} (s \cdot \nabla w(x)s)^2 \,\mathrm{d}\mathcal{H}^{d-1}(s) \,\mathrm{d}x \,\mathrm{d}t. \end{aligned} \tag{4.42}$$

Proof. The proof runs along the lines of the proof of Lemma 4.5.4 and we therefore only highlight the adaptations. Recalling the splitting (4.36)–(4.39), the second integral in (4.36) and I_2, I_3 can be controlled uniformly in $x \in \widetilde{\Omega}$ in terms of $\eta_n \|w_n(t)\|^2_{W^{2,\infty}(\widetilde{\Omega})^d}$, where (η_n) is a sequence with $\eta_n \to 0$ as $n \to \infty$. Thus, recalling the representation in (4.40) this shows

$$G = \liminf_{n\to\infty} \int_0^T \int_\Omega \int_{B(0,R(x))} \rho_n(\xi) \,\mathrm{d}\xi \fint_{S^{d-1}} (s \cdot \nabla w_n(x)s)^2 \,\mathrm{d}\mathcal{H}^{d-1}(s) \,\mathrm{d}x \,\mathrm{d}t,$$

where $R(x) = \operatorname{dist}(x, \partial\widetilde{\Omega})$ and G denotes the left-hand side of (4.42) for brevity. In view of Assumption 4.2.1 (ii), (iii), given any $\varepsilon > 0$, we get

$$G \geq \liminf_{n\to\infty} \int_0^T \int_\Omega d(1-\varepsilon) \fint_{S^{d-1}} (s \cdot \nabla w_n(x)s)^2 \,\mathrm{d}\mathcal{H}^{d-1}(s)\,\mathrm{d}x\,\mathrm{d}t.$$

As $v \mapsto \int_\Omega \fint_{S^{d-1}} (s \cdot \nabla v(x)s)^2 \,\mathrm{d}\mathcal{H}^{d-1}(s)\,\mathrm{d}x$ is convex, using $w_n|_\Omega \rightharpoonup w|_\Omega$ weakly in $L^2(0,T;H^1(\Omega;\mathbb{R}^d))$ by assumption, we obtain

$$G \geq d(1-\varepsilon) \int_0^T \int_\Omega \fint_{S^{d-1}} (s \cdot \nabla w(x)s)^2 \,\mathrm{d}\mathcal{H}^{d-1}(s)\,\mathrm{d}x\,\mathrm{d}t.$$

As $\varepsilon > 0$ is arbitrary, this concludes the proof. □

Lemma 4.5.6. *Let $u_n \in \mathcal{S}_n(\widetilde{\Omega};\mathbb{R}^d)$ and $u, v \in H^1_0(\Omega;\mathbb{R}^d)$ be such that $u_n \to u$ strongly in $L^2(\widetilde{\Omega};\mathbb{R}^d)$ and $\sup_n |u_n|_n < \infty$. Then,*

$$\int_{\widetilde{\Omega}} \rho_n(x'-\cdot)\mathscr{D}(u_n)(x',\cdot)\mathscr{D}(v)(x',\cdot)\,\mathrm{d}x' \to d \fint_{S^{d-1}} (s\cdot\nabla us)\,(s\cdot\nabla vs)\,\mathrm{d}\mathcal{H}^{d-1}(s)$$

strongly in $L^1(\widetilde{\Omega};\mathbb{R}^d)$ as $n \to \infty$.

Proof. Step 1. Assume momentarily that $v \in C_c^\infty(\Omega;\mathbb{R}^d)$. Let $\eta \in C_c^\infty(\mathbb{R}^d)$, with $\|\eta\|_{L^1(\mathbb{R}^d)} = 1$ and set $\eta_k(x) := k^d\eta(kx)$. Moreover, set $u_n^k := \eta_k * u_n$ and $u^k := \eta_k * u$, where we implicitly extended u_n and u to $\mathbb{R}^d$ by 0. We have that $u_n^k \to u^k$ strongly in $L^2(\widetilde{\Omega};\mathbb{R}^d)$, because mollification is a compact operator, see, e.g., [39, Corollary 4.28]. Moreover, due to the mollification, also $u_n^k \to u_n$ strongly in $L^2(\widetilde{\Omega};\mathbb{R}^d)$, and $u^k \to u$ strongly in $H^1(\widetilde{\Omega};\mathbb{R}^d)$.

Then, we have that

$$\left\| \int_{\widetilde{\Omega}} \rho_n(x'-\cdot)\mathscr{D}(u_n)(x',\cdot)\mathscr{D}(v)(x',\cdot)\,\mathrm{d}x' - \fint_{S^{d-1}} (s\cdot\nabla u(\cdot)s)(s\cdot\nabla v(\cdot)s)\,\mathrm{d}\mathcal{H}^{d-1}(s) \right\|_{L^1(\widetilde{\Omega})}$$

is controlled from above by the sum of three terms I_1, I_2, and I_3, defined as

$$\begin{aligned}
I_1 = \Big\| & \int_{\widetilde{\Omega}} \rho_n(x'-\cdot)\mathscr{D}(u_n)(x',\cdot)\mathscr{D}(v)(x',\cdot)\,\mathrm{d}x' \\
& - \int_{\widetilde{\Omega}} \rho_n(x'-\cdot)\mathscr{D}(u_n^k)(x',\cdot)\mathscr{D}(v)(x',\cdot)\,\mathrm{d}x' \Big\|_{L^1(\widetilde{\Omega})} \\
I_2 = \Big\| & \int_{\widetilde{\Omega}} \rho_n(x'-\cdot)\mathscr{D}(u_n^k)(x',\cdot)\mathscr{D}(v)(x',\cdot)\,\mathrm{d}x' \\
& - \fint_{S^{d-1}} (s\cdot\nabla u^k(\,\cdot\,)s)(s\cdot\nabla v(\,\cdot\,)s)\,\mathrm{d}\mathcal{H}^{d-1}(s) \Big\|_{L^1(\widetilde{\Omega})} \\
I_3 = \Big\| & \fint_{S^{d-1}} (s\cdot\nabla u^k(\,\cdot\,)s)(s\cdot\nabla v(\,\cdot\,)s)\,\mathrm{d}\mathcal{H}^{d-1}(s) \\
& - \fint_{S^{d-1}} (s\cdot\nabla u(\,\cdot\,)s)(s\cdot\nabla v(\,\cdot\,)s)\,\mathrm{d}\mathcal{H}^{d-1}(s) \Big\|_{L^1(\widetilde{\Omega})}.
\end{aligned}$$

Now, we let first $n \to \infty$ and then $k \to \infty$ and show that each term converges to 0.

To check this for I_1, let us first note that, for all $w \in \mathcal{S}_n(\widetilde{\Omega};\mathbb{R}^d)$, by writing

$$\mathscr{D}(w)(x',x) = w(x') \cdot \frac{x'-x}{|x'-x|^2} - w(x) \cdot \frac{x'-x}{|x'-x|^2} = -w(x') \cdot \frac{x-x'}{|x'-x|^2} - w(x) \cdot \frac{x'-x}{|x'-x|^2},$$

using a change of variable $x' \mapsto x$, the symmetry of ρ_n and $\mathscr{D}(v)$, and Fubini's Theorem, we get

$$\begin{aligned}&\int_{\widetilde{\Omega}} \int_{\widetilde{\Omega}} \rho_n(x'-x)\mathscr{D}(w)(x',x)\mathscr{D}(v)(x',x)\,\mathrm{d}x'\,\mathrm{d}x \\ &= \int_{\widetilde{\Omega}} w(x) \cdot \left(- \int_{\widetilde{\Omega}} 2\rho_n(x'-x) \frac{x'-x}{|x'-x|^2} \mathscr{D}(v)(x',x)\,\mathrm{d}x' \right) \mathrm{d}x.\end{aligned}$$

Setting $\mathscr{D}_n^*\mathscr{D}(v)(x) := -\int_{\widetilde{\Omega}} 2\rho_n(x'-x)\frac{x'-x}{|x'-x|^2}\mathscr{D}(v)(x',x)\,\mathrm{d}x'$, Hölder's inequality gives

$$\begin{aligned}I_1 &= \int_{\widetilde{\Omega}} \left| \int_{\widetilde{\Omega}} \rho_n(x'-x)\mathscr{D}(u_n-u_n^k)(x',x)\mathscr{D}(v)(x',x)\,\mathrm{d}x' \right| \mathrm{d}x \\ &\le \int_{\widetilde{\Omega}} |(u_n-u_n^k)(x)|\,|\mathscr{D}_n^*\mathscr{D}(v)(x)|\,\mathrm{d}x \le \|u_n-u_n^k\|_{L^2(\widetilde{\Omega})^d} \|\mathscr{D}_n^*\mathscr{D}(v)\|_{L^2(\widetilde{\Omega})^d}.\end{aligned}$$

Since $u_n \to u$, $u_n^k \to u^k$, and $u^k \to u$ strongly in $L^2(\widetilde{\Omega};\mathbb{R}^d)$ as $n \to \infty$, we are left with checking that $\|\mathscr{D}_n^*\mathscr{D}(v)\|_{L^2(\widetilde{\Omega})^d}$ is uniformly bounded in n. As v is smooth and $\mathscr{D}(v)(x',x) = \mathscr{D}(v)(x,x')$, we obtain by Taylor expansion around x and x'

$$2\mathscr{D}(v)(x',x) = \frac{\xi}{|\xi|} \cdot \big(\nabla v(x') + \nabla v(x)\big) \frac{\xi}{|\xi|} + \frac{1}{2}\xi \cdot \big(\nabla^2 v(z') + \nabla^2 v(z)\big) : \left(\frac{\xi}{|\xi|} \otimes \frac{\xi}{|\xi|} \right)$$

for suitable points z and z', where we set $\xi := x'-x$ for brevity. Accordingly, we split $-\mathscr{D}_n^*\mathscr{D}(v)(x) = J_1 + J_2$, with

$$\begin{aligned}J_1 &:= \int_{\widetilde{\Omega}} \rho_n(x'-x) \frac{x'-x}{|x'-x|^2} \frac{x'-x}{|x'-x|} \cdot \big(\nabla v(x') + \nabla v(x)\big) \frac{x'-x}{|x'-x|}\,\mathrm{d}x', \\ J_2 &:= \int_{\widetilde{\Omega}} \rho_n(x'-x) \frac{x'-x}{|x'-x|^2} \frac{x'-x}{2} \cdot \big(\nabla^2 v(z') + \nabla^2 v(z)\big) : \left(\frac{x'-x}{|x'-x|} \otimes \frac{x'-x}{|x'-x|} \right) \mathrm{d}x'.\end{aligned}$$

To obtain an upper bound for J_2, we use Assumption 4.2.1 (ii) to get

$$|J_2| \le \|\nabla^2 v\|_{L^\infty(\widetilde{\Omega})^{d\times d\times d}} \int_{\mathbb{R}^d} \rho_n(\xi)\,\mathrm{d}\xi \le d\|\nabla^2 v\|_{L^\infty(\widetilde{\Omega})^{d\times d\times d}}.$$

To control J_1, we proceed analogously to [105, Formula (2.3)]. For $x \in \widetilde{\Omega}$, we set $R(x) := \operatorname{dist}(x, \partial\widetilde{\Omega})$ and let $\varepsilon \in (0, R(x))$ be arbitrary. Denoting by χ_M the characteristic function of the set M, we have for any $x' \in \widetilde{\Omega}$

$$-\chi_{[\varepsilon,\infty)}(|x'-x|) + 2\chi_{[\varepsilon,R(x))}(|x'-x|) = \chi_{[\varepsilon,\infty)}(|x'-x|) - 2\chi_{[R(x),\infty)}(|x'-x|),$$

and therefore also

$$\begin{aligned}
&-\chi_{[\varepsilon,\infty)}(|x'-x|)\rho_n(x'-x)\frac{x'-x}{|x'-x|^2}\frac{x'-x}{|x'-x|}\cdot(\nabla v(x')+\nabla v(x))\frac{x'-x}{|x'-x|}\\
&\quad+2\chi_{[\varepsilon,R(x))}(|x'-x|)\rho_n(x'-x)\frac{x'-x}{|x'-x|^2}\frac{x'-x}{|x'-x|}\cdot\nabla v(x)\frac{x'-x}{|x'-x|}\\
=&\chi_{[\varepsilon,\infty)}(|x'-x|)\rho_n(x'-x)\frac{x'-x}{|x'-x|^2}\frac{x'-x}{|x'-x|}\cdot\big(-(\nabla v(x')-\nabla v(x))\big)\frac{x'-x}{|x'-x|}\\
&\quad-2\chi_{[R(x),\infty)}(|x'-x|)\rho_n(x'-x)\frac{x'-x}{|x'-x|^2}\frac{x'-x}{|x'-x|}\cdot\nabla v(x)\frac{x'-x}{|x'-x|^2}.
\end{aligned}\tag{4.43}$$

Since $\xi\mapsto\frac{\xi}{|\xi|^2}\frac{\xi}{|\xi|}\cdot\nabla v(x)\frac{\xi}{|\xi|}$ is odd, integrating over a symmetric domain around x will give 0. Therefore, we have that

$$2\int_{\widetilde{\Omega}}\chi_{[\varepsilon,R(x))}(|x'-x|)\rho_n(x'-x)\frac{x'-x}{|x'-x|^2}\frac{x'-x}{|x'-x|}\cdot\nabla v(x)\frac{x'-x}{|x'-x|}\,\mathrm{d}x'=0.$$

In particular, integrating (4.43) with respect to x' gives

$$-\int_{\widetilde{\Omega}}\chi_{[\varepsilon,\infty)}(|x'-x|)\rho_n(x'-x)\frac{x'-x}{|x'-x|^2}\frac{x'-x}{|x'-x|}\cdot(\nabla v(x')+\nabla v(x))\frac{x'-x}{|x'-x|}\,\mathrm{d}x'=H_1+H_2$$

with

$$\begin{aligned}
H_1&=\int_{\widetilde{\Omega}}\chi_{[\varepsilon,\infty)}(|x'-x|)\rho_n(x'-x)\frac{x'-x}{|x'-x|^2}\frac{x'-x}{|x'-x|}\cdot\big(-(\nabla v(x')-\nabla v(x))\big)\frac{x'-x}{|x'-x|}\,\mathrm{d}x',\\
H_2&=-2\int_{\widetilde{\Omega}}\chi_{[R(x),\infty)}(|x'-x|)\rho_n(x'-x)\frac{x'-x}{|x'-x|^2}\frac{x'-x}{|x'-x|}\cdot\nabla v(x)\frac{x'-x}{|x'-x|^2}\,\mathrm{d}x'.
\end{aligned}$$

As ∇v is smooth, we can bound

$$\begin{aligned}
|H_1|&\le\int_{\widetilde{\Omega}}\chi_{[\varepsilon,\infty)}(|x'-x|)\rho_n(x'-x)\frac{1}{|x'-x|}|\nabla v(x')-\nabla v(x)|\,\mathrm{d}x'\\
&\le\|\nabla^2 v\|_{L^\infty(\widetilde{\Omega})^{d\times d\times d}}\int_{\mathbb{R}^d}\rho_n(\xi)\,\mathrm{d}\xi\le d\|\nabla^2 v\|_{L^\infty(\widetilde{\Omega})^{d\times d\times d}}.
\end{aligned}$$

We are left with estimating H_2 from above. To this end, pick $\xi(x)\in(\widetilde{\Omega}\setminus\operatorname{supp}\nabla v)\cap B(x,R(x))$. Then, $\nabla v(\xi(x))=0$ and by the choice of $\xi(x)$ also $|\xi(x)-x|\le R(x)$. Therefore, we get

$$\begin{aligned}
\left|\frac{1}{2}H_2\right|&\le\int_{\widetilde{\Omega}}\chi_{[R(x),\infty)}(|x'-x|)\rho_n(x'-x)\frac{1}{|x'-x|}\,|\nabla v(\xi(x))-\nabla v(x)|\,\mathrm{d}x'\\
&\le\|\nabla^2 v\|_{L^\infty(\widetilde{\Omega})^{d\times d\times d}}\int_{\widetilde{\Omega}}\chi_{[R(x),\infty)}(|x'-x|)\rho_n(x'-x)\frac{|\xi(x)-x|}{|x'-x|}\,\mathrm{d}x'\\
&\le d\|\nabla^2 v\|_{L^\infty(\widetilde{\Omega})^{d\times d\times d}}
\end{aligned}$$

since from the additional constraint $\chi_{[R(x),\infty)}(|x'-x|)$ on the integration domain, we have that $|\xi(x)-x| \leq R(x) \leq |x'-x|$. Hence, as ε is arbitrary, we conclude that $|J_1| \leq 3d\|\nabla^2 v\|_{L^\infty(\widetilde{\Omega})^{d\times d\times d}}$. In particular, the uniform L^2-bound of $\mathscr{D}_n^*\mathscr{D}(v)$ follows.

For showing that the term I_2 converges to 0, we can apply Lemma 4.5.4 as u_n^k and u^k are smooth. Indeed, by Young's Convolution Inequality and Proposition 4.4.2, we have

$$\sup_{n\in\mathbb{N}} \|u_n^k\|_{L^\infty(\widetilde{\Omega})^d} \leq \sup_{n\in\mathbb{N}} \|u_n\|_{L^2(\widetilde{\Omega})^d} \|\eta_k\|_{L^2(\mathbb{R}^d)} \leq c_k$$

and analogously for ∇u_n^k and $\nabla^2 u_n^k$. Moreover, this bound and Rellich's Theorem also imply that $\nabla u_n^k \to \nabla u^k$ strongly in $L^2(\widetilde{\Omega};\mathbb{R}^{d\times d})$.

Eventually, the third term I_3 vanishes as $u^k \to u$ in $H^1(\widetilde{\Omega};\mathbb{R}^d)$ by mollification.

Step 2. Let us now consider the case $v \in H_0^1(\Omega;\mathbb{R}^d)$. We approximate v by a smooth sequence $v^k \in C_c^\infty(\Omega;\mathbb{R}^d)$, i.e., we assume $\|v-v^k\|_{H_0^1(\Omega)^d} \to 0$, and estimate

$$\begin{aligned}
&\Big\| \int_{\widetilde{\Omega}} \rho_n(x'-\cdot)\mathscr{D}(u_n)(x',\cdot)\mathscr{D}(v)(x',\cdot)\,\mathrm{d}x' - \fint_{S^{d-1}} (s\cdot\nabla u(\cdot)s)\,(s\cdot\nabla v(\cdot)s)\,\mathrm{d}\mathcal{H}^{d-1}(s)\Big\|_{L^1(\widetilde{\Omega})} \\
&\leq \int_{\widetilde{\Omega}}\int_{\widetilde{\Omega}} \rho_n(x'-x)|\mathscr{D}(u_n)(x',x)|\,|\mathscr{D}(v-v^k)(x',x)|\,\mathrm{d}x'\,\mathrm{d}x \\
&\quad + \Big\| \int_{\widetilde{\Omega}} \rho_n(x'-\cdot)\mathscr{D}(u_n)(x',\cdot)\mathscr{D}(v^k)(x',\cdot)\,\mathrm{d}x' \\
&\qquad - \fint_{S^{d-1}} (s\cdot\nabla u(\,\cdot\,)s)(s\cdot\nabla v^k(\,\cdot\,)s)\,\mathrm{d}\mathcal{H}^{d-1}(s)\Big\|_{L^1(\widetilde{\Omega})} \\
&\quad + \int_\Omega \fint_{S^{d-1}} |s\cdot\nabla u(x)s|\,|s\cdot(\nabla v^k(x)-\nabla v(x))s|\,\mathrm{d}\mathcal{H}^{d-1}(s)\,\mathrm{d}x. \qquad (4.44)
\end{aligned}$$

We let first $n\to\infty$ and then $k\to\infty$. As $v \in H_0^1(\Omega;\mathbb{R}^d)$, we can apply Lemma 4.4.1, Hölder's inequality, and the definition (4.17) to estimate the first term on the right hand side of (4.44) as

$$\int_{\widetilde{\Omega}}\int_{\widetilde{\Omega}} \rho_n(x'-x)|\mathscr{D}(u_n)(x',x)|\,|\mathscr{D}(v-v^k)(x',x)|\,\mathrm{d}x'\,\mathrm{d}x \leq \|v-v^k\|_{H_0^1(\Omega)^d} \sup_{n\in\mathbb{N}} |u_n|_n,$$

which tends to 0 as $\sup_n |u_n|_n \leq c$ by assumption. The second term on the right hand side of (4.44) vanishes by Step 1, whereas the third term on the right hand side of (4.44) converges to 0 as v^k converges to v in $H^1(\Omega;\mathbb{R}^d)$. □

Remark 4.5.7 (Homogeneous Dirichlet boundary conditions). For the proof of the theorem above, it is instrumental to have homogeneous Dirichtlet boundary conditions, as otherwise one would only be able to establish an L^1-bound of $\mathscr{D}_n^*\mathscr{D}(v)$, see [67, Proposition A.1] and [55, Proposition 2.12].

As already mentioned, one cannot expect Lemma 4.5.6 to hold, if we replace v by a sequence $v_n \rightharpoonup v$. However, one can still prove a lower semicontinuity result, see, e.g., [86, Lemma A.1], [101, Proof of Theorem 1.1].

Lemma 4.5.8 ([86, Lemma A.1]). *Let η_k be a standard sequence of mollifiers, $u \in \mathcal{S}_n(\widetilde{\Omega};\mathbb{R}^d)$ and define $u^k := \eta_k * u$. Then, for any $A \subset\subset \widetilde{\Omega}$ measurable, we have*

$$\int_A \int_A \rho_n(x'-x)(\mathscr{D}(u^k)(x',x))^2 \,\mathrm{d}x' \,\mathrm{d}x \leq \int_{\widetilde{\Omega}} \int_{\widetilde{\Omega}} \rho_n(x'-x)(\mathscr{D}(u)(x',x))^2 \,\mathrm{d}x' \,\mathrm{d}x$$

for all k sufficiently large.

The proof directly follows from the linearity of $u \mapsto \mathscr{D}(u)$, the convexity of $y \mapsto y^2$, and Jensen's inequality.

4.6 Proof of Theorem 4.2.1

The proof is based on the classical evolutive Γ-convergence approach, inspired by Sandier and Serfaty [119], see also [110]. This requires to check the lim inf-inequalities (4.13)–(4.15), which makes for the main part of the proof.

Lemma 4.6.1 (Liminf-inequalities). *Let $u_n \in H^1(0,T;\mathcal{S}_n(\widetilde{\Omega};\mathbb{R}^d))$ be a sequence of solutions to the nonlocal viscoelastic problem (4.20), and $u \in C([0,T];L^2(\widetilde{\Omega};\mathbb{R}^d))$ from the compactness result Proposition 4.4.10. Then, extracting a not relabeled subsequence with $u_n \to u$ in $C([0,T];L^2(\widetilde{\Omega};\mathbb{R}^d))$, for almost every $t \in [0,T]$, the following liminf-inequalities hold*

$$\liminf_{n\to\infty} E_n(u_n(t)) \geq E(u(t)), \tag{4.45}$$

$$\liminf_{n\to\infty} \int_0^t D_n(\dot{u}_n(s)) \,\mathrm{d}s \geq \int_0^t D(\dot{u}(s)) \,\mathrm{d}s, \tag{4.46}$$

$$\liminf_{n\to\infty} \int_0^t D_n^*\big(-\mathrm{d}_n E_n(u_n(s))\big) \,\mathrm{d}s \geq \int_0^t D^*\big(-\mathrm{d}E(u(s))\big) \,\mathrm{d}s. \tag{4.47}$$

Note that the lim inf-inequality for the energy (4.45) has already been proved in [101, Theorem 1.2] as part of the Γ-convergence result, which we recalled in Theorem 4.4.5. We show the two remaining liminf-inequalities (4.46) and (4.47) in the subsequent Sections 4.6.1 and 4.6.2, respectively.

4.6.1 Proof of (4.46)

Let $(u_n)_n$ be a sequence of solutions to the nonlocal viscoelastic problem (4.20) and u be the respective limit from the compactness result Proposition 4.4.10. We resort to mollification and use Lemma 4.5.8. As $\Omega \subset\subset \widetilde{\Omega}$, for k large enough one has

$$\int_\Omega \int_\Omega \rho_n(x'-x)(\mathscr{D}(\eta^k * \dot{u}_n)(x',x))^2 \,\mathrm{d}x' \,\mathrm{d}x \leq |\dot{u}_n|_n^2,$$

and hence also

$$\liminf_{n\to\infty} \int_0^T \int_\Omega \int_\Omega \rho_n(x'-x)(\mathscr{D}(\eta^k * \dot{u}_n)(x',x))^2 \,\mathrm{d}x' \,\mathrm{d}x \,\mathrm{d}t \leq \liminf_{n\to\infty} \int_0^T |\dot{u}_n|_n^2 \,\mathrm{d}t. \tag{4.48}$$

From the a priori bound (4.35) and Proposition 4.4.2 we get that

$$\sup_{n\in\mathbb{N}} \int_0^T \|\dot{u}_n(t)\|^2_{L^2(\widetilde{\Omega})^d} \,\mathrm{d}t \le c. \tag{4.49}$$

Therefore, one can find a (non relabeled) subsequence $\dot{u}_n \rightharpoonup v$ in $L^2(0,T;L^2(\widetilde{\Omega};\mathbb{R}^d))$. By identifying weak limits, we see that $v = \dot{u}$. Moreover, (4.49) and Young's Convolution Inequality implies that $\sup_n \int_0^T \|(\dot{u}_n(t) * \eta^k)\|^2_{W^{2,\infty}(\widetilde{\Omega})^d} \,\mathrm{d}t \le c$. In particular, by a further weak compactness argument this also implies that $\eta^k * \dot{u}_n \rightharpoonup \eta^k * \dot{u}$ in $L^2(0,T;H^1(\Omega;\mathbb{R}^d))$. Thus, we can apply Lemma 4.5.5 and obtain

$$\begin{aligned}\liminf_{n\to\infty} \int_0^T \int_\Omega \int_\Omega \rho_n(x'-x)(\mathscr{D}(\eta^k * \dot{u}_n)(x',x))^2 \,\mathrm{d}x' \,\mathrm{d}x \,\mathrm{d}t \\ \ge d \int_0^T \int_\Omega \fint_{S^{d-1}} (s\cdot\nabla(\eta^k * \dot{u})(x)s)^2 \,\mathrm{d}\mathcal{H}^{d-1}(s) \,\mathrm{d}x \,\mathrm{d}t.\end{aligned} \tag{4.50}$$

Combining (4.48) and (4.50), we get

$$d \int_0^T \int_\Omega \fint_{S^{d-1}} (s\cdot\nabla(\eta^k * \dot{u})(t,x)s)^2 \,\mathrm{d}\mathcal{H}^{d-1}(s) \,\mathrm{d}x \,\mathrm{d}t \le \liminf_{n\to\infty} \int_0^T |\dot{u}_n(t)|_n^2 \,\mathrm{d}t.$$

Now, we take the limit as $k \to \infty$ and conclude as, owing to the definition of $|\cdot|_n$ and Lemma 4.4.6, the latter is exactly inequality (4.46). □

4.6.2 Proof of (4.47)

The Fenchel Inequality gives for all $v \in H^1(\Omega;\mathbb{R}^d)$

$$D_n^*(-\,\mathrm{d}_n E_n(u_n)) \ge -\,\mathrm{d}_n E_n(u_n)(v) - D_n(v).$$

The next lemma shows that one can pass to the limit in the above expression, which is the key ingredient to show (4.47).

Lemma 4.6.2 (Convergence). *Let $u_n \in H^1(0,T;\mathcal{S}_n(\widetilde{\Omega};\mathbb{R}^d))$ be a sequence of solutions to the nonlocal viscoelastic problem, $v \in H^1_0(\Omega;\mathbb{R}^d)$, and $u \in C([0,T];L^2(\widetilde{\Omega};\mathbb{R}^d))$ from Proposition 4.4.10. Then, extracting a non relabeled subsequence with $u_n \to u$ in $C([0,T];L^2(\widetilde{\Omega};\mathbb{R}^d))$ we find, as $n \to \infty$,*

$$-\,\mathrm{d}_n E_n(u_n(t))(v) \to -\,\mathrm{d}E(u(t))(v) \quad \text{for every } t \in [0,T], \tag{4.51}$$

$$D_n(v) \to D(v), \tag{4.52}$$

where $-\,\mathrm{d}_n E(u_n)(v)$ and $-\,\mathrm{d}E(u)(v)$ are as in (4.22) and (4.26), respectively.

Proof of Lemma 4.6.2. The claim for D_n (4.52) follows from Lemma 4.5.6, when setting $u_n = v$ and recalling the various forms of D in Lemma 4.4.6.

For the convergence of $-\mathrm{d}_n E_n(u_n(t))$, we expand the product in the integral of (4.22) as

$$\begin{aligned}-\mathrm{d}_n E_n(u_n(t))(v) = &-\alpha \int_{\widetilde{\Omega}}\int_{\widetilde{\Omega}} \rho_n(x'-x)\mathscr{D}(u_n(t))(x',x)\mathscr{D}(v)(x',x)\,\mathrm{d}x'\,\mathrm{d}x \\ &-\Big(\beta-\frac{\alpha}{d}\Big)\int_{\widetilde{\Omega}}\int_{\widetilde{\Omega}} \mathfrak{D}_n(u_n(t))(x)\mathfrak{D}_n(v)(x)\,\mathrm{d}x.\end{aligned}$$

Then we can employ Lemma 4.5.6 and Corollary 4.5.3 to pass to the limit. Eventually, using (4.8), Lemma 4.7.3, and a computation analogous to the one of Lemma 4.7.5 the proof is concluded. □

We now proceed with the proof of inequality (4.47) by first showing that $\liminf_{n\to\infty} D_n^*\big(-\mathrm{d}_n E_n(u_n(t))\big) \geq D^*\big(-\mathrm{d}E(u(t))\big)$ at almost every $t\in[0,T]$.

To this aim, let $\eta>0$ be small but arbitrary. By definition of D^* (see also (4.31)), we can find $v\in H_0^1(\Omega;\mathbb{R}^d)$ such that

$$D^*\big(-\mathrm{d}E(u(t))\big) \leq -\mathrm{d}E(u(t))(v) - D(v) + \eta.$$

Therefore, by (4.31), Lemma 4.6.2 implies

$$\begin{aligned}\liminf_{n\to\infty} D_n^*\big(-\mathrm{d}_n E_n(u(t))\big) &\geq \liminf_{n\to\infty}\Big(-\mathrm{d}_n E_n(u(t))(v) - D_n(v)\Big) \\ &= -\mathrm{d}E(u(t))(v) - D(v) \geq D^*\big(-\mathrm{d}E(u(t))\big) - \eta.\end{aligned}$$

Since η is arbitrary, we conclude by integrating over $t\in[0,T]$ and applying Fatou's Lemma. □

4.6.3 Conclusion of the proof Theorem 4.2.1

Let $u_n \in H^1(0,T;\mathcal{S}_n(\widetilde{\Omega};\mathbb{R}^d))$ be a sequence of solutions to the nonlocal viscoelastic problem (4.20), and $u\in C([0,T];L^2(\widetilde{\Omega};\mathbb{R}^d))$ from Proposition 4.4.10.

From the well-preparedness assumption $E_n(u_n^0)\to E(u^0)$ and the energy-dissipation equality (4.30), we obtain

$$\begin{aligned}&E(u(0)) = \liminf_{n\to\infty} E_n(u_n(0)) \\ &\geq \liminf_{n\to\infty} E_n(u_n(t,\cdot)) + \liminf_{n\to\infty}\int_0^t D_n(\dot{u}_n(s,\cdot))\,\mathrm{d}s + \liminf_{n\to\infty}\int_0^t D_n^*(-\mathrm{d}_n E_n(u_n(s,\cdot))\,\mathrm{d}s.\end{aligned} \tag{4.53}$$

Now, employing Lemma 4.6.1, we can further estimate the right-hand side of (4.53) as

$$\begin{aligned}&\liminf_{n\to\infty} E_n(u_n(t,\cdot)) + \liminf_{n\to\infty}\int_0^t D_n(\dot{u}_n(s,\cdot))\,\mathrm{d}s + \liminf_{n\to\infty}\int_0^t D_n^*(-\mathrm{d}_n E_n(u_n(s,\cdot))\,\mathrm{d}s \\ &\geq E(u(t)) + \int_0^t D(\dot{u}(s,\cdot))\,\mathrm{d}s + \int_0^t D^*(-\mathrm{d}E(u(s,\cdot))\,\mathrm{d}s.\end{aligned} \tag{4.54}$$

In order to conclude the proof, we need the classical chain rule for E.

Lemma 4.6.3 (Chain rule). *Assume that* $\dot{u} \in L^2(0,T;H_0^1(\Omega;\mathbb{R}^d))$ *and* $\mathrm{d}E(u) \in L^2(0,T;(H_0^1(\Omega;\mathbb{R}^d))^*)$. *Then, the chain rule holds, i.e.,*

$$\frac{\mathrm{d}}{\mathrm{d}t}E(u(t)) = \mathrm{d}E(u(t))(\dot{u}(t)) \qquad \text{for almost every } t \in [0,T].$$

We now check the regularity assumptions of the lemma above. As $E(u(0)) < \infty$ and $D^* \geq 0$, we obtain from (4.53)–(4.54)

$$\int_0^t \int_\Omega \mathbb{D}\varepsilon(\dot{u}(t,x)) : \varepsilon(\dot{u}(t,x)) \,\mathrm{d}x \,\mathrm{d}t < \infty,$$

which is nothing else but $\|\dot{u}\|_{L^2(0,T;H_0^1(\Omega;\mathbb{R}^d))} < \infty$ by Lemma 4.4.4. This, along with the fact that $u(0) \in H_0^1(\Omega;\mathbb{R}^d)$, also shows that $u \in L^2(0,T;H_0^1(\Omega;\mathbb{R}^d))$.

Next, we prove that $\mathrm{d}E(u) \in L^2(0,T;(H_0^1(\Omega;\mathbb{R}^d))^*)$. First note that from (4.26) we have

$$|\,\mathrm{d}E(u)(v)| \leq c \int_\Omega \varepsilon(u(x)) : \varepsilon(v(x)) \,\mathrm{d}x \leq c\|u\|_{H_0^1(\Omega)^d}\|v\|_{H_0^1(\Omega)^d}$$

for some constant $c > 0$. Therefore, we arrive at

$$\begin{aligned}
\int_0^t \|\,\mathrm{d}E(u(s))\|^2_{(H_0^1(\Omega;\mathbb{R}^d))^*} \,\mathrm{d}s &= \int_0^t \left(\sup_{v \in H_0^1(\Omega;\mathbb{R}^d):\|v\|_{H_0^1(\Omega)^d} \leq 1} |\,\mathrm{d}E(u)(v)| \right)^2 \mathrm{d}s \\
&\leq c \int_0^t \left(\sup_{v \in H_0^1(\Omega;\mathbb{R}^d):\|v\|_{H_0^1(\Omega)^d} \leq 1} \|u\|_{H_0^1(\Omega)^d}\|v\|_{H_0^1(\Omega)^d} \right)^2 \mathrm{d}s \\
&\leq c \int_0^t \|u(t)\|^2_{H_0^1(\Omega)^d} \,\mathrm{d}s \leq c\|u\|^2_{L^2(0,T;H_0^1(\Omega;\mathbb{R}^d))}.
\end{aligned}$$

In particular, the assumptions of Lemma 4.6.3 are fulfilled. Now, from (4.53)–(4.54), and the chain rule of Lemma 4.6.3, we obtain

$$\begin{aligned}
0 &\geq E(u(t)) - E(u(0)) + \int_0^t D(\dot{u}(s)) \,\mathrm{d}s + \int_0^t D^*\big(-\mathrm{d}E(u(s))\big) \,\mathrm{d}s \\
&= \int_0^t \Big(\mathrm{d}E(u(s))(\dot{u}(s)) + D(\dot{u}(s)) + D^*\big(-\mathrm{d}E(u(s))\big) \Big) \,\mathrm{d}s.
\end{aligned}$$

Since the integrand $\mathrm{d}E(u)(\dot{u}) + D(\dot{u}) + D^*(-\mathrm{d}E(u))$ is nonnegative due to the definition of the Fenchel-Legendre transform, we conclude that

$$\mathrm{d}E(u(t))(\dot{u}(t)) + D(\dot{u}(t)) + D^*\big(-\mathrm{d}E(u(t))\big) = 0 \qquad \text{for almost every } t \in [0,T].$$

Therefore, u is a (weak) solution of (4.21).

Uniqueness follows by standard arguments using the linearity of the limit problem. In particular, all extractions of subsequences as $n \to \infty$ were unnecessary and the whole sequence u_n converges to u. □

From the above proof, we readily get the following additional information.

Corollary 4.6.4 (Energy convergence)**.** *Let u_n be a sequence of solutions to the nonlocal viscoelastic problem (4.20) and u be the solution to the local viscoelastic problem (4.21) with $u_n \to u$ as in the setting of Theorem 4.2.1. Then, we have*

$$E_n(u_n(t)) \to E(u(t)) \quad \text{for almost all } t \in [0,T].$$

4.7 Calculations

In this section, we collect some elementary calculations.

Lemma 4.7.1 (Integrals over the unit sphere)**.**

$$\begin{aligned}
&\fint_{S^{d-1}} s_i^n s_j \,\mathrm{d}\mathcal{H}^{d-1}(s) = 0 && \forall i \neq j, i, j \in \{1,\dots,d\},\ \forall n \in \mathbb{N},\\
&\fint_{S^{d-1}} s_i^2 \,\mathrm{d}\mathcal{H}^{d-1}(s) = \frac{1}{d} && \forall i \in \{1,\dots,d\},\\
&\fint_{S^{d-1}} s_i^4 \,\mathrm{d}\mathcal{H}^{d-1}(s) = \frac{3}{d(d+2)} && \forall i \in \{1,\dots,d\},\\
&\fint_{S^{d-1}} s_i^2 s_j^2 d\mathcal{H}^{d-1}(s) = \frac{1}{d(d+2)} && \forall i \neq j, i, j \in \{1,\dots,d\}.
\end{aligned}$$

A proof can be found in [99, Theorem A.1], see also [11].

Lemma 4.7.2. *For $u \in H^1(\Omega;\mathbb{R}^d)$ we have*

$$\fint_{S^{d-1}} s \cdot \nabla u(x) s \,\mathrm{d}\mathcal{H}^{d-1}(s) = \frac{1}{d} \operatorname{div} u(x) \qquad \text{for a.e. } x \in \Omega.$$

Proof. A simple computation shows

$$\begin{aligned}
\fint_{S^{d-1}} s \cdot \nabla u(x) s \,\mathrm{d}\mathcal{H}^{d-1}(s) &= \sum_{ij} \partial_i u_j(x) \fint_{S^{d-1}} s_i s_j \,\mathrm{d}\mathcal{H}^{d-1}(s)\\
&= \sum_i \partial_i u_i(x) \frac{1}{d} = \frac{1}{d} \operatorname{div} u(x),
\end{aligned}$$

where we used Lemma 4.7.1. □

We can also give an expression for the product of quadratic forms on the sphere.

Lemma 4.7.3. *Let $u, v \in H^1(\Omega;\mathbb{R}^d)$. Then we have for almost every $x \in \Omega$*

$$\begin{aligned}
&\fint_{S^{d-1}} (s \cdot \nabla u(x) s)(s \cdot \nabla v(x) s) \,\mathrm{d}\mathcal{H}^{d-1}(s)\\
&= \frac{2}{d(d+2)} \varepsilon(u(x)) : \varepsilon(v(x)) + \frac{1}{d(d+2)} (\operatorname{div} u(x))(\operatorname{div} v(x)).
\end{aligned}$$

Proof. As for any matrix M we have $x \cdot Mx = x \cdot \frac{M+M^\top}{2}x$, we can replace ∇u by the symmetric gradient $\varepsilon(u)$ in the following calculations. For brevity we set $A := \varepsilon(u)$ and $B := \varepsilon(v)$. Then, we obtain by Lemma 4.7.1

$$\begin{aligned}
&\fint_{S^{d-1}} (s \cdot \nabla us)(s \cdot \nabla vs)\,\mathrm{d}\mathcal{H}^{d-1}(s) = \fint_{S^{d-1}} (s \cdot As)(s \cdot Bs)\,\mathrm{d}\mathcal{H}^{d-1}(s)\\
&= \sum_{ijkl} A_{ij}B_{kl} \fint_{S^{d-1}} s_i s_j s_k s_l \,\mathrm{d}\mathcal{H}^{d-1}(s)\\
&= \frac{3}{d(d+2)} \sum_i A_{ii}B_{ii} + \frac{1}{d(d+2)} \sum_{i\neq k} A_{ii}B_{kk} + \frac{1}{d(d+2)} \sum_{i\neq j} A_{ij}B_{ij} + \frac{1}{d(d+2)} \sum_{i\neq j} A_{ij}B_{ji}.
\end{aligned}$$

Next, note that, since $\partial_i u_i = \varepsilon(u)_{ii}$, we have

$$\sum_i A_{ii}B_{ii} + \sum_{i\neq k} A_{ii}B_{kk} = \sum_{i,k} A_{ii}B_{kk} = \left(\sum_i \partial_i u_i\right)\left(\sum_k \partial_k v_k\right) = \operatorname{div} u \operatorname{div} v.$$

Eventually, by virtue of the symmetry of A and B, we have

$$\begin{aligned}
2\sum_i A_{ii}B_{ii} + \sum_{i\neq j} A_{ij}B_{ij} + \sum_{i\neq j} A_{ij}B_{ji} &= 2\sum_i \sum_j A_{ij}B_{ji} = 2\sum_i (AB)_{ii}\\
&= 2\operatorname{tr}(AB^\top) = 2A : B = 2\varepsilon(u) : \varepsilon(v).
\end{aligned}$$

Putting this together yields the claim. □

Let us conclude by proving the claim on the equivalent forms of the energy in Theorem 4.4.5. We present a full argument for the sake of completeness, but one could also refer to [100, Proposition 4].

Lemma 4.7.4. *Let $u, v \in H^1(\Omega;\mathbb{R}^d)$. Then*

$$\begin{aligned}
&\int_\Omega \fint_{S^{d-1}} \left(s \cdot \nabla u(x)s - \frac{1}{d}\operatorname{div} u(x)\right)\left(s \cdot \nabla v(x)s - \frac{1}{d}\operatorname{div} v(x)\right)\mathrm{d}\mathcal{H}^{d-1}(s)\,\mathrm{d}x\\
&= \int_\Omega \frac{2}{d(d+2)}\varepsilon(u(x)) : \varepsilon(v(x)) + \left(\frac{1}{d(d+2)} - \frac{1}{d^2}\right)(\operatorname{div} u(x))(\operatorname{div} v(x))\,\mathrm{d}x.
\end{aligned}$$

In particular, we have

$$\begin{aligned}
E(u) &= \frac{\mu}{2}\int_\Omega |\varepsilon(u(x))|^2\,\mathrm{d}x + \frac{\lambda}{2}\int_\Omega \operatorname{div}^2 u(x)\,\mathrm{d}x\\
&= \frac{\beta}{2}\int_\Omega \operatorname{div}^2 u(x)\,\mathrm{d}x + \frac{\alpha}{2}d\int_\Omega \fint_{S^{d-1}} \left(s \cdot \nabla u(x) \cdot s - \frac{1}{d}\operatorname{div} u(x)\right)^2 \mathrm{d}\mathcal{H}^{d-1}(s)\,\mathrm{d}x,
\end{aligned}$$

where $\mu = \frac{2\alpha}{d+2}$ and $\lambda = \beta - \frac{2\alpha}{d(d+2)}$.

Proof. By Lemma 4.7.2 we have

$$\int_\Omega \fint_{S^{d-1}} (s \cdot \nabla u(x) s) \frac{1}{d} \operatorname{div} v(x) \, \mathrm{d}\mathcal{H}^{d-1}(s) \, \mathrm{d}x = \frac{1}{d^2} \int_\Omega \operatorname{div} u(x) \, \operatorname{div} v(x) \, \mathrm{d}x$$

and similarly for u and v interchanged. We can hence conclude

$$\begin{aligned}
&\int_\Omega \fint_{S^{d-1}} \left(s \cdot \nabla u(x) s - \frac{1}{d} \operatorname{div} u(x) \right) \left(s \cdot \nabla v(x) s - \frac{1}{d} \operatorname{div} v(x) \right) \mathrm{d}\mathcal{H}^{d-1}(s) \, \mathrm{d}x \\
&= \int_\Omega \fint_{S^{d-1}} (s \cdot \nabla u(x) s) \, (s \cdot \nabla v(x) s) \, \mathrm{d}\mathcal{H}^{d-1}(s) \, \mathrm{d}x - \frac{1}{d^2} \int_\Omega \operatorname{div} u(x) \, \operatorname{div} v(x) \, \mathrm{d}x.
\end{aligned}$$

Employing Lemma 4.7.3, we arrive at

$$\begin{aligned}
&\int_\Omega \fint_{S^{d-1}} (s \cdot \nabla u(x) s) \, (s \cdot \nabla v(x) s) \, \mathrm{d}\mathcal{H}^{d-1}(s) \, \mathrm{d}x - \frac{1}{d^2} \int_\Omega \operatorname{div} u(x) \, \operatorname{div} v(x) \, \mathrm{d}x \\
&= \int_\Omega \left(\frac{2}{d(d+2)} \varepsilon(u) : \varepsilon(v) + \frac{1}{d(d+2)} \operatorname{div} u(x) \, \operatorname{div} v(x) - \frac{1}{d^2} \operatorname{div} u(x) \, \operatorname{div} v(x) \right) \mathrm{d}x
\end{aligned}$$

concluding the first part of the claim. The representation of the energy follows by (4.4). □

Lemma 4.7.5 (Elastic energy)**.** *With $\mathbb{C}$ defined as in (4.8), we have*

$$\frac{\lambda}{2} \int_\Omega \operatorname{div} u(x)^2 \, \mathrm{d}x + \frac{\mu}{2} \int_\Omega |\varepsilon(u(x))|^2 \, \mathrm{d}x = \frac{1}{2} \int_\Omega \mathbb{C}\varepsilon(u(x)) : \varepsilon(u(x)) \, \mathrm{d}x.$$

Proof. Set for brevity $\varepsilon_{ij} := \varepsilon(u)_{ij}$. A direct calculation shows that

$$\begin{aligned}
\mathbb{C}\varepsilon : \varepsilon &= \sum_{ijkl} \mathbb{C}_{ijkl} \varepsilon_{ij} \varepsilon_{kl} = \sum_{ijkl} \left(\mu \delta_{ik} \delta_{jl} \varepsilon_{ij} \varepsilon_{kl} + \lambda \delta_{ij} \delta_{kl} \varepsilon_{ij} \varepsilon_{kl} \right) \\
&= \sum_{ij} \mu \varepsilon_{ij} \varepsilon_{ij} + \sum_{ik} \lambda \varepsilon_{ii} \varepsilon_{kk} = \mu |\varepsilon|^2 + \lambda (\operatorname{div} \varepsilon)^2.
\end{aligned}$$

□

Acknowledgments

This work was supported by the DFG project FR 4083/3-1, by the Deutsche Forschungsgemeinschaft (DFG, German Research Foundation) under Germany's Excellence Strategy EXC 2044 -390685587, Mathematics Münster: Dynamics–Geometry–Structure, by the Austrian Science Fund (FWF) projects 10.55776/F65, 10.55776/I4354, 10.55776/I5149, and 10.55776/P32788.

References

[1] R. A. Adams, J. J. F. Fournier. *Sobolev Spaces*. 2nd ed. Pure and Applied Mathematics 140. Amsterdam: Academic Press, 2003.

[2] D. Akinwande, C. Huyghebaert, C.-H. Wang, M. I. Serna, S. Goossens, L.-J. Li, H.-S. P. Wong, F. H. Koppens. Graphene and two-dimensional materials for silicon technology. *Nature* **573** (2019), no. 7775, 507–518.

[3] R. Alicandro, M. Cicalese. A general integral representation result for continuum limits of discrete energies with superlinear growth. *SIAM J. Math. Anal.* **36** (2004), no. 1, 1–37.

[4] R. Alicandro, M. Cicalese, A. Gloria. Integral representation results for energies defined on stochastic lattices and application to nonlinear elasticity. *Arch. Ration. Mech. Anal.* **200** (2011), no. 3, 881–943.

[5] M. J. Allen, V. C. Tung, R. B. Kaner. Honeycomb carbon: a review of graphene. *Chem. Rev.* **110** (2010), no. 1, 132–145.

[6] N. L. Allinger. *Molecular structure: understanding steric and electronic effects from molecular mechanics*. Hoboken, NJ: Wiley, 2010.

[7] L. Ambrosio, N. Gigli, G. Savaré. *Gradient flows in metric spaces and in the space of probability measures*. 2nd ed. Lectures in Mathematics ETH Zürich. Basel: Birkhäuser, 2008.

[8] M. Arndt, M. Griebel. Derivation of higher order gradient continuum models from atomistic models for crystalline solids. *Multiscale Model. Simul.* **4** (2005), no. 2, 531–562.

[9] E. Askari, F. Bobaru, R. B. Lehoucq, M. L. Parks, S. A. Silling, O. Weckner. Peridynamics for multiscale materials modeling. *J. Phys. Conf. Ser.* **125** (2008), no. 1, 012078.

[10] A. Bach, A. Braides, M. Cicalese. Discrete-to-continuum limits of multibody systems with bulk and surface long-range interactions. *SIAM J. Math. Anal.* **52** (2020), no. 4, 3600–3665.

[11] J. A. Baker. Integration over spheres and the divergence theorem for balls. *Amer. Math. Monthly* **104** (1997), no. 1, 36–47.

[12] J. M. Ball. Progress and puzzles in nonlinear elasticity. In: *Poly-, Quasi- and Rank-One Convexity in Applied Mechanics*. Ed. by P. Schröder Jörg and Neff. Vienna: Springer, 2010, pp. 1–15.

[13] J. M. Ball. Some open problems in elasticity. In: *Geometry, mechanics, and dynamics*. Ed. by P. Newton, P. Holmes, A. Weinstein. New York, NY: Springer, 2002, pp. 3–59.

[14] J. C. Bellido, J. Cueto, C. Mora-Corral. Bond-based peridynamics does not converge to hyperelasticity as the horizon goes to zero. *J. Elasticity* **141** (2020), no. 2, 273–289.

[15] X. Blanc, C. Le Bris, P.-L. Lions. Atomistic to continuum limits for computational materials science. *M2AN Math. Model. Numer. Anal.* **41** (2007), no. 2, 391–426.

[16] X. Blanc, C. Le Bris, P.-L. Lions. From molecular models to continuum mechanics. *Arch. Ration. Mech. Anal.* **164** (2002), no. 4, 341–381.

[17] X. Blanc, M. Lewin. The crystallization conjecture: a review. *EMS Surv. Math. Sci.* **2** (2015), no. 2, 225–306.

[18] F. Bobaru, J. T. Foster, P. H. Geubelle, S. A. Silling, eds. *Handbook of peridynamic modeling*. Advances in Applied Mathematics. Boca Raton, FL: CRC Press, 2017.

[19] F. Bonelli, N. Manini, E. Cadelano, L. Colombo. Atomistic simulations of the sliding friction of graphene flakes. *Eur. Phys. J. B* **70** (2009), no. 4, 449–459.

[20] M. Born, J. R. Oppenheimer. Zur Quantentheorie der Molekeln. *Ann. Physik* **389** (1927), no. 20, 457–484.

[21] I. Boustani. New quasi-planar surfaces of bare boron. *Surface Science* **370** (1997), no. 2-3, 355–363.

[22] A. Braides. Γ-*convergence for beginners*. Oxford Lecture Series in Mathematics and its Applications 22. Oxford: Oxford University Press, 2002.

[23] A. Braides. Discrete-to-continuum variational methods for lattice systems. In: *Proceedings of the International Congress of Mathematicians—Seoul 2014. Vol. IV*. Seoul: Kyung Moon Sa, 2014, pp. 997–1015.

[24] A. Braides. *Local minimization, variational evolution and* Γ-*convergence*. Lecture Notes in Mathematics 2094. Cham: Springer, 2014.

[25] A. Braides, M. Caroccia. Asymptotic behavior of the Dirichlet energy on Poisson point clouds. *J. Nonlinear Sci.* **33** (2023), no. 5, Paper No. 80.

[26] A. Braides, A. Causin, M. Solci, L. Truskinovsky. Beyond the classical Cauchy-Born rule. *Arch. Ration. Mech. Anal.* **247** (2023), no. 6, Paper No. 107.

[27] A. Braides, M. Colombo, M. Gobbino, M. Solci. Minimizing movements along a sequence of functionals and curves of maximal slope. *C. R. Math. Acad. Sci. Paris* **354** (2016), no. 7, 685–689.

[28] A. Braides, L. D'Elia. Homogenization of discrete thin structures. *Nonlinear Anal.* **231** (2023), Paper No. 112951.

[29] A. Braides, G. Dal Maso, A. Garroni. Variational formulation of softening phenomena in fracture mechanics: the one-dimensional case. *Arch. Ration. Mech. Anal.* **146** (1999), no. 1, 23–58.

[30] A. Braides, A. Defranceschi, E. Vitali. Variational evolution of one-dimensional Lennard-Jones systems. *Netw. Heterog. Media* **9** (2014), no. 2, 217–238.

[31] A. Braides, M. S. Gelli. Continuum limits of discrete systems without convexity hypotheses. *Math. Mech. Solids* **7** (2002), no. 1, 41–66.

[32] A. Braides, M. S. Gelli. From discrete systems to continuous variational problems: an introduction. In: *Topics on concentration phenomena and problems with multiple scales*. Ed. by A. Braides, V. Chiadò Piat. Lect. Notes Unione Mat. Ital. 2. Berlin: Springer, 2006, pp. 3–77.

[33] A. Braides, A. J. Lew, M. Ortiz. Effective cohesive behavior of layers of interatomic planes. *Arch. Ration. Mech. Anal.* **180** (2006), no. 2, 151–182.

[34] A. Braides, M. Solci. *Geometric flows on planar lattices*. Pathways in Mathematics. Cham: Birkhäuser, 2021.

[35] A. Braides, M. Solci, E. Vitali. A derivation of linear elastic energies from pair-interaction atomistic systems. *Netw. Heterog. Media* **2** (2007), no. 3, 551–567.

[36] J. Braun. Connecting atomistic and continuous models of elastodynamics. *Arch. Ration. Mech. Anal.* **224** (2017), no. 3, 907–953.

[37] J. Braun, B. Schmidt. On the passage from atomistic systems to nonlinear elasticity theory for general multi-body potentials with p-growth. *Netw. Heterog. Media* **8** (2013), no. 4, 879–912.

[38] D. W. Brenner. Empirical potential for hydrocarbons for use in stimulating the chemical vapor deposition of diamond films. *Phys. Rev. B* **42** (1990), no. 15, 9458–9471.

[39] H. Brezis. *Functional analysis, Sobolev spaces and partial differential equations*. Universitext. New York, NY: Springer, 2011.

[40] M. J. Buehler. *Atomistic modeling of materials failure*. New York, NY: Springer, 2008.

[41] U. Burkert, N. Allinger. *Molecular mechanics*. 2nd ed. ACS monograph series 177. Washington, DC: American Chem. Soc., 1984.

[42] S. Cahangirov, M. Topsakal, E. Aktürk, H. Şahin, S. Ciraci. Two-and one-dimensional honeycomb structures of silicon and germanium. *Phys. Rev. Lett.* **102** (2009), no. 23, 236804.

[43] K. Chu, W.-s. Li, F.-l. Tang. Flatness-dependent thermal conductivity of graphene-based composites. *Phys. Lett. A* **377** (2013), no. 12, 910–914.

[44] G. M. Coclite, S. Dipierro, F. Maddalena, E. Valdinoci. Wellposedness of a nonlinear peridynamic model. *Nonlinearity* **32** (2019), no. 1, 1–21.

[45] S. Conti, G. Dolzmann, B. Kirchheim, S. Müller. Sufficient conditions for the validity of the Cauchy-Born rule close to SO(n). *J. Eur. Math. Soc. (JEMS)* **8** (2006), no. 3, 515–530.

[46] B. Dacorogna. *Direct methods in the calculus of variations*. 2nd ed. Applied Mathematical Sciences 78. New York, NY: Springer, 2008.

[47] G. Dal Maso. *An introduction to* Γ*-convergence*. Progress in Nonlinear Differential Equations and their Applications 8. Boston, MA: Birkhäuser, 1993.

[48] G. Dal Maso, M. Negri, D. Percivale. Linearized elasticity as Γ-limit of finite elasticity. *Set-Valued Anal.* **10** (2002), no. 2-3, 165–183.

[49] M. E. Dávila, L. Xian, S. Cahangirov, A. Rubio, G. Le Lay. Germanene: a novel two-dimensional germanium allotrope akin to graphene and silicene. *New J. Phys.* **16** (2014), no. 9, 095002.

[50] G. Del Nin, M. Petrache. Continuum limits of discrete isoperimetric problems and Wulff shapes in lattices and quasicrystal tilings. *Calc. Var. Partial Differential Equations* **61** (2022), no. 6, Paper No. 226.

[51] R. Delorme, I. Tabiai, L. Laberge Lebel, M. Lévesque. Generalization of the ordinary state-based peridynamic model for isotropic linear viscoelasticity. *Mech. Time-Depend. Mater.* **21** (2017), no. 4, 549–575.

[52] S. Deng, V. Berry. Wrinkled, rippled and crumpled graphene: an overview of formation mechanism, electronic properties, and applications. *Mater. Today* **19** (2016), no. 4, 197–212.

[53] Q. Du, M. Gunzburger, R. B. Lehoucq, K. Zhou. A nonlocal vector calculus, nonlocal volume-constrained problems, and nonlocal balance laws. *Math. Models Methods Appl. Sci.* **23** (2013), no. 3, 493–540.

[54] Q. Du, M. Gunzburger, R. B. Lehoucq, K. Zhou. Analysis and approximation of nonlocal diffusion problems with volume constraints. *SIAM Rev.* **54** (2012), no. 4, 667–696.

[55] Q. Du, X. Tian, Z. Zhou. Nonlocal Diffusion Models with Consistent Local and Fractional Limits. In: *A^3N^2M: Approximation, Applications, and Analysis of Nonlocal, Nonlinear Models*. Ed. by T. Mengesha, A. J. Salgado. The IMA Volumes in Mathematics and its Applications 165. Cham: Springer, 2023, pp. 175–213.

[56] Q. Du, K. Zhou. Mathematical analysis for the peridynamic nonlocal continuum theory. *ESAIM Math. Model. Numer. Anal.* **45** (2011), no. 2, 217–234.

[57] W. E, D. Li. On the crystallization of 2D hexagonal lattices. *Comm. Math. Phys.* **286** (2009), no. 3, 1099–1140.

[58] W. E, P. Ming. Cauchy-Born rule and the stability of crystalline solids: dynamic problems. *Acta Math. Appl. Sin. Engl. Ser.* **23** (2007), no. 4, 529–550.

[59] W. E, P. Ming. Cauchy-Born rule and the stability of crystalline solids: static problems. *Arch. Ration. Mech. Anal.* **183** (2007), no. 2, 241–297.

[60] E. Emmrich, R. B. Lehoucq, D. Puhst. Peridynamics: a nonlocal continuum theory. In: *Meshfree methods for partial differential equations VI*. Lect. Notes Comput. Sci. Eng. 89. Heidelberg: Springer, 2013, pp. 45–65.

[61] E. Emmrich, D. Puhst. Survey of existence results in nonlinear peridynamics in comparison with local elastodynamics. *Comput. Methods Appl. Math.* **15** (2015), no. 4, 483–496.

[62] E. Emmrich, O. Weckner. On the well-posedness of the linear peridynamic model and its convergence towards the Navier equation of linear elasticity. *Commun. Math. Sci.* **5** (2007), no. 4, 851–864.

[63] J. L. Ericksen. On the Cauchy-Born Rule. *Math. Mech. Solids* **13** (2008), no. 3-4, 199–220.

[64] B. Farmer, S. Esedoḡlu, P. Smereka. Crystallization for a Brenner-like potential. *Comm. Math. Phys.* **349** (2017), no. 3, 1029–1061.

[65] A. Fasolino, J. H. Los, M. I. Katsnelson. Intrinsic ripples in graphene. *Nat. Mater.* **6** (2007), no. 11, 858–861.

[66] J. Fischer, M. Wendland. On the history of key empirical intermolecular potentials. *Fluid Ph. Equilib.* **573** (2023), 113876.

[67] G. Foghem, M. Kassmann. A general framework for nonlocal Neumann problems. *Commun. Math. Sci.* **22** (2024), no. 1, 15–66.

[68] M. Friedrich, B. Schmidt. An analysis of crystal cleavage in the passage from atomistic models to continuum theory. *Arch. Ration. Mech. Anal.* **217** (2015), no. 1, 263–308.

[69] M. Friedrich, B. Schmidt. An atomistic-to-continuum analysis of crystal cleavage in a two-dimensional model problem. *J. Nonlinear Sci.* **24** (2014), no. 1, 145–183.

[70] M. Friedrich, B. Schmidt. On a discrete-to-continuum convergence result for a two dimensional brittle material in the small displacement regime. *Netw. Heterog. Media* **10** (2015), no. 2, 321–342.

[71] M. Friedrich, M. Seitz, U. Stefanelli. *Discrete-to-continuum linearization in atomistic dynamics*. 2024. arXiv: 2305.08469.

[72] M. Friedrich, M. Seitz, U. Stefanelli. *Nonlocal-to-local limit in linearized viscoelasticity*. 2024. arXiv: 2402.16386.

[73] M. Friedrich, M. Seitz, U. Stefanelli. Tilings with nonflat squares: a characterization. *Milan J. Math.* **90** (2022), no. 1, 131–175.

[74] M. Friedrich, U. Stefanelli. Graphene ground states. *Z. Angew. Math. Phys.* **69** (2018), no. 3. Paper No. 70, 18 pp.

[75] M. Friedrich, U. Stefanelli. Ripples in graphene: a variational approach. *Comm. Math. Phys.* **379** (2020), no. 3, 915–954.

[76] G. Friesecke, R. D. James, S. Müller. A hierarchy of plate models derived from nonlinear elasticity by gamma-convergence. *Arch. Ration. Mech. Anal.* **180** (2006), no. 2, 183–236.

[77] G. Friesecke, F. Theil. Molecular geometry optimization, models. In: *Encyclopedia of Applied and Computational Mathematics*. Ed. by B. Engquist. Berlin, Heidelberg: Springer, 2015.

[78] G. Friesecke, F. Theil. Validity and failure of the Cauchy-Born hypothesis in a two-dimensional mass-spring lattice. *J. Nonlinear Sci.* **12** (2002), no. 5, 445–478.

[79] Y. K. Galadima, S. Oterkus, E. Oterkus, I. Amin, A.-H. El-Aassar, H. Shawky. Modelling of viscoelastic materials using non-ordinary state-based peridynamics. *Eng. Comput.* **40** (2023), no. 1, 527–540.

[80] A. K. Geim, K. S. Novoselov. The rise of graphene. *Nat. Mater.* **6** (2007), no. 3, 183–191.

[81] I. M. Gelfand, S. V. Fomin. *Calculus of variations*. Englewood Cliffs, NJ: Prentice-Hall, Inc., 1963.

[82] E. Gnecco, E. Meyer, eds. *Fundamentals of Friction and Wear on the Nanoscale*. Cham: Springer, 2015.

[83] M. E. Gurtin. *An introduction to continuum mechanics*. Mathematics in Science and Engineering 158. London, New York, NY: Academic Press, Inc., 1981.

[84] R. C. Heitmann, C. Radin. The ground state for sticky disks. *J. Statist. Phys.* **22** (1980), no. 3, 281–287.

[85] A. Javili, R. Morasata, E. Oterkus, S. Oterkus. Peridynamics review. *Math. Mech. Solids* **24** (2019), no. 11, 3714–3739.

[86] M. Kružík, C. Mora-Corral, U. Stefanelli. Quasistatic elastoplasticity via peridynamics: existence and localization. *Contin. Mech. Thermodyn.* **30** (2018), no. 5, 1155–1184.

[87] M. Kružík, T. Roubíček. *Mathematical Methods in Continuum Mechanics of Solids*. Interaction of Mechanics and Mathematics. Cham: Springer, 2019.

[88] S. Y. Krylov, J. W. M. Frenken. Atomistic mechanisms for frictional energy dissipation during continuous sliding. *Sci. Rep.* **11** (2021), no. 1, 1–10.

[89] C. Le Bris, P.-L. Lions. From atoms to crystals: a mathematical journey. *Bull. Amer. Math. Soc. (N.S.)* **42** (2005), no. 3, 291–363.

[90] J. G. Lee. *Computational materials science: an introduction*. Boca Raton, FL: CRC press, 2016.

[91] I. N. Levine. *Quantum Chemistry*. 5th ed. Upper Saddle River, NJ: Prentice Hall, 2000.

[92] E. G. Lewars. *Computational Chemistry*. New York, NY, Boston, MA, Dordrecht, London, Moscow: Kluwer Academic Publishers, 2011.

[93] W. Li, X. Qian, J. Li. Phase transitions in 2D materials. *Nat. Rev. Mater.* **6** (2021), no. 9, 829–846.

[94] H. Liu, A. T. Neal, Z. Zhu, Z. Luo, X. Xu, D. Tománek, P. D. Ye. Phosphorene: an unexplored 2D semiconductor with a high hole mobility. *ACS nano* **8** (2014), no. 4, 4033–4041.

[95] S. G. Lobanov, O. G. Smolyanov. Ordinary differential equations in locally convex spaces. *Uspekhi Mat. Nauk* **49** (1994), no. 3(297), 93–168.

[96] U. Ludacka, M. R. A. Monazam, C. Rentenberger, M. Friedrich, U. Stefanelli, J. C. Meyer, J. Kotakoski. In situ control over graphene ripples and strain in the electron microscope. *npj 2D Mater. Appl.* **2** (2018), no. 1, 25.

[97] E. Madenci, S. Oterkus. Ordinary state-based peridynamics for thermoviscoelastic deformation. *Eng. Fract. Mech.* **175** (2017), 31–45.

[98] E. Mainini, P. Piovano, U. Stefanelli. Finite crystallization in the square lattice. *Nonlinearity* **27** (2014), no. 4, 717–737.

[99] T. Mengesha. Nonlocal Korn-type characterization of Sobolev vector fields. *Commun. Contemp. Math.* **14** (2012), no. 4, 1250028.

[100] T. Mengesha, Q. Du. Nonlocal constrained value problems for a linear peridynamic Navier equation. *J. Elasticity* **116** (2014), no. 1, 27–51.

[101] T. Mengesha, Q. Du. On the variational limit of a class of nonlocal functionals related to peridynamics. *Nonlinearity* **28** (2015), no. 11, 3999–4035.

[102] T. Mengesha, Q. Du. The bond-based peridynamic system with Dirichlet-type volume constraint. *Proc. Roy. Soc. Edinburgh Sect. A* **144** (2014), no. 1, 161–186.

[103] T. Mengesha, J. M. Scott. *Linearization and localization of nonconvex functionals motivated by nonlinear peridynamic models.* 2023. arXiv: 2306.15446.

[104] T. Mengesha, J. M. Scott. The solvability of a strongly-coupled nonlocal system of equations. *J. Math. Anal. Appl.* **486** (2020), no. 2, 123919, 21.

[105] T. Mengesha, D. Spector. Localization of nonlocal gradients in various topologies. *Calc. Var. Partial Differential Equations* **52** (2015), no. 1-2, 253–279.

[106] N. D. Mermin. Crystalline order in two dimensions. *Phys. Rev.* **176** (1968), no. 1, 250–254.

[107] N. D. Mermin, H. Wagner. Absence of ferromagnetism or antiferromagnetism in one- or two-dimensional isotropic Heisenberg models. *Phys. Rev. Lett.* **17** (1966), no. 22, 1133–1136.

[108] P. van Meurs, M. A. Peletier, N. Požár. Discrete-to-continuum convergence of charged particles in 1D with annihilation. *Arch. Ration. Mech. Anal.* **246** (2022), no. 1, 241–297.

[109] J. C. Meyer, A. K. Geim, M. I. Katsnelson, K. S. Novoselov, T. J. Booth, S. Roth. The structure of suspended graphene sheets. *Nature* **446** (2007), no. 7131, 60–63.

[110] A. Mielke. On evolutionary Γ-convergence for gradient systems. In: *Macroscopic and large scale phenomena: coarse graining, mean field limits and ergodicity*. Lect. Notes Appl. Math. Mech. 3. Cham: Springer, 2016, pp. 187–249.

[111] A. Mielke, T. Roubíček, U. Stefanelli. Γ-limits and relaxations for rate-independent evolutionary problems. *Calc. Var. Partial Differential Equations* **31** (2008), no. 3, 387–416.

[112] J. A. Mitchell. *A non-local, ordinary-state-based viscoelasticity model for peridynamics*. Tech. rep. SAND2011-8064. Albuquerque, NM, and Livermore, CA: Sandia National Laboratories (SNL), 2011.

[113] K. S. Novoselov, A. K. Geim, S. V. Morozov, D. Jiang, Y. Zhang, S. V. Dubonos, I. V. Grigorieva, A. A. Firsov. Electric field effect in atomically thin carbon films. *Science* **306** (2004), no. 5696, 666–669.

[114] C. Ortner, F. Theil. Justification of the Cauchy-Born approximation of elastodynamics. *Arch. Ration. Mech. Anal.* **207** (2013), no. 3, 1025–1073.

[115] C. Ortner. Gradient flows as a selection procedure for equilibria of nonconvex energies. *SIAM J. Math. Anal.* **38** (2006), no. 4, 1214–1234.

[116] A. K. Rappé, C. L. Casewit. *Molecular Mechanics across Chemistry*. Sausalito, CA: University Science Books, 1997.

[117] F. Rindler. *Calculus of variations*. Universitext. Cham: Springer, 2018.

[118] M. Ruf. Discrete stochastic approximations of the Mumford-Shah functional. *Ann. Inst. H. Poincaré C Anal. Non Linéaire* **36** (2019), no. 4, 887–937.

[119] E. Sandier, S. Serfaty. Gamma-convergence of gradient flows with applications to Ginzburg-Landau. *Comm. Pure Appl. Math.* **57** (2004), no. 12, 1627–1672.

[120] F. Santambrogio. {Euclidean, metric, and Wasserstein} gradient flows: an overview. *Bull. Math. Sci.* **7** (2017), no. 1, 87–154.

[121] M. Schäffner, A. Schlömerkemper. On Lennard-Jones systems with finite range interactions and their asymptotic analysis. *Netw. Heterog. Media* **13** (2018), no. 1, 95–118.

[122] B. Schmidt. A derivation of continuum nonlinear plate theory from atomistic models. *Multiscale Model. Simul.* **5** (2006), no. 2, 664–694.

[123] B. Schmidt. On the derivation of linear elasticity from atomistic models. *Netw. Heterog. Media* **4** (2009), no. 4, 789–812.

[124] B. Schmidt. On the passage from atomic to continuum theory for thin films. *Arch. Ration. Mech. Anal.* **190** (2008), no. 1, 1–55.

[125] R. E. Showalter. *Monotone operators in Banach space and nonlinear partial differential equations*. Mathematical Surveys and Monographs 49. Providence, RI: American Mathematical Society, 1997.

[126] S. A. Silling. Linearized theory of peridynamic states. *J. Elasticity* **99** (2010), no. 1, 85–111.

[127] S. A. Silling. Reformulation of elasticity theory for discontinuities and long-range forces. *J. Mech. Phys. Solids* **48** (2000), no. 1, 175–209.

[128] S. A. Silling, M. Epton, O. Weckner, J. Xu, E. Askari. Peridynamic states and constitutive modeling. *J. Elasticity* **88** (2007), no. 2, 151–184.

[129] J. C. Slater. *Quantum theory of matter*. 2nd ed. New York, NY: McGraw-Hill, 1968.

[130] U. Stefanelli. The Brezis-Ekeland principle for doubly nonlinear equations. *SIAM J. Control Optim.* **47** (2008), no. 3, 1615–1642.

[131] F. H. Stillinger, T. A. Weber. Computer simulation of local order in condensed phases of silicon. *Phys. Rev. B* **31** (1985), no. 8, 5262–5271.

[132] J. Tersoff. New empirical approach for the structure and energy of covalent systems. *Phys. Rev. B* **37** (1988), no. 12, 6991–7000.

[133] F. Theil. A proof of crystallization in two dimensions. *Comm. Math. Phys.* **262** (2006), no. 1, 209–236.

[134] F. Theil. Surface energies in a two-dimensional mass-spring model for crystals. *ESAIM Math. Model. Numer. Anal.* **45** (2011), no. 5, 873–899.

[135] D.-L. Tian, X.-P. Zhou. A viscoelastic model of geometry-constraint-based non-ordinary state-based peridynamics with progressive damage. *Comput. Mech.* **69** (2022), no. 6, 1413–1441.

[136] X. Wang, A. Tabarraei, D. E. Spearot. Fracture mechanics of monolayer molybdenum disulfide. *Nanotech.* **26** (2015), no. 17, 175703.

[137] O. Weckner, N. A. Nik Mohamed. Viscoelastic material models in peridynamics. *Appl. Math. Comput.* **219** (2013), no. 11, 6039–6043.

[138] L. Xian, A. P. Paz, E. Bianco, P. M. Ajayan, A. Rubio. Square Selenene and Tellurene: Novel Group VI Elemental 2D Materials with Nontrivial Topological Properties. *2D Mater.* **4** (2017), no. 4, 041003.

[139] K. Xu, P. Cao, J. R. Heath. Scanning tunneling microscopy characterization of the electrical properties of wrinkles in exfoliated graphene monolayers. *Nano Lett.* **9** (2009), no. 12, 4446–4451.

[140] M. Yang, S. Zhang, Y. Nie. On weak solutions for a nonlocal model with nonlocal damping term. *J. Math. Anal. Appl.* **525** (2023), no. 2, Paper No. 127306, 16.

[141] M. Yangari. Existence and uniqueness of weak solutions for nonlocal parabolic problems via the Galerkin method. *J. Math. Anal. Appl.* **463** (2018), no. 2, 910–921.

[142] H. Yserentant. *Schrödinger Equation for Chemistry*. In: *Encyclopedia of Applied and Computational Mathematics*. Ed. by B. Engquist. 2015.

[143] R.-w. Zhang, W.-x. Ji, C.-w. Zhang, P. Li, P.-j. Wang. Prediction of flatness-driven quantum spin Hall effect in functionalized germanene and stanene. *Phys. Chem. Chem. Phys.* **18** (2016), no. 40, 28134–28139.

[144] Y. Zhang, A. Rubio, G. Le Lay. Emergent elemental two-dimensional materials beyond graphene. *J. Phys. D: Appl. Phys.* **50** (2017), no. 5, 053004.

[145] F. Zhu, W.-j. Chen, Y. Xu, C.-l. Gao, D.-d. Guan, C.-h. Liu, D. Qian, S.-C. Zhang, J.-f. Jia. Epitaxial growth of two-dimensional stanene. *Nat. Mater.* **14** (2015), no. 10, 1020–1025.

Zusammenfassung

Makroskopische Eigenschaften aus atomistischen Systemen herzuleiten ist eine herausfordernde, aber lohnende, Aufgabe, welche wir in dieser Dissertation in drei Fällen aufgreifen wollen.

In einem ersten Beitrag charakterisieren wir dreidimensionale Grundzustände eines zweidimensionalen Masse-Feder-Systems, welches zusätzlich ein Winkel-Potenzial aufweist und Bindungswinkel von π bevorzugt. Die Diskrepanz zwischen der Interaktion nächster Nachbarn und dem Winkel-Potenzial bewirkt, dass flache Quadrate in die dritte Dimension geknickt werden. Dies gibt Anlass zu der Frage, wie man Parkettierungen mit nicht-flachen Quadraten charakterisieren kann. Wir zeigen, dass solche Anordnungen geriffelt, gewellt oder sogar aufgerollt sein können, diese Wellen aber effektiv nur in eine Richtung entstehen können.

Es wurde bereits gezeigt, dass Masse-Feder-Systeme im Übergang von einem atomistischen zu einem Kontinuumsmodell bei gleichzeitiger Linearisierung zu Modelle der klassischen linearen Elastizität konvergieren. Im zweiten Beitrag erweitern wir dieses Ergebnis auf den dynamischen Kontext. Wir zeigen, dass Lösungen der atomistischen Bewegungsgleichung mit Viskosität zur klassischen Impulsgleichung für die lineare elastische Energie konvergieren.

Während in der klassischen Kontinuumsmechanik mechanische Spannungen ausschließlich über Kontaktkräfte beschrieben werden, hat der atomistische Ansatz den Vorteil, dass er auch nicht-lokale Interaktionen, also solche mit langer Reichweite, berücksichtigt. Diese beiden Ansätze wurden zu einem nichtlokalen Kontinuumsmodell kombiniert, welches als *Peridynamik* bezeichnet wird. In einigen Fällen ist es möglich, klassische Formulierungen der Kontinuumsmechanik zu erhalten, wenn man die Reichweite der nichtlokalen Interaktionen gegen 0 gehen lässt, also im sogenannten nichtlokal-zu-lokalen Limes. Wir präsentieren ein dynamisches nichtlokal-zu-lokal Konvergenzergebnis, indem wir die quasistatische Entwicklung eines viskoelastischen peridynamischen Modells mit nichtlokalem Viskositätspotenzial betrachten. Dies kann als eine nichtlokale Version eines Kelvin-Voigt rheologischen Modells interpretiert werden. Wir beweisen, dass Lösungen des nichtlokalen Modells im nichtlokal-zu-lokalen Limes zur Lösung der lokalen Gleichung konvergieren.